CONCEPTUAL AND NUMERICAL MODEL OF INFILTRATION FOR THE YUCCA MOUNTAIN AREA, NEVADA

U.S. GEOLOGICAL SURVEY

Water Resources Investigation Report ##-###

DRAFT

Prepared in cooperation with the
NEVADA OPERATIONS OFFICE
U.S. DEPARTMENT OF ENERGY, under
Interagency Agreement DE-AI08-92NV10874

Dept.
Seal

version

INFIL_R1.WPD

September 20, 1996

CONCEPTUAL AND NUMERICAL MODEL OF INFILTRATION FOR THE YUCCA MOUNTAIN AREA, NEVADA

by Alan L. Flint, Joseph A. Hevesi and Lorraine E. Flint

U.S. GEOLOGICAL SURVEY

Water Resources Investigation Report ##-###

Prepared in cooperation with the
NEVADA OPERATIONS OFFICE
U.S. DEPARTMENT OF ENERGY, under
Interagency Agreement DE-AI08-92NV10874

Denver, Colorado
1996

U.S. DEPARTMENT OF THE INTERIOR

BRUCE BABBITT, Secretary

U.S. GEOLOGICAL SURVEY

Gordon P. Eaton, Director

The use of trade, product, industry, or firm names is for descriptive purposes only and does not imply endorsement by the U.S. Government

---

For additional information write to:

Chief, Earth Sciences Investigations Program
Yucca Mountain Project Branch
U.S. Geological Survey
Box 25046, MS 421
Denver Federal Center
Denver, CO 80225

Copies of this report can be purchased from:

U.S. Geological Survey
Earth Science Information Center
Open-File Reports Section
Box 25286, MS 517
Denver Federal Center
Denver, CO 80225

CONTENTS

ABSTRACT 1

INTRODUCTION 2
Background 2
Purpose and Objectives 4
Previous Work 5

PROCESSES, THE PHYSICS OF INFILTRATION 8
Field Water Balance 9
Precipitation 11
Run-on / Runoff 15
Infiltration 16
Evapotranspiration 19
Redistribution 23
Flow at the soil-bedrock interface 24
Net infiltration 25

STUDY AREA DESCRIPTION 26
Geographic and Physiographic Setting 26
Climate 28
Past 28
Present 31
Future 31
Geology 33
Distribution 35
Properties 35
Watershed Characteristics 36
Defined watersheds 37
Topographic surfaces 38
Soils 39
Distribution 40
Properties 41
Vegetation 43

DATA COLLECTION / DATA ANALYSIS 46
Precipitation 46
Run-on / Runoff 54
Infiltration 57
Evapotranspiration 59
Redistribution 60
Neutron hole moisture profile analysis 60

Geochemistry analysis 63
Flow at the soil-bedrock interface 66
Net infiltration 68

NUMERICAL MODEL 69
Precipitation 70
Run-on/Runoff 72
Infiltration 74
Evapotranspiration 74
Solar radiation 74
Modified Priestley-Taylor equation 75
Redistribution 77
Net infiltration 82
Model Calibration 83
Stochastic Simulations of Infiltration 85

ASSUMPTIONS AND LIMITATIONS 88

FUTURE WORK 89

SUMMARY 90

Appendix I -- All Yucca Mountain Project data referred to in this report, listed by data tracking number 104

Appendix II -- Neutron borehole locations and information used in numerical model 107

Appendix III -- Program MARKOV 108

Appendix IV -- Program PPTSIM 119

Appendix V -- Program INFIL 127

FIGURES

1. Location of a) North American Deserts and the original 3 sites for characterization, and b) physiographic provinces. 2
2. Yucca Mountain regional study area with Death Valley Ground-Water Unit and infiltration study boundary. 5
3. Field scale schematic of infiltration. 9
4. Diagrammatic water balance components using notation described in equation 1. 10
5. Conceptual model of the energy balance equation for evapotranspiration. 21
6. a)Water content and water potential at the soil-bedrock interface at a depth of 2.1 m in borehole USW UZ-N52. The horizontal lines are the air-entry water potentials for a 2.5 um open fracture and a filled fracture, and b) associated flux calculated as the hydraulic conductivity of the fracture times a unit gradient 25
7. Infiltration study area and modeling domain with original site-scale model boundary (Wittwer and others, 1992) and potential repository location. 27
8. Historical climate change estimates from a) SPECMAP studies with a hypothetical transfer to precipitation, b) high-frequency fluctuations in climate change from the GRIP studies and c) recharge estimated from climate change cycles using the Maxey-Eakin method 30
9. Predominate direction of weather patterns and seasonal sources of moisture across the southwestern U.S. 31
10. Map of area with general geologic designations (after Sawyer and others, 1994.) 35
11. Saturated hydraulic conductivity of the surficial bedrock units 36
12. Map of major watersheds at Yucca Mountain. 37
13. Map of soil thickness designated in 4 categories, 0 - < 0.5, 0.5 - < 3 m, 3 - < 6 m, and ≥ 6 m. 40
14. Map of surficial soils. 41
15. Relationship of a) soil texture to saturated hydraulic conductivity using Campbell (1985) for soil without rock fragments and modified to correct for percent rock fragments, and b) modeled versus measured conductivity 42

16. Moisture retention curves calculated from measured soil texture (Campbell, 1985) compared to measured data for soil model units a) 1, b) 2, and c) 4, and texture models for d) all soil model units 43
17. Map of vegetation associations. 44
18. Rate of rainfall for a) a summer thunderstorm and b) winter precipitation 47
19. Estimated daily precipitation for Yucca Mountain using 15 years of measured data simulated at 90 neutron boreholes. 49
20. Probability of occurrence of daily precipitation at Yucca Mountain using 3rd order Markov chains. A 4-day window was used and 1 equals precipitation. 50
21. Data and fitted model for the cumulative probability distribution of precipitation quantity at station 4JA a) for the month of February and b) for the month of July. 51
22. Probability distribution of precipitation quantity for a) precipitation data from Area 12 and b) precipitation data from Yucca Mountain. 53
23. Hydrograph for Pagany Wash and Wren Wash, March 11, 1995. 57
24. Map of maximum infiltration capacity into initially air-dry soil. 58
25. Map of minimum infiltration capacity. 58
26. Illustration of the change in infiltration capacity for soil model unit 5 with time, related to precipitation rate and minimum infiltration capacity 58
27. Map of field capacity of surficial soils 59
28. Field storage capacity of soils calculated as field capacity multiplied by soil depth 59
29. Measured evaporation pan data and calculated potential evapotranspiration using energy balance for 1991-1993. 59
30. Average depth of penetration of the wetting front for years 1990-1993 and soil depth for 34 boreholes (Flint and Flint, 1995). 61
31. Changes in water content over time and depth for borehole USW UZ-N1. 62
32. Changes in water content over time and depth for borehole USW UZ-N15. 63
33. Saturation, porosity and $^{36}Cl/Cl$ ratios for boreholes USW UZ-N15, USW UZ-N16, USW UZ-N17 and USW UZ-N11. ^{36}Cl data is indicated for depth ranges as between pairs of points. 66

34. Saturation, porosity and $^{36}Cl/Cl$ ratios for boreholes USW UZ-N53, USW UZ-N54 and USW UZ-N55. ^{36}Cl data is indicated over a depth range. 66
35. Water potential measurements near borehole USW UZ-N15 using heat dissipation probes, a) measured at 4 depths for 1995 and b) used to calculate flux. 68
36. One hundred-year stochastic simulations of precipitation at a) Yucca Mountain and b) Area 12. 71
37. Average annual precipitation distributed spatially using an elevation correlation. 72
38. Simulated daily evapotranspiration for Yucca Mountain using 15 years of measured precipitation simulated at 90 neutron boreholes 76
39. Volumetric water content simulated at one location in Split Wash for a) 15 years and b) 100 years using the YM stochastic rainfall model 81
40. Simulation of mean net infiltration for neutron boreholes using 100-year stochastic simulations of precipitation from a) Yucca Mountain and b) Area 12 83
41. Calibration of modeled net infiltration using neutron boreholes a) USW UZ-N50 and b) USW UZ-N63. 84
42. Precipitation modeled with no channel enhancement factor and with 30 percent channel enhancement factor compared to simulated average annual precipitation for 15 years of data. 84
43. Precipitation versus infiltration modeled for each borehole with no channel enhancement factor and with 30 percent channel enhancement factor, and mean yearly infiltration for all boreholes. Linear regressions predicting values for each data set are shown. 84
44. Precipitation versus net infiltration, modeled 100-year simulation, estimated using Maxey-Eakin method and calculated from neutron borehole data 85
45. Infiltration simulated using stochastic precipitation simulations with average annual precipitation values of a) 165 mm/year and b) 205 mm/year 86
46. Conceptual model of infiltration numerically modeled using average annual precipitation resulting in an average of 4.5 mm/year flux over the modeling domain 87
47. Close-up view of the potential repository area in figure 46 87
48. Alternative conceptual model of infiltration numerically modeled assuming all infiltration is

through the channels, and assuming an average of 10 mm/yr, resulting in an average flux of 0.5 mm/yr over the modeling domain 87

TABLES

1. Generalized lithostratigraphy of Yucca Mountain area and ages 34
2. Properties of rock matrix and fractures for all lithostratigraphic units exposed in the study area. 36
3. Surficial soil units recombined from mapped surficial units. 40
4. Summary of soil properties. 41
5. Plant species most commonly found at Yucca Mountain. 45
6. Model parameters and cumulative probability for various minimum amounts of daily precipitation for stations 4JA and Area 12 calculated for months 53
7. Infiltration fluxes estimated by the chloride mass balance method (adapted from Fabryka-Martin and others, 1994) with a comparison of point and areally averaged estimates of net infiltration. 64

CONVERSION FACTORS

Multiply	*By*	*To Obtain*
millimeter (mm)	0.03937	inch (in)
meter (m)	3.28	foot (ft)
watt (w)	0.2388	calorie per second (C/s)
kilopascal (KPa)	0.01	bar
kilometer (km)	0.6214	mile (mi)
square kilometer (km^2)	0.386	square mile (mi^2)
millimeter per year (mm/yr)	0.00328	foot per year (ft/yr)
cubic centimeter (cm^3)	3.531×10^{-5}	cubic foot (ft^3)
cubic centimeter per second (cm^3/s)	3.531×10^{-5}	cubic foot per second (ft^3/s)

Degree Celsius (°C) may be converted to degree Fahrenheit (°F) by using the following equation:

$$°F = 9/5\ °C + 32.$$

CONCEPTUAL AND NUMERICAL MODEL OF INFILTRATION FOR THE YUCCA MOUNTAIN AREA, NEVADA

By Alan L. Flint, Joseph A. Hevesi and Lorraine E. Flint

ABSTRACT

Studies are currently underway to determine the suitability of Yucca Mountain, Nevada, as the United States' first high-level nuclear waste repository. Values of net infiltration are required to determine pre-waste emplacement groundwater travel times and to evaluate the performance of the repository as a waste-containment system. The objectives of this study were to develop a conceptual model of infiltration processes at the site, to implement that conceptual model in a numerical model, and to evaluate the ability of the numerical model to explain available hydrologic data. The conceptual model describes the effect that observed processes of precipitation, runoff, evapotranspiration, and redistribution of water within the shallow unsaturated zone have on predicted rates of net infiltration and concludes that the timing of precipitation and soil depth are the two most significant variables to describe. The conceptual model was developed to explain available infiltration data and was tested using a numerical model based on energy- and water-balance calculations. Test results indicated a satisfactory preliminary calibration of a more detailed numerical model of infiltration and also a simplified version that is more efficient in modeling the over 250,000 30-m grid cells in the study area. Stochastic simulations of precipitation provide insight into the temporal and spatial distribution of net infiltration throughout the area of Yucca Mountain under current-climatic conditions and wetter conditions. Spatially, and for an average precipitation year (approximately 170 mm), net infiltration ranges from zero, for a soil thickness of 6 meters or more, to over 80 mm/yr for a thin soil on north-facing slopes and at high elevations that overlies highly-permeable bedrock. Infiltration averages 4.5 mm/yr. On a year-to-year basis, net infiltration ranges, on a site average,

from zero, in dry years, to over 20 mm/yr when average precipitation exceeds 300 mm. The neutron-borehole locations were modeled using the precipitation for the current climate model (approximately 169 millimeters per year) and produce an average net infiltration of 5.5 mm/yr. The simulated future climate (approximately 330 mm/yr) produced an average net infiltration of almost 30 mm/yr.

INTRODUCTION

Background

High-level radioactive waste is accumulating in the United States. In 1983 there were about 4,600 m^3 (160,000 ft^3) of spent fuel from commercial nuclear power plants in the United States. It is estimated that this volume will increase to over 19,000 m^3 (670,000 ft^3) by the year 2000 and to over 33,000 m^3 (1,200,000 ft^3) by the year 2010 (Weber and Wiltshire, 1985). In 1982, Congress passed the Nuclear Waste Policy Act, authorizing the Department of Energy (DOE) to investigate several sites for possible use as deep geologic repositories. In addition, the DOE was to oversee the design, construction, and operation of two repositories. Out of nine sites initially selected for consideration, three were nominated by the DOE for further site characterization. These included a site in Deaf Smith County on the Texas panhandle, the Hanford site in Washington, and Yucca Mountain in Nevada. While all sites were considered arid or semi-arid, Yucca Mountain was the only site located in one of the desert regions of the United States (fig. 1).

(Figure 1. Location of a) North American Deserts and the original 3 sites for characterization, and b) physiographic provinces.)

In 1987, as part of amendments to the Nuclear Waste Policy Act, site characterization was limited to Yucca Mountain for which a comprehensive plan of characterization was planned. (U.S. Department of Energy, 1988). At Yucca Mountain, the potential repository host rock is in

the Topopah Spring Tuff of the Paintbrush Group, a densely welded and fractured volcanic tuff. The water table is an average of 510 m (1,700 ft) below the land surface beneath the crest of Yucca Mountain. The potential location of the repository is in the unsaturated zone at an average of 300 m (1,000 ft) beneath the land surface. Initially, the repository was to be located in the saturated zone. However, due to potential difficulties arising from retrieval of radioactive wastes and the desire to limit radionuclide contact with regional groundwater, among other issues, the potential repository horizon was moved to the unsaturated zone (Roseboom, 1983).

Thick unsaturated zones beneath interfluvial areas, as proposed by Winograd (1981) for the disposal of radioactive waste, would have extremely small, if measurable, net infiltration due to high storage capacity and evapotranspiration. Roseboom (1983) noted that 30-60 feet of soil overlaying rock would produce similar low net infiltration rates. The absence of these thick zones, as is the case at Yucca Mountain, may be replaced by an interbedded layer of high porosity, nonwelded tuff acting as a natural capillary barrier (Roseboom, 1983). This presupposes that the thin soils at Yucca Mountain will not behave as Winograd (1981) originally suggested, due to the low storage capacity and the presence of underlying fractured tuff. The higher storage capacity of the interbedded nonwelded tuff certainly equals that of the soil but there is no evapotranspiration at that depth to remove the stored water. This would allow for a delay in percolation of net infiltration, just as in thick soils. However, without the near surface processes of evapotranspiration, the net infiltration could not be eliminated. (Throughout the text the word soil is used synonymously with unconsolidated materials, which include alluvial, colluvial and eolian deposits.)

As part of the licensing process, the DOE must project the performance of the repository for 10,000 years considering the full range of environmental conditions that may affect the repository during that time (Justus and Stablein, 1989). To attain safe storage, the design relies on the site's natural features and processes to isolate the waste. Assuming a release of the radioactive material from the waste canisters occurs, one possible mechanism for radionuclide transport is advection by the unsaturated flow of water. To evaluate and quantify the significance

of radionuclide transport through the tuff, knowledge of the boundary conditions in the unsaturated zone is required. The lower boundary condition is controlled by the elevation of the regional water table. The upper boundary condition is controlled by the net infiltration of water at the soil surface. As part of the site characterization process, the U.S. Geological Survey (USGS) is collecting hydrologic data from this area to characterize the present-day infiltration processes and the net-infiltration rates through the surficial materials at Yucca Mountain. Net infiltration is defined as the moisture flux below the zone influenced by surface processes and is the result of infiltration of natural precipitation. Net infiltration is the ultimate source for the movement of groundwater (percolation) through the thick unsaturated zone at Yucca Mountain. This groundwater percolation is a possible vehicle for transport of radionuclides released from stored waste in a repository to the accessible environment. The net infiltration rates and the spatial and temporal distribution of net infiltration are important characteristics of this site which help define a boundary condition for numerical modeling of flow and transport at Yucca Mountain, which is necessary to extrapolate site responses under changing climate and site conditions over long time periods.

Purpose and Objectives

Infiltration is one of the most dynamic water-moving processes at Yucca Mountain. For the most part, other major water-moving processes in the subsurface are relatively inactive. Net infiltration is the upper boundary condition for flux in the unsaturated zone. Whipple (1996), in an analysis of the safety of Yucca Mountain as a nuclear waste repository, states that the infiltration rate and its related movement is the single most important factor in determining how long the buried canisters might survive. This conclusion was also reached by Gauthier and Wilson (1994) and both they and Whipple (1996)explicitly state that it is necessary to consider climate change and the resultant change on net infiltration and percolation to evaluate the safety or suitability of Yucca Mountain.

The purpose and objective of the report is then to present the current state of knowledge

on the temporal and spatial distribution of net infiltration under the current climate (<50 yrs), and associated uncertainties, and to present the possible future temporal and spatial distributions of net infiltration under simulated future climatic conditions using numerical models, and to evaluate the ability of the numerical model to explain available hydrologic data. The conceptual model describes the effect that observed processes of precipitation, overland flow, evapotranspiration, and redistribution of water within the shallow unsaturated zone have on predicted rates of net infiltration. As part of this presentation, a detailed description of the conceptual model of infiltration, which includes the relative importance of the different mechanisms of infiltration and the role of atmospheric and biotic conditions, and soil and rock properties on the control of net infiltration at Yucca Mountain, will be presented. The developed conceptual model is the foundation for the numerical model where the important mechanism and properties are correctly incorporated.

The study area (fig. 2) is located within the Death Valley Ground-Water Unit boundary (which is the USGS saturated zone flow model boundary). The infiltration study area was chosen to match the expanded USGS/Lawrence Berkeley National Lab (LBNL) 3-dimensional unsaturated-zone flow model (Wu and others, 1996) so that output from the numerical model of infiltration could directly feed the unsaturated zone flow model.

(Figure 2. Yucca Mountain regional study area with Death Valley Ground-Water Unit and infiltration study boundary.)

Previous Work

There are several ways recharge is estimated in arid environments. These include estimating discharge, water balance and soil physics techniques, geochemistry and transfer equations based on other variables (i.e. precipitation). Direct measurements of net infiltration at Yucca Mountain can not be done due to the low moisture flux resulting from the low precipitation and high potential evapotranspiration rates characteristic of this site. Several

estimates of net infiltration have been suggested for Yucca Mountain and vicinity. Winograd and Thordarson (1975) used measurements of discharge from springs at Ash Meadows (south of Yucca Mountain near the Nevada-California border) to estimate net infiltration for the lower carbonate aquifer. They estimated that about three percent of the precipitation falling on carbonate-rock uplands within the boundaries of the Ash Meadows basin becomes net infiltration. Watson and others (1976) investigated the Maxey-Eakin method (Maxey and Eakin, 1949) of estimating net infiltration to groundwater basins in Nevada. With the Maxey-Eakin method, average annual precipitation (AAP) is used to classify areas of a basin into five infiltration zones, each with a different percent of precipitation becoming net infiltration (<200, 200-300, 300-380, 380-500 and >500 mm/yr, yielded 0, 3, 7, 15, and 25 percent of AAP as net infiltration). Hevesi and Flint (1996), using a modified technique, with improved estimates of AAP, estimated the net infiltration in the Yucca Mountain area to be 0.2 to 1.4 mm/yr increasing to more than 10 mm/yr in the mesas to the north. Czarnecki (1984), in a study of the effects of possible increases in net infiltration on the groundwater flow system at Yucca Mountain and vicinity, used estimates of net infiltration based on the Maxey-Eakin method. Czarnecki separated the area into three zones based on values of AAP. Estimated rates of net infiltration ranged between 0 and 2.0 mm/yr. Rush (1970) also used this method to estimate net infiltration for the western two-thirds of Jackass Flats (about 6.5 km east of Yucca Mountain) and obtained results of about 1.5 mm/yr. Lichty and McKinley (1995) provide an analysis of recharge for two analog basins in central Nevada using two independent modeling approaches, one a water balance approach, the other using water and chloride mass balance. Using two precipitation rates, the results yielded 10-30 mm/yr using 270 mm/yr precipitation, and 300-320 mm/yr using 640 mm/yr precipitation, which is consistent with the modified Maxey-Eakin results used by Hevesi and Flint (1996, see Figure 7), for areas of similar precipitation (yielding 25 and 260 mm/yr respectively).

Scott and others (1983) developed a conceptual hydrologic model of Yucca Mountain. They estimated net infiltration to be 6 mm/yr; 3 percent of an AAP value of 200 mm/yr . Montazer and Wilson (1984) developed a conceptual hydrologic model similar to Scott and

others (1983). In their model, they also assumed 3 percent of the precipitation as net infiltration but used different values for AAP. They suggested 4.5 mm/yr as a upper estimate on net infiltration at Yucca Mountain.

Net infiltration estimates for basins in Nevada have also been obtained using chloride-balance calculations. Dettinger (1989) applied this method to sixteen basins in Nevada. His estimates compared closely to those obtained using the Maxey-Eakin method and water balance calculations. Dettinger (1989) states that the chloride-balance method is practical, at a reconnaissance level, for estimating average rates of net infiltration for many desert basins of the western United States. The application of chloride-balance methods, however, assume piston flow in porous media and may not be as applicable for fractures rock under shallow soils. As a preliminary estimate Fabryka-Martin and others (1994) used chloride-balance calculation at Yucca Mountain and estimated net infiltration rates of 0 to 5.4 mm/yr. These estimates were made for porous, nonwelded volcanic tuffs but were overlain by fractured welded volcanic tuffs and may be subject to the same errors of discrete fracture flow versus piston flow.

Several researchers have looked specifically at soil fill materials which should behave differently from shallow soils located over fractured bedrock. Assuming steady-state conditions, Winograd (1981) estimated net infiltration through the thick soil valley fill at Sedan Crater, about 48 km (30 miles) northeast of Yucca Mountain, to be about of 2 mm/yr. Nichols (1987) used a numerical model to perform water balance calculations for the unsaturated zone at a burial site for low-level radioactive waste near Beatty, Nevada. His model was used to determine under what conditions net infiltration might have occurred during a 15-year study period. Nichols (1987) estimated a rate of net infiltration of 0.04 mm/yr in the thick soil materials but with potentially lower precipitation rates than Sedan Crater (See the precipitation maps of Hevesi and others, 1991a,b).

The first estimates of the spatial variability of net infiltration at Yucca Mountain were done by Flint and Flint (1994). Their values ranged from 0.02 to 13.40 mm/yr, distributing net

infiltration by location of bedrock units underlying the soil. Calculations were made based on hydraulic-property measurements of the bedrock unit closest to the surface, the water content of each unit at a depth assumed to be in steady-state flow conditions, and an assumed unit gradient. Their net infiltration estimates were for deep, steady-state matrix flow and did not account for shallow, transient flow or fracture flow.

The spatial variability of net infiltration was calculated by Hudson and Flint (1996) based on a statistical correlation between measured changes in water content in boreholes using a neutron moisture meter and average annual precipitation, depth to bedrock, and whether the borehole was in a channel. Once correlated, the spatial distribution of these parameters were used to develop a spatially distributed map of infiltration. Estimates of net infiltration range from 0 to 45 mm/yr. Their analysis was limited by the spatially limited borehole data and did not account for differences in geology (welded, nonwelded, fractured, etc.) under the soil or seasonal variations in precipitation. Their analysis was also limited to the time frame of the measurements (1984-1995) and does not provide insight into the effects of different climatic scenarios because it is strictly a statistical correlation.

PROCESSES, THE PHYSICS OF INFILTRATION

Figure 3 illustrates a generalized view of the terminology and processes involved in the water balance at Yucca Mountain. The term infiltration is used to describe water entering the soil across the air-soil interface and the associated movement away from that interface when water is made readily available at the soil surface. Redistribution is the continued movement of water through the soil profile when no more water is available to infiltrate into the soil surface. Net infiltration is used to describe that water which has moved to a depth that is variable in space and time and below which the water cannot be readily removed by surface (evapotranspiration) processes. A hypothetical net-infiltration boundary is presented in figure 3. Percolation is defined as the downward or lateral flow of water in the unsaturated zone. Recharge is the movement of water from the unsaturated zone into the saturated zone.

(Figure 3. Field scale schematic of infiltration.)

Field Water Balance

Determination of net infiltration rates using water-balance calculations requires very precise and accurate measurements of the components of the water-balance equation (eq. 1). In the absence of such measurements, the water-balance equation can still be applied in analyzing the spatial and temporal distribution of infiltration rates using the following input: 1) a conceptual understanding of the physical processes involved, 2) deterministic or stochastic numerical models for approximating each of the physical processes, 3) an adequate coupling of the physical processes and 4) direct or indirect measurements of as many of the components of the water balance as possible to provide some means of calibrating the numerical model. The dominant physical processes in the general field water balance equation are precipitation, evapotranspiration, overland flow (runoff and run-on), infiltration, and redistribution of the soil moisture. It is also important to consider the variability of these processes in space and time. A calibrated model can correct, to a certain extent, for a lack of detailed measurements, if it can bound the solution to robust field observation. This concept will be further developed in the section on the numerical model.

Water transport and retention processes in surficial materials (soils and bedrock) are affected by high variability in solar radiation fluxes, diurnal and seasonal temperature cycles, relative humidity, and periodic inputs from precipitation (in the form of either rain or snow) followed by extended periods of drought conditions. Despite the complexity, we can describe the process conceptually or even quantitatively if the approximate models are based on sound physical principles. The conceptual or quantitative models can provide valuable insight into the behavior of the real system. A description of the field water balance provides a starting point for following discussions of the conceptual and numerical infiltration models. The water balance is based on the principle of the conservation of mass for water:

$$P + A + U + \Delta W_s + \Delta S_s + \Delta B_s + L_i + R_{on} - R_{off} - D - E - T - L_o - E_x = 0 \quad (1)$$

where P is precipitation, A is applied water (man induced), U is upward flow, ΔW_s is change in soil water storage, ΔS_s is change is surface storage, ΔB_s is change in above ground biomass storage, L_i is lateral flow in, R_{on} is surface run-on, R_{off} is surface runoff, D is deep drainage or percolation, E is evaporation, T is transpiration, L_o is lateral flow out and E_x is extraction of water (man induced). Equation 1 states that the sum of all inputs, outputs and changes in storage in the hydrologic system must equal zero. To be applied, equation 1 must be defined over some arbitrary time interval (i.e day, year) and over some arbitrary volume or depth in the soil (fig. 4).

(Figure 4. Diagrammatic water balance components using notation described in equation 1.)

In most cases, the general form of the water-balance equation can be greatly simplified by assuming one or more of the terms to be zero or negligible in magnitude. For example, the terms B_s, R_{on} and R_{off} can often be set to zero in cases involving arid and semi-arid sites where overland flow occurs only in direct response to relatively infrequent, larger magnitude precipitation events. In the case of one-dimensional flow with zero or negligible run-on and runoff under current climatic conditions, negligible upward flow, man-induced fluxes and surface storage, the water-balance equation becomes:

$$P + \Delta W_s - D - E - T = 0 \quad (2)$$

Although greatly simplified, this equation usually provides a more practical starting point for analyzing net infiltration (D). For some applications, equation 2 is further simplified by setting P to zero (for periods having no precipitation), assuming D to be negligible compared to the other terms, and combining E and T into a single term of evapotranspiration (ET). In this form, the water balance can provide a method of using measurements of ΔW_s to estimate ET (Nichols and Cuenca, 1993). In essence we are saying that equation 1, in spite of the difficulty of

quantifying each of the terms, provides the conceptual framework for the analyses that follow. Lesser know variables are approximated with bounding values, while other terms are dropped based on understanding of the site-specific relative importance of different terms.

As the individual terms comprising the water balance are quantified under conditions for which the simplifying assumptions are applicable, equation 2 can be expanded to provide a more general application. For example, the B_s, R_{on} and R_{off} terms should be included in the mass balance during periods of precipitation resulting in significant overland flow. As another example, precipitation occurring as snow can be handled as a surface storage term. In some cases, man induced fluxes (A and E_x) may be significant as point applications. Large volumes of water may be applied on an annual basis on roads and drill pads for dust control. Settling ponds and septic systems may provide deeper penetration into soils. Surface applications of water from pump tests may be applied to channels or sprayed over large areas to reduce concentrated flow. Water may be pumped from shallow water tables or perched-water zones.

Although the application or extraction of water may be significant for short periods of time or where it is concentrated in small areas, overall they should have little effect on the time and spatial scales of a nuclear waste repository. For the following analysis, man-induced fluxes will be assumed to be zero and only the natural system will be considered. At any time during site characterization these man-induced fluxes can be reconsidered as necessary.

Precipitation

Precipitation is usually considered as the starting point in the hydrologic cycle. In arid and semi-arid environments where man-induced inputs such as irrigation can be neglected, precipitation is the primary input to the water balance because inputs from surface water bodies such as lakes, rivers, or ephemeral streams tend to be negligible in comparison. The primary physical process causing precipitation is the cooling of air masses to the dew point, resulting in cloud formation and precipitation. There are several different processes that can cause air masses

to cool to the dew point; cyclonic (or frontal), convective, and orographic. Cyclonic-type processes tend to cause lower intensity, longer duration precipitation over larger areas and often produce precipitation in the form of snow, especially for the higher (> 2,000 m) elevations. In contrast to cyclonic-type processes, convective-type processes tend to cause higher intensity, shorter duration precipitation over localized areas, usually produce lightning, and often produce hail. Orographic processes usually act as a precipitation-enhancing mechanism for both cyclonic- and convective-type processes, and tend to cause an increase in the frequency and amount of precipitation with an increase in elevation.

In the southwestern United States (southern Great Basin and Mojave Deserts), cyclonic-type processes are the dominant cause of precipitation during the winter, whereas convective-type processes are the dominant cause of precipitation during the summer for most locations. During the spring and fall, also referred to as the winter-to-summer and the summer-to-winter transition periods (Houghton, 1969; Pyke, 1972), cyclonic-type processes are dominant for most locations in the Great Basin and Mojave Deserts. The prevalence of convective-type processes tends to be greater during the spring and fall (transition periods) relative to the winter, and reaches a maximum during the summer months of July, August, and September.

Synoptic-scale weather systems causing precipitation during the winter are generally controlled by the position of the jet stream. Winter storms originate in the eastern Pacific from the gulf of Alaska to southern California. The polar and subtropical jet streams or storm tracks steer developing storm systems eastward and inland. During the fall and spring the average position of the jet stream tends to steer storm systems eastward and southeastward from Washington, Oregon, and northern California into the northern and central Great Basin, resulting in a higher average precipitation frequency for this area as compared to the Mojave Desert. In the spring, the west-to-east storm track migrates northward as cold air retreats and warm air invades from the south. In the southern Great Basin and Mojave Deserts, precipitation occurring during the winter is largely dependent on whether the jet stream can establish a steering pattern which moves storm systems eastward from southern California and southeastward from northern

and central California. Such positioning of the jet stream may in turn depend strongly on global circulation patterns such as the *El Niño* Southern Oscillation (ESNO), the mechanics of which are not yet fully understood. On average, precipitation occurring during the winter represents the greater part of total annual precipitation in the Mojave Desert (Hevesi and Flint, 1996).

In contrast to the dominant winter weather systems, synoptic-scale weather systems causing precipitation during the summer are controlled primarily by the Southwestern Summer Monsoon (Houghton, 1969; Pyke, 1972). The Southwest Monsoon is an atmospheric circulation pattern caused by the existence of a strong, stationary high-pressure cell in the southwestern United States that develops primarily during the months of July and August. The high-pressure center, which is usually located in southern Utah, may be accompanied by an upper-level low-pressure area centered over extreme southern California. The air circulation draws moisture from the Gulf of Mexico westward and northward into New Mexico, Arizona, and parts of Nevada. Depending on the positions of the high and low pressure cells, the monsoonal flow may also draw moisture northward and northeastward from the Gulf of California and the Pacific Ocean off Baja California into the Mojave and Great Basin Deserts. These moist air masses tend to become unstable from surface heating as they move into the southwestern Deserts, and localized convective cells can develop (either as scattered, isolated cells or as more organized bands or clusters). Summer convective-type storms may develop in the presence of an irregular cloud cover associated with large-scale air masses, or they may develop within band-type cloud patterns. Storm clouds are made up of a number of individual thunder clouds, each of which contains several convective cells which actually produce the rain. The life-cycle of individual cells consists of a developing stage, a mature stage, and a dissipating stage. The total duration of the life-cycle for an individual cell is usually limited to tens of minutes. However, the down draft associated with dissipation tends to form new cells, and this process of cell regeneration often produces convective storm precipitation durations on the order of one or two hours.

Geomorphology pays a significant role in controlling the occurrence of convective rainfall. Differential heating effects induced by slopes or rock outcrops and convergence of

winds induced by local topography provide initial lift to buoyant air. These lifting mechanisms result in the formation of convective clouds which rapidly build to heights that are sufficiently cool for the formation of raindrops. The spatial distribution of rainfall produced by convective storms is determined primarily by the characteristics of cell clusters and their movement relative to the local terrain. These typically result in a central core area of 1 to 5 km in diameter receiving relatively uniform amounts of rainfall surrounded by more or less elliptical isohyets grading off to zero rainfall at distances of less than 10 km from the storm center. The amount of rain falling in the central core is partly dependent on the movement of cell clusters during the storm. Precipitation depths for individual storms are usually of the order of a few tens of millimeters, while maximum values appear to be around 70-80 mm to, very exceptionally, 100 mm for arid zones (Jones, 1981). There is an asymmetric average storm intensity profile for storms of short duration, with the highest intensities falling in the first part of the storm.

In arid lands with low ground level elevations and little topographic relief, it is not uncommon to see rain descending from the base of clouds failing to reach the ground. This phenomenon, known as virga, is due to the depletion by evaporation of the falling rain. Because of direct evaporation from rain prior to reaching the ground, caution is required when using stable isotope ratios in studies of the evaporation history of terrestrial water in arid lands. Rainfall often has lighter isotopic compositions with increasing elevation, whereas there is a tendency for small rains at lower altitudes to be relatively rich in heavy isotopes due to evaporation from falling rain (Benson and Klieforth, 1989).

The various processes governing the occurrence and intensity of precipitation reaching the ground surface are not mutually exclusive and often occur in some combination. Although the processes are fairly well understood, the use of deterministic models to define precipitation as a component of the water balance can be problematic because of the large number of variables involved, particularly in the modeling of air flow. Fortunately, precipitation is a comparatively simple component of the water balance to measure, and precipitation records of 30 years and longer are available for locations in the vicinity of the potential repository site and for locations

in the Great Basin and Mojave Deserts. These records can be used for establishing a statistical characterization of precipitation. Probability distribution functions for precipitation intensity and frequency can be quantified and used to develop stochastic models of precipitation. Correlations with other parameters, such as elevation or geographic location, can be analyzed and defined using statistical and geostatistical models.

Run-on / Runoff

Horton (1933) observed that when rainfall reaches the ground surface, the water infiltrates the surface soils at a rate that decreases with time. He concluded that for any given soil there is a limiting curve that defines the maximum possible rates of infiltration versus time, which he called the curve of infiltration capacity. The curve of infiltration capacity for a given soil type indicates that if at any time during a rainfall event the rate of rainfall exceeds the infiltration capacity, excess water will pond on the surface and may contribute to overland flow or runoff. In arid and semi-arid environments, baseflow (groundwater discharge or seepage from sub-surface flow, such as through-flow) contributions to streamflow (channel-flow) often does not occur (hence, the prevalence of intermittent streams and dry riverbeds), and streamflow only occurs in response to overland flow caused by precipitation. If overland flow occurs, the path by which the water reaches a channel and the rate and magnitude of streamflow generation depends upon such controls as topography, geology, soils and vegetation. The St. Venant equations, which are derived using the conservation of mass and momentum, can be used as a deterministic numerical approximation to gradually varied, unsteady overland flow if surface geometries and surface roughness coefficients are known, and if the spatial and temporal distribution of precipitation intensities over the catchment being modeled are known. The kinematic-wave approximation of the St. Venant equations allows for simplifying assumptions in the modeling of inertial forces, and is often applied to modeling urban runoff and streamflow in smaller drainages where backwater effects and flood-wave propagation are not important. The kinematic-wave approximation also requires assumptions concerning the predominance of laminar or turbulent flow. Hydrograph simulations using the kinematic-wave approximation have indicated that for

small arid-land catchments, laminar flow theory is adequate for modeling overland flow (Woolhiser and others, 1990).

Because of the heterogeneity of the soil surface and the irregular patterns of precipitation in space and time a partial-area-contribution concept was developed (described in Freeze and Cherry, 1979). The concept recognizes that certain portions of the watershed regularly contribute overland flow to channels, whereas others seldom or never do. Most overland-flow hydrographs originate from small portions of the watershed that constitute no more than 10%, and often as little as 1-3%, of the basin area, and even on these restricted areas only 10-30% of the total rainfall can cause overland flow (Freeze and Cherry, 1979).

During the process of runoff, areas within the basin may receive run-on. A large area of exposed bedrock with a low infiltration capacity may cause rapid runoff, but the down-gradient soil receives this runoff as run-on. In many cases the precipitation on the soil surface and the run-on combined still do not exceed the infiltration capacity of the soil and the runoff is contained before reaching the channel. In those instances when runoff reaches the channel, the early part of the runoff event infiltrates into the channel materials (at rates up to their infiltration capacity, which is generally high in sand and gravels) as the water moves down gradient. In many cases no overland flow escapes the basin because most of the water can be taken up in the deeper channel soil.

Infiltration

To understand the development of specific infiltration equations the development of the transient, unsaturated flow equation must first be understood. As in the case of surface water flow, the conservation of mass and momentum (energy) again provide the framework for the governing flow equations.

The basic steady-state, 1-dimensional equation (Darcy's law) for liquid water flow is:

$$J_w = \frac{Q_w}{At} = -K\left(\frac{\Delta\psi_h}{\Delta z}\right) \quad (3)$$

where J_w is water flux density, Q_w is quantity of water, A is area, t is time, K is the saturated hydraulic conductivity and $\Delta\psi_h$ hydraulic (total water) potential between two points separated by a distance Δz measured along the direction of flow.

Darcy's law was modified for unsaturated steady-state flow by making K dependent on the unsaturated water content as $K(\theta)$ resulting in the Buckingham-Darcy flux law (Jury and others, 1991):

$$J_w = -K(\theta)\left(\frac{\Delta\psi_h}{\Delta z}\right) \quad (4)$$

Under transient flow conditions water is stored or removed from storage over time. This change in storage will lead to a change in water flux density and is described in equation 4:

$$\frac{\partial\theta_v}{\partial t} = \frac{\partial J_w}{\partial z} \quad (5)$$

where θ_v is volumetric water content. At a specific location, for a given volume, the water content of the soil will increase if the water flux density coming into that volume is greater than the water flux density going out. If the reverse is true, then soil water content is decreasing (draining) at that location. To understand changing infiltration rates the general flow equation (eq. 4) for J_w is substituted into the equation of continuity (eq. 5) to obtain:

$$\frac{\partial\theta_v}{\partial t} = \frac{\partial}{\partial z}\left(K(\theta)\frac{\partial\psi_h}{\partial z}\right) \quad (6)$$

which is referred to as the Richards equation in the case of 1-dimensional unsaturated ground-water flow. $K(\theta)$ is hydraulic conductivity as a function of water content which allows for unsaturated flow. Liquid-water flow occurs in response to a hydraulic potential gradient and not in response to a water content gradient. For vertical flow into soils, the hydraulic gradient is a combination of gravitational and matric potentials. For vertical water flow in soils, equation 6 becomes:

$$\frac{\partial \theta_v}{\partial t} = \frac{\partial}{\partial z}\left(K(\theta)\frac{\partial(\psi_m + \psi_z)}{\partial z}\right) \tag{7}$$

where ψ_m is matrix potential and ψ_z is gravitational potential. Equation 7 is limited to isothermal, one-dimensional cases of transient state flow. Once boundary and initial conditions have been established, these equations can be solved numerically. An approximate solution for vertical infiltration into a homogeneous soil with water ponded on the surface was developed by Philip (1957):

$$I = S_p t^{1/2} + A_p t \tag{8}$$

in which I is cumulative infiltration, S_p is sorptivity and A_p is a soil parameter. An equation for vertical infiltration rate is obtained by differentiating equation 8 and setting the derivative $\partial I/\partial t$ equal to I which gives:

$$i = \frac{1}{2} S_p t^{-1/2} + A_p \tag{9}$$

where i is infiltration rate, or infiltration capacity. Although infiltration rate may be initially high, the infiltration rate is reduced as a function of the square root of time, as can be seen in equation 9. This reduction is the infiltration capacity as a function of time which was noted by Horton (1933). It is the relation between the rate of precipitation and the initial, declining and

final infiltration rate that determines when and if runoff will occur. Although infiltration capacity is an empirical concept it was theoretically predicted by Rubin and Steinhards (1963 and 1964) and Rubin and others (1964). The final constant infiltration rate described by Horton (1933), is numerically equivalent to the saturated hydraulic conductivity of the soils and is about 30 percent to 60 percent of the coefficient A_p in Philip's (1957) approximate equation (eq. 9).

For Philip's equation to apply, the top boundary must be maintained at saturation. In most situations, such as natural precipitation, this top boundary condition is not met. If the precipitation rate is less than the saturated conductivity, the soil may never be saturated at the surface, no ponding will occur, and the infiltration rate will be equal to the precipitation rate. Even if the actual precipitation rate is greater than the saturated hydraulic conductivity there will be some time between the beginning of precipitation and the time the surface saturates and ponding begins. The time before which ponded conditions develop is not only dependent on the precipitation rate and the soil physical properties but also on the initial soil-water content. Soils that are initially wetter will have a lower initial infiltration capacity and will reach saturation and runoff sooner. Even if the precipitation rate exceeds the final infiltration rate, runoff may not occur if the precipitation duration is short-lived. In rainfall-infiltration-runoff relations the precipitation intensity, duration, and the history of the change in soil-water content are quite important in determining if and when runoff will occur.

Evapotranspiration

Evapotranspiration is the combined process of evaporation and plant transpiration. The difference in evapotranspiration between temperate and arid regions arise largely from differences in precipitation. To quantify this, precipitation must be compared with the water equivalent of energy available for evaporation and sensible heat flux. On an annual basis, in temperate climates the precipitation exceeds the energy available for evapotranspiration, whereas in arid regions, generally precipitation is smaller (approximately 170 mm of water per year in the Yucca Mountain area) than the available energy for evapotranspiration (876 mm of water per

year could be evaporated from the Yucca Mountain area).

Vegetation adapts to its environment and, consequently, temperate crops usually cover the ground completely, whereas arid crops do not. This has great impact on the description of evaporation. For example, the bare-soil evaporation is generally negligibly small in the temperate regions, but can be dominant in arid zones. Because of the temporal and spatial distributions of precipitation over short time intervals, however, precipitation can easily exceed the water equivalent of the available energy and it is possible that a part of the precipitation will reach the deeper soil layers. It is the timing and amount of precipitation, not the amount alone, that controls deep infiltration in arid lands.

The general theory of evapotranspiration suggests that the availability of moisture, the availability of energy for evapotranspiration and transport of water vapor away from the evaporating surface are the most important aspects of evapotranspiration. There are a variety of ways that areal evapotranspiration can be calculated. These include turbulence methods, profile methods, such as using the atmospheric boundary layer, energy-budget methods and water-balance methods (Brutsaert, 1982). The following discussion is directed toward a combination of turbulence and energy-budget methods. In applying the energy-budget method the first component, the energy available for evaporation, is simply stated as:

$$R_n - G = \lambda E + H \qquad \textbf{(10)}$$

where the left side is available energy, the right side is the turbulent flux, R_n is net radiation, G is soil-heat flux, H is sensible heat flux, λE is the latent heat flux, λ is the latent heat of vaporization, and E the rate of evaporation. Net radiation is the balance of incoming short wave, K↓, ground-reflected short wave, K↑, incoming long wave, L↓, and outgoing long wave, L↑. The rate of evaporation can be solved by knowing the other parameters and using simple algebra. In general when net radiation and soil heat flux are known or estimated, the remaining energy is partitioned into latent and sensible heat flux, the proportion depending on the water availability.

A conceptual model of the energy balance components is presented in figure 5.

(Figure 5. Conceptual model of the energy balance equation for evapotranspiration.)

Even with adequate water availability, evapotranspiration is limited due to the ability of the atmosphere to take up water. Atmospheric turbulence can mix the moist air near the surface with drier air above and maintain an evaporation gradient. Without mixing, the atmosphere near the evaporation surface would soon become saturated and the gradient for evaporation would diminish and evaporation would become diffusion limited. Turbulence methods are used to calculate the mixing of the moist air near the evaporating surface with the drier air above, and therefore calculate one component of evapotranspiration.

A combination model, such as the Penman-Monteith equation (Monteith, 1965) for actual evaporation, combines the energy balance and aerodynamic equations for evaporation in the form:

$$\lambda E = \frac{S}{S+\gamma}(R_n - G) + \frac{\rho C_p}{r_a}(D_z - D_0) \qquad (11)$$

where S is the slope of the saturation vapor pressure-temperature curve, γ is the psychrometric constant, ρ is air density, C_p, the specific heat of air at constant pressure, r_a, the aerodynamic resistance to the diffusion of water, D, wet-bulb depression, and the subscripts 0 and z denote the surface and a height above the surface, respectively. Implicit in this model is the assumption that the sources of sensible and latent heat are at the same height and temperature, there is adequate fetch and the canopy can act as a single big leaf. This assumption may work for a full canopy or a bare soil surface, but not a sparse canopy which is typical of the Yucca Mountain area. As a result the Penman-Monteith equation cannot be applied. Using an energy combination theory, Shuttleworth and Wallace (1985) developed an equation for use in sparse canopies that has been successfully applied by several researchers (LaFleur and Rouse, 1990; Stannard, 1993). The

application of this equation for the Yucca Mountain site is not practical for long term estimates of ET because of the lack of available data. Long-term measurements of water content from neutron holes along with meteorological measurements are available, however. This suggests the use of an equation such as that developed by Priestley and Taylor (1972)

$$\lambda E = \alpha \frac{S}{S+\gamma} (R_n - G) \qquad (12)$$

where α, an empirical coefficient, was determined to be 1.26 for freely evaporating surfaces (Priestley and Taylor, 1972; Stewart and Rouse, 1977; and Eichinger and others, 1996). Close examination of equations 11 and 12 show that the aerodynamic term in equation 11 is modeled as $(\alpha-1)[S/(S+\lambda)](R_n-G)$, which has been successfully used because the radiation term generally dominates the aerodynamic term (Stewart, 1983). The Priestley-Taylor equation has been modified by several researchers to relate their empirical coefficient, α, to seasonal changes in soil water content (Davies and Allen, 1973; Flint and Childs, 1991), and has been described as successfully used in arid and semi-arid environments (de Bruin, 1988; Stannard, 1993). This equation has the added benefit of minimal data requirements. For soil-water-limited conditions the relation between α and soil water content is empirical but works well for many surface conditions (Davies and Allen, 1973; Flint and Childs, 1991). For a semi-arid site, Stannard (1993) found α to be independent of soil moisture and depended only on leaf-area index and cumulative evaporation following precipitation. The cumulative evaporation is, however, directly correlated to a reduction in soil-water content and will account for either drainage or evaporation. Therefore, leaf-area index and a term to account for increases and decreases in soil-water content (precipitation and evaporation) would produce an equivalent equation to that of Stannard (1993) and allow the additional information of soil-water holding capacity, and depth to restricting layer (bedrock or cemented soil horizons), which varies significantly over the site to be incorporated into the model.

Redistribution

Redistribution refers to the continued movement of water through a soil profile after infiltration has ceased at the soil surface. This is a complex process, because the lower part of the profile ahead of the wetting front will increase in water content and the upper part of the profile near the surface will decrease in water content. As the distance from the surface to the downward moving wetting front increases, the average water content behind the wetting front decreases. The total water content in the profile (mass balance) stays the same, minus evapotranspiration, since the length of the wetting front increases as the average water content behind the wetting front decreases. The soil drains to its field capacity, which has been defined as the water content of the near-surface soil profile at which drainage becomes negligible. True field capacity cannot exist because water will drain continually under gravity as long as no impermeable barrier is present in the soil, until it comes into equilibrium with a water table, or until the gravitation potential is balanced by capillary forces. Water retention (field capacity) in a profile depends on the water transmission properties of the entire profile and on the hydraulic head gradient rather than only on the energy state of water at a particular point in the profile. An important consideration is that the longer the water can be held within the root zone, the more potential there is for removal by evapotranspiration, and the less potential for deep drainage.

Redistribution can be modeled using a finite-difference approximation of equation 7 and appropriate model geometry and boundary conditions for representing precipitation and evapotranspiration (Campbell, 1985). The nonlinearity of the partial-differential equation is represented by the moisture characteristic curve, which defines relative permeability and water potential as continuous functions of relative saturation. The parameters defining the curves must be measured or estimated for the soil or rock being modeled. Differences in soil or rock materials can be represented by selecting an appropriate combination of model parameters and model geometry. In most cases, a 1-dimensional model is adequate for representing vertical distribution. However, 3-dimensional redistribution of moisture beneath channels may not be accurately represented in some cases by a 1-dimensional redistribution model.

Flow at the soil-bedrock interface

One of the most significant processes in infiltration under shallow soils is that the soil-water content at the soil-bedrock interface tends to approach or reach saturation under heavy or long-term precipitation because the hydraulic conductivity of the bedrock matrix is, in most cases, several orders of magnitude less than that of the soil. The saturated or near-saturated conditions allows water to move into large, unfilled fractures and percolate below the root zone (which may exist within the top one or two meters of the fractured bedrock). Filled fractures will not allow water to flow as rapidly (because of their reduced hydraulic conductivity) but may take on water from the overlying soil as it wets up sooner than unfilled fractures because of the smaller pores in the fracture filling. For example as the soil at the tuff-soil contact dried in early 1992 in borehole USW UZ-N52 (figure 6a, b) a hypothetical 2.5 um unfilled fracture would drain (no longer conducting water, fig 6b) once the soil reached -0.15 MPa (which is the air-entry value or water potential at which the fracture starts to drain). The 2.5 um filled fracture would continue to conduct water for several more weeks at its highest rate (which is still lower than an unfilled fracture, fig 6b) until the soil reached -0.4 MPa and it begins to drain. The same process would occur in reverse as the soil wet up again in 1993, a 2.5 um unfilled fracture would start conducting water at its highest rate only when the soil wets up to -0.15 MPa whereas the filled fracture would be conducting water at its highest when soil is -0.4 MPa or wetter. In deep soils water may reach field capacity in the near surface but the water supply may not be enough to move the wetting front below the root zone, which may be several meters deep. For this reason, under water-limited conditions it is more likely that deep penetration of water will occur under shallow soils in fractured bedrock than in deep soils with large storage capacity and deep root zones. An exception to this occurs in soil channels where water is concentrated during episodic runoff events and wetting fronts can penetrate to depths of 10 meters or more. Under these conditions water infiltrates at its maximum infiltration capacity, described by equation 9, and downward percolation may be rapid enough to allow the infiltrated water to penetrate below the root zone. Once water penetrates to a depth below the zone of evapotranspiration, the redistribution of this water, however slow, will probably result in net infiltration across the

soil/bedrock interface. (Upward vapor flow, lateral flow, and exfiltration due to the existence of an upward potential gradient may also occur, but these processes would likely be secondary to downward percolation due to a unit or near-unit gradient, or the continued advance of the wetting front). Infiltration into bedrock under deep soils (> 10 meters) will likely occur only through filled fractures and/or through the bedrock matrix, because saturated or near-saturated conditions are less likely to develop (the frequency at which these conditions develop becomes extremely low but still possible), and thus the water potentials seldom become high enough to initiate flow in open fractures.

(Figure 6. a)Water content and water potential at the soil-bedrock interface at a depth of 2.1 m in borehole USW UZ-N52. The horizontal lines are the air-entry water potentials for a 2.5 um open fracture and a filled fracture, and b) associated flux calculated as the hydraulic conductivity of the fracture times a unit gradient)

Under arid conditions paleosols often have developed within several meters of the surface (or cemented horizons of carbonate). These conditions may cause lateral redistribution and still maintain the increased saturation within the root zone. Because of this stratification and vertical heterogeneity in soil material, the occurrence of channel flow does not guarantee deep percolation throughout the length of the channel.

Net infiltration

For this report, net infiltration is defined as the drainage term (D) in the water-balance equation (eq. 2). Net infiltration is the water which penetrates below a depth from which it cannot be readily removed by evapotranspiration processes. Where shallow soil overlies fractured bedrock, that depth may be 2 meters, however, under deep soil fill that depth may be 3 to 4 meters. Net infiltration is actually a time-averaged downward flux which occurs in response to the time-averaged potential gradient below the hypothetical zero-flux plane. The zero-flux plane represents the depth above which the potential for flux generally upward but may have

reversals due to transient infiltration events and response to evapotranspiration. Below the zero-flux plane the gradient is always downward. Water that gets below this zone is what we have defined as net infiltration. The depth of the zero-flux plane fluctuates in response to daily, seasonal, and annual variability in meteorological conditions, and is also dependent on the site-specific characteristics of a given location, such a plant rooting depth. Values of net infiltration at depths above the zero-flux plane are inherently dependent on the time period being considered, and may not be representative of deeper percolation rates (especially in the case of transient conditions). Deeper percolation fluxes, although more representative of long-term, time-averaged conditions, may not be representative of the response of the hydrologic system to current climatic conditions but are a residual of past climatic conditions. An understanding of the response of the hydrologic system to current climatic conditions is a prerequisite for predicting the response of the system to potential future climatic conditions. Developing an understanding of the distribution of net infiltration in time and space and quantifying it as a dynamic upper-boundary condition for the deeper percolation fluxes in the approximately 500-meter thick unsaturated zone of Yucca Mountain is the main focus of the work presented in this report.

STUDY AREA DESCRIPTION

Geographic and Physiographic Setting

Yucca Mountain, located in southern Nevada (fig. 2) about 160 km northwest of Las Vegas, occurs within the Basin and Range physiographic province (Grayson, 1993) (fig. 1). The basin and range physiography is defined by the linear mountains and valleys of this area which have a distinct north to northwest trend. The region ranges in altitude from 86 meters below sea level at Death Valley, the lowest point in the United States, to about 3600 meters above sea level. Altitudes of basins are generally below 150 m and the mountains are generally above 2400 m. Physiographic elements of the Yucca Mountain area (fig. 7) can be divided into (1) ridges and valleys of Yucca Mountain, (2) irregular rugged topography north of Yucca Wash, (3) piedmont slopes surrounding Yucca Mountain on the south and east, (4) Fortymile Wash east of Yucca

Mountain and (5) the broad soil flats to the east and west of Yucca Mountain (U.S. Geological Survey, 1983).

(Figure 7. Infiltration study area and modeling domain with original site-scale model boundary (Wittwer and others, 1992) and potential repository location.)

Within the Basin and Range physiographic province are several topographic regions. Yucca Mountain is in the region named for Death Valley which is the largest and most prominent desert basin in the region (fig. 2). The Death Valley region is primarily in the northern Mojave Desert, extending into the Great Basin Desert, and is in the rainshadow of the Sierra Nevada Mountains. This results in a climate that is arid to semiarid throughout the region. Precipitation on the valley floors of the Amargosa Desert, Death Valley and basins at lower altitudes in the southern part of the region is less than 70 mm/yr, on average. Precipitation in the mountain ranges is commonly in the range from 100 to 150 mm/yr with annual precipitation as much as 500-750 mm in the Sheep Range and Spring Mountains (fig. 2), the highest ranges in the region. The mean-annual free-water-surface evaporation for the area ranges from 1250 to greater than 2500 mm/yr.

The Death Valley region (fig. 2) is the ground-water discharge area for a large part of the region. It is composed largely of closed topographic basins that apparently coincide with several closed ground-water flow systems. In these systems, recharge occurs sparingly at higher altitudes by infiltration of precipitation or by infiltration of ephemeral runoff. Discharge occurs largely by spring flow and by evaporation and transpiration in the playas. The deepest part of the system consists of carbonate aquifers that connect closed topographic basins at depth. Discharge from the system occurs in several intermediate areas that are geomorphically, stratigraphically and structurally controlled, but ultimately, most ground-water flow discharges to Death Valley.

The closed basin in which Yucca Mountain resides is referred to as ground-water unit DV-03 by Bedinger and others (1989). This unit and a smaller, adjacent basin DV-02 (Bedinger

and others, 1989) have been used to define the boundary of a regional 3-dimensional ground-water flow model for predicting the effect of climatic changes on regional hydrology and possible waste migration from Yucca Mountain (Frank D'Agnese, U.S. Geological Survey, written communication, 1994). The combined areas of DV-03 and DV-02, an area approximately 45,874 km^2, are referred to as the Death Valley Ground-Water Unit by Hevesi and Flint (1996)(fig. 2) and were used to map estimates of annual average precipitation and recharge on a regional basis.

This unit is underlain by extensive Paleozoic carbonate-rock aquifers and associated confining beds. The carbonate aquifers under-drain the area and there are also structural and lithologic controls that compartmentalize the ground-water flow in this unit, which results in very complex flow patterns. Discharge from this unit occurs in Sarcobatus Flat, Amargosa Desert and Pahrump Valley, and ultimately in Death Valley. The predominant direction of drainage for surface water and ground-water flow in this unit is generally from north to south because of a decrease in average topographic elevations in this direction in the southern Basin and Range.

Climate

Climate will likely be the most dynamic hydrologic process at Yucca Mountain over the next 10,000 years. The evaluation of past climate is needed to evaluate the control of climate on the hydrologic conditions at depth. The evaluation of current climate is necessary to relate changes in climate to near-surface processes, such as infiltration, runoff, redistribution and evapotranspiration. Future climate is the only climate that really matters for the success of a nuclear waste repository. The following sections provide some insight into the climate at Yucca Mountain.

Past

Gauthier and Wilson (1994) present a coherent picture of the literature that describe regional past climate and how it might be interpreted for the Yucca Mountain area. The same arguments are made here and applied to possible infiltration and recharge scenarios. There is strong evidence that Pleistocene climate underwent semi-regular progression of climate changes associated with glacial cycles (Imbrie and Imbrie, 1980, Imbrie, 1985). Based on these cycles, climate can be divided into two categories, glacial (or pluvial) and interglacial. Studies of pack-rat middens (e.g., Spaulding, 1985), ostracodes (e.g., Forester, 1994; Forester and Smith, 1994), lake levels (e.g., Benson and Klieforth, 1989), and water-table levels (e.g., Paces and others, 1993, and Marshall and others, 1993), indicate that, in the southwestern United States as a whole, the glacial periods are typically reflected as wet climates, while the interglacials are typically dry. The present climate is an interglacial, dry climate.

The glacial cycles are about 100,000 years long, on average, and appear to correlated with various changes in the amount of solar radiation that reaches the Earth, known as the Milankovitch insolation cycles (Imbrie and Imbrie, 1980). The changes are caused by the eccentricity in the Earth's orbit around the Sun (a 100,000 year period), the tilt of the Earth's axis (a 41,000 year period), and the precession of the Earth's axis (19,000 and 23,000 year periods). Winograd and others (1988) suggest a slightly different time scale, one not aligned with the Milankovitch insolation cycles: however, Imbrie and others (1993) argue that the difference is not significant. While vein-calcite data from Winograd and others (1992) represents more local conditions, published records only extend to 60,000 years ago, not to present time. The most complete record of global climate change exists for $\delta^{18}O$ data from ocean sediments in the SPECMAP study (fig. 8a) (Imbrie and others, 1984). These records show similar frequency of climate change as the vein calcite data, and can easily be used to simulate climate change for the Yucca Mountain area. Recent $\delta^{18}O$ data from Greenland ice cores (GRIP, 1993) shows the same general cooling and warming trends as the ocean-floor data, but with tremendous fluctuations superimposed on the general trends (fig. 8b). The fluctuations appear to have a time scale of 1000 to 2000 years (Gauthier and Wilson, 1994). This high-frequency climate change is not as apparent in the vein-calcite data of Winograd and others (1988) or Winograd and others (1992),

indicating that these fluctuations may not be present at Yucca Mountain. These rapid changes, if present, may have a much more significant influence on net infiltration at Yucca Mountain in a 10,000 year time frame and may need further evaluation.

Using the $\delta^{18}O$ time data, simulated hydrologic conditions can be modeled. Koltermann and Gorelick (1992) used this technique to estimate mean flood discharge. Flint and others (1993) used this technique to provide the upper-boundary conditions for an infiltration model. The fluctuations in climate were assigned net infiltration values as a linear function of $\delta^{18}O$. Although Koltermann and Gorelick (1992) use a linear relation between the $\delta^{18}O$ and mean flood discharge we have not verified that there is a linear relation between $\delta^{18}O$ and precipitation but believe the following approach provides a possible scenario for evaluating the sensitivity of Yucca Mountain to climate change. For this analysis when $\delta^{18}O$ was at a minimum, net infiltration was set at a minimum and when $\delta^{18}O$ was at a maximum, net infiltration was set at a maximum. By using Spaulding's (1985) estimate of a 40 percent increase in mean-annual precipitation during the Pleistocene, and the Hevesi and Flint (1996) estimate of 160 mm/year for the current climate, a possible mean-annual precipitation estimate can be made for the last 600,000 years (fig. 8a). This is based on the assumption that when the $\delta^{18}O$ was the highest in the oceans the climate was the coldest on the continent, and therefore, the precipitation was also the highest. By using the estimated mean-annual precipitation values in figure 8a and the modified Maxey-Eakin recharge model of Hevesi and Flint (1996), a time-varying model of recharge can be developed for the Yucca Mountain area (fig. 8c). In this model, a mean-recharge rate (over the last 600,000 years) of almost 5 mm/year with a maximum of 10 mm/year (18,000 yr. B.P.) and a minimum of near 1 mm/year today. This regional analysis only looks at the lower frequency climate change and does not account for the high frequency, short duration climate changes as seen in data of GRIP (1993) which may or may not be applicable to the Yucca Mountain area. In addition this regional analysis averages watershed scale areas and does not exclude spatially variable infiltration patterns within a watershed leading to high net infiltration in some areas and non in others.

(Figure 8. Historical climate change estimates from a) SPECMAP studies with a hypothetical transfer to precipitation, b) high-frequency fluctuations in climate change from the GRIP studies and c) recharge estimated from climate change cycles using the Maxey-Eakin method.) All $\delta^{18}O(^{o}/_{oo})$ *are referenced to Vienna Standard Mean Ocean Water (VSMOW)*

Present

The most recently published estimates of average annual precipitation at the site are between 170 mm/yr (Hevesi and others, 1991b) and 160 mm/yr (Hevesi and Flint, 1996). Average-annual precipitation can be used as an indicator of current climatic conditions and can be used as an input parameter for hydrologic studies. (The variability in annual and seasonal precipitation, storm intensity, duration and frequency may be more important in the analysis of infiltration but is only partially incorporated into this analysis.) Weather patterns within the study area vary seasonally. Summer precipitation primarily comes from the south and southeast. The southerly winds carrying the summer precipitation tend to curve east over southern Nevada (French, 1983). Winter winds carrying precipitation flow from the west resulting in a regional rain shadow east of the Sierra-Nevada Mountains (fig. 9). Below 38°30'N latitude, southern Nevada can be divided into deficit and excess zones of precipitation with an ill-defined transition zone which covers the Nevada Test Site (NTS) and Yucca Mountain (French, 1983). Generally, stations east of longitude 115°45W receive from 1.5 to 2.5 times more precipitation than stations at similar altitudes located west of longitude 116°45W (Winograd and Thordarson, 1975). Even in the relatively small study area there is significant variability imposed by orographic influences causing average annual precipitation to vary from less than 130 mm yr^{-1} to over 200 mm yr^{-1} (Hevesi and Flint, 1996).

(Figure 9. Predominate direction of weather patterns and seasonal sources of moisture across the southwestern U.S.)

Future

Various mechanisms operate on different scales of time to affect climate. Based on current knowledge of climate dynamics and the geologic record of past changes, major global climatic fluctuations likely will occur within the next 10,000 years (Spaulding, 1985). The two most likely forcing mechanisms that may cause significant climatic change in the next 10,000 years are increasing atmospheric carbon dioxide, and changes in the Earth's orbit, though each at a different frequency. Surface warming caused by increasing atmospheric carbon dioxide concentrations in the troposphere may be rapid enough that the effects may be visible today (Kellogg and Schware, 1981; Schlesinger, 1983). The increase in carbon dioxide should increase the annual temperature by 2 to 3 degrees C and increase average-annual precipitation. Changes due to astronomic parameters in the Milankovitch changes are a much lower frequency and are not readily apparent. These changes should bring back glacial climatic conditions with a lowering in the mean-annual temperature on the order of 5 to 10 degrees C and an increase in precipitation by 40 percent (Spaulding, 1985). There are may ways to develop future climate scenarios for Yucca Mountain. One could assume that the current climate will remain constant over the life of the repository or simply reproduce past climate conditions and determine under what condition, if any, Yucca Mountain may fail as a repository. There still needs to be an evaluation of anthropogenic effects on climate, such as increases in CO_2. Man-induced changes in climate have not occurred in the past and an evaluation of their effects is essential in determining the suitability of Yucca Mountain. Botkin and others (1991) suggest that global warming may result in ENSO-like conditions. If this is the case then the precipitation at Yucca Mountain is likely to be increase from 40 to 80 percent which is typical of ENSO conditions. Knox (1991) presents several methods that have been proposed for projecting future climates. These include extrapolating current instrument records, using paleoclimate analogs, using general circulation models (GCM's), using coupled mesoscale models within GCM's and using statistical submodels to GCM's to upscale from coarse grid GCM's to regional scale. The last two are currently being evaluated using model results from the National Center for Atmospheric Research (NCAR) for double CO_2 concentrations (simulated global warming) and a 21ka glacial maximum and then upscaling with the stochastic precipitation model being presented here.

Geology

Yucca Mountain is located within the southern portion of the southwestern Nevada volcanic field in an area where a thick section of Tertiary volcanic rocks overlie Paleozoic sedimentary strata (Byers and others, 1976). These strata record the evolution of at least seven calderas that compose the Timber Mountain-Oasis Valley caldera complex (Sawyer and others, 1994). The study area consists of a series of north-trending, eastward-dipping structural blocks that are bounded by mostly west-dipping normal faults (Carr and others, 1986). These fault blocks are composed principally of thick, welded ash-flow tuff deposits that are separated by thinner, silicic lavas, and tuffaceous sedimentary units. Formations of the Paintbrush Group (table 1), erupted from 12.8 to 12.7 Ma and form most of the exposures in the study area (Sawyer and others, 1994; Christiansen and Lipman, 1965; Scott and Bonk, 1984). Yucca Mountain is underlain by two densely welded and devitrified ash-flow tuffs (the Tiva Canyon and Topopah Spring Tuffs) that are separated by a comparatively thin interval of mostly nonwelded, vitric pyroclastic deposits referred to as the PTn (Paintbrush Tuff nonwelded). These deposits include the Yucca Mountain and Pah Canyon Tuffs, which are negligible to the south of the study area, nonwelded within the study area and are relatively thick to the north, where portions can be densely welded. Underlying the Topopah Spring Tuff is the rhyolitic Calico Hills Formation (nonwelded and referred to as CHn), and the Prow Pass and Bullfrog Tuffs of the Crater Flat Group. These rocks are primarily zeolitized with relatively thin zones of increased welding and devitrification and are separated by thin bedded tuff units. These rocks comprise a large proportion of the surface exposures over the study area (table 1).

Volcanic exposures on the fringes of the study area to the north include lava flows and pyroclastic rocks of the Rhyolites of Windy Wash, Timber Mountain Group and the Paintbrush Group (fig. 10).

Table 1. Generalized lithostratigraphy of Yucca Mountain area and ages (after Buesch and others, 1996; Moyer and Geslin, 1995; Sawyer and others, 1994).

Formal Nomenclature	Age (Ma)
TIMBER MOUNTAIN GROUP (Tm)	
Rainier Mesa Tuff	**11.6**
PAINTBRUSH GROUP	
Tiva Canyon Tuff (Tpc)	**12.7**
crystal-rich member (Tpcr)	
vitric zone (rv)	
nonlithophysal zone (rn)	
lithophysal zone (rl)	
crystal-poor member (Tpcp)	
upper lithophysal zone (pul)	
middle nonlithophysal zone (pmn)	
lower lithophysal zone (pll)	
lower nonlithophysal zone (pln)	
vitric zone (pv)	
Pre-Tiva Canyon Tuff bedded tuff (Tpbt4)	
Yucca Mountain Tuff (Tpy)	
Pre-Yucca Mountain Tuff bedded tuff (Tpbt3)	
Pah Canyon Tuff (Tpp)	
Pre-Pah Canyon Tuff bedded tuff (Tpbt2)	
Topopah Spring Tuff (Tpt)	**12.8**
crystal-rich member (Tptr)	
vitric zone (rv)	
nonlithophysal zone (rn)	
lithophysal zone (rl)	
crystal-poor member (Tptp)	
upper lithophysal zone (pul)	
middle nonlithophysal zone (pmnl)	
lower lithohysal zone (pll)	
lower nonlithophysal zone (pln)	
vitric zone (pv)	
Pre-Topopah Spring Tuff bedded tuff (Tpbt1)	
CALICO HILLS FORMATION (Tac)	**12.9**
Bedded tuff (Tacbt)	
Basal sandstone (Tacbs)	
WAHMONIE FORMATION (Tw)	**13.0**
CRATER FLAT GROUP	
Prow PassTuff (Tcp)	
Pre-Prow Pass bedded tuff (Tcpbt)	
Bullfrog Tuff (Tcb)	**13.5**
Tram Tuff (Tct)	

Distribution

The surface exposures over the study area (fig. 10) incorporate rocks with a large range of properties leading to varying degrees of infiltration of surface water. Over the potential repository area the rocks are generally the welded rocks from the crystal-poor Tiva Canyon Tuff, and the crest of the mountain is composed of higher porosity rocks of the crystal-rich, nonlithophysal Tiva Canyon Tuff. Several exposures of high-porosity PTn rocks are scattered around the study area, particularly in downcut washes to the south and north of the potential repository area. Ridgetops to the north of the potential repository area are composed of highly-fractured vitric rocks of the crystal-rich Tiva Canyon Tuff. Volcanic exposures to the north of the main study area, and included in the expanded site-scale model (Wu and others, 1996) are a mixture of rocks with varying properties from highly-fractured densely-welded rocks from lava flows to high-porosity pyroclastic rocks and bedded tuffs.

(Figure 10. Map of area with general geologic designations (after Sawyer and others, 1994.))

Properties

Matrix properties, including porosity, bulk density, particle density, saturated-hydraulic conductivity (K_s) and moisture retention characteristics (Flint, 1996) of volcanic tuffs, have been specifically determined for the rocks of the Tiva Canyon, Yucca Mountain, Pah Canyon, and Topopah Spring Tuffs and interlayered bedded tuffs, as well as the Calico Hills Formation and Prow Pass Tuff. These properties have been associated with each of the lithostratigraphic units included in Scott and Bonk (1984) and are listed in table 2. All properties were collected and determined following a full quality-assurance program. All data associated with this report that are qualified for use in site characterization are listed by data tracking number in Appendix I. The

saturated-hydraulic conductivity of the surficial-bedrock units is distributed spatially and illustrated in figure 11. Also included in the table are estimated properties of fractures for each unit. Fractures are prevalent in the welded rocks and frequent to infrequent in the nonwelded rocks. Fracture densities and apertures are not well characterized for all lithostratigraphic units, but estimates have been made from borehole core logs. Properties of fractures are dependent on fracture aperture and whether the fractures are open or filled with calcium carbonate or siliceous materials. Calculations can easily be made of porosity and K_s of fractures with assumed or estimated density and aperture and because flux in fractures is assumed to occur only under saturated or near-saturated conditions, unsaturated flow parameters are not required. Average K_s of fractures with a range of apertures are 2.5 um = 410 mm/day, 25 um = 15,700 mm/day and, 250 um = 745,000 mm/day. K_s has been measured on fracture-fill materials and averages 43.2 mm/day. Estimates of K_s were calculated using these values of fracture conductivity for the percent of area per square meter of rock given the fracture density and aperture available for water to flow through. This was added to the K_s of the rock matrix and weighted averages calculated for lithostratigraphic unit for 6 fracture types, whether open or filled and for each of the 3 aperture classes noted above. Weighted averages could be calculated if the proportion of fracture apertures for each rock type were known. As an example the 6 fracture types (3 sizes, filled or unfilled) were equally weighted to produce the last column in table 2. For the model INFIL, discussed later, and to produce figure 11, the fractures were assumed to be filled 250 um fractures (the second-to-last column in table 2).

(Figure 11. Saturated hydraulic conductivity of the surficial bedrock units.)

(Table 2. Properties of rock matrix and fractures for all lithostratigraphic units exposed in the study area.)

Watershed Characteristics

Yucca Mountain has largely been influenced by an interrelationship of tectonism and geomorphic processes. The topography has been defined by erosional processes on the eastern sloping ridge and along faults and fault scarps that have created a series of washes that are down cut

to varying degrees into different bedrock layers. The topography is generally controlled by the high-angle faults, which tilt the resistant volcanic strata eastward. Slopes are locally steep on the west-facing escarpments eroded along the faults and in some of the valleys that cut into the more gentle eastward-facing dip slopes. Narrow valleys and ravines are cut in bedrock; wider valleys are floored by soil deposits into which terraces have been cut by intermittent streams. Locally, small sandy fans extend up the lower slopes and spread out on the valley floors. East of the crest of Yucca Mountain, drainage is into Fortymile Wash; west of the crest, streams flow southwestward down fault-controlled canyons and discharge in Crater Flat. The site area can be divided into two parts, that to the north of Drill Hole Wash and the area to the south. The washes in the southern area trend eastward, are relatively short (less than 2 km) and are defined by erosional channels which produce gently sloping sideslopes. The washes north of Drill Hole Wash are northwest trending and 3-4 km long. They are controlled by fault features and have steeper sideslopes.

Defined watersheds

The Drill Hole Wash, Busted Butte, and Solitario Canyon watersheds are the three main surface drainage that directly overly the potential repository area (Squires and Young, 1984). Two additional surface drainage that are adjacent to the potential repository area are the Yucca Wash and the Fortymile Wash watersheds (fig. 12). The Drill Hole Wash, Busted Butte, and Yucca Wash watersheds are well defined west-to-east drainage that are direct tributaries to the Fortymile Wash watershed. The Solitario Canyon watershed, which is not a tributary of the Fortymile Wash drainage system, is a north-to-south drainage that feeds the Crater Flat soil basin to the west of Yucca Mountain. The Crater Flat basin and the Fortymile Wash watershed are both tributaries of the Amargosa River watershed, which is the major surface drainage of the Death Valley closed basin (Osterkamp and others, 1994; Hevesi and Flint, 1996).

(Figure 12. Map of major watersheds at Yucca Mountain.)

The Drill Hole Wash and Busted Butte watersheds consist of several smaller drainage

which can be considered as separate and distinct hydrologic systems, primarily based on physiographic differences. In general, these smaller drainage can be grouped according to whether the dip slope of the bedded tuffs or faults are the primary geologic structure affecting erosional processes and thus the physiographic position of the drainage. The Solitario Canyon drainage is controlled by the north to south striking Solitario Canyon normal fault. All other drainage overlying the potential repository area are primarily controlled by the east-southeast dip slope of the bedded tuffs on the uplifted side of the Solitario Canyon fault. The upper Drill Hole Wash drainage (the main tributary of the Drill Hole Wash watershed) and the Pagany Wash drainage (an important tributary of the Yucca Wash watershed), which are both directly north and northeast of the potential repository area, are controlled primarily by northwest-to-southeast right-lateral strike-slip faults. Other important differences in these smaller drainage include changes in the underlying bedrock and important fault zones (such as the Ghost Dance fault) which may or may not be affecting the drainage.

Topographic surfaces

The topography at this site can be described in terms of generalized topographic positions which represent infiltration zones; ridgetop, sideslope, terrace, and channel. Over an area within the boundaries of the original USGS/LBNL 3-dimensional site-scale model (Wittwer and others, 1992) (fig. 7) which extends from Yucca Wash in the north, between the Solitario Canyon and Bow Ridge faults and to Busted Butte in the south, the ridgetop locations (which include ridge and shoulder) encompass about 14 percent of the total area, the sideslopes 62 percent, the terraces 22 percent and the active channels 2 percent (Flint and Flint, 1994). The infiltration study area for this report (fig. 7), which includes the expanded USGS/LBNL 3-dimensional site-scale model (Wu and others, 1996), encompasses about 1 percent ridge, 6 percent shoulder, 41 percent sideslope, 7 percent footslope, 44 percent terrace and 2 percent channel. The ridgetop locations are generally flat to gently sloping and are higher in altitude than the other topographic positions. They have thin (less than a meter) to no surficial deposits but are relatively stable morphologically. Existing soils are fairly well developed, and thin calcium carbonate layers are common. Bedrock at ridgetop

locations is moderately to densely welded (Flint and others, 1995) and moderately to highly fractured. The slopes and elevations of the ridgetops lead to the retainment of snowfall in the winter for several weeks at a time.

Because of the difficulty of drilling boreholes at steep, sideslope locations, field data for this topographic position are limited to sites on the lower sideslopes of washes. This location is distinguished from the terrace and channel locations by depth of soils and slope. Soil cover is thin to nonexistent, and in most locations, bedrock is densely welded and highly fractured. The sideslopes are approximately north or south facing in the southern section of the site and, therefore, have different seasonal solar radiation loads. In the northern washes, though directed more southwest-northeast, the steepness of the slopes accentuates the seasonal radiation differences. In some locations, side channels concentrate runoff water.

Terraces and channels are located at lower elevations in the main washes and have thin soil cover in the upper washes and thick soils farther down. A very small percentage of exposed bedrock exists in the washes. The soil has varying degrees of calcium carbonate cementation that commonly is quite extensive. The porosity of the soil ranges from 15 to 50 percent with an average of about 30 percent. The surface is relatively flat and dissected by old soil channels and active channels. Channels differ from terraces because of periodic runoff in the channels under extreme precipitation conditions. The channels occupy a very small surface area of the wash but may contribute significantly to net infiltration during runoff events.

Soils

Soil deposits are found in the valley floors and washes. These include fluvial sediments and debris-flow deposits. These deposits have varying degrees of soil development and thickness and have a gravelly texture with rock fragments constituting between 20 and 80 percent of the total volume. The soils range from 100-m thick in the valleys to less than 30-m thick in the mouths of the washes. Midwash, most soil fill is less than 15-m deep in the center. Many of these soils have

developed cemented calcium-carbonate layers. More stable surfaces, generally on the flat upland ridges, have developed soils 0.5 to 2-m thick with high clay contents. Soil thickness was classified into 4 categories: 0 to <0.5, 0.5 to <3.0, 3.0 to <6.0 and ≥6.0 (fig. 13) which make up 48 percent, 7 percent, 5 percent and 40 percent of the area, respectively.

(Figure 13. Map of soil thickness designated in 4 categories, 0 - < 0.5, 0.5 - < 3 m, 3 - < 6 m, and ≥ 6 m.)

Distribution

The surficial units of Lundstrom and others (1994), Lundstrom and others (1995a), Lundstrom and others (1995b), and Lundstrom and others (1995c), were recombined into eight soil taxonomic units using the description in soil taxonomy (USDA, 1975), with the two units used by Lundstrom and others (1994), Lundstrom and others (1995a), Lundstrom and others (1995b), and Lundstrom and others (1995c) of rock (r) and disturbed ground (d) remaining the same. Soils are primarily Aridisols with some Entisols (USDA, 1975) in the active washes and sand ramps. The recombined surficial units and associated coverages are described in table 3 and illustrated in figure 14.

Table 3. Surficial soil units recombined from mapped surficial units.
[%, percent].

Model Unit	Recombined Soil Unit	Included Surfical Unit	Area (%)
1	Typic Argidurids	0, 1, 1-3, 2, Tpg	7.9
2	Typic Haplocalcids	3, 3f, 3-4, 4, 4f, 4s, 4/1, 4f-5f, 3-5	17.5
3	Typic Haplocambids	5, 5f, 5s, 5/1, 5-6, 5f-6f, 6, 6f, 5-7	13.0
4	Typic Torriorthents	7, 7f ,6-7, 6f-7f	1.8
5	Lithic Haplocambids	cu, cs	46.0
6	Typic Torripsamments	e, eo, ey, 1/e0, 3/eo, ef/e	4.8

Model Unit	Recombined Soil Unit	Included Surfical Unit	Area (%)
1	Typic Argidurids	0, 1, 1-3, 2, Tpg	7.9
7	Lithic Haplargids	rc	1.2
8	Rock	r	0.3
9	Typic Calciargids	cf	6.4
10	Disturbed Ground	d	1.1

(Figure 14. Map of surficial soils.)

Properties

Field and laboratory analyses were conducted on the soil on and around Yucca Mountain. Large-volume, field bulk-density samples were collected from the surface to 0.3 m using an irregular-hole, bulk-density device, a bead cone (Flint and Childs, 1984). Bulk density, grain density, porosity, rock fragment content, sand, silt and clay percentages were determined. Saturated-hydraulic conductivity was measured using a double-ring infiltrometer (Hofmann and others, 1993) on soils in measurable locations and modeled using textural data for the fine soil fraction (<2 mm) using equation 6.12 of Campbell (1985). Log-log water characteristic curves were determined using equations 2.15, 2.16, 2.17, 2.18, 5.10 and 5.11 of Campbell (1985) and were converted to van Genuchten curves using RETC (van Genuchten and others, 1991). Soil-water content at -0.1 bar and -60 bars water potential are used as field capacity and the upper limit of plant-available water, respectively, and will be discussed in the appropriate sections. The soil properties are summarized in table 4, where conductivity, alpha, and n are modeled from texture, rock fragment content and bulk density measured in the field and water contents are calculated from the water retention curves.

Table 4. Summary of soil properties.

[m/s, meters per second; Pa, pascals; %, percent; g/cm^3, grams per centimeter]

Model unit	Saturated hydraulic conductivity (modeled, m/s)	alpha (1/Pa)	n	Porosity (%)	Rock fragments (%)	Bulk density (g/cm^3)	Water content at -0.1 bar water potential (%)	Water content at -60 bars water potential (%)
1	5.6E-6	0.00052	1.24	36.6	10.5	1.60	24.2	5.4
2	1.2E-5	0.00062	1.31	31.5	11.6	1.73	17.3	2.3
3	1.3E-5	0.00066	1.36	32.5	18.7	1.70	16.3	1.7
4	3.8E-5	0.00087	1.62	28.1	21.9	1.81	7.3	0.2
5	6.7E-6	0.00056	1.78	33.0	15.2	1.69	20.0	3.5
6	2.7E-5	0.00074	1.40	33.9	11.7	1.66	15.0	1.1
7	5.6E-6	0.00055	1.26	37.0	17.1	1.58	23.4	4.6
8	--------	--------	-----	--------	--------	--------	--------	--------
9	5.7E-6	0.00055	1.30	32.2	19.1	1.72	18.9	2.8
10	--------	--------	-----	--------	--------	--------	--------	--------

To test the validity of using textural analysis as a surrogate for hydrologic properties field measured hydraulic conductivities were compared with the geometric-mean particle diameter (Shirazi and Boersma, 1984) and the model predictions of Campbell (1985) (fig. 15a). There appears to be adequate correlation to use textural data, however, the presence of rock fragments has dramatic effects on soil properties (see Childs and Flint, 1990, for a comprehensive discussion). To account for the presence of rock fragments, the log of predicted hydraulic conductivity from Campbell (1985) and the gravimetric rock-fragment content were regressed against the log of the measured values of hydraulic conductivity to produce a modified Campbell equation with an r^2 of 0.85 (fig. 15b). The equation was then applied to each model unit in Table 4 to determine the saturated-hydraulic conductivity. This analysis only applies to the top 0.3 m which is likely not applicable to depths greater than 0.5 to 1 m because of textural changes with depth. However, because most of the surface over the potential repository is generally < 0.5 meters (fig. 13) the application of this data for these shallow soil is not totally inappropriate.

(Figure 15. Relationship of a) soil texture to saturated hydraulic conductivity using Campbell

(1985) for soil without rock fragments and modified to correct for percent rock fragments, and b) modeled versus measured conductivity.)

Texture was also used for the calculation of moisture retention curves for the surficial soils using Campbell (1985). Six moisture retention curves were measured in the laboratory on each of soil model units 1, 2, and 4 using tempe cells, pressure pots and chilled-mirror psychrometers (Flint, 1996) to measure water potential over a full range of saturations (fig. 16a, 16b and 16c). Curves were fit to the combined data sets for each soil unit. Curves calculated from the average textural data for the soil model units are very similar to the curves from the measured data for the 3 units. It was considered, therefore, that texture could be used to calculate curves and associated modeling parameters for the remaining 5 soil model units and all curves are illustrated in figure 16d. These parameters are those listed in Table 4 and are used in the numerical model.

(Figure 16. Moisture retention curves calculated from measured soil texture (Campbell, 1985) compared to measured data for soil model units a) 1, b) 2, and c) 4, and texture models for d) all soil model units.)

Vegetation

In arid environments, range plants are very often subject to stress because of water deficits and plant distributions, community types and production are determined by the availability and distribution of water (Lane and others, 1984). Seasonal plant activity is also governed to a large degree by water availability, but also by temperature and light. Due to the tremendous variability in precipitation in these environments, plant productivity is reflected in the gradual adaptation of vegetation to variability in environmental factors.

The study area is situated within the broad transition, referred to as Transition Desert, between the northern boundary of the Mojave Desert and the southern boundary of the Great Basin Desert. The northern boundary of the Mojave Desert is usually delimited by the northern limits of

Larrea tridentata (Beatley, 1976). On Yucca Mountain, Mojave Desert vegetation occurs at lower elevations on bajadas and in washes. Transition Desert associations are situated topographically above the *larrea* ecotone. Over broad areas, *Coleogyne ramosissima* is the species most identified with the Transition Desert (Beatley, 1976). These associations are located primarily on ridges and canyons. Associations on Yucca Mountain are very heterogeneous and are composed of a large diversity of shrub associates (fig. 17).

(Figure 17. Map of vegetation associations.)

Vegetation characterization research has been conducted on the Nevada Test Site and at Yucca Mountain periodically for the past 30 years (Beatley, 1976; O'Farrell and Emery, 1976; Wallace, 1980; O'Farrell and Collins, 1983), and most recently by EG&G Energy Measurements for the Environmental Assessment for the Yucca Mountain Project (USDOE, 1986). Three dominant vegetation associations occur in the EG&G study area (fig. 17), which extends from Solitario Canyon in the west to Fortymile Canyon in the east and from Yucca Wash to the north to Busted Butte in the south. These associations are identified by the major plant species and are described in the Annual Report FY89 & FY90 (EG&G, 1991). The most common vegetation associations are *Larrea-Lycium-Grayia* which covers approximately 35% of the surface area at Yucca Mountain, *Coleogyne* (30%), and *Lycium-Grayia* (26%). *Larrea-Lycium-Grayia* predominates on the eastern bajadas of central Yucca Mountain. It occurs at intermediate elevations in the study area ranging from 1,000 to 1,500 m. Soils in this association are very gravelly to rocky, particularly near the steeper slopes. *Coleogyne* occurs across the northern third of the study area. This association occurs from the valley floors at elevations of approximately 1,030 m to the flat ridge tops at roughly 1,710 m; however, it generally does not occur on the steep slopes connecting these two areas. It occupies areas with relatively shallow soils. Slopes are fairly gentle with most ranging from 1-10%. The dominant species is Blackbrush *(Coleogyne ramosissima)* and because this species tends to exclude other species, this association is the least diverse. *Lycium-Grayia* occurs on steep slopes throughout the study area and dominate on the ridgetop of Yucca Mountain south of Antler Ridge. This association is the most complex and diverse of the associations with several species (Mormon

teas, *Ephedra* spp. and *buckwheats, Eriogonum* spp.) forming subassociations and dominating in local areas. Soils in this association are very shallow and generally extremely rocky. An additional association, *Larrea-Ambrosia,* though only covering 9% of the area, occurs in the south and southeastern sections of the study area. This is characterized by deep, loose sandy soils without a well-developed surface pavement. Elevations range from 900 to 1,050 m and slopes are gentle (0-5%). The dominant plant species is Bursage (*Ambrosia dumosa)* which contributes almost half of the total cover. The dominant and subdominant species are included in table 5 with an effort to characterize the seasonal activity, rooting depth and minimum xylem water potential of each species based on available information from Hansen and others (written communication, 1996). The percent cover of these species has changed from year to year, sometimes dramatically, in particular following the drought years of 1987-1990, and are therefore not included. Minimum xylem water potential was used to calculate the -60 bar lower limit of plant-available water. Rooting depths were used to estimate extraction depths in the model INFIL discussed later.

Additional detailed information from Hansen and others (written communication, 1996) has provided insight into details of plant habits and distributions that support estimates of evapotranspiration based on energy-balance calculations and modeling of radiation loads over the surface of Yucca Mountain. North- and south-facing slopes receive different amounts of solar radiation, resulting in differences in temperature and water availability in the habitats located on these aspects. South-facing slopes tend to be warmer and drier while north-facing slopes tend to be cooler and wetter. Plant species exhibit differential preference or tolerance for these growing conditions. Preliminary data (Hansen and others, written communication, 1996) indicates that some species, often typical of the flora of the Great Basin area, such as yellow rabbitbrush, green ephedra, big sagebrush and burrobrush are commonly found on north-facing slopes, while bursage and range rhatany, often typical of the flora of the warmer Mojave Desert, are commonly found on south-facing slopes.

Table 5. Plant species most commonly found at Yucca Mountain. Where possible, information is included on life style.

Scientific Name	Common Name	Life Form	Active Months	Rooting Depth (cm)	Minimum Xylem Potential (bars)
Acamptopappus shockleyi	Goldenhead	shrub			
Ambrosia dumosa	Bursage	shrub	Mar-Dec	86 cm	-50
Atriplex confertifolia	Shadscale	shrub	never truly dormant	70 cm	-100
Coleogyne ramosissima	Blackbrush	shrub			
Ephedra nevadensis	Mormon tea	shrub	Feb-May, rain	>100	-70
Ephedra viridis	Green ephedra	shrub			
Eriogonum fasciculatum	Calif. buckwheat	shrub			
Grayia spinosa	Spiny hopsage	shrub	Feb-Jul, temp	97	-60
Haplopappus cooperi	Goldenbush	shrub			
Hilaria jamesii		grass			
Hymenoclea salsola	Cheese bush	shrub	Feb-Dec	81	-37
Krameria parvifolia	Range rhatany	shrub	Mar-Dec, temp	50	-72
Larrea tridentata	Creosote bush	shrub	never truly dormant	168	-60
Lycium andersonii	Desert thorn	shrub	Feb-Sep	122	-52
Menodora spinescens	Spiny menodora	shrub			
Oryzopsis hymenoides	Indian ricegrass	grass			
Salazaria mexicana	Bladdersage	shrub			
Stipa speciosa	Desert needlegrass	grass			

DATA COLLECTION / DATA ANALYSIS

Precipitation

Measurements of precipitation at the potential repository site are critical in providing a starting point for developing the water balance, as discussed previously. Measurements of precipitation at Yucca Mountain are also needed for defining current climatic conditions at the site.

Site specific data collected from 5 automated weather stations installed and operated by the U.S. Geological Survey for water years 1988-1994 is provided by Flint and Davies (1995). Measurements were obtained using tipping-bucket precipitation gages to provide a record of the temporal distribution of precipitation intensity, including the timing, frequency, and duration of precipitation. Additional site specific data were collected by the USGS for water years 1992 and 1993 from a dense network of approximately 130 nonrecording rain gages located mostly over the area of the potential repository site (Ambos and others, 1995). Although the data does not provide an accurate measure of the timing of precipitation or of the temporal distribution of precipitation intensity and duration, the network of nonrecording gages is important for providing data on the spatial distribution of accumulated precipitation amounts over the area of the potential repository. Total precipitation amounts for all major storm events from October, 1991, through October, 1993 measured using the nonrecording rain gage network is provided by Hevesi and others (1994a). Results by Hevesi and others (1994a) also include a geostatistical analysis of the spatial variability of total precipitation resulting from storm periods, with a comparison of results for winter versus summer storms.

Analysis of precipitation data measured at Yucca Mountain indicates that winter precipitation tends to be of lower intensity but longer duration as compared to summer precipitation. In general, severe winter storms were often observed to persist for more than one day, while durations of severe summer storms were often less than one to two hours. One of the highest intensity precipitation events recorded at Yucca Mountain, although non-QA, occurred on August 31, 1991 (figure 18a), with maximum instantaneous intensities of more than 175 mm/hr occurring within the 40 minute duration of the storm. This storm, which had a maximum total storm depth of approximately 40 mm at one location, resulted in flash flooding and debris flows in Abandoned Wash on Yucca Mountain (D. Bauer, written communication, 1992). Widespread overland flow throughout the Yucca Mountain area did not occur because the storm was isolated and centered over the south-central part of the mountain (Hevesi and others, 1994a). In comparison, the severe winter storm of March 9-11, 1995, resulted in maximum intensities of only 14 mm/hr during a 35-hr period of near-continuous precipitation (figure 18b). The total duration of this storm was two days

and the average total storm depth was approximately 65 mm. The total amount of precipitation on March 10 and the increase in precipitation intensity after 25 hours of precipitation, combined with wetter than average antecedent conditions following the wettest January on record, caused widespread overland flow throughout the Yucca Mountain area during the morning of March 11, 1995.

(Figure 18. Rate of rainfall for a) a summer thunderstorm and b) winter precipitation.)

Regional data, which are collected and maintained by various federal, state, and private agencies, are important for determining how conditions measured at Yucca Mountain compare to the spatial and temporal distribution of precipitation on a regional scale, (although they are not operating under an approved YMP QA program). This is especially important because records for Yucca Mountain are short (<10 years) compared to records of 30 years and longer which are available at the regional sites. Records of daily precipitation amounts ranging from 1921 through 1995 were obtained from a regional network of over 150 precipitation stations located throughout the Yucca Mountain region, including stations located in parts of central Nevada, southern California, southwestern Utah, and northwestern Arizona. The network defines a set of regionally-distributed locations where measurements of precipitation have a potential relevance for defining present-day (1921-1995) climatic conditions for the Yucca Mountain region. A complete description of the network and the daily precipitation data up through 1993 is provided by Hevesi and Flint (1996) and by Hevesi and others (1996). A regional analysis of the orographic effects on the spatial distribution of average annual precipitation for the Yucca Mountain region using data from 1921-1993 is presented by Hevesi and Flint (1996). A regional analysis of the spatial and temporal distribution of precipitation throughout the Yucca Mountain region for two water years (1992 and 1993) that were affected by ENSO is presented by Hevesi and others (1996). This report also includes a comparison of these two ENSO years to the complete record of each station.

For this report, a 15-year record of daily precipitation for the area of Yucca Mountain was needed to analyze and develop the remaining components of the water balance (as discussed in

greater detail in following sections). The record was required for calibrating the numerical model of infiltration. Site-specific data which were available for various locations on Yucca Mountain were combined with the regional data to develop a record providing the best estimates of total daily precipitation amounts from January 1, 1980 through September 30, 1995, although non-QA. The daily totals were adjusted using elevation to provide a spatial distribution of precipitation that is consistent with the correlation between average annual precipitation and elevation (Hevesi and Flint, 1996). Figure 19 shows the average daily totals for the locations of the 90 neutron boreholes used for monitoring infiltration at Yucca Mountain (Flint and Flint, 1995), and is an approximate representation of average daily total precipitation for the area of the potential repository site. (Locations of all boreholes can be found in Appendix II). For 1980 through 1987, the developed record is less certain because site specific data were not available for this period; the estimated daily totals are interpolated using records from NTS stations and nearby regional stations. Beginning in 1988, site specific data from 3 U.S. Geological Survey weather stations (stations 1, 3, and 4) (Flint and Davies, 1996) were included in the interpolation model, greatly reducing the uncertainty in the developed record.

(Figure 19. Estimated daily precipitation for Yucca Mountain using 15 years of measured data simulated at 90 neutron boreholes.)

Records from the NTS stations and the regional network were also used to analyze the temporal distribution of daily precipitation and to define the parameters of a stochastic model of daily precipitation which was used for 100-year simulations of infiltration. Using the program MARKOV (appendix III), the 32 transition probabilities for a 3rd-order, 2-state Markov chain model of the occurrence of measurable daily precipitation were estimated for each month by the equation (Gregory and others, 1992, 1993; Haan, 1977):

$$P_{ij}^{q} = \frac{n_{ij}^{q}}{\sum_{j=1}^{m} n_{ij}^{q}} \qquad (13)$$

where q is the month and n is the number of times state I transitioned to state j. The program uses a 4-day sliding window to determine the probability of precipitation occurrence following a sequence of wet or dry days for the three preceding days. Figure 20 indicates the calculated transition probabilities of the occurrence of precipitation following 6 selected sequences for three preceding days for each month using the record for station 4JA. In general, the results define the probability of precipitation on the 4th day given a known state of precipitation for the preceding 3 days. For example, the probability of having precipitation on the 3rd day following three days of no precipitation is 6 percent in January. The probability of having a precipitation event is generally lowest in the summer and generally less than 10 percent given no precipitation the previous 3 days. Once a precipitation event has occurred the probability of an event the following day jumps to a high of over 50 percent in January and a low of 23 percent in May. The bimodal character of the temporal distribution of precipitation occurrence is indicated by a comparison of the monthly transition probabilities. The probability of precipitation following a sequence of dry days is greatest during January, February, and March, with July and August indicating an increased probability as compared to June and September. The probability of having a sequence of alternating wet and dry days is greatest during July, which is consistent with isolated thunderstorm activity during the monsoon. The probability of having precipitation following 3 consecutive wet days is greatest for January, February, March, and July. For all months, the probability of precipitation is less than 10 percent following a period of three consecutive dry days but once precipitation has occurred the probability of precipitation on the following day is higher than 20 percent for all months. The absolute probability of a series of events occurring could be determined by multiplying the individual probability of each event in series. For example, to determine the absolute probability of getting three days of precipitation in a row in January multiply the probability of getting one day (0001, 6 percent) times the probability of getting two days (0011, 52 percent) times the probability of getting three days (0111, 44 percent) which yields an absolute probability of < 2 percent.

(Figure 20. Probability of occurrence of daily precipitation at Yucca Mountain using 3rd order Markov chains. A 4-day window was used and 1 equals precipitation.)

The probability of the magnitude of daily precipitation was defined using a modified exponential-type cumulative probability distribution function:

$$P_S = e^{(-A_S(PPT)^{B_S}+A_S)} \quad (14)$$

where P is the cumulative probability for a month or season S of daily precipitation amount, PPT (hundredths of inches), and A and B are fitted parameters . For this report, January, February, and March were designated as winter, April, May, and June as spring, July, August, and September as summer, and October, November, and December as fall. The program MARKOV (appendix III) was used to estimate cumulative probabilities for daily precipitation amounts using intervals of 0.254, 1.27, 2.54, 6.35, 12.7, 19.0, 25.4, 38.1, 50.8, 63.5, and 76.2 mm. These intervals correspond to intervals of 0.01, 0.05, 0.10, 0.25, 0.50, 0.75, 1.0, 1.5, 2.0, 2.5, and 3.0 inches because the precipitation records for the regional and the NTS stations are terms of inches. The measurement resolution for this data is 0.01 inches, thus the probability of a precipitation amount of 0.254 mm or greater for any day having precipitation is 1.0. MARKOV uses nonlinear regression to solve equation 14 to obtain values for the A and B parameters for each month. Figures 21a and b show the fit of the model to the measured probabilities obtained using the record for station 4JA for the months of February (fig. 21a) and July (fig. 21b). The modified exponential model was observed to provide a good fit to the full range of measured daily precipitation magnitudes for all months, and was found to provide a better overall fit to the data than the standard exponential probability-distribution function. The fitted model predicts that at station 4JA approximately 10 percent of all days having precipitation will result in accumulations of 15 mm or greater in February, and 7 mm or greater in July. The model also predicts that approximately 1.5 percent of days having precipitation will result in accumulations of 40 mm or greater in February, and 100 mm or greater in July. Because the model is asymptotic to a probability of zero, unrealistically high magnitudes of daily precipitation are given some small probability of occurrence. Upper limits on the predicted magnitudes of daily precipitation were defined for the model based on the maximum daily accumulation observed for each month, which was 35.3 mm for February and 62.7 mm for July at station 4JA.

(Figure 21. Data and fitted model for the cumulative probability distribution of precipitation quantity at station 4JA a) for the month of February and b) for the month of July.)

The fitted monthly values for the A and B parameters obtained for two selected NTS stations, 4JA and Area 12, are listed in table 6. The approximate cumulative probabilities and the corresponding minimum total daily precipitation amounts predicted using the monthly model, along with the observed maximum daily precipitation for each month, are also listed in table 6. The model indicates that the probability of having a total daily precipitation amount of at least 1 mm is higher than 50 percent throughout most of the year at 4JA, and throughout all of the year at Area 12. The highest probability of total daily precipitation of at least 10 mm occurs for February at 4JA and for January at Area 12, while the lowest probability for at least 10 mm occurs for July at 4JA and for June at Area 12. In contrast, the highest probability of total daily precipitation of at least 50 mm occurs for July at 4JA and for February at Area 12, while the lowest probability for at least 50 mm occurs for May at 4JA and for June at Area 12. The probability of moderate precipitation amounts of at least 1 to 10 mm tends to be highest during the winter months for both stations, while the probability of more severe storms producing total daily accumulations of at least 50 to 100 mm tends to be highest during the summer months for both stations. The modeled probability of having at least 100 mm total daily precipitation at both stations tends to be the highest for those months in which the highest maximum precipitation amounts were observed. The probability of having at least 100 mm precipitation is as high as 1.3 percent in July at 4JA, which was a month during which a maximum accumulation of 62.7 mm was measured at the site. The probability of at least 100 mm total daily precipitation is 0.4 percent in August at Area 12, and the maximum measured accumulation at this site 71.1 mm during August.

A comparison of the fitted models for selected months from each season for stations 4JA and Area 12 is provided in figure 22. The models are bounded by the minimum daily precipitation amount of 0.254 mm and by the maximum observed daily precipitation for each month. For both stations, the models for February provides the greatest minimum precipitation magnitudes for

cumulative probabilities greater than 3 percent, while the models for August provides the greatest minimum precipitation magnitudes for cumulative probabilities less than 1 percent. For cumulative probabilities of approximately 70 percent and higher, the February and October models for 4JA provide the highest minimum precipitation amounts (> 2 mm). For cumulative probabilities less than 10 percent, however, the models for Area 12 provide greater minimum precipitation amounts (> 10 mm). The fitted models indicate that more half the precipitation events in the summer are small (<2 mm), largely due to virga and to the short duration of summer storms. However summer precipitation events have the largest probability of being over 25 mm at 4JA and 60 mm at Area 12. Overall, the models for Area 12 predict higher daily precipitation magnitudes as compared to 4JA, which is somewhat expected due to the higher elevation of Area 12 (approximately 7,600 ft for Area 12 compared to approximately 3,400 ft. for 4JA). It should be noted that the models do not by themselves directly predict the relative wetness of various sites or months; the frequency of precipitation occurrence, as predicted by the Markov model, must be considered in conjunction with models predicting precipitation magnitudes.

(Figure 22. Probability distribution of precipitation quantity for a) precipitation data from Area 12 and b) precipitation data from Yucca Mountain.)

Table 6. Model parameters and cumulative probability for various minimum amounts of daily precipitation for stations 4JA and Area 12 calculated for months.
[mm, millimeter]

Station	Month	Model Parameters A	Model Parameters B	Minimum Daily Precipitation Amount (mm) 1	5	10	25	50	100	Observed Maximum Precipitation (mm)
				Cumulative Probability						
4JA	January	0.16	0.73	7.6E-1	2.9E-1	1.2E-1	1.4E-2	6.5E-4	6.1E-6	30.0
	February	0.08	0.84	8.4E-1	4.0E-1	1.9E-1	2.6E-2	1.3E-3	8.0E-6	35.3
	March	0.06	0.93	8.4E-1	3.6E-1	1.4E-1	8.7E-3	9.2E-5	2.8E-8	30.0
	April	0.86	0.42	5.2E-1	1.2E-1	4.6E-2	7.2E-3	9.7E-4	7.9E-5	26.4
	May	0.12	0.86	7.5E-1	2.2E-1	6.0E-2	1.7E-3	6.8E-6	6.0E-10	15.7
	June	0.60	0.46	5.8E-1	1.7E-1	7.6E-2	1.4E-2	2.2E-3	2.1E-4	31.0

	July	14.02	0.04	4.1E-1	1.3E-1	8.1E-2	4.0E-2	2.3E-2	1.3E-2	62.7
	August	4.24	0.13	4.3E-1	1.2E-1	6.8E-2	2.7E-2	1.2E-2	5.5E-3	81.8
	September	1.13	0.78	8.1E-1	3.4E-1	1.5E-1	1.8E-2	8.0E-4	5.4E-6	29.7
	October	0.07	0.96	8.4E-1	3.3E-1	1.1E-1	4.8E-3	2.3E-5	1.4E-9	22.6
	November	0.17	0.70	7.6E-1	2.8E-1	1.2E-1	1.5E-2	9.0E-4	1.2E-5	22.6
	December	0.58	0.41	6.5E-1	2.5E-1	1.3E-1	4.1E-2	1.1E-2	2.4E-3	47.0
Area 12	January	0.03	1.04	9.2E-1	5.5E-1	3.0E-1	3.9E-2	1.1E-3	7.9E-7	47.2
	February	0.21	0.57	7.8E-1	3.9E-1	2.3E-1	7.0E-2	1.7E-2	2.2E-3	75.9
	March	0.10	0.74	8.4E-1	4.4E-1	2.4E-1	5.4E-2	6.7E-3	2.1E-4	64.3
	April	0.19	0.68	7.5E-1	2.9E-1	1.2E-1	1.7E-3	1.2E-4	2.0E-5	34.8
	May	0.10	0.87	8.0E-1	3.0E-1	1.1E-1	5.9E-3	7.3E-5	2.6E-8	27.9
	June	0.12	0.86	7.6E-1	2.2E-1	6.4E-2	1.9E-3	8.9E-6	6.0E-10	18.5
	July	0.13	0.71	8.1E-1	3.8E-1	2.0E-1	3.8E-2	4.2E-3	1.2E-4	48.8
	August	0.80	0.34	6.2E-1	2.3E-1	1.3E-1	4.5E-2	1.5E-2	4.0E-3	71.1
	September	0.40	0.42	7.0E-1	3.0E-1	1.7E-1	5.3E-2	1.5E-2	2.6E-3	68.3
	October	0.48	0.48	6.4E-1	2.2E-1	1.0E-1	2.2E-2	3.9E-3	3.7E-4	39.6
	November	0.04	0.96	9.0E-1	5.2E-1	2.7E-1	4.1E-2	1.8E-3	4.6E-6	47.5
	December	0.42	0.49	6.7E-1	2.5E-1	1.2E-1	2.8E-2	5.5E-3	5.7E-4	63.5

Run-on / Runoff

Episodic run-on and runoff (overland flow) has been observed at Yucca Mountain throughout the study period (1984-1995). Most of the overland flow observed within the three main watersheds overlying the potential repository area occurred on a very limited scale and for short durations. The most significant runoff events which involved widespread overland flow and channel flow occurred in 1984, 1992, and 1995. Streamflow data consisting of crest-stage and continuous-stage records were obtained for some of the runoff events (Pabst and others, 1993; Osterkamp and others, 1994). Major runoff events occurring in Fortymile Wash during 1992 and 1993 were also documented (Savard, 1995).

Both summer- and winter-type precipitation were observed to cause episodic runoff in various drainages during the 1984-95 study period. A severe summer storm during July of 1984 resulted in a flash flood in Pagany Wash (Britch, 1990). The duration of runoff was approximately 1-hour, during which most of the channel in this major sub-drainage was experiencing channel flow. In addition to field observations, moisture profiles obtained from neutron boreholes which had been recently installed in the wash provided indirect measurements of the runoff event. The

moisture profiles indicated rapid advance of the wetting front under saturated and near-saturated conditions to a depth of approximately 5 meters within a period of 1 to 2 days following the runoff. This event occurred during an active warm-season ENSO which had resulted in several smaller summer storms occurring previous to the storm causing the runoff. In addition to this wetter than average summer period, the ENSO had been unusually strong during the 1983-84 period, causing some of the wettest conditions measured in the Yucca Mountain region since 1940 (Hevesi and others, 1996; Philander, 1990). The 11-year records of moisture profiles obtained from most of the (98) neutron boreholes initially installed at Yucca Mountain indicated that comparatively wet antecedent conditions existed in surficial materials prior to the 1984 runoff event (Flint and Flint, 1995). Measurements of total daily precipitation at the nearest precipitation station indicated a total of 50 mm precipitation on the day of the runoff event (Britch, 1990). Assuming that most of the precipitation that resulted in runoff in Pagany Wash occurred during a convective-type summer storm having a duration of less than 1 to 2 hours, it can be assumed that the precipitation intensity exceeded the infiltration capacity of the unsaturated soils, which was likely to have been diminished by the wetter-than-average antecedent conditions. Unfortunately, more detailed measurements of precipitation and streamflow are not available for Pagany Wash during this important episode of runoff at Yucca Mountain.

A second important runoff event caused by a severe convective-type storm occurred in Abandoned Wash during August of 1991. As discussed previously, this storm resulted in some of the highest precipitation intensities recorded at Yucca Mountain during the 1984-95 study period (fig. 18a). Maximum intensities of 175 mm/hr were recorded during a 40-minute period over a very localized area centered on Abandoned Wash. Although detailed measurements of the spatial distribution of total precipitation resulting from this storm period were made (Hevesi and others, 1994a), neutron boreholes had not yet been installed in Abandoned Wash and streamflow measurements were not made. Streamflow measurements would have been very difficult for this event because of braided channel flow and the occurrence of major debris flows. The debris flow deposits and erosional features provided the field evidence that significant runoff had occurred in this wash (D. Bauer, written communication, 1992). For this runoff event, the record of moisture

profiles indicated that antecedent conditions at Yucca Mountain were comparatively dry, and thus overland flow was caused by the unusually high precipitation intensities which exceeded the infiltration capacity of the dry soils.

During 1992, the installation of crest-stage and continuous-stage streamflow gages at various locations on Yucca Mountain was initiated by the U.S. Geological Survey partly to help support work on understanding precipitation-runoff relations (D. Beck, written communication, 1992). Streamflow data were obtained for several episodes of runoff which occurred in various drainages (sub-drainages) during the winters of 1991-92, 1992-93, and 1994-95, all of which were years affected by an active cold-season ENSO. The largest runoff events occurred during the months of January and March in the winter of 1994-95, which included the wettest January recorded in 36 years. In contrast to the 1984 and 1991 summer runoff events, the 1995 runoff occurred in response to a higher frequency and longer duration of storms which created saturated antecedent conditions in surficial materials. Runoff in January 1995 occurred following six days of continuous precipitation, and runoff on March 11, 1995 occurred on the second day of a two-day storm event (fig. 18b). In both cases, maximum precipitation intensities were low compared to the intensities during the 1991 summer runoff event, but the duration and amount of total precipitation were much greater, and the antecedent conditions were much wetter. Field observations indicated that runoff during the winter of 1995 was generated when the precipitation intensity exceeded the storage capacity of the soils and the infiltration capacity of the underlying bedrock.

Streamflow hydrographs were obtained for gages in Wren Wash and Pagany Wash during the storm periods of January and March, 1995 (US Geological Survey, 1995). The preliminary hydrographs obtained for 3 continuous-stage gaging stations during the March 11 runoff event are indicated in figure 23. Runoff was measured at the Wren Wash gage beginning just before midnight on March 10 and increased steadily to a maximum of 30 cubic feet per second after approximately 2.5 hours, and then decreased steadily during the next 15 hours until runoff stopped. The gages in Pagany Wash measured a maximum flow of 50 to 55 cubic feet per second, however runoff was not measured until 1 to 2.5 hours after it was measured in Wren Wash because the gages

in Pagany Wash are relatively further downstream than the gage in Wren Wash. Runoff was measured at the lower Pagany Wash gage before it was measured at the upper gage because of runoff contributions to the lower channel from an adjacent ridge, which may have been enhanced due to the road on the top of the ridge. The rapid increase in measured discharge at the upper gage occurred approximately 45 minutes prior to the rapid increase in measured discharge at the lower gage, providing an important measure of the effects of channel geometry, channel roughness, and infiltration losses on the propagation of the flood-wave downstream. The duration and magnitude of flow at the lower gage is well correlated to the measured precipitation intensities (fig. 18b) when the flood-wave lag-time is accounted for. Although the flow at the upper gage is indicated as decreasing and stopping 5 to 7.5 hours prior to the flow measured at the lower gage, measurements at the upper gage were likely affected by channel erosion during the later part of the runoff event. In general, these hydrographs provide a lumped measure of the hydrologic response of catchments on Yucca Mountain to the spatial and temporal distribution of precipitation during a large winter storm, and can be used to help calibrate the various components of the water balance.

(Figure 23. Hydrograph for Pagany Wash and Wren Wash, March 11, 1995.)

Infiltration

Most precipitation infiltrates into the soil directly where it falls. Where there is exposed bedrock, local runoff occurs, but that water is quickly taken into the soils as they become thicker down slope (where the soil aggregates). Lateral flow following infiltration has been observed to occur along the soil-bedrock interface but has not been observed to occur beyond 10 meters in deep soils (Flint and Flint, 1996). The relation between infiltration and runoff can be tied to two concepts: infiltration capacity and total storage capacity. Runoff events in 1984 and 1985 were from summer thunderstorms during which the infiltration capacity was exceeded by the precipitation rate whereas the winter storms of 1992 and 1995 exceeded the storage capacity of the soil. Infiltration capacity (eq. 9), which varies with time and depends on initial-water content, is dependent on the sorptivity which is a function of water content. Sorptivity for an air-dry soil can be estimated using

an equation from Selker (written communication, 1995):

$$S = \sqrt{2K_s \psi_f n} \quad (15)$$

where K_s is saturated-hydraulic conductivity, ψ_f is wetting-front potential, which is calculated as twice the air-entry potential (1/alpha) from table 4, and n is porosity. The results of the solution to equation 15 for an initially dry soil are inserted into equation 9 and solved to determine the maximum infiltration capacity (fig. 24). Assuming that sorptivity goes to zero as the soil approaches saturation then minimum infiltration capacity is equal to the saturated-hydraulic conductivity of the soil (fig. 25). The maximum surface infiltration capacity of Yucca Mountain is generally around 300 mm/hr but ranges from 30 to over 500 mm/hr. For an initially dry soil fairly high precipitation rates would not generate runoff, at least for a short time. As an example the infiltration capacity as a function of time for soil model unit 5 is presented in figure 26. A hypothetical 100-mm/hr storm would not cause runoff for at least 10 minutes, but ponding would occur shortly thereafter. (The exact time cannot be determined from this analysis as equation 9 requires ponded conditions, and this should be considered a minimum time). Even assuming an initially dry soil, the summer precipitation event presented in figure 18a would cause runoff by the end of the storm. Under ponded conditions the infiltration capacity is below 50 mm/hr after an hour and reaches its minimum infiltration capacity within 4 hours and would likely cause runoff because of the high average intensity and duration of the summer storm.

(Figure 24. Map of maximum infiltration capacity into initially air-dry soil.)

(Figure 25. Map of minimum infiltration capacity.)

(Figure 26. Illustration of the change in infiltration capacity for soil model unit 5 with time, related to precipitation rate and minimum infiltration capacity.)

Generally, the surface materials of Yucca Mountain have an average minimum infiltration capacity of approximately 30 mm/hr, but the infiltration can be as little as zero on bedrock exposures to 90 mm/hr in the channel materials (fig. 25). Runoff would occur during a storm

exceeding 30 mm/hr, such as that presented in figure 18a, if it was persistent enough to cause the soil-water content to approach saturation. The relatively high-intensity winter storm in figure 18b did not exceed 15 mm/hr, which is half of the average minimum infiltration capacity for the Yucca Mountain area (fig. 25) and would not have caused runoff by exceeding the infiltration capacity. In general, most winter precipitation is less than the average minimum infiltration capacity and only causes runoff if the total soil water storage is exceeded. The total soil water storage is calculated as the soil porosity multiplied by soil depth. Another useful term is the field capacity of the soil, (generally taken as the maximum amount of water held in the soil against gravity), multiplied by soil depth. Field capacity, which is calculated as the soil-water content at -0.1 bars (table 4), ranges from 7.3 percent to 24.2 percent (table 4, fig. 27), and when multiplied by the depth to bedrock (fig. 13) produces a range in field storage capacity between 0, for exposed bedrock, to 1.2 m for thick soils (fig. 28). Soils tend to reach field capacity fairly quickly as excess water drains off. After field capacity is reached water will continue to drain but fairly slowly. Precipitation added to a soil already at its field storage capacity can still be stored up to the total soil water storage capacity but beyond that runoff must occur.

(Figure 27. Map of field capacity of surficial soils.)

(Figure 28. Field storage capacity of soils calculated as field capacity multiplied by soil depth.)

Evapotranspiration

Measurements of potential evapotranspiration using a Class A pan have been made for several years. Although not directly applicable to estimating actual evapotranspiration the data show that advective conditions exist at Yucca Mountain since measured pan evaporation exceeds calculated potential evaporation (calculated using eq. 12) by almost 100 percent (fig. 29). There is also considerable variability in pan evaporation due to the variability in cloudiness, humidity and atmospheric turbidity. Measurement of actual evapotranspiration in arid climates is a more challenging endeavor. The low availability of water and the small gradients make many techniques (i.e. Bowen ratio) problematic. Some success using eddy correlation instrumentation have made the

technique look promising but requires an intensive field program. For the most part, inverse modeling the neutron hole data against a specified evapotranspiration equation has had the most success but is limited by the assumptions of the model, assumptions about available energy, assumptions concerning changes in moisture profiles measured at monthly time intervals, and the errors in the neutron hole data.

(Figure 29. Measured evaporation pan data and calculated potential evapotranspiration using energy balance for 1991-1993.)

Redistribution

Redistribution is an important process to understand in order to determine if infiltrating water becomes net infiltration. There are several ways to evaluate redistribution in the surface soils and bedrock at Yucca Mountain. Monthly neutron hole logging and analysis of the resultant changes in water content profiles has been used to provide a temporal and spatial distribution of redistribution. Geochemical analysis of chloride (Cl), bomb-pulse ^{36}Cl and bomb-pulse tritium (^{3}H) has also been evaluated.

Neutron hole moisture profile analysis

The analysis of moisture profiles in 99 boreholes from the four topographic positions at Yucca Mountain included both quantitative and subjective methods and represented a large areal coverage over a 9-year period of time (Flint and Flint, 1995). Analyses of the measured profiles indicated that the thinner the soil cover, that is, storage capacity, the deeper the measured increase in volumetric water content, indicating greater net infiltration, which is especially evident when surface flow concentrates runoff at locations underlain by fractured bedrock (fig. 30). The more deeply the water penetrates, the less likely that it will be lost to evapotranspiration. When surface

flow is negligible, the deepest infiltration was on the ridgetops and the shallowest infiltration was in the washes, although there is little difference in infiltration characteristics between the terrace and channel boreholes. Exceptions were noted, however, following appreciable runoff events. For these cases, large volumes of water often infiltrated more than 5 m into the soil in the washes, which is below the estimated root zone. At these sites, however, conditions causing significant channel runoff occurred episodically and only in a few washes during any single event. In addition, the active channels where runoff occurs comprise less than 2 percent of the surface area of the watersheds and therefore are not considered to contribute significantly to overall net infiltration in the watershed. More precipitation infiltrates during the winter when the evapotranspiration is low and runoff occurs rarely, due to lower-intensity storms and to slowly melting snow on the ridgetops for several weeks each winter. This slow rate of input over long time periods allows for larger volumes of water to penetrate below the root zone and thereby escape the high evapotranspiration demands of the following summer.

(Figure 30. Average depth of penetration of the wetting front for years 1990-1993 and soil depth for 34 boreholes (Flint and Flint, 1995).)

Shallow infiltration processes at Yucca Mountain were categorized into four zones that generally can be identified on the basis of the manner in which volumetric water contents change with depth and time. The zones are described as follows: (1) The ridgetop is flat to gently sloping, higher in elevation and has thin soils mostly developed in place with clays and a higher water-holding capacity that reduces rapid evaporation and drainage. The ridgetops generally are located where the bedrock is moderately to densely welded and, therefore, fractured. These conditions lead to deeper penetration of infiltration pulses than in the other topographic positions, but relatively smaller volumes of water. In some locations, however, where runoff is channeled, large volumes of water can infiltrate. (2) Sideslopes are steep, commonly have very shallow to no soil cover, and are usually developed in welded, fractured tuff which creates conditions conducive to rapid runoff. The low storage capacity at the surface and the exposure of fractures at the surface can allow small volumes of water to infiltrate to greater depths, especially on slopes with north-facing exposures

and, therefore, lower evapotranspiration demands. Shallow soil at the bases of the slopes can easily become saturated and initiate flow into the underlying fractures. (3) Soil terraces are flat, broad deposits of layered rock fragments and fine soil with a large storage capacity. There is, therefore, little runoff and little movement of water to any depth in the profile before evapotranspiration removes it. Consequently, this zone contributes the least to net infiltration in the watershed. (4) Active channels differ little from the terraces but are located in a position to collect and concentrate runoff which, although it occurs infrequently, can then penetrate deeply. However, this mechanism is not considered to be a major contributor to aerially distributed net infiltration because of the infrequency of precipitation resulting in runoff and because the channels encompass a very small percentage of the watershed area may be significant for localized pulse of net infiltration.

There are numerous heterogeneities and exceptions to this categorization. In general, however, changes in moisture profiles over time measured at a borehole tend to be characterized by the model zone in which the site is located. In an environment that has a high evaporative demand, it is more important to assess the depth of water penetration than the volume of water entering the profile in order to estimate net infiltration. This penetration is influenced by the potential for surface storage (depth of soils, layering and caliche, slope and aspect), the timing of the precipitation (winter or summer), the presence of fractures, and the degree of saturation of the wetting front when it reaches fractured bedrock.

The influence of redistribution following channel runoff is clearly evident in the neutron probe data. Figure 31 presents almost ten years of neutron probe data from N1 showing the periodic penetration of a wetting front following winter precipitation. There is also a large pulse of water following the runoff event in 1995. The initially high water contents in the soil profile can be related to the runoff event in 1984, prior to the drilling of the borehole. It appears to take over 6 years to come back to an equilibrium condition following the runoff (fig. 31).

Redistribution in bedrock directly under a shallow (0.7 m) soil channel clearly shows a wetting front moving slowly to over 15 m (fig. 32). The total increase in borehole water storage

below 3 m was equivalent to 500 mm of water in 1995. If roots fail to penetrate to greater than 3 m then this water would be considered to be net infiltration. Two nearby boreholes (N36 and N17), in the same geologic materials, show similar patterns of redistribution but with a lower volume due to the lack of surface runoff. The total increases in borehole water storage below 3 m were equivalent to 150 mm and 110 mm, respectively, in 1995. These values are considerably lower, but likely more typical of the soil thickness and underlying rock type for the general topographic area (away from the small channel). This is a measure of water that has imbibed into the matrix and is detectable by the neutron probe. Additional water may have penetrated to greater depths through fractures but is not indicated in the neutron hole profile.

(Figure 31. Changes in water content over time and depth for borehole USW UZ-N1.)
(Figure 32. Changes in water content over time and depth for borehole USW UZ-N15.)

Geochemistry analysis

Geochemistry data provides additional insight into the infiltration and redistribution at Yucca Mountain. In particular, chloride concentrations and $^{36}Cl/Cl$ ratios provide information about the characteristics of water movement. The chloride mass-balance technique :

$$P\ C_o = I_n\ C_p \qquad \textbf{(16)}$$

where P is average annual precipitation (assumed to be 170 mm/yr), C_o is average chloride concentration in precipitation (assumed to be 0.62 mg/L), which includes dry fallout, C_p is the average chloride concentration in porewater (measured at a specific location) and I_n is the net infiltration rate (calculated from eq. 16). The major assumptions in the chloride mass-balance approach are: one-dimensional, downward, piston flow, a well-mixed soil-water reservoir, no run-on or runoff and constant average annual precipitation and Cl deposition rate. Although these assumptions may not be valid, there is a relative usefulness in comparison of different areas. Calculated infiltration rates using this approach assumes the assumption hold but are referred to as

apparent flux.

Chloride mass-balance calculations (table 7) determined using soil and rock samples from Fabryka-Martin and others (1994) suggest that apparent flux under an soil terrace (UZ16), an inactive old channel (N54), and a moderately-active channel (N37), are 0.02 mm/y, 0.02 mm/yr and 0.5 mm/yr, respectively. Mass-balance calculations using rock samples from the PTn and the CHn (Calico Hills nonwelded) yield much higher fluxes. Flux estimates in the PTn and the CHn directly under the soil samples at UZ16 yield apparent fluxes of 3.0 mm/yr and 3.5 mm/yr. Flux estimates in the PTn under N54 is 3.3. This difference may indicate that some lateral redistribution of higher fluxes in the nearby sideslopes occurs by the time the water reaches the PTn. The flux estimates for the PTn under N55, a south-facing slope, and N53, a north-facing slope, which are on opposite sides of the terrace in which N54 is located, yield 2.4 and 3.3 mm/yr respectively, again indicating that the flux may be redistributed by the time it reaches the PTn.

Table 7. Infiltration fluxes estimated by the chloride mass balance method (adapted from Fabryka-Martin and others, 1994) with a comparison of point and areally averaged estimates of net infiltration.
[m, meter; mm/yr, millimeters per year; borehole locations can be found in Appendix II]

Borehole	Unit	Depth interval (m)	Apparent flux (mm/yr)	Point estimate of net infiltration (from figure 45)	3600 m^2 areal average of net infiltration (from figure 45)
USW UZ-N37	Soil	0-13	0.5	0.0	0.0
USW UZ-N53	PTn		3.3	6.1	2.9
USW UZ-N54	Soil	0-7.8	0.02	0.0	0.0
	PTn		3.3		
USW UZ-N55	PTn		2.4	0.6	0.3
USW UZ-N11	PTn		3.2	3.3	3.1
UE-25 UZ#16	Soil	0-7.4	0.02	0.0	0.0
	PTn	50-55	3.0		
	Calico Hills	368-440	3.5		

USW UZ-14	PTn	44-75	1.2	7.3	3.1
	Calico Hills	470-477	5.9		
UE-25 UZ#4	PTn	91-96	1.1	5.0	2.5
UE-25 UZ#5	PTn	29-36	2.5	5.0	2.9
	PTn	94-97	1.4		

Flux estimates under an soil terrace (UZ14) yields flux estimates of 1.2 in the PTn and 5.9 in the CHn. The difference may be related to the lateral redistribution of higher fluxes in the nearby sideslopes into the PTn. However, the higher flux in the CHn is likely related to the higher flux coming from the perched-water body above the CHn indicating that less than 20 percent of the water comes into the perched-water body through the soil terrace and the underlying PTn (at that location). Directly under an active channel (UZ4) flux estimates are 1.1 mm/yr in the PTn and under a nearby borehole (UZ5) located at the terrace-sideslope interface, flux estimates are 1.4 to 2.5 mm/yr in the PTn (table 7). The lower than expected values directly under the channel may be explained possibly by lateral redistribution of water before it reaches the PTn, or simply by lower infiltration rates under the channels than expected. (Discussion of the model estimates of net infiltration included in table 6 will be discussed under the modeling section).

Results from $^{36}Cl/Cl$ ratios provide additional estimates of infiltration by evaluating the shape and magnitude of the of the bomb-pulse profile and the depth to the center of mass of the ^{36}Cl bomb pulse in soils. Norris and others (1987) measured the peak ^{36}Cl at 0.5 m and estimated a flux of 2 mm/yr averaged over 35 years in a soil terrace in Yucca Wash. Tyler and others (1996) present ^{36}Cl data and suggest that the infiltration waters are recycling with the root zone (0-2 m). Fabryka-Martin and others (1994) find the center of mass of the ^{36}Cl to be much deeper than that of Norris and others (1987): 3.3 to 4.8 m for N37 and 2.1 to 3.0 m for N54. Because N37 is in a more active channel than N54 the differences should be expected. The depth of penetration of the center of mass for the ^{36}Cl for N37 and N54 yields an estimate of 10 to 15 mm/yr and 6 to 9 mm/yr respectively. These are considerably higher than that calculated from the chloride mass-balance

technique but can be explained by a somewhat deeper penetration of a wetting front following a runoff event, but the lack of significant penetration beyond the root zone (pulses of water can penetrate 3-4 m within days after a runoff event but most is extracted by evapotranspiration).

Bomb pulse ^{36}Cl is found at much greater depths in boreholes overlain by thin soils. Bomb-pulse ^{36}Cl was found to the total depth (18-25 m) of boreholes N15, N16, N17 and N11 (fig. 33), which have less than 2 m of soil cover. Although net infiltration values cannot be determined from the presence of ^{36}Cl in fractured rock, it is important to realize that fast flow through the fracture network in the surface tuffs can occur when the soil-tuff interface is saturated and fracture flow is initiated.

(Figure 33. Saturation, porosity and $^{36}Cl/Cl$ ratios for boreholes USW UZ-N15, USW UZ-N16, USW UZ-N17 and USW UZ-N11. ^{36}Cl data is indicated for depth ranges as between pairs of points.)

Three boreholes, in particular, demonstrate the conceptual model of infiltration in deep and shallow soils as well as the influence of faults on the penetration of net infiltration deeper into Yucca Mountain. Boreholes N53, N54 and N55 are located on a north-facing slope overlain by 0.5-m of soil, a channel terrace overlain by 10-m of soil and a south-facing slope overlain by 0.5-m of soil, respectively. The PTn in borehole N55 is faulted in one and possibly two locations and has measured bomb-pulse ^{36}Cl throughout the PTn and into the Topopah Spring Tuff (fig. 34). Borehole N53 has no evidence of a fault and has bomb-pulse ^{36}Cl well past the middle of the PTn, but which failed to reach the Topopah Spring Tuff (fig. 34). Borehole N54 has such thick soil that the bomb-pulse ^{36}Cl failed to penetrate below about 3 meters in the soil profile (fig. 34). Hudson and Flint (1996) suggest that fast pathways from the surface may simply be faults which allow water to pass more quickly through the PTn. The full penetration of ^{36}Cl in the faulted borehole, N55, and only partial penetration of an unfaulted borehole, N53, supports this hypothesis. The lack of any penetration in the borehole with thick soil cover, N54, also supports the hypothesis proposed by Hudson and Flint (1996) that fast pathways cannot exist from the surface under thick soil cover

unless sufficient flow concentration occurs.

(Figure 34. Saturation, porosity and $^{36}Cl/Cl$ ratios for boreholes USW UZ-N53, USW UZ-N54 and USW UZ-N55. ^{36}Cl data is indicated over a depth range.)

Flow at the soil-bedrock interface

Several years of neutron probe measurements of water content (i.e. fig. 30, fig. 32) indicate that periodic fracture flow is initiated when the soil becomes saturated or nearly saturated at the interface. Fractures filled with calcium carbonate may carry less volume of water but can flow under drier conditions and therefore may carry water for longer periods of time due to the lower air-entry potential. Thicker soils (>3 meters) overlying the fractured bedrock store water and retard the penetration of the wetting front (i.e. fig. 30, fig. 31). Evapotranspiration can then remove infiltrating water before fracture flow can be initiated.

The existence of boreholes in the fractured tuffs may introduce additional fractures or enhance the flow in the existing network causing an overestimate of fracture flow and, therefore, net infiltration. An independent line of evidence for the estimate of net infiltration was developed using one year of water-potential measurements from heat-dissipation probes at the soil-bedrock interface (fig. 35a). Measurement were made at 4 depths: 7, 15, 36.5 and 73.7 cm (which is at the soil-tuff interface). Within two weeks of installation (February, 1995) heavy winter precipitation saturated the soil-bedrock interface to within 36 cm of the soil surface (note that in early March the heat-dissipation probe at 36.5 cm was saturated as well as the probe at 73.7 cm). The probe at the soil-tuff interface remained saturated until the end of March then dried out to < -10 bars by September. The probes closer to the surface dried out faster with the near-surface probes wetting up periodically due to summer precipitation events. The absolute value of water potential beyond -100 bars is questionable but provided a relative indication of drying conditions.

The water-retention curve for this location (soil model unit 5) was used to convert water

potential to water content. The water content of the profile was calculated and is presented in figure 35b. A series of selected data were chosen and the rate of water loss was calculated between the dates using the change in water content. In early March the profile was changed at a rate of over 10 mm/day but dropped to less than 2 mm/day within 30 days. The evaporation rate was estimated to be no more than 2 mm/day based on potential ET calculations using the Priestley-Taylor equation, yielding a maximum flux into the bedrock of 8 mm/day. The average flux for 30 days averaged 5 mm/day to yield a total flux into the bedrock of 150 mm. The estimate for the nearby borehole (N17) by Hudson and Flint (1996) is 110 mm for the same time period. The saturated-hydraulic conductivity, including the 250-um filled fractures, estimated in Table 2 for this location is 0.322 mm/day (GIS code 17, Tiva Canyon Tuff, caprock) which is far exceeded by the 8 mm/day. Fractures in a nearby exposure are mostly unfilled and the assumption of filled fractures to produce figure 11 may not be appropriate and should be further evaluated.

(Figure 35. Water potential measurements near borehole USW UZ-N15 using heat dissipation probes, a) measured at 4 depths for 1995 and b) used to calculate flux.

The amount of infiltration that penetrates the soil-bedrock interface is determined by the balance between the timing of evapotranspiration and gravity drainage at the soil-bedrock interface. Occurrences of high-frequency, high-magnitude winter precipitation, combined with sparse vegetation and a shallow soil cover over fractured bedrock, provide conditions which can lead to a substantial amount water penetrated the soil-bedrock interface over a limited time period.

Net infiltration

Net infiltration is temporally and spatially distributed and occurs at different depths in the soils and bedrock on and around Yucca Mountain. It is a function of the depth of the root zone and the time and distribution of precipitation. Water penetrating below 2 m in bedrock cannot be easily removed by ET due to a lack of plant roots. In soils, where plant roots have been observed to penetrate up to 5 m, water can be removed to that depth. It is assumed that in deep soils, water that

penetrates below a depth of 6 m becomes net infiltration, although that depth may be shallower. Roots have been estimated to penetrate up 2 m in the fractured bedrock underlying shallow soils (< 0.5 m) (Hanson and others, written communication, 1995). It is, therefore, assumed the water that penetrates more than 2 m into the bedrock becomes net infiltration. In moderately-deep soils (5 to 6 m) it is indeterminate at what depth into the bedrock roots may penetrate and therefore what depth water becomes net infiltration. Plant rooting is a dynamic function that depends on the specific location of the plant and the climatic history. Several years of drought removed much of the vegetative cover over Yucca Mountain and therefore the depth of penetration of a wetting front to become net infiltration could be considerably less. Gradual recovery of the vegetative cover would likely deepen that depth. Because of the dynamics of the root zone, similar precipitation patterns occurring during different years, may yield very different net infiltration values depending on the specific vegetative cover that developed over the preceding several years.

NUMERICAL MODEL

The basic process of developing a numerical water balance model at Yucca Mountain is to: 1) correctly apply the physics of the water-balance processes to arid climates, 2) define the physical setting (i.e., slope, aspect, soil properties, rock properties, vegetation, etc,) as adequately as possible, 3) calibrate the model by matching observations and data to model output as much as possible without altering, beyond reason, physics and physical setting and 4) perhaps the most important step is to test the model and model assumptions against data independent of the calibration data, and 5) run the model for all geomorphic or topographic positions, soils and climates to see how the system responds in areas that we have no data and under climates that have not been observed. This fourth step has only been done for limited cases and therefore the following models should only be considered as preliminary.

The program INFIL (appendix V) is a FORTRAN 77 computer code that is designed to produce an estimate for net infiltration for any location within the USGS/LBNL expanded 3-dimensional site-scale model boundary. The programs require two external data sets specific to the

location being modeled. One data set contains physiographic and hydrologic information (physical data set) for the site and the other data set contains estimates or measurements of daily precipitation (precipitation data set). This physical data set requires location identification, northing, easting, slope, aspect, elevation, latitude, longitude, soil type, soil depth, underlying geologic formation, geomorphic position and the location of the surrounding topography that blocks the site for diffuse or direct-beam solar radiation. Using this information as input, the model will calculate daily values of net infiltration using a water-balance approach but will not solve the water-balance equation (eq. 2) directly. The solution to net infiltration is described in the following sections.

The program is based on a model of solar radiation which is used to drive the evapotranspiration function. The radiation load is calculated based on slope, aspect, elevation, latitude, longitude and surrounding topography. The site specific data of soil type and underlying geologic formation are converted to hydrologic parameters using lookup tables within the program. The programs uses a mass balance approach partitioning of the input function of precipitation and then calculates runoff, evapotranspiration, change in storage and net infiltration, which is based on the soil hydrologic properties, soil depth and the hydrologic properties of the underlying bedrock. There are two submodels that are user selectable called BUCKET and RICHARDS. The submodel BUCKET simplifies the modeling of redistribution in the soil profile, as discussed in following sections, to decrease computer run time and allow more analysis of changing climatic conditions whereas the submodel RICHARDS uses Richards equation (eq. 7) to model soil-moisture content with depth and allows for more detailed understanding of soil layers and the role for fractures.

Precipitation

The program PPTSIM (appendix IV) was developed to provide stochastic simulations of daily precipitation at a point location. The stochastic precipitation model consists of a pseudo-random number generator which provides a normalized uniform deviate for a two-step process of simulating daily precipitation. The first step uses a 3rd-order two-state Markov chain process to determine the occurrence of daily precipitation and the second step uses a modified, exponential,

cumulative-probability-distribution function to determine the magnitude of daily precipitation. This model can either be run separately to provide an input file of simulated precipitation or can be incorporated as a subroutine in the infiltration program. The model requires an input file which contains the simulation seed (any prime number), 16 of the 32 Markov transition probabilities, and the coefficients for the modified, exponential, cumulative-probability-distribution function. As discussed previously, 32 Markov transition probabilities were defined separately for each month and the coefficients for the probability distribution function were defined for 4 seasons using the program MARKOV (appendix III). A total of 100 separate 100-year stochastic simulations, or realizations, were generated using the sample statistics for the record at station 4JA, which is the closest station to Yucca Mountain that has a record of daily precipitation longer than 30 years. The simulation provided an average-annual precipitation amount of 131 mm and a maximum daily amount of 100 mm, which are in good agreement with the measured average annual amount of 133 mm and the measured maximum daily amount of 89 mm. The stochastic simulations were corrected for elevation to provide a simulated record consistent with estimates of average-annual precipitation at Yucca Mountain (Hevesi and Flint, 1996). A single 100-year simulation for Yucca Mountain is presented in figure 36a indicating an average-annual precipitation of approximately 165 mm/yr. Stochastic simulations were also generated using sample statistics obtained for station Area 12 (fig. 36b), located at an elevation of 2,316 meters in the northern part of the NTS, approximately 50 km northeast of Yucca Mountain. The simulation provided an average-annual precipitation amount of 332 mm, a maximum annual total of 600 mm, and a maximum daily total of 108 mm. The Area 12 simulation was used to represent potentially wetter climatic conditions at Yucca Mountain. This is an improvement over simply increasing precipitation intensity by scaling the 4JA simulations (in addition to the elevation adjustment) because the Area 12 simulation provides an increase in both the intensity and the frequency of precipitation, and this is considered to be more representative of wetter climatic conditions.

(Figure 36. One hundred-year stochastic simulations of precipitation at a) Yucca Mountain and b) Area 12.)

These simulations do not include spatially distributed data. Although spatially distributed simulations can be generated by using data input from any available station there is no link in the simulation between one location and another. For example, if stochastic simulations were performed using temporally and spatially independent simulations for each of the nodes comprising the 30-meter grid spacing of the model, daily precipitation would be generated somewhere within the study area for each day simulated, and the probability of generating precipitation throughout the entire study area would be extremely small. To provide acceptable simulations of precipitation that are spatially distributed over the 30-meter grid, the spatial correlation of precipitation on the scale of the modeling domain must be accounted for. Although work is continuing, a temporally and spatially integrated simulation has not yet been completed. For this study, a uniform spatial distribution of precipitation that is adjusted to orographic effects using an empirical scaling function is applied to the stochastic simulation of daily precipitation at one point. Daily precipitation values are scaled to the elevation of the surrounding area using the relation between elevation and average-annual precipitation (Hevesi and Flint, 1996), which leads to approximately a 1 percent change in precipitation for every 14 meters change in elevation. Spatially, then, each simulation looks like a topographic map with the precipitation values depending on the daily value for the individual stochastic simulation (fig. 37). For central Yucca Mountain there is less than a 5 percent change in precipitation between the ridge tops and the wash a bottoms. Although this simplification may be at least somewhat valid for winter precipitation, it does not provide a very realistic representation of the much higher degree of spatial variability and the comparatively poor correlation with physiography observed for summer precipitation on the scale of the modeling domain (Hevesi and others, 1994a). In addition, simulations of total daily precipitation are likely to be poor representations of summer storms which tend to have durations less than 1 hour but can produce high-intensity precipitation for short durations (Hevesi and others, 1994a). Under such conditions, channel runoff may be generated in the 1-hour time period, but would not necessarily be generated if the 1-hour storm intensity was averaged over a 1-day period. Since winter precipitation is much more important in determining net infiltration the error associated with this assumption is acceptable at this time. Further development of a spatially variable stochastic model will help resolve some of the problems.

(Figure 37. Average annual precipitation distributed spatially using an elevation correlation.)

Run-on/Runoff

A numerical model of surface runoff for the Yucca Mountain area is being developed by modifying and/or directly incorporating subroutines and parts of subroutines obtained from the KINEROS program, which is an event-based, distributed, finite-difference model of kinematic overland flow and sediment transport (Woolhiser and others, 1990). The model calculates overland flow and stream discharge in response to precipitation, infiltration, watershed and channel geometry, and surface roughness factors. The KINEROS model is an event-based program where redistribution and evapotranspiration following precipitation events are not accounted for. Both the BUCKET and RICHARDS submodels are continuous models which account for changes in soil moisture due to evapotranspiration and net infiltration, which in turn provide the antecedent conditions for the following precipitation event. In most cases, significant overland flow does not occur in response to precipitation at Yucca Mountain, and the routing of excess precipitation is not required. However, for an accurate modeling of net infiltration beneath channels, episodic runoff events must be accounted for, and a method is needed for routing excess precipitation into channel areas.

In the first approach presently used in the model, excess precipitation is accumulated as a storage term for each grid element and the spatial distribution of excess precipitation is analyzed. Excess precipitation can also be modeled as a moving storage term in both the BUCKET AND RICHARDS submodels. If excess precipitation is generated at a grid element, this volume is transferred during the following time step to adjacent elements having lower elevations at a rate determined by the calculated slope and aspect as well as estimates for roughness coefficients. The flow rate is added to the precipitation input term for the downstream element, which in turn may generate more excess precipitation if the field capacity for that element has been exceeded. The time steps must be on the order of minutes or hours rather than days for a representative routing of excess precipitation. In an alternative approach, the KINEROS model is called as subroutine during

days having significant excess precipitation being generated at grid elements. The subroutine determines the total discharge from the watershed or the modeling domain at the end of the time step and the simulations of infiltration or channel loss is used as input to the BUCKET or RICHARDS submodels for the next time step. The output from either the BUCKET or the RICHARDS submodel is then used to reset the proper water contents and excess precipitation amounts for the KINEROS model. The sequence is repeated for the length of the model run. A third approach to modeling overland flow as part of a continuous model for determining net infiltration is to fully integrate the kinematic-wave governing equation to all grid elements in the modeling domain. With the exception of the first approach, the other methodologies for modeling overland flow as a part of the BUCKET and RICHARDS submodels were still in a developmental and testing stage at the time this report was written.

Infiltration

All precipitation is modeled as infiltration except when the storage capacity of the soil is exceeded and runoff occurs. In the submodel RICHARDS all precipitation is put into the first 10-cm element. If storage capacity is exceeded then runoff occurs (as mentioned above). In the submodel BUCKET all precipitation is put into the entire soil profile. The analysis of rate of rainfall versus infiltration has not yet been incorporated into the numerical model. Incorporation of a rate of rainfall into the stochastic rainfall model and the submodels RICHARDS and BUCKET will be done at a later time.

Evapotranspiration

Solar radiation

The solar radiation subroutine is the basis for a spatially distributed evapotranspiration model. The subroutine is essentially the model SOLRAD of Flint and Childs (1987). The model

uses detailed site geometry and atmospheric properties. The site geometry includes latitude, longitude, slope, aspect, elevation, and angle about a horizontal surface of the ridges that block the sky from direct-beam or diffuse radiation. The atmospheric inputs are ozone, precipitable water, atmospheric turbidity, circumsolar-diffuse radiation, and ground albedo. These values are input as monthly averages. The position of the sun is calculated every 1 hour starting at sunrise on each day. Direct-beam and diffuse sky radiation are then calculated based on the atmospheric input parameters and applied to the surface based on the slope and aspect. Diffuse sky radiation is reduced by that amount of sky which would be blocked by the surrounding topography. The direct beam radiation is also blocked when the solar position would be behind the surrounding topography. Ground-reflected radiation is added to the site based on the area of the surrounding topography, the ground albedo and the direct-beam and diffuse sky radiation that reflects from the surrounding topography.

Modified Priestley-Taylor equation

Evapotranspiration is modeled by modifying the Priestley-Taylor equation (eq. 12) where α is replaced with α' which is modeled as:

$$\alpha' = \alpha \, (1 - e^{\beta\Theta}) \tag{17}$$

where α is taken as 1.27, β is a fitting parameter set to -1.5 and Θ is relative saturation:

$$\Theta = \frac{(\theta - \theta_r)}{(\theta_s - \theta_r)} \tag{18}$$

where θ is soil-water content, θ_s is porosity, θ_r is residual saturation for plant transpiration (soil-water content at -60 bars water potential, which is the approximate mean minimum xylem potential for the plants in table 5). The parameter $S/(S+\gamma)$, extracted from Table A.3 in Campbell (1977), is modeled as:

$$\frac{S}{(S+\gamma)} = -13.281 + \frac{0.083684}{K} T_a - \frac{0.00012375}{K^2} T_a^2 \quad (19)$$

where T_a is air temperature, in degrees Kelvin, and is modeled as a daily mean as:

$$T_a = \left(17.3 - 11.74 \; SIN \left(\frac{DN}{366} * 2 * \Pi + 1.3 \right) \right) + 273.15 \quad (20)$$

where DN is the day of the year. Net radiation (R_n, w/m^2) is modeled as:

$$R_n = -71 + 0.72 * K\downarrow \quad (21)$$

where K↓ is incoming solar radiation (w/m^2). Soil-heat flux (G, w/m^2) is modeled as:

$$G = -20 + 0.386 \; R_n \quad (22)$$

The evapotranspiration is solved on an hourly basis and summed over the period of one day, and the change in water content (θ) is updated at the beginning of the next day. This modification of the Priestley-Taylor equation allows for the soil-water content to limit evapotranspiration. If moisture conditions change due to precipitation then α' approaches 1.26 allowing evapotranspiration to approach the equilibrium evaporation rate. In this preliminary model a leaf-area index term has not been applied as would be appropriate (Stannard, 1993). Instead, the parameters in equation 17 were set to average vegetation values. A dynamic plant function which changes leaf-area index under water excess or deficient would improve the application of the model under changing climate regimes (future-climate scenarios). For a fully vegetated surface α would still be set to 1.26 but β would vary from between approximately -1.0 and -10.0.

Following the methodology presented by Hevesi and others (1994b), actual ET is simulated for each element in the RICHARDS submodel by applying the modified Priestley-Taylor equation to the relative saturation obtained at each time step, and multiplying this result by the root-zone weight obtained for each element to calculate the actual ET rate for each element. Figure 38

indicates daily ET simulation results calculated as the average for the total ET obtained for the locations of the 90 neutron boreholes used for model calibration. The simulation was obtained using the developed Yucca Mountain daily-precipitation record for 1980 through 1990. The results indicate the general seasonal variability in ET along with considerable inter- and intra-annual variability due to variability in the frequency and magnitude of storms which determines the amount of moisture available for ET. Maximum daily ET rates of more than 1.5 mm were simulated during the wettest years of 1983 and 1995. Minimum daily ET rates of less than 0.1 mm were simulated in the winter of 1990 following a period of drought.

(Figure 38. Simulated daily evapotranspiration for Yucca Mountain using 15 years of measured precipitation simulated at 90 neutron boreholes.)

In the RICHARDS submodel, the alpha coefficient in the modified Priestley-Taylor equation can also be defined as a depth- and/or time-dependent function (Hevesi and others, 1994b). For example, the modified Priestley-Taylor equation can be defined as a seasonally-dependent function to represent active and dormant stages in plant communities during the annual cycle, adjusted to depth to allow for differences in active versus dormant cycles between shallow- and deeper-rooted plants. The combination of these various options for representing the root zone provides a wide range of flexibility in modeling ET using the RICHARDS submodel. The disadvantage of increasing the flexibility of the model is that the number of parameters which must be defined or calibrated also increases. The parameters and equations comprising the ET module used in the RICHARDS submodel are defined in the following section on redistribution.

Redistribution

Redistribution is calculated differently for the two infiltration models. In the submodel BUCKET, redistribution is calculated instantaneously (every 24 hours) and is averaged over the entire soil profile. For the shallow soil which covers most of the potential-repository area this is probably acceptable during heavy precipitation events and probably unimportant for light events.

For deeper soils this method has a tendency to move water deeper than would be expected but does not lead to increases in net infiltration. Simulations of ET using the BUCKET submodel may also be inaccurate because the distribution of moisture throughout the soil profile is not accounted for. For example, ET should be greater for soils having moisture concentrated in the top of the profile versus the bottom of the profile. For soils which are only 0.5 meters deep, this inaccuracy is not likely to be significant as compared to other processes being simulated by the BUCKET submodel over simulation times of 10 years and longer.

In the RICHARDS submodel, vertical redistribution is simulated using a one-dimensional finite-difference approximation of the Richards governing flow equation (eq. 7). The model domain consists of a 10-m deep profile discretized into 0.10 m equidimensional elements for each location. Elements are assigned soil or rock material properties based on the soil-depth class and material-property parameters designated for each location (tables 2, 4). Initial conditions for all elements are defined using an assumed constant potential of -1 bar (100 J/Kg) for the entire profile. The upper boundary of the profile is defined as an impermeable (no-flow) boundary while the lower boundary is defined as a constant-potential boundary using the initial conditions of -1 bar. Following the example provided by Campbell (1985), the non-linear partial-differential governing flow equation is solved for each time step using Newton-Raphson iteration and the Thomas algorithm. The vertical redistribution profile is linked to the water-balance equation using specified flux terms in the governing flow equation:

$$\frac{\partial \theta_v}{\partial t} = \frac{\partial}{\partial z}\left(K(\theta)\frac{\partial(\psi_m + \psi_z)}{\partial z}\right) + PPT - ET + FRAC_{in} - FRAC_{out} - POND \qquad (23)$$

where PPT is simulated or measured precipitation, ET is the simulated evapotranspiration volume converted to a constant flux for the given time step, $FRAC_{in}$ is the flux from fractures into rock matrix, $FRAC_{out}$ is the flux into fractures from either the soil or the rock matrix, and $POND$ is the flux to a storage term for excess precipitation, which in the RICHARDS submodel becomes the

source of runoff. The *PPT* source term is defined as a constant flux term for the top element only. Precipitation intensity is calculated as the average 24-hour rate using the simulated or measured values of total daily precipitation. Thus, the *PPT* source term provides a constant input flux for the entire day for each day precipitation occurs. As discussed previously, all precipitation is assumed to infiltrate to 0.1 meters as long as the storage capacity is available in the top element.

The ET source term is calculated for all elements in the root zone using equation 17 and the root-zone weighting model, which are both dependent on the water contents simulated during the previous time step for each element in the root zone. The root-zone weighting model is dependent on the relative saturation calculated using the simulated water content θ_i and the residual water content θ^R_i for each element I in the root zone using a dynamic conditioning function:

$$W_i^D = \frac{\theta_i^R - \theta_r}{\sum_{i=1}^{m} (\theta_i - \theta_i^R)} \qquad (24)$$

where W^D_i is the normalized weight for each element and m is set to 100 for the total number of elements in the finite difference model. The normalized root-density weights are modeled as a function of depth using:

$$W_i^F = \left[\frac{W_i^r (1 - B_i)}{\sum_{i=1}^{m} W_i^r} \right] + B_i^o \qquad (25)$$

where B_i is a factor defining the estimated percentage of bare soil evaporation from total evapotranspiration for the top element. For the top element ($I = 1$), $B^o_i = B_i$, for all other elements, B^o_i is set to zero. The term W^r_i is calculated as a function of depth using an estimated root-density equation:

$$W_i^r = \left[((A_k - R_k)\, Z_i)^{B_k} + C_k\right]^{0.5} \qquad (26)$$

where A, B, and C are estimated model parameters for a given soil-depth class k, R is the estimated root-zone depth for a given soil-depth class, and Z is the depth below surface for element I. The dynamic conditioning function is combined with the normalized root-density weights to provide the final normalized root-zone weighting factors using:

$$W_i = \frac{(W_i^r (W_i^D)^{0.5})(1 - W_i^A)}{\sum_{i=1}^{m} W_i^r (W_i^D)^E} \qquad (27)$$

where the W_i^A terms are derived using a static conditioning function to limit total evapotranspiration in the lower part of the root zone as water is removed from the upper part of the root zone. The static conditioning function is defined by:

$$W_i^A = \frac{Z_i^{E_k}}{100} \qquad Z_i > 100\,, \quad W_i^A = 0 \qquad Z_i \le 100 \qquad (28)$$

where E is a parameter defined for each soil depth (and thus each root depth) class k, and Z is depth below surface in cm. Equation 28 allows for actual ET to be 100 percent of potential ET only under the condition that the wetting front is within the top 1 meter of the root zone, or under the condition that the top meter is fully saturated. All element weights W are set to zero beneath the root zone.

In the simplest approach to modeling fracture flow for 1-dimensional redistribution, the $FRAC_{in}$ terms are all set to zero and the sum of the $FRAC_{out}$ terms are added to the matrix flux at 10 meters to obtain an estimate of net infiltration. For each time step, the $FRAC_{out}$ terms for each element are set to zero unless the relative saturation of the bottom soil element or any bedrock element is greater than 0.95, in which case the $FRAC_{out}$ term is set to the estimated fracture saturated conductivity for that element using the values presented in table 2. Total fracture flow is summed for each time step and totaled for each day along with the matrix flux at 10 meters to provide an

estimate of daily net infiltration.

A modified version of this approach, referred to in this report as the cascading fracture model, uses a fracture storage term which sets $FRAC_{in}$ for each element equal to the saturated conductivity of the matrix, as long as water is available in the fracture storage term which is calculated as the sum of the $FRAC_{out}$ terms. The $FRAC_{out}$ term provides available water to the next underlying element, and the excess water is transferred down the profile for each time step using the fracture storage term until all water has been imbibed into the matrix or the fracture storage term is still greater than zero for the bottom element, in which case it becomes an estimate of the fracture-flow contribution to net infiltration. This approach represents an improvement over the first approach, which allows net infiltration to occur at a depth of 0.5 meters even though this is less than the depth of the modeled root zone. In both methods, the use of the $FRAC_{out}$ terms minimizes but does not necessarily prevent the creation of ponding conditions in bedrock.

Using a similar approach as for fracture flow, the *POND* specified flux term provides an estimate of excess precipitation created in the soil profile which then becomes available for overland flow. The term is set to zero for each element unless relative saturations become greater than 0.95, in which case the excess water is simply removed from the profile. The *POND* term prevents ponding conditions from occurring in the soil profile (including the bottom soil element at the soil-bedrock interface).

Examples of simulated redistribution profiles using the cascading fracture model are provided by figures 39 a and b. For this location, the soil depth is 0.5 meters and the root-zone depth is 1.5 meters. Figure 39a indicates simulated water contents using the developed 15-year record (1980 through 1995) for Yucca Mountain. The results illustrate the episodic pulses of increased wetting front penetration in response to increased precipitation during 1980, 1983, 1985, 1988, 1992, 1993, and 1995. In all cases, the advance of the wetting front was halted by evapotranspiration occurring throughout the root zone, and the effect of the root zone in drying the profile to the residual-water content of approximately 0.05 creates a distinct boundary at the bottom

of the root zone. The slight increases in water contents beneath the root zone which occurred during the wet years were caused by the cascading fracture model, which transferred moisture from the soil-bedrock interface at 0.5 meters to an average depth of 2 meters. The 100-year simulation provided results similar to the 15-year simulation, with a slight but continuous wetting of the bedrock beneath the root zone. These results indicate that longer simulation times are needed for this model in order to assess the contribution of fracture flow to net infiltration; the fracture-flow term at the bottom of the profile was zero for the entire period of both simulations. The RICHARDS submodel was still in the calibration phase at the time this report was written, and thus figure 39 can only be used as an example of simulation results, not as indication of actual net infiltration rates at Yucca Mountain. Although work on the calibration of the RICHARDS submodel is being continued, simulation run times are very long when multiple locations are being modeled simultaneously (as in the case of watersheds), and a sufficient number of calibration tests have not yet been completed.

(Figure 39. Volumetric water content simulated at one location in Split Wash for a) 15 years and b) 100 years using the YM stochastic rainfall model.)

Flow at the soil-bedrock interface

Flow at the soil-bedrock interface is calculated differently for the two infiltration submodels. In the submodel BUCKET, once the soil profile has reached field capacity, excess water is removed from the soil profile and added to a bucket or holding tank. Water is removed from the bucket by evapotranspiration and drainage. Because the bucket is assumed to be at the tuff/soil interface a smaller percentage of evapotranspiration is removed than may be realistic in moderately deep soils (0.5 to 3 m). Flow at the soil-bedrock interface in the submodel RICHARDS is simply a continuation of the Richards-equation approach described above. The most significant difference is that in the submodel RICHARDS water can flow into the matrix at less than the saturated-hydraulic conductivity (which is used in BUCKET) and provides a more realistic view of flux across the

tuff/soil contact and also the effect of fracture flow on the redistribution of water in bedrock and on net infiltration rates.

Net infiltration

In the submodel BUCKET net infiltration is modeled as the saturated-hydraulic conductivity of the underlying bedrock when water exists in the bucket. It is assumed that when water builds up at the tuff/soil interface that it infiltrates on a daily basis under a unit gradient. At the same time, evapotranspiration is taking water from the bucket. The ponded condition may exist for several days and the total net infiltration is simply the saturated-hydraulic conductivity multiplied by the number of days infiltration existed. Using this method the water-balance equation (eq. 2) is not solved directly. Rather the model determines if field capacity is exceeded by precipitation and water drains to the bedrock interface. Based on field observation this is a fairly robust process and easily predicted based on measurements of precipitation and estimates of soil storage capacity. The critical value then, need to calculated net infiltration, is the saturated-hydraulic conductivity of the underlying bedrock, which can be modified during model calibration.

Simulations of net infiltration for all neutron boreholes were done using 100-year stochastic simulations from figure 36a,b and are plotted in figure 40 for Yucca Mountain (fig. 40a) and Area 12 (fig. 40b). Net infiltration averaged over 5 mm/year for the neutron-hole locations using the Yucca Mountain simulation (169-mm average precipitation) but had a maximum of over 25 mm in one year with minimums of zero for several years. Net infiltration averaged almost 30 mm/yr using the Area 12 simulation (330 mm average precipitation) with a high of over 100 mm/yr and a low of just under 10 mm/yr. The Area 12 simulation is based on data collected at one of the highest points on Rainier Mesa and is higher than the average precipitation for the area (Hevesi and Flint, 1996). Estimates of the net infiltration at Rainier Mesa ranges from 10 to 20 mm/yr (J. Wang, written communication, 1996) which is consistent with the higher model estimate of 30 mm/yr that is based on higher than average precipitation for Rainier Mesa.

(Figure 40. Simulation of mean net infiltration for neutron boreholes using 100-year stochastic simulations of precipitation from a) Yucca Mountain and b) Area 12.)

Model Calibration

There were several model-calibration techniques and several phases of calibration. Solar radiation was compared to measured solar radiation data, the air-temperature model was compared to measured air-temperature data and evapotranspiration calculated by the Preistley-Taylor was compared to water loss from neutron-moisture profiles. The combined submodel BUCKET was then calibrated using neutron-probe data by summing the water in the soil profile and comparing that to the model simulation for the same time using an estimate of the actual precipitation. Two examples are presented, borehole N50, with deep soil (2.7 m) (fig. 41a) and borehole N63 with shallow soil (1.7 m) (fig. 41b). This comparison provided some assurance that the water-balance technique employed by the submodel BUCKET could correctly maintain the proper soil moisture and therefore would allow for more accurate determination of when the water-storage capacity was exceeded and ponding at the soil-bedrock interface had occurred. The next step was to determine if the fluxes calculated when ponding occurred matched the fluxes estimated from the neutron-probe data. Site-specific precipitation data at neutron holes was not available until the early 1990's (Ambos and others, 1995) and has not been incorporated into the analysis of the neutron-hole data between 1984 and 1995. Because the BUCKET submodel requires daily values of precipitation a direct comparison of neutron-hole flux and model flux is difficult. There is, however, enough data for year-to-year comparisons between the flux at the neutron holes and the modeled flux. Yearly precipitation values estimated by Hudson and Flint (1996) using geostatistical analyses, the open squares, were compared to the estimated values for each borehole location, the crosses, (fig. 42) using precipitation estimated from 15 years of measured data (fig. 19). There is general agreement between the yearly values with the estimates, but the differences at various elevations are notable. Precipitation was also increased by 30 percent to simulate increases due to concentration of water in the channels, as indicated by the open circles. These data were then used to model infiltration at each borehole using the submodel BUCKET (fig. 43). The average-annual precipitation and

infiltration estimates from Hudson and Flint (1996) are again noted by the open squares. Models were fit to each data set and it can be seen that the regression model of infiltration modeled with the BUCKET submodel, using the increase in precipitation to simulate channels, matches the calculated yearly values of flux from Hudson and Flint (1996) very well, whereas infiltration modeled without the 30 percent channel enhancement factor is slightly lower (fig. 43). The only support for using a 30 percent enhancement factor is the improved match to the neutron hole data. The submodel RICHARDS uses the same submodels for evapotranspiration and therefore only the soil redistribution (Richards' equation) is different. Because of the lack of precipitation data it is felt that detailed statistical analysis would not be appropriate. General trends are adequate to suggest the model represents, in general, the influence of the site properties as well as they are currently known.

(Figure 41. Calibration of modeled net infiltration using neutron boreholes a) USW UZ-N50 and b) USW UZ-N63.)

(Figure 42. Precipitation modeled with no channel enhancement factor and with 30 percent channel enhancement factor compared to simulated average annual precipitation for 15 years of data.)

(Figure 43. Precipitation versus infiltration modeled for each borehole with no channel enhancement factor and with 30 percent channel enhancement factor, and mean yearly infiltration for all boreholes. Linear regressions predicting values for each data set are shown.)

Stochastic Simulations of Infiltration

The 100-year periods with stochastically distributed precipitation were used in conjunction with the BUCKET submodel to generate relations between yearly average precipitation and average infiltration for Yucca Mountain and Area 12. These simulation results were compared with similar relations determined from 15 years of measured precipitation and neutron-moisture meter data, as well as the Maxey-Eakin model. The YM and A12 simulations of net infiltration and the actual neutron-hole estimates are presented in figure 44. There is generally good agreement between the estimates based on measured neutron-hole data and the simulated YM data. The periodic spikes in

the YM simulation appear as ENSO events and compare well to actual ENSO events measured. In general ENSO years are associated with increases in precipitation which may lead to increase in net infiltration. In the case for Yucca Mountain almost all ENSO years lead to major increases in net infiltration, thus the direct correlation from ENSO to net infiltration. The 15-year record between 1980 and 1995 does not appear to be typical when compared to the 100-year YM simulation. When viewed as a time series there are certainly 15-year periods in the 100-year series that would compare to the 15 years of measured data (fig. 40a). For example, the 15 years between year 35 and year 50 (fig. 40a) has a much higher occurrence of ENSO events than the average, whereas between year 20 and year 35 there are only two significant events. This should clearly point out that the meteorological conditions are variable enough that the short time frame of the measurements at Yucca Mountain (<15 years) do not necessarily represent the mean values at 100-, or even 50-year time scales. A polynomial model of the YM simulation and a model of the combined YM and A12 simulation is presented as a comparison to the Maxey-Eakin model. There is generally good agreement between the three models.

(Figure 44. Precipitation versus net infiltration, modeled 100-year simulation, estimated using Maxey-Eakin method and calculated from neutron borehole data.)

Two single-year simulations were obtained using the BUCKET submodel and the complete area of the USGS/LBNL 3-dimensional site-scale model represented by the 30-meter grid. The first simulation (fig. 45a) used as input the twelfth year of the YM simulation, which represented a mean precipitation value (165 mm) and a mean flux (5.4 mm) value for the 3-dimensional site-scale model boundary and the YM simulation (fig. 36a and fig. 40a). The second simulation (fig. 45b) used the first year of the YM simulation which had an aerially-distributed mean-precipitation value of 205 mm and a mean flux of 8 mm (fig. 36b and fig. 40b). Since channel flow is not specifically modeled in the BUCKET submodel the precipitation was increased to simulate runoff events and downstream channel loss. The results compare well with the estimated 3 percent net infiltration in channels estimated by Hudson and Flint (1996).

(Figure 45. Infiltration simulated using stochastic precipitation simulations with average annual precipitation values of a) 165 mm/year and b) 205 mm/year.)

The stochastic rainfall-infiltration model predicts substantial year-to-year and location-to-location variability of net infiltration. The timing of precipitation is, in some cases, more dramatic than the total year precipitation. For example, in some years during which precipitation is less than 150 mm, there are net infiltration values calculated for the neutron holes in excess of 12 mm (fig. 44). On the other hand, the stochastic model predicts that precipitation of between 150 mm/yr and 350 mm/yr, infiltration seldom exceeds 12 mm/yr (fig. 44). This shows a lower significance of the absolute year value and more of an influence of the seasonality. To produce a conceptual model of net-infiltration values that would be useful as input for the 3-dimensional site-scale model, a compromise between year-to-year variability and long-term trends was needed. By fitting a polynomial model through the 100-year simulation (YM), a scaling factor could be produced to convert the second simulation to a mean value for the 3-dimensional site-scale model area. A factor was developed to scale the simulation results as shown in figure 45b, which had an average annual precipitation value of 205 mm. The scaling factor provided a representation of the average net infiltration for an precipitation value of 169 mm. The polynomial regression line for the YM simulation from figure 44 predicted 6.5 mm net infiltration for an annual precipitation of 205 mm, and 4.5 mm net infiltration for 169 mm of precipitation. The net infiltration estimates for all the grid blocks were then scaled as 6.5:4.5 to produce figure 46. Channel flow is estimated as 3 percent of annual precipitation (169 mm/yr) which is based on Hudson and Flint (1996). Further work on incorporating channel flow in the submodel BUCKET will be done using the model KINEROS at a later date. A close-up perspective of the potential repository area is presented in figure 47. It has been argued that channel flow is the only significant form of net infiltration at Yucca Mountain (Kwicklis and Rousseau, 1996) based on an estimate of percolation flux in Pagany Wash and Drill Hole Wash. To provide an alternate conceptual model describing this perspective, channels were modeled as the only source of infiltration using an estimated 10 mm/yr infiltration rate proposed by Kwicklis and Rousseau (1996) (fig. 48). This model results in an average flux over the modeling domain of 0.5 mm/yr.

(Figure 46. Conceptual model of infiltration numerically modeled using average annual precipitation resulting in an average of 4.5 mm/year flux over the modeling domain.)
(Figure 47. Close-up view of the potential repository area in figure 46.)
(Figure 48. Alternative conceptual model of infiltration numerically modeled assuming all infiltration is through the channels, and assuming an average of 10 mm/yr, resulting in an average flux of 0.5 mm/yr over the modeling domain.)

Flux estimates were taken from the average flux map (fig. 46) at specific points to compare to the chloride mass-balance flux estimates in table 7. The closest 30-m grid point to each borehole was used as the point estimate of net infiltration. There is fairly good agreement between the apparent flux estimates and the model estimates. The model estimates at UZ4, UZ5, and UZ14 are, however, higher than the chloride mass-balance estimates. Because the infiltration pattern varies over short distances, such as between channels and terraces, the apparent flux at depth may be integrating a much larger area. A larger area (3600 m^2) is averaged around the borehole to evaluate this effect. In several cases this averaging had little effect indicating longer correlation lengths. The exception is in active channels (UZ4 and UZ14) where the areal average is more consistent with the chloride mass balance. The reduction at UZ5 is likely due to the close proximity of a terrace which makes the areal average of flux less than the point estimate for sideslopes. (Due to the problems with the assumptions in fractured media, noted under the geochemistry analysis, these apparently close estimates of flux may be coincidental. It is possible, however, that with thin soils overlying fractured tuffs the overall system may behave more like porous media and less like a single fracture.)

ASSUMPTIONS AND LIMITATIONS

Many of the assumptions and limitation were addressed in the text. Such as the instantaneous redistribution of water (every 24 hours) in the BUCKET submodel and the flow of water into the fractures only when the soil-tuff interface become fully saturated. The size, filling and influence of the fractures in the underlying bedrock is also assumed and untested. The assumptions that the

fractures are all filled with calcium carbonate and can be represented by a mean diameter of 250 um is basically untested although partially based on field observation. It is also assumed that water infiltrating into the underlying bedrock becomes net infiltration for the BUCKET submodel.

The root dynamics in fractured bedrock are untested and more of the water may be removed than is incorporated into the models. One-dimensional flow is assumed for each 30 m grid block, therefore any lateral flow between grid blocks is discounted. There is evidence for lateral flow in the shallow soil but the distance that water moves is undetermined. The significance of lateral flow in concentrating water under the thicker soils in the valley terraces needs to be investigated.

Finally, the inaccuracy of representing summer precipitation as a continuous 24-hour precipitation intensity is likely to cause errors in predicting runoff caused by severe summer thunderstorms having durations of less than 1 to 2 hours. The assumption that daily precipitation values can be scaled to the elevation of the surrounding area using the relation between elevation and average-annual precipitation (Hevesi and Flint, 1996). This assumption leads to approximately a 1 percent change in precipitation for every 14 meters change in elevation. For central Yucca Mountain there is less than a 5 percent change in precipitation between the ridge tops and the wash bottoms. Although this simplification may be at least somewhat valid for winter precipitation, it does not provide a very realistic representation of the much higher degree of spatial variability and the comparatively poor correlation with physiography observed for summer precipitation on the scale of the modeling domain. Further development of a spatially variable stochastic model will help resolve some of the problems.

FUTURE WORK

The conceptual model has been incorporated into the numerical model; however, several assumptions need to be tested before confidence in the model results can be developed. The model is very dependent on the soil properties, the bedrock properties and the evapotranspiration function. Each of these should be tested in more detail and any new information incorporated into the

numerical model. Detailed evapotranspiration measurements would provide a good verification check of the Priestley-Taylor equation. At the same time, measurements of soil heat flux and net radiation could provide an adequate comparison to the rest of the energy balance equation. Laboratory and field measurements of the soil properties, particularly soil water retention functions, are needed spatially. Field measurements of the saturated hydraulic conductivity of the underlying bedrock is perhaps the most important measurement needed. It is likely that with larger amounts of precipitation, the amount of fracture filling decreases causing an increase in net infiltration. This possibility and the real values of bulk saturated hydraulic conductivity need to be verified with field experiments.

SUMMARY

Studies are currently underway to determine the suitability of Yucca Mountain, Nevada, as the United States' first high-level nuclear-waste repository. Values of net infiltration are required to determine pre-waste emplacement groundwater-travel times and to evaluate the performance of the repository as a waste-containment system. A conceptual model is proposed that describes the processes of precipitation, runoff, evapotranspiration, and redistribution of water within the shallow unsaturated zone, in particular, the initiation of fracture flow at the soil-bedrock interface. The conceptual model is consistent with most of the available infiltration data and matches the independent chloride mass-balance approach. The properties and processes most important in determining if net infiltration occurs are the timing and amount of precipitation, the storage capacity of the soil (which includes soil depth), the seasonality and amount of evapotranspiration and the hydrologic properties of the underlying bedrock, including fracture properties. The role of faults in near-surface infiltration is more difficult to ascertain. The bomb-pulse ^{36}Cl indicates that, once initiated under shallow soils, fracture flow can move water quickly through the Tiva Canyon Tuff, indicating that there may be no unique fast-flow pathways through the shallow welded rocks. The bomb-pulse ^{36}Cl and neutron-borehole data analysis indicates that deeper soils retard the penetration of water and prevent rapid movement into fractures. The fastest pathways into the near surface, therefore appear to exist in any fractured rock under shallow soils, where near-saturated conditions

can develop. The rock surrounding the surface-exposed faults may have increased fracture density which could increase the volume of water entering the near surface but may not necessarily increase the flow velocity. There is, however, evidence that where faults exist within the PTn water can quickly penetrate into the underlying Topopah Spring Tuff, as long as the location of the fault is under shallow soils where near-surface fracture flow could be initiated. Based on the observations, faults may have little role in increasing surface infiltration but may play a major role in allowing water to quickly pass through the PTn.

The numerical models were developed to correctly account for the properties and processes that exist at Yucca Mountain. The model results indicated a satisfactory preliminary calibration of a more detailed numerical submodel of infiltration (RICHARDS) and also a simplified version (BUCKET) that allowed for a more efficient analysis of the spatial variability of infiltration across the study area (>220 km^2). The models were used to provide 100-year simulations of infiltration which allowed for an evaluation of the temporal and spatial distribution of net infiltration throughout the area of Yucca Mountain under current-climatic conditions and possible future-climatic conditions (doubling precipitation increased net infiltration by a factor of 4). Infiltration is temporally and spatially variable but averaged 4.5 mm/yr over the study area and 6.5 mm/yr over the potential repository area for the current climate. The most important aspect of infiltration is that temporally, it may be 0 mm/yr for several years and 10-20 mm/yr for one year, whereas spatially it may be 0 mm/yr for much of the area and exceed 80 mm/yr for other areas. It is not the amount of precipitation alone that determines net infiltration, but also the timing. Therefore, estimates of climate change require daily estimates of precipitation or need to provide insight into the parameters necessary to generate daily precipitation using stochastic models. Without this information the influence of wetter or drier climates cannot be adequately evaluated for the Yucca Mountain area.

REFERENCES

Ambos, D.S., Hevesi, J.A. and Flint, A.L., 1995, Precipitation data for water years 1992 and 1993 from a network of nonrecording gages at Yucca Mountain, Nevada: U.S. Geological Survey Open-File Report 95-146, Denver, Co., 100 p.

Beatley, J.C., 1976, Vascular plants of the Nevada Test Site and central-southern Nevada: ecological and geographical distributions: U.S. Energy Research and Development Administration Rep. TID-26881, 308 p.

Bedinger, M.S., Langer, W.H., and Reed, J.E., 1989, Ground-Water Hydrology: *In* Studies of geology and hydrology in the Basin and Range Province, southwestern United States, for isolation of high-level radioactive waste-- characterization of the Death Valley region, Nevada and California, Bedinger, M.S., Sargent, K.A., and Langer, W.H., (eds.), U.S. Geol. Survey Prof. Paper 1370-F, Washington D.C., 49 p.

Benson, L. and Klieforth, H., 1989, Stable isotopes in precipitation and ground water in the Yucca Mountain region, southern Nevada: paleoclimatic implications: *in* Aspects of climate variability in the Pacific and the Western Americas, D.H. Peterson, (ed.), Geophysical Monograph, vol. 55, p. 41-59.

Botkin, D.B., Nisbet, R.A., Bicknell, S., Woodhouse, C., Bentley, B., and Ferren, W., 1991, Global climate change and California's natural ecosystems: *In* Global Climate Change and California, Potential Impacts and Responses, (Knox, J.B. and Scheuring, A.F., eds.), University of Calif. Press, Berkeley, CA., p. 123-146.

Britch, M.J., 1990, Watershed modeling at Yucca Mountain, Nevada: unpublished M.S. thesis, Oregon State University, Corvallis, OR, July, 112 p.

Brutsaert, W.H., 1982, Evaporation into the atmosphere: Reidel Publishing Company, Boston, 299 p.

Buesch, D.C., Spengler, R.W., Moyer, T.C., and Geslin, J.K., 1996, Proposed stratigraphic nomenclature and macroscopic identification of lithostratigraphic units of the Paintbrush Group exposed at Yucca Mountain, Nevada: U.S. Geological Survey Open-File Report 94-469, 45 p.

Byers, Jr., F.M., Carr, W.J., Orkild, P.P., Quinlivan, W.D., and Sargent, K.A., 1976, Volcanic suites and related cauldrons of the Timber Mountain-Oasis Valley Caldera Complex, southern Nevada: U.S. Geol. Survey Prof. Paper 919, 70 p.

Campbell, G.S., 1977, An introduction to environmental biophysics, Springer-Verlag, New York, p. 159.

Campbell, G.S., 1985, Soil physics with BASIC transport models for soil-plant systems: Developments in Soil Sci., vol. 14, Elsevier, NY, 150 p.

Carr, W.J., Byers, F.M., Jr., and Orkild, P.P., 1986, Stratigraphic and volcano-tectonic relations of the Crater Flat Tuff and some older volcanic units, Nye County, Nevada: U.S. Geol. Survey Prof. Paper 1323, 28 p.

Childs, S.W. and Flint, A.L., 1990, Nature of forest soils with rock fragments: *Proceedings* North American Forest Soils Conference, Stan Gessel (ed.), Edmonton, Alberta, Chapter 7, 267 p.

Christiansen, R.L., and Lipman, P.W., 1965, Geologic map of the Topopah Spring Northwest quadrangle, Nye County, Nevada: U.S. Geological Survey Geologic Quadrangle map GQ-444, scale 1:24,000.

Czarnecki, J.B., 1984, Simulated effects of increased recharge on the ground-water flow system of Yucca Mountain and vicinity, Nevada-California: U.S. Geological Survey Water-Resources Investigations Report 84-4344, 33 p.

Davies, J.A. and Allen, C.D., 1973, Equilibrium, potential and actual evaporation from cropped surfaces in southern Ontario: J. Appl. Meteorol., vol. 12, p. 649-657.

de Bruin, H.A.R., 1988, Evaporation in arid and semi-arid regions: *In* Estimation of natural groundwater recharge, I. Simmers (ed.), Reidel Publ. Company, Boston, MA., p. 73-88.

Dettinger, M.D., 1989, Reconnaissance estimates of natural recharge to desert basins in Nevada, U.S.A., by using chloride-balance calculations: Journal of Hydrology, vol. 106, p. 55-78.

Eichinger, W.E., Parlange, M.B. and Stricker, H., 1996, On the concept of equilibrium evaporation and the value of the Priestley-Taylor coefficient: Water Resources Research, vol. 32, no. 1, p. 161-164.

EG&G, Energy Measurements, 1991, Yucca Mountain biological resources monitoring program: Annual Report FY89 &FY90: EGG 10617-2084, Santa Barbara Operations, Goleta, Calif.

Fabryka-Martin, J.T, Wightman, S.J., Murphy, W.J., Wickham, M.P., Caffee, M.W., Nimz, G.J., Southon, J.R., Sharma, P., 1993, Distribution of chlorine-36 in the unsaturated zone at Yucca Mountain: an indicator of fast transport paths: *Proceedings*, FOCUS '93: Site Characterization and Model Validation, American Nuclear Soc., La Grange Park, IL, Sept. 26-29, 1993, Las Vegas, NV, p. 58-68.

Fabryka-Martin, J.T., , Wightman, S.J., Robinson, B.A., and Vestal, E.W., 1994, Infiltration processes at Yucca Mountain inferred from chloride and chlorine-36 distributions: Los Alamos Report LA-CST-TIP-94-022, Level 4 Milestone Report 3417, Los Alamos National Lab., Los Alamos, NM., 37 p.

Flint, A.L. and Childs, S.W., 1987, Calculation of solar radiation in mountainous terrain: Journal of Agricultural and Forest Meteorology, vol. 40, p. 233-249.

Flint, A.L. and Childs, S.W., 1984, Development and calibration of an irregular hole bulk density sampler: Soil Science Society America Journal, vol. 48, p. 374-378.

Flint, A.L. and Childs, S.W., 1991, Modification of the Priestley-Taylor equation for estimating evapotranspiration for soil water limited conditions: J. Agric. and Forest Meteorology, vol. 56, p. 247-260.

Flint, A.L. and Davies, W.J., 1996, Meteorological data for water years 1988-94 from 5 weather stations at Yucca Mountain, Nevada: U.S. Geological Survey Open-File Report. (*in press*)

Flint, A.L. and Flint, L.E., 1994, Spatial distribution of potential near surface moisture flux at Yucca Mountain: *Proceedings,* Fifth International Conference on High Level Radioactive Waste Management, American Nuclear Society, La Grange Park, IL, May 22-26, 1994, Las Vegas, NV., p. 2352-2358.

Flint, A.L., Flint, L.E., and Hevesi, J.A., 1993, Influence of long term climate change on net infiltration at Yucca Mountain, Nevada: *Proceedings*, Fourth International High Level Radioactive Waste Conference, Las Vegas, NV., April 25-30.

Flint, L.E. and Flint, A.L., 1995, Shallow infiltration processes at Yucca Mountain-- Neutron logging data 1984-93: U.S. Geological Survey Open-File Report 95-4035.

Flint, L.E., Flint, A.L., Rautman, C.A., and Istok, J.D., 1995, Physical and hydrologic properties of rock outcrop samples at Yucca Mountain, Nevada: U.S. Geological Survey Open-File Report 95-280, 52 p.

Flint, L.E., 1996, Matrix properties of hydrogeologic units at Yucca Mountain, Nevada: U.S. Geological Survey Water-Resources Investigations Report, Denver, CO. (*in review*)

Forester, R.M., 1994, Late glacial to modern climate near Yucca Mountain, Nevada: *Proceedings*, 5th International High-Level Radioactive Waste Management Conference, American Nuclear

Society, Las Vegas, NV., p. 2750-2754.

Forester, R.M. and Smith, A.J., 1994, Late glacial climate estimates for southern Nevada: the ostracode fossil record: *Proceedings*, 5th International High-Level Radioactive Waste Management Conference, American Nuclear Society, Las Vegas, NV., p. 2553-2561.

Freeze, R.A. and Cherry, J.A., 1979, Groundwater. Prentice-Hall, New Jersey, p. 67.

French, R.H., 1983, Precipitation in southern Nevada: Journal of Hydraulic Engineering, v. 109, no. 7, July, p. 1023-1036.

Gauthier, J.H. and Wilson, M.L., 1994, Chapter 8, Infiltration and percolation rates, *In* Total-system performance assessment for Yucca Mountain - SNL second iteration (TSPA-1993), Sandia Report, SAND93-2675, p. 8.1-8.17.

Grayson, D.K., 1993, The Desert's Past: a Natural Prehistory of the Great Basin: Smithsonian Institution Press, Washington D.C., 356 p.

Gregory, J.M., Wigley, T.M.L., and Jones, P.D., 1992, Determining and interpreting the order of a two-state Markov chain: application of models of daily precipitation: Water Resources Research, vol. 28, p. 1443-1446.

Gregory, J.M., Wigley, T.M.L., and Jones, P.D., 1993, Application of Markov chains to area-average daily precipitation series and interannual variability in seasonal totals: Climate Dynamics, vol. 8, p. 299-310.

Greenland Ice-Core Project Members (GRIP), 1993, Climate instability during the last interglacial period recorded in the GRIP ice core: Nature, vol. 364, p. 203-207.

Haan, C.T., 1977, Statistical Methods in Hydrology: Iowa State University Press, Ames, IA., 378 p.

Hevesi, J.A., Istok, J.D., and Flint, A.L., 1991a, Precipitation estimation in mountainous terrain using multivariate geostatistics: I. Structural Analysis: Journal of Applied Meteorology, vol. 31, no. 7, p. 661-676.

Hevesi, J.A., Flint, A.L. and Istok, J.D., 1991b, Precipitation estimation in mountainous terrain using multivariate geostatistics: II. Isohyetal Maps: Journal of Applied Meteorology, vol. 31, no. 7, p. 661-676.

Hevesi, J.A., Ambos, D.S. and Flint, A.L., 1994a, A preliminary characterization of the spatial variability of precipitation at Yucca Mountain, Nevada: *Proceedings,* Fifth International

Conference on High Level Radioactive Waste Management, American Nuclear Society, La Grange Park, IL, May, 1994, Las Vegas, NV., p. 2520-2529.

Hevesi, J.A., Flint, A.L. and Flint, L.E., 1994b, Verification of a 1-dimensional model for predicting shallow infiltration at Yucca Mountain: *Proceedings,* Fifth International Conference on High Level Radioactive Waste Management, American Nuclear Society, La Grange Park, IL, May, 1994, Las Vegas, NV., p. 2323-2332.

Hevesi, J.A., Ambos, D.S., and Flint, A.L., 1996, Synoptic scale analysis of precipitation for water years 1992 and 1993 at Yucca Mountain, Nevada: U.S. Geological Survey Open-File Report. (*in review*)

Hevesi, J.A. and Flint, A.L., 1996, Regional estimation of precipitation and recharge in southern Nevada: U.S. Geological Survey Water-Resources Investigations Report. *(in review)*

Hofmann, L.L., Guertal, W.R., Davies, W.J., and Flint, A.L., 1993, A large-scale, automated, constant head, double-ring infiltrometer: Agronomy Abstracts, Soil Sci. Soc. Am., Madison, WI, Nov., 1993.

Horton, R.E., 1933, The role of infiltration in the hydrologic cycle: Trans. Am. Geophys. Union, 14th Annual Meetings, p. 446-460.

Houghton, J.G., 1969, Characteristics of Rainfall in the Great Basin: Desert Research Institute, University of Nevada, Reno, NV., 205 p.

Hudson, D.B., and Flint, A.L., 1996, Estimation of shallow infiltration and presence of potential fast pathways for shallow infiltration in the Yucca Mountain area, Nevada: U.S. Geological Survey Water-Resources Report. *(in review)*

Imbrie, J. and Imbrie, J.Z., 1980, Modeling the climatic response to orbital variations: Science, vol. 207, p. 943-953.

Imbrie, J., 1985, A theoretical framework for the pleistocene ice ages: Journal of the Geological Soc. of London, vol. 142, p. 417-432.

Imbrie, J., Mix, A.C., and Martinson, D.G., 1993, Milankovitch theory viewed from Devils Hole: Letters to Nature, Nature, vol. 363, p. 531-533.

Imbrie, J, Hay, J., Martinson, D.G., McIntyre, A., Mix, A.C., Morley, J.J., Pisias, N.G., Press, W.L., and Shackleton, N.J., 1984, The orbital theory of pleistocene climate: Support from a

revised chronology of the marine ^{18}O record: *In* Milankovich and Climate, Part I, A. Berger, J. Imbrie, J. Hay, S. Gupka, B. Saltzman (Eds.), Reidel, Boston, MA., p. 269-305.

Jones, K.R., 1981, Arid Zone Hydrology for Agricultural Development: FAO Irrigation and Drainage Paper, Food and Agriculture Org. of the United Nations, Rome, Italy, 264 p.

Jury, W.A., Gardner, W.R., and Gardner, W.H., 1991, Soil Physics, John Wiley & Sons, Inc., New York, 328 p.

Justus, P.S. and Stablein, N.K., 1989, Geoscientists help make 10,000-year decisions--U.S. Nuclear Regulatory Commission: Geotimes, January, p. 14-15.

Kellogg, W.W. and Schware, R., 1981, Climate Change and Society: Westview Press, Boulder, CO., p. 178.

Knox, J.B., 1991, Global climate change: impacts on California: An introduction and overview: *In* Global Climate Change and California, Potential Impacts and Responses, (Knox, J.B. and Scheuring, A.F., eds.), University of Calif. Press, Berkeley, CA., p. 1-24.

Koltermann, C.E. and Gorelick, S.M., 1992, Paleoclimatic signature in terrestrial flood deposits: Science, vol. 256, p. 1775-1782.

Kwicklis, E.M. and Rousseau, J.P., 1996, Implications for waste isolation: *In* Hydrogeology of the unsaturated zone, North Ramp area of the Exploratory Studies Facility, Yucca Mountain, Nevada, Rousseau, J.P., Kwicklis, E.M., and Gillies, D.C., (eds.), U.S. Geological Survey Water Resources Investigations Report. (*in review*)

Lafleur, P.M. and Rouse, W.R., 1990, Application of an energy combination model for evaporation from sparse canopies: Agric. Forest Meteorology, vol. 49, p. 135-153.

Lane, L.J., Romney, E.M., and Hakonson, T.E., 1984, Water balance calculations and net productions of perennial vegetation in the northern Mojave Desert: J. Range Manage., vol. 37, no. 1, p. 12-18.

Lichty, R.W. and McKinley, P.W., 1995, Estimates of ground-water recharge rates for two small basins in central Nevada: U.S. Geological Survey Water Resources Investigation Report 94-4104, 31 p.

Lundstrom, S.C., Wesling, J.R., Taylor, E.M., and Paces, J.B., 1994, Preliminary surficial deposits map of the northeast quarter of the Busted Butte 7.5-minute quadrangle: U.S.

Geological Survey Open-File Report 94-341, scale 1:12000.

Lundstrom, S.C., Mahan, S.A., and Paces, J.B., 1995a, Preliminary surficial deposits map of the northwest quarter of the Busted Butte 7.5-minute quadrangle: U.S. Geological Survey Open-File Report 95-133, scale 1:12000.

Lundstrom, S.C., and Taylor, E.M., 1995b, Preliminary surficial deposits map of the southern half of the Topopah Spring NW 7.5-minute quadrangle: U.S. Geological Survey Open-File Report 95-132, scale 1:12000.

Lundstrom, S.C., Whitney, J.W., Paces, J.B., Mahan, S.A., and Ludwig, K.R., 1995c, Preliminary surficial deposits map of the southern half of the Busted Butte 7.5-minute quadrangle, Nye County, NV: U.S. Geological Survey Open-File Report 95-311, scale 1:12000.

MacMahon, J.A., 1985, Deserts, Audubon Society Nature Series: Alfred Knopf Publ., New York, NY., 368 p.

Marshall, B.D., Peterman, Z.E., and Stuckless, J.S., 1993, Strontium isotopic evidence for a higher water table at Yucca Mountain: *Proceedings,* Fourth International Conference of High Level Radioactive Waste Management, Las Vegas, NV, April 26-30, 1993, American Nuclear Society, La Grange Park, IL., p. 1984-1952.

Maxey, G.B. and Eakin, T.E., 1949, Ground water in White River Valley, White Pine, Nye, and Lincoln Counties, Nevada: Nevada State Eng., Water Resources Bull. no. 8, 59 p. (prepared in cooperation with U.S. Dep. Inter., U.S. Geol. Surv.).

Montazer, P. and Wilson, W.E., 1984, Conceptual hydrologic model of flow in the unsaturated zone, Yucca Mountain, Nevada: U.S. Geological Survey Water-Resources Investigations Report 84-4345, 55 p.

Monteith, J.L., 1965, Evaporation and Environment: Symp. Sor. Exp. Biol., vol. 19, p. 205-234.

Moyer, T.C. and Geslin, J.K., 1995, Lithostratigraphy of the Calico Hills Formation and Prow Pass Tuff (Crater Flat Group) at Yucca Mountain, Nevada: U.S. Geological Survey Open-File Report 94-460, 59 p.

Nichols, W.D., 1987, Geohydrology of the unsaturated zone at the burial site for low level radioactive waste near Beatty, Nye County, Nevada: U.S. Geological Survey Water-Supply Paper 2312, 52 p.

Nichols, W.E., and Cuenca, R.H., 1993, Evaluation of the evaporative fraction for parameterization of the surface energy balance: Water Resources Research, vol. 29, no. 11, p. 3681-3690.

Norris, A.E., Wolfsberg, K., Gifford, S.K., Bentley, H.W., and Elmore, D., 1987, Infiltration at Yucca Mountain, Nevada, traced by ^{36}Cl: Nuclear Instrum. Methods Physical Research, vol. B29, p. 376-379.

O'Farrell, T.P. and Collins, E., 1983, 1982 Biotic survey of Yucca Mountain, Nevada Test Site, Nye County, Nevada: EG&G Energy Measurements, Santa Barbara Operations, Goleta, Ca., 41 p.

O'Farrell, T.P. and Emery, L.A., 1976, Ecology of the Nevada Test Site: a narrative summary and annotated bibliography: U.S. Department of Energy Report No. NVO-167, 249 p.

Osterkamp, W.R., Lane, L.J., and Savard, C.S., 1994, Recharge estimates using a geomorphic/distributed-parameter simulation approach, Amargosa River Basin: Water Resources Bulletin, vol. 30, no. 3, p. 493-507.

Pabst, M.E., Beck, D.A., Glancy, P.A., and Johnson, J.A., 1993, Streamflow and selected precipitation data for Yucca Mountain and vicinity, Nye County, Nevada, water years 1983-85: U.S. Geological Survey Open-File Report 93-438, Carson City, NV., 66 p.

Paces, J.B., Taylor, E.M., Bush, C., 1993, Late quaternary history and uranium isotopic compositions of ground water discharge deposits, Crater Flat, Nevada: *Proceedings,* Fourth International Conference of High Level Radioactive Waste Management, Las Vegas, NV, April 26-30, 1993, American Nuclear Society, La Grange Park, IL., p. 1573-1580.

Philander, S.G., 1990, *El Niño, La Niña*, and the Southern Oscillation: Academic Press, Inc., San Diego, CA., 28 p.

Philip, J.R., 1957, Theory of infiltration. 4. Sorptivity and algebraic equations: Soil Science, vol. 84, p. 257-264.

Priestley, C.H.B. and R.J. Taylor, 1972, On the assessment of surface heat flux and evaporation using large-scale parameters: Man. Weather Rev., vol. 100, p. 81-92.

Pyke, C.W., 1972, Some meteorological aspects of the seasonal distribution of precipitation in the Western United States and Baja California: University of California, Water Resources Center Contribution 139, 205 p.

Roseboom, E.H., 1983, Disposal of high-level nuclear waste above the water table in arid regions:

U.S. Geological Survey Circular 903, 21 p.

Rubin, J., and Steinhards, R., 1963, Soil water relations during rain infiltration: I. Theory: Soil Sci. Soc. Am. Proc., vol. 28, p.

Rubin, J., and Steinhards, R., 1964, Soil water relations during rain infiltration: III. Water uptake at incipient ponding: Soil Sci. Soc. Am. Proc., vol. 28, p. 614-619.

Rubin, J., Steinhards, R., and Reiniger, P., 1964, Soil water relations during rain infiltration: II. Moisture content profiles during rains of low intensities: Soil Sci. Soc. Am. Proc., vol. 28, p. 1-5.

Rush, F.E., 1970, Regional ground-water system in the Nevada Test Site area, Nye, Lincoln, and Clark Counties, Nevada: Nevada Department of Conservation and Natural Resources Reconnaissance Series Report 54, 25 p.

Savard, C.S., 1995, Selected hydrologic data from Fortymile Wash in the Yucca Mountain area, Nevada, water year 1992: U.S. Geological Survey Open-File Report 94-317, Denver, CO., 38 p.

Sawyer, D.A., Fleck, R.J., Lanphere, M.A., Warren, R.G., and Broxton, D.E., 1994, Episodic volcanism in the Miocene southwest Nevada volcanic field: Stratigraphic revision, $^{40}Ar/^{39}Ar$ geochronologic framework, and implications for magmatic evolution: Geological Society of America Bulletin, vol. 106, p. 1304-1318.

Schlesinger, M.E., 1983, A review of climate model simulations of CO_2 - induced climatic change: Climate Research Institute Report no. 41, Oregon State University, Corvallis, OR., 135 p.

Scott, R.B., and Bonk, J., 1984, Preliminary geologic map of Yucca Mountain, Nye County, Nevada, with geologic sections: U.S. Geological Survey Open-File Report 84-494, 9 p., map scale 1:12,000.

Scott, R.B., R.W. Spengler, S. Diehl, A.R. Lappin, and M.P. Chornack, 1983, Geologic character of tuffs in the unsaturated zone at Yucca Mountain, southern Nevada: *In* Mercer, J.W., P.S.C. Rao, and I.W. Marine, (eds.), Role of the unsaturated zone in radioactive and hazardous waste disposal, Ann Arbor Science, Ann Arbor, MI., p. 289-335.

Shirazi, M.A. and Boersma, L., 1984, A unifying quantitative analysis of soil texture: Soil Sci. Soc. Amer. J. vol. 48, p. 142-147.

Shuttleworth, W.J., and J.S. Wallace, 1985, Evaporation from sparse crops -- an energy combination theory: Q.J.R. Meteorol. Soc., vol. 111, p. 839-855.

Spaulding, W.G., 1985, Vegetation and climates of the last 45,000 years in the vicinity of the Nevada Test Site, south-central Nevada: U.S. Geological Survey Professional Paper 1329, Alexandria, VA., 55 p.

Squires, R.R., and Young, R.L., 1984, Flood potential of Fortymile Wash and its principal southwestern tributaries, Nevada Test Site, southern Nevada: U.S. Geological Survey Water-Resources Investigations Report 83-4001, Carson City, NV., 33 p.

Stannard, D.I., 1993, Comparison of Penman-Monteith, Shuttleworth-Wallace, and the modified Priestley-Taylor evapotranspiration models for wildland vegetation in semi-arid rangelands: Water Resources Res., vol. 29, no. 5, p. 1379-1392.

Stewart, R.B., 1983, A discussion of the relationships between the principal forms of the combination equation for estimating crop evaporation: Agric. Meteorol., vol. 30, p. 111-127.

Stewart, R.B., and Rouse, W.R., 1977, Substantiation of the Priestley and Taylor parameter α=1.26 for potential evaporation in high latitudes: J. Appl. Meteorol., vol. 16, p. 649-650.

Tyler, S.W., Chapman, J.B., Conrad, S.H, Hammermeister, D.P., Blout, D.O., Miller, J., and Ginanni, J.M., 1996, Soil water flux on the Nevada Test Site: spatial and temporal variations over the last 120,000 years: Water Resources Research, vol. 32, no. 6, p. 1481-1499.

U.S. Department of Agriculture, 1975, Soil Taxonomy: Soil Conservation Service Agriculture Handbook No. 436, Washington, D.C., 754 p.

U.S. Geological Survey, 1995, Water resources data Nevada, water year 1996. U.S. Geological Survey Water-Data Report NV-95-1, Carson City, NV., 734 p.

U.S. Department of Energy, 1986, Environmental assessment, Yucca Mountain site, Nevada Research and Development Area, Nevada: DOE/RW-0073, Office of Civilian Radioactive Waste Management, Washington, D.C., p.

U.S. Department of Energy, 1988, Yucca Mountain site characterization plan: DOE/RW-0199, U.S. Department of Energy, Office of Civilian Radioactive Waste Management Office, Washington, D.C.

U.S. Geological Survey, 1983, A summary of geologic studies through January 1, 1983, of a

potential high-level radioactive waste repository site at Yucca Mountain, southern Nye County, Nevada: U.S. Geol. Survey Open-File Report 84-792, Denver, CO., 103 p.

van Genuchten, M.Th., Leij, F.J., and Yates, S.R., 1991, The RETC code for quantifying hydraulic functions of unsaturated soils: EPA/600/2-91/065, 93 p.

Wallace, A. (ed.), 1980, Soil-plant-animal relationships bearing on revegetation and land disturbance in Nevada deserts: Great Basin Naturalist Memoirs No. 4, Brigham Young University Press, Provo, UT., 227 p.

Watson, P., Sinclair, P., and Waggoner, R., 1976, Quantitative evaluation of a method for estimating recharge to the desert basins of Nevada: Journal of Hydrology, vol. 31, p. 335-357.

Weber, I.P. and Wiltshire, S.D., 1985, The Nuclear Waste Primer, a Handbook for Citizens: The League of Women Voters Education Fund, 38 p.

Whipple, C.G., 1996, Can nuclear waste be stored safely at Yucca Mountain?: Scientific American, June, p. 72-79.

Winograd, I.J. and Thordarson, W., 1975, Hydrogeologic hydrochemical framework, south-central Great Basin, Nevada-California, with special reference to the Nevada Test Site: U.S. Geological Survey Professional Paper 712-C, 126 p.

Winograd, I.J., 1981, Radioactive waste disposal in thick unsaturated zones: Science, vol. 212, no. 4502, p. 1457-1464.

Winograd, I.J., Szabo, B.J., Coplen, T.B., and Riggs, A.C., 1988, A 250,000-year climate record from Great Basin vein calcite: Implications for Milankovitch theory: Science, vol. 242, p. 1275-1280.

Winograd, I.J., Coplen, T.B., Landwehr, J.M., Riggs, A.C., Ludwig, K.R., Szabo, B.J., Kolesar, P.T., and Revesz, K.M., 1992, Continuous 500,000-year climate record from vein calcite in Devils Hole, Nevada: Science, vol. 258, p. 255-260.

Wittwer, C.S., Bodvarsson, G.S., Chornack, M.P., Flint, A.L., Flint, L.E., Lewis, B.D., Spengler, R.W., and Rautman, C.A., 1992, Design of a three-dimensional site-scale model for the unsaturated zone at Yucca Mountain, Nevada: *Proceedings,* Third International Conference on High Level Radioactive Waste Management," American Nuclear Society, La Grange Park, IL, April 12-16, 1992, Las Vegas, NV., p. 263-271.

Woolhiser, D.A., Smith, R.E., and Goodrich, D.C., 1990, KINEROS, A kinematic runoff and erosion model: Documentation and user manual: U.S. Department of Agriculture, Agricultural Research Service, ARS-77, 130 p.

Wu, Y.S., Bandurraga, T.M., Ahlers, C.F., Finsterle, S., Chen, G., Haukwa, C., Bodvarsson, G.S., Kwicklis, E., Rousseau, J., and Flint, L.E., 1996, Calibration and extension of the LBNL/USGS three-dimensional site-scale model of Yucca Mountain, Nevada: LBNL-UC#, Lawrence Berkeley National Laboratory, Berkeley, CA., 275 p.

Appendix I -- All Yucca Mountain Project data referred to in this report, listed by data tracking number.

Neutron Logging Data

GS940708312212.010*:	Volumetric water content from neutron moisture meter counts for 74 boreholes from time they were drilled until 5/2/89.
GS940708312212.011:	Volumetric water content from neutron moisture meter counts for 99 boreholes from 5/3/89 or from the time they were drilled, until 12/31/93.
GS941408312212.017:	Subsurface water content at Yucca Mountain--neutron logging data from 1/1/94 through FY94.
GS950808312212.001:	Volumetric water content calculated from field calibration equations using neutron counts from 99 boreholes at Yucca Mountain from 1-Oct-94 to 31-May-95.
GS960108312212.001:	Volumetric water content calculated from field calibration equations using neutron counts from 99 boreholes at Yucca Mountain from 1-Jun-95 to 30-Sep-96.

Core Properties

GS920508312231.012:	USW UZ-N54 and USW UZ-N55 core analysis: bulk density, porosity, particle density and in situ saturation for core dried in 105° C oven.
GS930108312231.006:	USW UZ-N53 core analysis: bulk density, porosity, particle density and in situ saturation for core dried in 105° C oven.
GS940408312231.004:	Core analysis of bulk density, porosity, particle density, and in situ saturation for 3 neutron USW UZ-N57, UZ-N61 and UZ-N62.
GS940108312231.002:	Core analysis of bulk density, porosity, particle density and in situ saturation for 17 neutron boreholes: Data for core dried in RH oven and 105° C oven for USW UZ-N31, UZ-N32, UZ-N33, UZ-N34, UZ-N35, UZ-N38, UZ-N58, UZ-N59, UE-25 UZN#63 and USW UZ-N64; data for core dried in 105° C only for USW UZ-N11, UZ-N15, UZ-N16, UZ-N17, UZ-N27, UZ-N36, and UZ-N37.
GS940508312231.006:	Core analysis of bulk density, porosity, particle density and in situ saturation for borehole UE-25 UZ#16.
GS950608312231.007:	Physical properties and water potentials of core from borehole USW NRG-6
GS950408312231.004:	Physical properties and water potentials of core from borehole USW SD-9
GS950408312231.005:	Physical properties and water potentials of core from borehole USW UZ-14
GS950308312231.003:	UE-25 UZ#16 pycnometer data
GS951108312231.009:	Physical properties, water content and water potential for borehole USW SD-7
GS951108312231.011:	Physical properties, water content and water potential for borehole USW UZ-7a
GS951108312231.010:	Physical properties and water content for borehole USW NRG-7/7A
GS950308312231.002:	Laboratory measurements of bulk density, porosity, and water content for USW SD-12
GS960808312231.004:	Physical properties, water content and water potential for lower depths in boreholes USW SD-12 and USW SD-7

Permeability and Moisture-Retention Measurements:

GS950608312231.006:	Water permeability of core from SD-9
GS960808312231.002:	Relative humidity calculated porosity measurements on samples from borehole USW SD-9 used for saturated hydraulic conductivity.
GS960808312231.001:	Water permeability and relative humidity calculated porosity for boreholes UE-25 UZ#16 and USW UZ-N27.
GS950608312231.008:	Moisture retention data from boreholes USW UZ-N27 and UE-25 UZ#16.
GS960808312231.005:	Water permeability and relative humidity calculated porosity measurements on samples from boreholes USW SD-9, USW UZ-14, USW SD-12 and USW SD-7

S960808312231.003:	Moisture retention data for samples from boreholes USW SD-9, USW UZ-14, USW SD-7 and USW SD-12.

Soil Properties and Coverages:

GS940108315142.004:	Preliminary Surficial Deposits Map of the Northeast Quarter of the Busted Butte 7.5 Minute Quadrangle
GS940708315142.008:	Preliminary Surficial Deposits Map of the Northwest Quarter of the Busted Butte 7.5 Minute Quadrangle ..
GS940108315142.005:	Preliminary Map of the Surficial Deposits of the Southern Half of the Topopah Spring NW 7.5 Minute Quadrangle
GS950408315142.004:	Preliminary Map of the Surficial Deposits of the Southern Half of the Busted Butte 7.5 Minute Quadrangle
GS960108312211.001:	FY95 Laboratory Measurements of Physical Properties of Surficial Materials at Yucca Mt, NV Part II
GS960108312211.002:	Gravimetric and Volumetric Water Content and Rock Fragment Content of 31 Selected Sites at Yucca Mt, NV, FY95 Laboratory Measurements of Physical Properties of Surficial Materials at Yucca Mt, NV Part III
GS950708312211.002:	FY95 Laboratory Measurements of Physical Properties of Surficial Materials at Yucca Mt, NV
GS930883117421.002:	Quaternary Deposits Subsurface Soil Data from Soil Pits at Midway Valley
GS940783117421.001:	Quaternary Deposits Subsurface Soil Data from Midway Valley Soil Pits
GS960408312212.005:	Preliminary surficial materials properties map
GS930883117421.002:	Quaternary deposits subsurface soil data from soil pits MWV-P1 through MWV-P7, MWVP-12 through MWVP-17, MWV-P22 through MWVP-26, MWVP-28 through MWVP-33 and MWVP-37 through MWV-P40..
GS940783117421.001:	Quaternary deposits subsurface soil data from Midway Valley soil pits MWV-P9, MWV-P19 through MWV-P21, Collected by S. Lundstrom
GS960908312212.009:	Cumulative infiltration and surface flux rates calculated from raw millivolt readings for FY95
GS950308312213.004:	Cumulative infiltration and surface flux rates conducted in 40 Mile Wash and near UE-25 UZN#7 calculated from raw millivolt readings
GS950908312211.004:	Laboratory measurements of water-retention data.

Precipitation and Evaporation:

GS940808312111.005*:	Precipitation data for water years 1992 and 1993 from a network of nonrecording gages at Yucca Mountain, Nevada, by Dale S. Ambos, Alan L. Flint and Joseph A. Hevesi
GS920708312111.006:	Precipitation data collected from 5 weatherstations August 1991.
GS960908312111.004:	FY95 meteorology data. Data collected at 5 weather stations during FY95.
GS950108312210.001*:	Class A pan Evaporation depth for 1/1/90 to 09/30/94
GS960908312211.004:	Heat dissipation probe data: Bleach Bone Ridge 3/95 - 11/95.

GS960500312212.006*:	Estimation of shallow infiltration and presence of potential fast pathways for shallow infiltration in the Yucca Mountain Area, NV by D.B. Hudson and A.L. Flint

No conclusions in this paper are dependent on the data from the above paper. Information used from this report is for corroborative purposes only, therefore this paper is not considered as source data.

All regional precipitation data (specifically station 4JA and station Area 12)*

*Indicates data that is not qualified for site characterization. Because all stochastic simulations are based on regional precipitation data that is considered non-QA, the model results may be considered as non-QA. However, since all other data used to develop the model is considered as "QA", and each stochastic rainfall simulation which is based on non-QA data, is simply a realization of a possible rainfall distribution, the resultant model should be considered as "QA" for that realization. The model results of net infiltration are simply realizations of a defined precipitation pattern, which does not imply that the precipitation pattern is real, but has a calculated probability of occurring. It is, therefore, the opinion of these authors that all data and model realizations should be considered as "QA" with the exception of the parameters listed in table 6. Other unqualified data, such as pan evaporation data, and neutron moisture meter data collected prior to May of 1989, are used for discussion of processes only and in support of conclusions based on site characterization data. No major conclusions are based solely on any unqualified data.

Appendix II. Locations of neutron boreholes, and information used in numerical model.
[depth class, 1= 0-0.5 m, 2= 0.5-3 m, 3= 3-6 m and 4= >6m; GIS Code corresponds to Table 2; topographic position, 1=channel, 2=sideslope and ridgetop; UTM, universal transverse mercator]

Borehole		UTM Easting (meters)	UTM Northing (meters)	Slope	Aspect	Elevation (meters)	Soil Model Unit	Depth Class	GIS Code	Topographic Position
UE-25 UZN #	1	549587	4079666	8.4	118.9	1217.7	4	4	32	1
UE-25 UZN #	2	549859	4079446	14.9	24.1	1203.0	5	1	30	2
UE-25 UZN #	3	549860	4079454	12.2	27.9	1201.2	4	2	30	2
UE-25 UZN #	4	549863	4079464	9.3	41.3	1201.5	4	4	30	2
UE-25 UZN #	5	549865	4079472	7.7	63.9	1201.8	4	4	31	2
UE-25 UZN #	6	549866	4079477	6.7	78.6	1200.3	4	4	31	1
UE-25 UZN #	7	549867	4079482	5.7	93.9	1200.6	4	4	31	1
UE-25 UZN #	8	549869	4079488	4.5	113.7	1200.6	4	4	31	1
UE-25 UZN #	9	549871	4079500	5.9	138.7	1201.2	4	4	31	2
UE-25 UZN #	10	549440	4079830	13.1	97.8	1230.8	4	1	31	1
USW UZ N-	11	547685	4083086	6.6	59.7	1592.3	7	2	31	2
UE-25 UZN #	12	550036	4079461	3.6	130.8	1190.9	4	4	30	1
UE-25 UZN #	13	550512	4079271	3.0	127.4	1164.6	4	4	12	1
UE-25 UZN #	14	550505	4079254	2.8	110.9	1165.6	4	4	12	2
USW UZ N-	15	547941	4082330	5.7	179.5	1557.2	7	2	17	2
USW UZ N-	16	547872	4082348	6.0	181.3	1559.7	7	2	18	2
USW UZ N-	17	547924	4082370	4.0	134.2	1563.0	5	2	17	2
UE-25 UZN #	18	549597	4078795	2.1	166.1	1225.0	4	4	30	1
UE-25 UZN #	19	549594	4077946	7.0	63.6	1226.8	4	4	31	1
UE-25 UZN #	20	549396	4077968	4.4	98.9	1227.4	4	4	30	1
UE-25 UZN #	21	549400	4077982	4.6	114.4	1227.7	4	4	30	1
UE-25 UZN #	22	549404	4078005	7.2	144.2	1228.0	4	3	28	2
UE-25 UZN #	23	549386	4078033	13.0	165.6	1232.3	5	1	28	2
USW UZ N-	24	548622	4079259	14.2	174.1	1288.4	4	1	31	1
USW UZ N-	25	548367	4079387	10.1	124.1	1321.3	4	1	30	1
USW UZ N-	26	548307	4079487	11.8	139.5	1336.2	4	1	28	1
USW UZ N-	27	547649	4080342	1.2	215.3	1481.0	5	2	18	2
UE-25 UZN #	28	549623	4077765	6.0	130.4	1206.4	4	1	1	2
UE-25 UZN #	29	549579	4077619	7.2	104.3	1211.0	5	1	20	2
UE-25 UZN #	30	549597	4077447	12.4	70.3	1206.7	5	1	28	2
USW UZ N-	31	548839	4078114	6.0	128.2	1266.1	4	3	30	1
USW UZ N-	32	548853	4078134	13.4	172.9	1267.4	5	2	30	2
USW UZ N-	33	548358	4079887	10.1	59.7	1320.4	4	3	32	1
USW UZ N-	34	548375	4079914	4.1	87.2	1318.0	4	3	33	2
USW UZ N-	35	548706	4077509	7.4	83.5	1294.5	4	3	31	1
USW UZ N-	36	549082	4081057	4.8	168.9	1414.9	5	2	17	2
USW UZ N-	37	549129	4079106	4.1	89.8	1257.0	4	4	30	1
USW UZ N-	38	549016	4079096	9.7	45.8	1264.6	4	3	30	2
USW UZ N-	40	549285	4078704	7.5	129.1	1243.3	5	2	28	2
USW UZ N-	41	549072	4078609	6.0	188.5	1255.2	4	3	28	1
USW UZ N-	42	548870	4078566	9.6	46.4	1273.8	4	1	28	1
USW UZ N-	43	548993	4078648	7.6	115.3	1264.6	4	4	30	2
USW UZ N-	44	548935	4078708	15.0	165.6	1268.6	4	1	28	1
USW UZ N-	45	549044	4078642	6.2	133.2	1258.8	4	4	30	1
USW UZ N-	46	547915	4080553	18.3	223.3	1371.9	4	1	33	1
USW UZ N-	47	547926	4080464	4.6	184.1	1365.5	4	4	33	1
USW UZ N-	48	548740	4077074	9.3	83.2	1283.5	4	1	30	1
USW UZ N-	49	548712	4077082	11.2	121.8	1289.0	5	2	28	2
USW UZ N-	50	548892	4077057	17.1	21.9	1271.9	4	2	30	2
USW UZ N-	51	548891	4077083	8.7	73.8	1270.7	4	3	30	1
USW UZ N-	52	548890	4077093	7.5	96.6	1271.6	4	2	30	2
USW UZ N-	53	549296	4076851	9.4	88.1	1236.3	5	2	28	2
USW UZ N-	54	549303	4076905	4.8	122.0	1233.2	4	3	28	1
USW UZ N-	55	549299	4076975	9.2	160.7	1241.5	5	2	30	2
UE-25 UZN #	56	549674	4076943	3.5	104.0	1207.6	4	4	30	1
USW UZ N-	57	548263	4075345	4.5	84.7	1271.9	5	2	45	2
USW UZ N-	58	548273	4075368	3.5	86.1	1274.4	4	2	46	1
USW UZ N-	59	548281	4075393	6.9	143.2	1274.1	4	3	45	1
UE-25 UZN #	60	550006	4076750	3.5	120.1	1186.3	4	4	20	1
USW UZ N-	61	548282	4075409	11.7	161.6	1275.3	4	3	44	2
USW UZ N-	62	547491	4075939	7.0	182.1	1488.6	5	2	18	2
USW UZ N-	63	549875	4079516	8.9	166.1	1202.1	5	2	30	2
USW UZ N-	64	547827	4078562	6.1	103.7	1460.3	5	2	18	2
USW UZ N-	65	548780	4076402	5.2	145.5	1332.6	5	1	18	2
USW UZ N-	66	548580	4076342	7.3	150.8	1327.7	5	1	20	2
USW UZ N-	67	549169	4074882	4.3	123.6	1194.8	4	3	17	1
USW UZ N-	68	549232	4074982	4.0	114.1	1196.3	4	4	11	1
USW UZ N-	69	549352	4075134	3.6	134.7	1194.2	4	4	11	1
USW UZ N-	70	548045	4079636	15.2	134.1	1384.4	4	1	28	1
USW UZ N-	71	547518	4077128	8.3	177.3	1501.1	5	1	17	2
USW UZ N-	72	547585	4077141	13.5	101.6	1490.2	5	1	18	2
USW UZ N-	73	547677	4077136	15.4	109.1	1483.5	5	1	19	2
USW UZ N-	74	547565	4077231	11.4	95.2	1494.7	5	1	17	2
USW UZ N-	75	547722	4077262	9.5	79.1	1462.7	5	2	18	2
USW UZ N-	76	547713	4077229	9.3	95.6	1511.2	5	1	18	2
USW UZ N-	77	546382	4075448	3.8	160.7	1189.0	4	4	20	1
USW UZ N-	78	546869	4076069	10.9	310.6	1274.7	5	1	17	2
USW UZ N-	79	546890	4076123	11.5	254.5	1266.4	4	1	19	1
USW UZ N-	80	547155	4076093	15.8	272.6	1320.4	4	1	32	2
USW UZ N-	81	546665	4076144	7.3	275.2	1239.0	4	2	20	1
USW UZ N-	82	546390	4076049	2.2	128.4	1211.6	4	4	19	1
USW UZ N-	84	546751	4077031	7.3	268.7	1253.3	4	4	17	2
USW UZ N-	86	546926	4077001	10.5	262.0	1271.6	4	1	20	2
USW UZ N-	87	546751	4077031	7.3	268.7	1253.2	4	3	17	2
USW UZ N-	88	546953	4077057	13.0	270.2	1280.8	5	1	19	2
USW UZ N-	89	546660	4076999	2.9	205.1	1246.6	4	4	20	1
USW UZ N-	90	546660	4076998	2.9	205.1	1246.6	4	4	19	1
USW UZ N-	96	547519	4076647	8.4	159.2	1491.4	5	2	17	2
UE-25 UZN #	97	549623	4077766	6.0	130.3	1206.4	4	4	28	2
USW UZ N-	98	548632	4079256	13.5	170.8	1287.2	4	1	31	1

Appendix III -- Program MARKOV

```
      PROGRAM MARKOV
C
C   J. Hevesi, A. Flint, USGS
C   PROGRAM "MARKOV.FOR", Version 1.0
C   TO CALCULATE THE 3RD-ORDER MARKOV CHAIN,
C   2 STATE TRANSITION PROBABILITIES FOR DAILY PRECIPITATION.
C   A DAY WITH PRECIPITATION (WET) IS (1), A DAY WITHOUT
C   PRECIPITATION (DRY) IS (0) ..
C   EXAMPLE:  1111 = WET,WET,WET,WET-- 4 DAYS OF PRECIPITATION
C         0000 = DRY,DRY DRY,DRY-- 0 DAYS OF PRECIPITATION
C         0101 = DRY,WET,DRY,WET-- 2 DAYS OF PRECIPITATION
C
C         A FREQUENCE OF -999 INDICATES THAT THE SEQUENCE HAD ZERO
C         PROBABILITY OF OCCURANCE, ANY OTHER NEGATIVE FREQUENCY
C         HAD 5 OR LESS OCCURANCES AND SHOULD BE VIEWED WITH CAUTION
C         DUE TO THE LIMITED SAMPLE SIZE
c
c---- Global parameters
c
      USE MSIMSL
            CHARACTER*9  STATION
      CHARACTER*8  CODE
      CHARACTER*2  NOTE1(40000),NOTE2(40000),FLG1(40000),FLG2(40000)
      REAL PPT(40000)
      INTEGER*2 IMON(40000),IDAY(40000),IYEAR(40000)
      INTEGER*2 IMON2(40000),IDAY2(40000),IYEAR2(40000)
            INTEGER*2 LPYR(100), MON(12)
      CHARACTER*20 INFILE, OUTFIL1,OUTFIL2
      CHARACTER*80 HEADER
      INTEGER*2 MONB,DAYB,YEARB,MONF,DAYF,YEARF
      INTEGER ISTART,IBUG
            real maxmon(12)
c
c
c---- Markov parameters
c
      REAL CNT(0:20,20)
      REAL TOT(0:20,20)
      REAL FRQ(0:20,20)
      REAL FIRSTAMT,SECNDAMT,THIRDAMT,FORTHAMT
      real i3, ippt
      CHARACTER*2 note01,note02,note03,note04
c
c---- Pdist parameters
c
      REAL PPT2(40000)
      REAL PCUT(20)
      INTEGER NPCUT(20), NPCUTM(12,20), NPCUT2(20), NPCUTM2(12,20)
      INTEGER NDMON3(12),NDMON4(12),NPPTMN(12),NMONTH(12)
      INTEGER NNMON(12),NDMON5(12)
```

```
      REAL frqcut(12,20),avgfrq(12,20),lnfrq(12,20)
      INTEGER nfrqcut(12)
c
C
c---- nonlinear regression parameters
c
    integer ldr,nobs,nparm
    parameter(nparm=2,ldr=nparm)
    external pptfunc
      real aguess,bguess,acoef,bcoef
      integer iseas
      common pcut,lnfrq,nfrqcut,iseas
c
      istart =  1
      ibug   =  0
      aguess = .5
      bguess = .5
c
c
 15  FORMAT(A)
    OPEN(UNIT=7,FILE='markov.ctl')
    READ(7,15) HEADER
    READ(7,15) INFILE
    READ(7,15) OUTFIL1
    READ(7,15) OUTFIL2
c       read(7,*)  aguess,bguess
c
c
    READ(7,*)  MONB, DAYB, YEARB
      READ(7,*)  MONF, DAYF, YEARF
C
c
c---- Open files and print headers ----------
c
    OPEN(UNIT=8,FILE=INFILE)
    OPEN(UNIT=9,FILE=OUTFIL1)
    OPEN(UNIT=10,FILE=OUTFIL2)
    WRITE(10,15) OUTFIL2
      WRITE(9,15) HEADER
    WRITE(9,15) OUTFIL1
    WRITE(9,30)
C
 30  FORMAT(/1X,'TOTAL DAYS WITH PRECIPITATION EXCEEDING EACH BIN',
   1      /1X,'MINIMUM, LEVELS ARE IN HUNDREDTHS OF INCHES',
   2     //1X,'MONTH',1X,'TOTAL',2X,' >0',2X,' >4',2X,' >9',
   3       2X,'>24',2X,'>49',2X,'>74',1X,' >99',1X,'>149',
   4       1X,'>199',1X,'>249',1X,'>299',
   5      /1X,'-----',1X,'-----',2X,'---',2X,'---',2X,'---',
   6       2X,'---', 2X,'---',2X,'---',1X,'----',1X,'----',
   7       1X,'----',1X,'----',1X,'----',/)
C
C
```

```
C---- Set up months and leap years ----------------------------------72
C    ----------------------------
C    This logic needed to check gaps for Markov Chain
c    year 1 = 1901
c    year 4 = 1904 = 1st leap year
c    this logic works only for 1901 thru 1999
c
     DO 100 I = 1,100
       LPYR(I) = 0
 100  CONTINUE
     DO 110 I = 4,100,4
       LPYR(I) = 1
 110  CONTINUE
C
     MON(1) = 31
C    MON(2) = 28  (Leap year logic included in loops)
     MON(3) = 31
     MON(4) = 30
     MON(5) = 31
     MON(6) = 30
     MON(7) = 31
     MON(8) = 31
     MON(9) = 30
     MON(10) = 31
     MON(11) = 30
     MON(12) = 31
C
C---- Initialize monthly counters
c
     DO I = 1,12
       NPPTMN(I) = 0
       NDMON3(I) = 0
       NDMON4(I) = 0
       NDMON5(I) = 0
       NNMON(I) = 0
            maxmon(i) = -999.
     enddo
C
c---- set up bins for distribution of daily ppt
c
          NCUT   = 11
     PCUT(1) = 1.
     PCUT(2) = 5.
     PCUT(3) = 10.
     PCUT(4) = 25.
     PCUT(5) = 50.
     PCUT(6) = 75.
     PCUT(7) = 100.
     PCUT(8) = 150.
     PCUT(9) = 200.
     PCUT(10) = 250.
     PCUT(11) = 300.
```

```
      PCUT(12) = 1000.
C
c---- initialize counters for bins (max 20 bins)
c
      DO 114 I = 1,12
        DO 114 J = 1,20
          NPCUTM(I,J) = 0
          NPCUTM2(I,J) = 0
 114  CONTINUE
C
C
C---- Find user specified starting date in ppt input file ----------72
C     ------------------------------------------------
c
 200  ND  = 1
      READ(8,210,end = 5900) station,
     1        CODE,IMON(ND),IDAY(ND),IYEAR(ND),
     2        PPT(ND),NOTE1(ND),NOTE2(ND)

C
 210   FORMAT(A9,A8,I2,1X,I2,1X,I2,2X,F8.1,A2,1X,A2)
      if(istart.eq.1) then
        IF (IMON(ND).NE.MONB) GOTO 200
        IF (IDAY(ND).NE.DAYB) GOTO 200
        IF (IYEAR(ND).NE.YEARB) GOTO 200
      endif
C
C
c---- Found starting date, now read in rest of ppt file ------------72
c     ------------------------------------------------
c
 300  ND = ND + 1
      NDY = NDY + 1
      READ(8,210,END=310) STATION,CODE,IMON(ND),IDAY(ND),
     1     IYEAR(ND),PPT(ND),NOTE1(ND),NOTE2(ND)
C
            if(istart.eq.1) then
              IF((IMON(ND).EQ.MONF).AND.(IDAY(ND).EQ.DAYF)
     1     .AND.(IYEAR(ND).EQ.YEARF)) THEN
                ND = ND + 1
                GOTO 310
              ENDIF
        GOTO 300
      endif
 310  continue
c
c
c
c---- start module for calculating monthly cumulative distributions --72
c     ------------------------------------------------------------
C
 400  ND = ND - 1
```

```
      IMONF = 12
      NNN = 0
      nn = 0
C
C---- Begin loop for years -----------
c
      DO 410 I = IYEAR(1),IYEAR(ND)
        write(*,*) i
        IF(I.EQ.IYEAR(1)) THEN
          IMON0 = IMON(1)
        ELSE
          IMON0 = 1
        ENDIF
        MON(2) = 28 + LPYR(I)
        IF(I.EQ.IYEAR(ND)) IMONF = IMON(ND)
c
c---- Begin loop for months ----------------
c
        DO 420 J = IMON0,IMONF
          IF((I.EQ.IYEAR(1)).AND.(J.EQ.IMON0)) THEN
            IDAY0 = IDAY(1)
          ELSE
            IDAY0 = 1
          ENDIF
          IF((I.EQ.IYEAR(ND)).AND.(J.EQ.IMONF)) MON(J) = IDAY(ND)
C
          NMISST = 0
          NMIS2 = 0
          NPPTT = 0
          NPPT2 = 0
          NPPT3 = 0
          PPTMAX = -999.
          DO 422 J2 = 1,NCUT
            NPCUT(J2) = 0
            NPCUT2(J2) = 0
 422      CONTINUE
c
c---- Begin loop for days in each month ------------
c
          DO 430 K = IDAY0,MON(J)
            nn = nn + 1
            ppt2(nn) = -999.
            flg1(nn) = ' M'
            flg2(nn) = ' Z'
                  iday2(nn) = k
                  imon2(nn) = j
                  iyear2(nn) = i
            nmiss = 1
            nppt = 0
c
            DO 450 II = 1,ND
              IF(((IYEAR(II).EQ.I).AND.
```

```
     1        (IMON(II).EQ.J)).AND.
     2        (IDAY(II).EQ.K)) THEN
               ppt2(nn) = ppt(ii)
               flg1(nn) = note1(ii)
               flg2(nn) = note2(ii)
               NMISS = 0
               NPPT  = 1
             ENDIF
   450       CONTINUE
C
           IF((ppt2(nn).ne.-999.).AND.
     1      (flg1(nn).ne.' M').AND.
     2      (flg1(nn).ne.' A').AND.
     3      (flg1(nn).ne.' S')) THEN
                    if(maxmon(j).lt.ppt2(nn)) maxmon(j) = ppt2(nn)
             NPPT3 = NPPT3 + 1
             DO 455 L = 1,NCUT
               IF(ppt2(nn).ge.PCUT(L)) NPCUT(L) = NPCUT(L)+1
   455         CONTINUE
           ENDIF

           IF(((flg1(nn).EQ.' M').OR.
     1        (flg1(nn).EQ.' A')).OR.
     2        (flg1(nn).EQ.' S')) NMIS2 = NMIS2 + 1
           NMISST = NMISST + NMISS
           NPPTT  = NPPTT + NPPT
C
   430     CONTINUE
C
                                  NDMON3(J)=NDMON3(J)+NPPT3
C
         DO L = 1,NCUT
           NPCUTM(J,L)  = NPCUTM(J,L) + NPCUT(L)
         enddo
         NMONTH(J) = NMONTH(J) + 1
C
   420   CONTINUE
   410 CONTINUE
C
C---- Loop for writing monthly frequencies for each bin ----------72
c    ------------------------------------------------
C
c---- print out absolute cumulative frequencies
c
      DO J = 1,12
               nfrqcut(j) = 0
c              pptfrq(j) = npcutm(j,1)/ndmon3(j)
        WRITE(9,770) J,NDMON3(J),(NPCUTM(J,L), L=1,11)
   770    FORMAT(1X,I5,1X,I4,1X,I4,1X,I4,1X,I4,1X,I4,1X,I4,
     1        1X,I4,1X,I4,1X,I4,1X,I4,2X,I3,2X,I3,2X,I3)
      enddo
c
```

```
c---- print out relative cumulative frequencies
c
    write(9,772)
 772  format(//)
    do L = 1,11
            do J = 1,12
              avgfrq(j,l) = 0.00001
              frqcut(j,L) = float(npcutm(j,L))/float(npcutm(j,1))
            enddo
c
c------- calculate average frequencies for the following
c       monthly groupings:
c         1,2,3  =  winter
c         4,5,6  =  spring
c         7,8,9  =  summer
c       10,11,12  =  fall
c
            do j = 1,12
              lnfrq(j,l) = 0
              avgfrq(j,L) = float(npcutm(j,l))
           1              /float(npcutm(j,1))
         if(avgfrq(j,l).gt.0) then
           nfrqcut(j) = nfrqcut(j) + 1
                                else
                                  avgfrq(j,l) = .00001
                                endif
         lnfrq(j,l)  = avgfrq(j,l)
c
       enddo
     enddo
c
c
          do l = 1,11
c           write(*,773) pcut(l), (lnfrq(j,l), j=1,6)
            write(9,773) pcut(l), (lnfrq(j,l), j=1,6)
          enddo
c         write(*,'(/)')
          write(9,'(/)')
     do l = 1,11
c           write(*,773) pcut(l), (lnfrq(j,l), j=7,12)
            write(9,773) pcut(l), (lnfrq(j,l), j=7,12)
     enddo
 773    format(1x,f6.0,1x,6f7.4)

c         write(*,'(/)')
          write(9,'(/)')
c
c
c------ Call the nonlinear regression IMSL routine ----------
c
          write(*,774)
          write(9,774)
```

```
 774  format(8x,'month',6x,'a coeff.',6x,'b coeff.',
     1      6x,'maximum ppt(in x 100)')
              do iseas = 1,12
                call nonlinr(nfrqcut,iseas,aguess,acoef,bguess,bcoef)
        write(*,*) iseas,acoef,bcoef,maxmon(iseas)
        write(9,*) iseas,acoef,bcoef,maxmon(iseas)
                write(10,*) iseas,acoef,bcoef,maxmon(iseas)
              enddo

c
c---- Begin Markov Chain analysis
C    Use binary system for assigning values to sequences
c    0 = dry day, 1 = wet day
c    this can be automated to create a universal order Markov model
c    ------------------------------------------------------------
C
c    0000 = 0
c    0001 = 1
c
c    0010 = 2
c    0011 = 3
c
c    0100 = 4
c    0101 = 5
c
c    0110 = 6
c    0111 = 7
c
c    1000 = 8
c    1001 = 9
c
c    1010 = 10
c    1011 = 11
c
c    1100 = 12
c    1101 = 13
c
c    1110 = 14
c    1111 = 15
c
c
c---- initialize the counters for each month
c    ---------------------------------------
c
     do j = 1,12
       do i = 0,15
         tot(i,j) = 0
         cnt(i,j) = 0
         frq(i,j) = 0.
       enddo
     enddo
C
```

```
C---- Read through daily record using 4-point moving window
c     ------------------------------------------------
c
      firstamt = 0
      secndamt = 0
      thirdamt = 0
      forthamt = 0
      if(ppt2(1).gt.0) firstamt = 1
      if(ppt2(2).gt.0) secndamt = 1
      if(ppt2(3).gt.0) thirdamt = 1
      note01   = flg1(1)
      note02   = flg1(2)
      note03   = flg1(3)
      do i = 4,nn
        forthamt = 0
        if(ppt2(i).gt.0) forthamt = 1
        note04 = flg1(i)
        if((note01.eq.' M').or.(note01.eq.' A').or.(note01.eq.' S'))
     1     firstamt = -9999.
        if((note02.eq.' M').or.(note02.eq.' A').or.(note02.eq.' S'))
     1     secndamt = -9999.
        if((note03.eq.' M').or.(note03.eq.' A').or.(note03.eq.' S'))
     1     thirdamt = -9999.
        if((note04.eq.' M').or.(note04.eq.' A').or.(note04.eq.' S'))
     1     forthamt = -9999.
c
        ippt = 1*(forthamt)+2*(thirdamt)+4*(secndamt)+8*(firstamt)
        i3 = -1.
        do i2 = 0,15
          i3 = i3 + 1
          if(ippt.eq.i3) cnt(i2,imon2(i)) = cnt(i2,imon2(i)) + 1
        enddo
c
c
        FIRSTAMT = SECNDAMT

        SECNDAMT = THIRDAMT
        THIRDAMT = FORTHAMT
              note01   = note02
              note02   = note03
              note03   = note04
      enddo
      do j = 1,12
        do i = 1,15,2
          tot(i,j) = cnt(i-1,j) + cnt(i,j)
          if(tot(i,j).ne.0) then
            frq(i-1,j) = cnt(i-1,j)/tot(i,j)
            frq(i,j)   = cnt(i,j)/tot(i,j)
          else
            frq(i-1,j) = 999.
            frq(i,j)   = 999.
          endif
```

```
          if(tot(i,j).lt.5) then
            frq(i-1,j) = -frq(i-1,j)
            frq(i,j)   = -frq(i,j)
          endif
        enddo
      enddo
c
c
c---- Ouput Results from Markov Chain Analysis
c     ----------------------------------------
c
            WRITE(9,24)
  24 FORMAT(///'    3RD ORDER MARKOV CHAIN, 2 STATES'//)
     write(9,41)
     DO J = 1,12
               write(9,60) j, (frq(i,j), i=0,7)
          write(10,60) j, (frq(i,j), i=0,7)
             enddo
c
     WRITE(9,42)
     DO J = 1,12
               write(9,60) j, (frq(i,j), i= 8,15)
               write(10,60) j, (frq(i,j), i=8,15)
             enddo
C
  41 FORMAT(1X,'MONTH',' FREQ0000',' FREQ0001',' FREQ0010',
    1' FREQ0011',' FREQ0100',' FREQ0101',' FREQ0110',' FREQ0111')
  42 FORMAT(/1X,'MONTH',' FREQ1000',' FREQ1001',' FREQ1010',
    1' FREQ1011',' FREQ1100',' FREQ1101',' FREQ1110',' FREQ1111')
  60 FORMAT(2X,I2,8(F9.3))
C
     GOTO 9000
c
c---- error trap ---------
c
 5900 write(*,5910)
 5910 format(/1x,'STARTING DATE NOT FOUND !')
C
 9000 CONTINUE
     CLOSE(7)
     CLOSE(8)
     close(9)
            close(10)
     END
c
c=============================================================
c
            subroutine nonlinr(nfrqcut,iseas,aguess,acoef,
     1           bguess,bcoef)
            integer   iseas,nfrqcut(12)
            real      pcut(20),lnfrq(12,20)
            INTEGER   LDR, NOBS, NPARM
```

```
      real     aguess,acoef,bcoef,bguess
      PARAMETER  (NPARM=2, LDR=NPARM)
      INTEGER   IDERIV, IRANK, NOUT
      REAL      DFE, R(LDR,NPARM), SSE, THETA(NPARM)
      EXTERNAL  pptfunc
C
      COMMON PCUT,LNFRQ

      nobs = nfrqcut(iseas)
      theta(1) = aguess
      theta(2) = bguess
C
      IDERIV = 0
      CALL RNLIN (pptfunc, NPARM, IDERIV, THETA, R, LDR, IRANK, DFE,
     &     SSE)
      acoef = theta(1)
      bcoef = theta(2)
      return
      END
C
c-------------------------------------------------------------
c
      SUBROUTINE pptfunc (NPARM, THETA, IOPT, IOBS, FRQ, WT, E, DE,
     &          IEND)
c     real wgt(11)
      INTEGER   NPARM, IOPT, IOBS, IEND
      REAL      THETA(NPARM), FRQ, WT, E, DE(1)
      INTEGER   iseas,NOBS,nfrqcut(12)
      REAL      EXP, XDATA(20), YDATA(20),PCUT(20),LNFRQ(12,20)
      INTRINSIC  EXP
      COMMON    PCUT,LNFRQ,nfrqcut,iseas

      nobs = nfrqcut(iseas)
      YDATA(IOBS)=PCUT(IOBS)
      xdata(iobs)=lnfrq(iseas,iobs)
C
      IF (IOBS .LE. NOBS) THEN
         wt = 1.0e0
         frq = 100.0
       IEND = 0
         E = ydata(iobs)-((log(xdata(iobs))-theta(1))/(-theta(1)))
     1     **(1/theta(2))
      ELSE
       IEND = 1
      END IF
      RETURN
      END
c=============================================================
```

Appendix IV -- Program PPTSIM

```
      PROGRAM PPTSIM
c     J. Hevesi, A. Flint, USGS
c     Program PPTSIM, Version 1.0
C     9/16/96
C
      INTEGER MON
      INTEGER ISEED(500)
      REAL SPOLD1,SPOLD2,SPOLD3,YEARTOT,YEARMAX,PSIMMMO
      REAL A(12), B(12), PLIM(12), MAXMON(12)
      REAL FRQ0000(12), FRQ0001(12), FRQ0011(12), FRQ0100(12)
      REAL FRQ0110(12), FRQ0101(12), FRQ0010(12), FRQ0111(12)
      REAL FRQ1000(12), FRQ1001(12), FRQ1011(12), FRQ1100(12)
      REAL FRQ1110(12), FRQ1101(12), FRQ1010(12), FRQ1111(12)
C
      REAL RVECT(50000)
      character*20 MODFILE,OUTFILE,OUTSIM
      CHARACTER*80 HEADER
      REAL PSIMHIN, PSIMMM
      INTEGER YR, MO, DY, MOOLD, YROLD, DYOLD, NMEAS
      INTEGER NUMYR
      INTEGER LPYR(500), NDMON(20)
      REAL SUMMEAS, MAXMEAS, MAXMEAS2,SUMMEAS2
      REAL SUMSIM, AVGSIM, MAXSIM, MAXSIM2,SUMSIM2
      COMMON ITAB(55),N1,N2
C
C
C---- Read PARAMETER file, open input/output files, print headers ----72
C
 15   FORMAT(A)
      OPEN(UNIT=7,FILE='PPTSIM.CTL')
      READ(7,15) HEADER
            read(7,15) MODFILE
            READ(7,15) OUTFILE
            read(7,15) OUTSIM
      READ(7,*) NUMYR,ISEED(1)
C
            open(unit=8,file=modfile)
            OPEN(UNIT=9,FILE=OUTFILE)
            open(unit=10,file=outsim)
C
      WRITE(*,15) HEADER
      WRITE(9,15) HEADER
      WRITE(*,40) MODFILE,OUTFILE,OUTSIM
      WRITE(9,40) MODFILE,OUTFILE,OUTSIM
 40   FORMAT(1X,'MODEL PARAMETERS INPUT FILE :   ',A20,
     1    /1X,'OUTPUT FOR SUMMARY RESULTS:     ',A20,
     2    /1x,'OUTPUT FOR SIMULATION RESULTS:  ',A20,//)
            3
            WRITE(9,39)
 39   FORMAT(1X,'    YEAR   TOTAL PPT(mm)   MAXIMUM PPT(mm)',/)
```

```
          READ(8,15) HEADER
      DO 20 I = 1,12
        READ(8,*) MON, A(I), B(I), MAXMON(I)
 20   CONTINUE
        DO 25 I = 1,12
        READ(8,*) IM,FRQ0000(IM),FRQ0001(IM),FRQ0010(IM),FRQ0011(IM),
     1          FRQ0100(IM),FRQ0101(IM),FRQ0110(IM),FRQ0111(IM)
 25   CONTINUE
        DO 26 I = 1,12
        READ(8,*) IM,FRQ1000(IM),FRQ1001(IM),FRQ1010(IM),FRQ1011(IM),
     1          FRQ1100(IM),FRQ1101(IM),FRQ1110(IM),FRQ1111(IM)
 26   CONTINUE
c
           do j= 1,12
         if(frq0000(j).lt.-9) frq0000(j) = 0.
         if(frq0001(j).lt.-9) frq0001(j) = 0.
         if(frq0010(j).lt.-9) frq0010(j) = 0.
         if(frq0011(j).lt.-9) frq0011(j) = 0.
         if(frq0100(j).lt.-9) frq0100(j) = 0.
         if(frq0101(j).lt.-9) frq0101(j) = 0.
         if(frq0110(j).lt.-9) frq0110(j) = 0.
         if(frq0111(j).lt.-9) frq0111(j) = 0.
         if(frq1000(j).lt.-9) frq1000(j) = 0.
         if(frq1001(j).lt.-9) frq1001(j) = 0.
         if(frq1010(j).lt.-9) frq1010(j) = 0.
         if(frq1011(j).lt.-9) frq1011(j) = 0.
         if(frq1100(j).lt.-9) frq1100(j) = 0.
         if(frq1101(j).lt.-9) frq1101(j) = 0.
         if(frq1110(j).lt.-9) frq1110(j) = 0.
         if(frq1111(j).lt.-9) frq1111(j) = 0.
           enddo
           numseed = 1
           ns = 1
c
    DO 3000 I = 1,NS
C
c----- initialize parameters
c
    SUMMEAS = 0.
    SUMMEAS2 = 0.
    SUMSIM  = 0.
    SUMSIM2 = 0.
    MAXMEAS = -999.
    MAXMEAS2 = -999.
    MAXSIM  = -999.
    MAXSIM2 = -999.
    SPOLD = 1
          spold1 = 0.
          spold2 = 0.
          YEARMAX = -999.
          YEARTOT = 0.
```

```
          YROLD = 1
C
C---- Initialize RAN1 psuedo-random number generator FUNCTION
c    N = 40000 good for 109 year simulation using 1 seed
c
     IDUM = -ISEED(I)
     RDUM = RAN1(IDUM)
     N    = 40000
     IDUM = ISEED(I)
     DO 150 II = 1,N
       RVECT(II) = RAN1(IDUM)
 150  CONTINUE
c
C
C---- Set up months and leap years for 200 years starting at 1900
c
     DO 160 I2 = 1,200
        LPYR(I2) = 0
 160  CONTINUE
     DO 170 I2 = 4,200,4
        LPYR(I2) = 1
 170  CONTINUE
C
     NDMON(1) = 31
     NDMON(2) = 28
     NDMON(3) = 31
     NDMON(4) = 30
     NDMON(5) = 31
     NDMON(6) = 30
     NDMON(7) = 31
     NDMON(8) = 31
     NDMON(9) = 30
     NDMON(10) = 31
     NDMON(11) = 30
     NDMON(12) = 31
C
C
c---- Begin simulation ----------
c    ----------
C
     N = 0
     NMEAS = 0
     NDMO = 0
C
     DO 1000 I3 = 1,NUMYR
       YR = I3
       NDY2 = 0
       DO 1000 J = 1,12
         MO = J
         NDMON2 = NDMON(J)
         IF(J.EQ.2) NDMON2 = NDMON(J) + LPYR(I3)
         DO 1000 K = 1,NDMON2
```

```
          N = N + 1
          DY = K
          NDY2 = NDY2 + 1
C
C
          IF(N.EQ.1) THEN
            MOOLD = MO
            DYOLD = DY
            YROLD = YR
          ENDIF
c
C---- -- Calculate precip using fitted model ----------
C       and markov chain transition probabilities.
c       For the 1st 3 days simulated;
c       plim(mo) = probality of having measurable precip
C
          IF(N.LE.3) THEN
c
C       -------- Do 1st 3 days of simulation
c
                  plim(j) = abs(frq0001(j))
            IF(RVECT(N).LE.PLIM(J)) THEN
              RVECT(40001) = RAN1(IDUM)
              PSIMHIN = ((ALOG(1-RVECT(40001))-A(J))/(-A(J)))
     1           **(1/B(J))
            ELSE
              PSIMHIN = 0.
            ENDIF
c
          ELSE
c
c       -------- Markov chain = 111x
c
            IF ((SPOLD1.GT.0.).AND.(SPOLD2.GT.0.).AND.
     1        (SPOLD3.GT.0)) THEN
              IF(RVECT(N).Lt.abs(FRQ1111(J))) THEN
                RVECT(40001) = RAN1(IDUM)
                PSIMHIN = ((ALOG(1-RVECT(40001))-A(J))/(-A(J)))
     1                **(1/B(J))
              ELSE
                PSIMHIN = 0.
              ENDIF
C
c       -------- Markov chain = 110x
c
            ELSE IF ((SPOLD1.GT.0.).AND.(SPOLD2.GT.0.).AND.
     1        (SPOLD3.EQ.0.)) THEN
              IF(RVECT(N).Lt.abs(FRQ1101(J))) THEN
                RVECT(40001) = RAN1(IDUM)
                PSIMHIN = ((ALOG(1-RVECT(40001))-A(J))/(-A(J)))
     1                **(1/B(J))
              ELSE
```

```
              PSIMHIN = 0.
            ENDIF
c
c     -------- Markov chain = 101x
c
          ELSE IF ((SPOLD1.GT.0.).AND.(SPOLD2.EQ.0.).AND.
     1       (SPOLD3.GT.0.)) THEN
            IF(RVECT(N).Lt.abs(FRQ1011(J))) THEN
              RVECT(40001) = RAN1(IDUM)
              PSIMHIN = ((ALOG(1-RVECT(40001))-A(J))/(-A(J)))
     1                **(1/B(J))
            ELSE
              PSIMHIN = 0.
            ENDIF
C
C     -------- Markov chain = 100x
c
          ELSE IF ((SPOLD1.GT.0.).AND.(SPOLD2.EQ.0.).AND.
     1       (SPOLD3.EQ.0.)) THEN
            IF(RVECT(N).Lt.abs(FRQ1001(J))) THEN
              RVECT(40001) = RAN1(IDUM)
              PSIMHIN = ((ALOG(1-RVECT(40001))-A(J))/(-A(J)))
     1                **(1/B(J))
            ELSE
              PSIMHIN = 0.
            ENDIF
c
c     -------- Markov chain = 011x
c
          ELSE IF ((SPOLD1.EQ.0.).AND.(SPOLD2.GT.0.).AND.
     1       (SPOLD3.GT.0)) THEN
            IF(RVECT(N).Lt.abs(FRQ0111(J))) THEN
              RVECT(40001) = RAN1(IDUM)
              PSIMHIN = ((ALOG(1-RVECT(40001))-A(J))/(-A(J)))
     1                **(1/B(J))
            ELSE
              PSIMHIN = 0.
            ENDIF
C
c     -------- Markov chain = 010x
c
          ELSE IF ((SPOLD1.EQ.0.).AND.(SPOLD2.GT.0.).AND.
     1       (SPOLD3.EQ.0.)) THEN
            IF(RVECT(N).Lt.abs(FRQ0101(J))) THEN
              RVECT(40001) = RAN1(IDUM)
              PSIMHIN = ((ALOG(1-RVECT(40001))-A(J))/(-A(J)))
     1                **(1/B(J))
            ELSE
              PSIMHIN = 0.
            ENDIF
c
c     -------- Markov chain = 001x
```

```
c
          ELSE IF ((SPOLD1.EQ.0.).AND.(SPOLD2.EQ.0.).AND.
     1      (SPOLD3.GT.0.)) THEN
            IF(RVECT(N).Lt.abs(FRQ0011(J))) THEN
              RVECT(40001) = RAN1(IDUM)
              PSIMHIN = ((ALOG(1-RVECT(40001))-A(J))/(-A(J)))
     1                **(1/B(J))
            ELSE
              PSIMHIN = 0.
            ENDIF
C
C       -------- Markov chain = 000x
c
          ELSE IF ((SPOLD1.EQ.0.).AND.(SPOLD2.EQ.0.).AND.
     1      (SPOLD3.EQ.0.)) THEN
            IF(RVECT(N).Lt.abs(FRQ0001(J))) THEN
              RVECT(40001) = RAN1(IDUM)
              PSIMHIN = ((ALOG(1-RVECT(40001))-A(J))/(-A(J)))
     1                **(1/B(J))
            ELSE
              PSIMHIN = 0.
            ENDIF
C
          ENDIF
C
C
C---- Calculate monthly statistics and print out for each month. -----72
c    Missing record is not included in calculation of average
c    monthly statistics.
c
        IF(MO.NE.MOOLD) THEN
          NN = N - 1
        ENDIF
          NDMO  = 0
          SUMMEAS2 = 0.
          SUMSIM2  = 0.
        ENDIF
C
C

IF((PSIMHIN).GT.MAXMON(J)) PSIMHIN = MAXMON(J)
        PSIMMM  = PSIMHIN*0.254
        SUMSIM  = SUMSIM + PSIMMM
        SUMSIM2 = SUMSIM2 + PSIMMM
        IF(MAXSIM.LT.PSIMMM) MAXSIM = PSIMMM
        IF(MAXSIM2.LT.PSIMMM) MAXSIM2 = PSIMMM
C
C
c---- -- Print out daily simulation results ----------
c      SPOLD1 = precip for 1st day in 3-day sequence
c      SPOLD2 = precip for 2nd day in 3-day sequence
C
```

```
          YEARTOT = YEARTOT + PSIMMMO
          IF(YEARMAX.LT.PSIMMMO) YEARMAX = PSIMMMO
          IF(YROLD.NE.YR) THEN
            WRITE(9,230) YROLD,YEARTOT,YEARMAX
 230    FORMAT(1X,I10,2X,F10.3,2X,F10.3)
       YEARTOT = 0.
            YEARMAX = -999.
          ENDIF
C
          IF(YR.EQ.NUMYR.AND.MO.EQ.12.AND.DY.EQ.31) THEN
            WRITE(9,231) YR,YEARTOT,YEARMAX
 231    FORMAT(1X,I10,2X,F10.3,2X,F10.3)
       YEARTOT = 0.
            YEARMAX = -999.
          ENDIF

C
          WRITE(10,220) MO,DY,YR,NDY2,PSIMMM
 220        FORMAT(1X,I2,1X,I2,1X,I3,1X,I4,1X,F8.2)
          PSIMMMO = PSIMMM
          DYOLD = DY
          YROLD = YR
          MOOLD = MO
          SPOLD1 = SPOLD2
          SPOLD2 = SPOLD3
          SPOLD3 = PSIMHIN
C
 1000 CONTINUE
C
    AVGSIM  = (SUMSIM/N)*365.25
C
 3000 CONTINUE
C
    WRITE(*,5010) N,ISEED(NS),AVGSIM,MAXSIM
    WRITE(9,5010) N,ISEED(NS),AVGSIM,MAXSIM
 5010 FORMAT(/1X,'TOTAL NUMBER OF DAYS SIMULATED      = ',I12,
    1     /1X,'SEED FOR SIMULATION              = ',I12,
    2     /1X,'SIMULATED AVERAGE ANNUAL PPT (mm)   = ',F12.4,
    3     /1X,'SIMULATED MAXIMUM DAILY PPT (mm)    = ',F12.4)
C
    CLOSE(9)
          CLOSE(10)
    END
C
C=============================================================
C---- Uniform normal deviate generater using random number algorithm
C    RAN1 FUNCTION
C    FROM PRESS ET AL "NUMERICAL RECIPES" (1990) FOR
C    USING LINEAR CONRUENTIAL GENERATORS FOR PRODUCING
C    AN INDEPENDENT SERIES OF RANDOM NUMBERS FOR THE
C    GENERATION OF A UNIFORM DEVIATE
c
```

```
      FUNCTION RAN1(IDUM)
      REAL R(97)
      PARAMETER (M1=259200,IA1=7141,IC1=54773,RM1=1./M1)
      PARAMETER (M2=134456,IA2=8121,IC2=28411,RM2=1./M2)
      PARAMETER (M3=243000,IA3=4561,IC3=51349)
      DATA IFF /0/
      IF (IDUM.LT.0.OR.IFF.EQ.0) THEN
        IFF = 1
        IX1 = MOD(IC1-IDUM,M1)
        IX1 = MOD(IA1*IX1+IC1,M1)
        IX2 = MOD(IX1,M2)
        IX3 = MOD(IX1,M3)
        DO 11 J = 1,97
          IX1 = MOD(IA1*IX1+IC1,M1)
          IX2 = MOD(IA1*IX2+IC2,M2)
          R(J) = (FLOAT(IX1)+FLOAT(IX2)*RM2)*RM1
11      CONTINUE
        IDUM = 1
      ENDIF
      IX1 = MOD(IA1*IX1+IC1,M1)
      IX2 = MOD(IA2*IX2+IC2,M2)
      IX3 = MOD(IA3*IX3+IC3,M3)
      J  = 1+(97*IX3)/M3
      IF(J.GT.97.OR.J.LT.1) PAUSE
      RAN1 = R(J)
      R(J) = (FLOAT(IX1)+FLOAT(IX2)*RM2)*RM1
      RETURN
      END
```

Appendix V -- Program INFIL

```
      PROGRAM INFIL
c           Program INFIL.FOR, Version 1.0
c           J. Hevesi and A. Flint, USGS                                    c
c           (9/2/96)
C           COMPILED USING WIN3.11, FORTRAN POWERSTATION
c           solar and net radiation routine developed by A. Flint after
c           potential ET routine developed by A. Flint after Priestley-Taylor
c           Richards eq. finite difference routine after Campbell
c           modified Priestley-Taylor ET function after Flint
c           begin modifications 03/27/96 by J. Hevesi:
c

      INTEGER IMODEL,ILOOP,ibucket,fracmod,itime
           INTEGER NROCKID,NSOILID,ROCKID,SOILID
      INTEGER MAXITER,MAXIT,MINIT,ITER,NIM2,imflag
      INTEGER I,M,DBGFLAG,ILOCOUT,NDAYS,NDAYOUT,DEPTHFLG,IRTZ,MOISTCR
           INTEGER yrbeg,yrend,dnbeg,dnend,month,day
      INTEGER PPTYUC,DBGFLAG2
c
c---- precip input file parameters
c    40,000 days = 109.514 years
c
      INTEGER YR(40000),DN(40000)
           REAL PPT(40000)
C
C---- map parameter input file variables
C     5000 locations too big for 32 Mbytes ram (4/5/96)
c     1000 locations was OK for 40 Mbytes ram
C
      INTEGER LOCID(200),TOPOID(200),DEPTHCLASS(200),
     1       SOILTYPE(200),ROCKTYPE(200)
      REAL EASTING(200),NORTHING(200),ELEV(200),SL(200),
     1    ASP(200),DEPTH(200),BR(200),RTZDPTH(200)
      REAL RIDGE(200,0:36)
C
      DOUBLE PRECISION LAT(200),LON(200)
C
c---- Mass balance statistics ----------------------------------------
c
           REAL SUMFRC(200),AVGFRCY(200),MAXFRCY(200),
     1    MINFRCY(200),MAXFRCD(200)
      real sumfbot(200),sumfin(200),sumfout(200),
     1    avgfbot(200),avgfin(200),avgfout(200)
           REAL SUMEVP(200),AVGEVPD(200),MAXEVPD(200),
     1    MINEVPD(200),AVGEVPY(200)
c          maxevpy(2000)
c
           REAL SUMPND(200),AVGPNDY(200),MAXPNDY(200),
     1    MINPNDY(200),MAXPNDD(200)
           REAL SUMFLB(200),AVGFLBY(200),MAXFLBY(200)
```

```
C
C
      REAL years,TPET,PETRS,PPTLOC
      REAL HSTEP,DT,MAXDT,MINDT,DTMIN,JTIME,DTX
C
      REAL SSINK,TSINK,SW,SW2,SSW2,AVGSW2
            REAL SFRAC,SFRAC2,SSFRAC,AVGFRAC
            real sfracin,sfrin,sfracout,sfrout,sfrbot,sfr80
            REAL SSPPT,AVGPPT2,SSET,AVGET,SPOND2,SSPOND,AVGPOND
            real ssfrin,ssfrout,ssfrbot,ssfr80
C
            REAL PPTFACT,ETFACT,PONDFACT,FR1FACT,FR2FACT,pptfact2
      REAL AVGPPT,MAXPPT,SPPT,AVGELEV,MAXELEV,MINELEV,SELEV
      REAL AVGSL,SSL,MAXSL
C
      DOUBLE PRECISION BETA(366),PG(366),WP(366),CSR(366),OZONE(366)
      REAL TR,RD,DR,PI
C
c----- Richards eq. parameters for rock and soil types ---------
c     max of 300 different rock types, 20 different soil types
c
      REAL ROCKCAP(0:300),ROCKRESID(0:300),ROCKPORO(0:300),
     1    ROCKALBETA(0:300),ROCKTALPHA(0:300),ROCKKS(0:300),
     2    ROCKPE(0:300),ROCKBVAL(0:300),ralpha(0:300),
     3    ROCKFRACKS(0:300),POTIR(0:300),ROCKVGN(0:300),imbibe(0:300)

      REAL FIELDCAP(20),SOILRESID(20),SOILPORO(20),sorp(20),
     1    SOILALBETA(20),SOILTALPHA(20),POTIS(20),salpha(20),
     2    SOILKS(20),SOILPE(20),SOILBVAL(20),SOILPOND(20),SOILVGN(20)
c
c
c----- Richards eq. parameters ------------
c     (dimensioned for 100 nodes)
c
C     INITIAL WATER CONTENT (WAT)
C     KS    = saturated hydraulic conductivity (Kg/m^2 sec)
C     PE    = air entry matric potential, (-J/Kg)
C     B     = moisture characteristic B value (Brooks and Corey)
C     BD    = bulk density (not used in program)
C     Z     = depth below surface (meters), positive down
C     DZ    = distance between element nodes (meters)
C     DT    = Richards eq. time step (seconds)
C           FLBOT = downward matric flux across bottom element (net infiltration)
C           FL    = downward matric flux into top element
C           M     = number of finite difference elements = 100
c
c---- Dynamic root zone parameters ----------------------------
c
            INTEGER IDPTH
      REAL ROOTW(0:101),DELVWC(0:101),RTZFN(0:101),RTZADJ(0:101)
            REAL RTZA(10),RTZB(10),RTZC(10),RTZD(10),BSOIL(10),VWCF2(10)
            REAL IDPTH2
```

```
      REAL SRTZFN,SRTZF2,SDELVWC,BSOIL2,DELVWCF
c
c---- Thomas Algorithm parameters (after G. Camplbell) ----------
c
      DOUBLE PRECISION DZ,SE,IM,FLBOT,fltop,fl80,flbr,WD,GR,TI,IM2,IM3,
     1            sfltop,sflbr,sfl80,sflbot
c
      DOUBLE PRECISION A(0:101),B(0:101),C(0:101),CP(0:101),
     1 F(0:101),Z(0:101),V(0:101),DP(0:101)

      DOUBLE PRECISION WC(200,0:101),WN(200,0:101),POT(200,0:101),
     1 K(200,0:101),SOURCE(200,0:101),
     2 SINK(200,0:101),FRAC(200,0:101),
     3 POND(200,0:101),REALPHA(200,0:101),
     4 FRACIN(200,0:101),FRACOUT(200,0:101)
c
      DOUBLE PRECISION KS(200,0:101),PE(200,0:101),BVAL(200,0:101),
     1     BCN(200,0:101),PORO(200,0:101),
     2     ALBETA(200,0:101),TALPHA(200,0:101),SOILP(200,0:101),
     3     FRACKS(200,0:101)
c
c
      real etresid(200,0:101),rockcp(200,0:101),
     1    vgn(200,0:101),vgm(200,0:101),vgalpha(200,0:101)
c        resid(2000,0:101)
c    2    rockn(2000,0:101),rockm(2000,0:101)
c
c
c---- following parameters are specific to the BUCKET model
c
      real soilvwc(200),runoffmm(200),drainvwc(200),
     1    buckmm(200),netinfil(200)
      real massbal,balance
      real infilmm,imb,tet,dsoilmm
      real yearppt,yeartet,yeardsw,yearnet,yearinf,yearoff,
     1    yearpet,yearbal
      real totppt,tottet,totdsw,totnet,totinf,totoff,
     1    totpet,totbal
c---------
c
      CHARACTER*20 INFILE,OUTFILE,PPTFILE,DBGFILE,FLXFILE,PROFILE
           CHARACTER*20 MAPFILE,DBGFIL2
      CHARACTER*80 HEADER,DUMBHEAD
c
C
c
c=================================================================
c============================== begin main program ===============
c
c          open control file and all I/O files
C    start modification to use BUCKET model as an option 8/15/96
c    IMODEL = 0 for bucket model, 1 for finite difference model
```

```
C    ILOOP  = 0 for looping through time 1st
c    ILOOP  = 1 for looping through locations 1st
c
C
 5   FORMAT(A)
C
     OPEN(UNIT=7,FILE='INFIL22g.CTL')
     READ(7,5) HEADER
           READ(7,*) IMODEL,ILOOP,IBUCKET
     READ(7,*) YRBEG,DNBEG,YREND,DNEND
           READ(7,*) MAXITER,MAXDT,MINDT,MAXIT,MINIT,HSTEP
           READ(7,*) IM2,IM3,itime
           READ(7,*) ILOCOUT,NDAYOUT
           READ(7,*) PPTFACT,ETFACT,FR1FACT,FR2FACT,PONDFACT
     READ(7,*) PPTYUC
     READ(7,5) PPTFILE
           READ(7,*) DEPTHFLG,IRTZ,DELVWCF,MOISTCR,FRACMOD
     READ(7,5) INFILE
     READ(7,5) OUTFILE
           READ(7,5) FLXFILE
           READ(7,5) PROFILE
           READ(7,5) MAPFILE
           READ(7,*) DBGFLAG,DBGFLAG2
           READ(7,5) DBGFILE
           READ(7,5) DBGFIL2
C
C------- read in parameters for dynamic root-zone function -------
C
C          IF (IRTZ.EQ.1) THEN
     do i = 1,4
             READ(7,5) DUMBHEAD
     enddo
           READ(7,*) NUMDEPTH
           DO I = 1,NUMDEPTH
             READ(7,*) IDPTH,IDPTH2,RTZA(IDPTH),RTZB(IDPTH),
    1        RTZC(IDPTH),RTZD(IDPTH),BSOIL(IDPTH),
    2        VWCF2(IDPTH)
           ENDDO
C
C------- read in soil properties data -----------
C
     do i = 1,4
             READ(7,5) DUMBHEAD
     enddo
           READ(7,*) NSOILID
           DO I = 1,NSOILID
             READ(7,*) SOILID,FIELDCAP(SOILID),SOILRESID(SOILID),
    1        SOILPORO(SOILID),SOILALBETA(SOILID),
    2        SOILTALPHA(SOILID),SOILKS(SOILID),SOILPE(SOILID),
    3        SOILBVAL(SOILID),SALPHA(soilid),SOILVGN(SOILID),
    4        SORP(SOILID),soilpond(soilid),POTIS(SOILID)
     ENDDO
```

```
C
C------- read in rock properties data -----------
C
    do i = 1,4
            READ(7,5) DUMBHEAD
           enddo
           READ(7,*) NROCKID
           DO I = 1,NROCKID
             READ(7,*) ROCKID,ROCKCAP(ROCKID),ROCKRESID(ROCKID),
   1
ROCKPORO(ROCKID),ROCKALBETA(ROCKID),
   2         ROCKTALPHA(ROCKID),ROCKKS(ROCKID),ROCKPE(ROCKID),
   3         ROCKBVAL(ROCKID),RALPHA(rockid),ROCKVGN(ROCKID),
   4         ROCKFRACKS(ROCKID),IMBIBE(ROCKID),POTIR(ROCKID)
    ENDDO
C
C------- finished reading control file, open all files ---------------
c
C    INFILE  = site specific parameter input file
c    OUTFILE = main output file (same as screen output)
c    PPTFILE = daily precipitation input file
c    DBGFILE = program development output file
c    FLXFILE = daily flux output for specified location
c    PROFILE = spyglass profile data for model calibration
c    MAPFILE = simulation results for areal mapping
C
    OPEN(UNIT=11,FILE=PPTFILE)
    OPEN(UNIT=8,FILE=INFILE)
    OPEN(UNIT=9,FILE=OUTFILE)
    OPEN(UNIT=10,FILE=PROFILE)
           OPEN(UNIT=12,FILE=FLXFILE)
           OPEN(UNIT=13,FILE=DBGFILE)
           OPEN(UNIT=14,FILE=MAPFILE)
           OPEN(UNIT=15,FILE=DBGFIL2)
c
C
C---- SET DAILY ATMOSPHERIC PARAMETERS FOR YUCCA MOUNTAIN ----------
C    ------------------------------------------------
c
    CALL ATMOS(OZONE,WP,BETA,CSR,PG)
C
C
C---- read precipitation file (will be modified to subroutine)
c           (improved logic of julian day counter to handle leep years)
c           ND = total number of days for simulation
c
    ND = 0
    SPPT = 0.
    MAXPPT = 0.
 20           ND = ND +1
      READ(11,*,END=30) month,day,yr(nd),dn(nd),ppt(nd)
c           1   YR(nd),DN(nd),PPT(nd)
```

```
        if((yr(nd).ge.yrend).and.(dn(nd).ge.dnend)) then
          nd = nd + 1
          goto 30
        endif
              if(yr(nd).lt.yrbeg) then
          nd = nd - 1
          goto 20
        endif
                                  if((yr(nd).eq.yrbeg).and.(dn(nd).lt.dnbeg)) then
          nd = nd - 1
          goto 20
              endif
        SPPT = SPPT + PPT(nd)
        IF(MAXPPT.LT.PPT(nd)) MAXPPT = PPT(nd)
c
      GOTO 20
c
 30   ND = ND - 1
      YEARS = FLOAT(ND)/365.25
      AVGPPT = SPPT/YEARS
      WRITE(*,5) HEADER
      WRITE(*,35) ND,YEARS,SPPT,AVGPPT,MAXPPT
 35   FORMAT(//1X,'TOTAL NUMBER OF DAYS READ IN  = ',I8,
     1     /1X,'TOTAL NUMBER OF YEARS READ IN = ',F8.3,
     2     /1X,'TOTAL DAILY PRECIP          = ',F8.1,
     3     /1X,'AVERAGE ANNUAL PRECIP (MM)   = ',F8.1,
     4     /1X,'MAXIMUM DAILY PRECIP (MM)    = ',F8.1/)
C
C
      IF(IBUCKET.EQ.1) THEN
            WRITE(*,36)
 36     FORMAT(//1X,'IBUCKET = 1'//)
        pause
      ENDIF
c
c----       read in INFILE for parameters needed to define material
c           properties for Richards Eq and Et function, for
c           net radiation calculations, and for the BUCKET model
c           (either as neutron borehole data or for generating maps)
c
c
            NLOC   = 1
            SSL    = 0.
            SELEV  = 0.
            MAXSL  = -99999.
            MAXELEV = -99999.
            MINELEV =  99999.
C
      illopx = 0
 500  READ(8,*,END=510) LOCID(nloc),EASTING(nloc),NORTHING(nloc),
     1     LAT(nloc),LON(nloc),SL(nloc),ASP(nloc),ELEV(nloc),
     2     SOILTYPE(nloc),DEPTHCLASS(nloc),ROCKTYPE(nloc),
```

```
    3   TOPOID(nloc),(RIDGE(nloc,II), II=1,36)
c
      if(lon(nloc).lt.0) lon(nloc) = -lon(nloc)
            NLOC  = NLOC + 1
            SSL   = SSL + SL(NLOC-1)
            SELEV = SELEV + ELEV(NLOC-1)
            IF (MAXSL.LE.SL(NLOC-1)) MAXSL = SL(NLOC-1)
            IF (MAXELEV.LE.ELEV(NLOC-1)) MAXELEV = ELEV(NLOC-1)
            IF (MINELEV.GE.ELEV(NLOC-1)) MINELEV = ELEV(NLOC-1)
      if(ibucket.eq.1) then
              nloc = 2
              iloopx = 1
              goto 510
            endif
          GOTO 500

 510      NLOC  = NLOC-1
    if(nloc.eq.0) then
      nloc = 1
      goto 3500
    endif
    AVGSL  = SSL/NLOC
    AVGELEV = SELEV/NLOC
C
    if(ibucket.NE.1) then
          WRITE(*,515) NLOC,AVGELEV,MAXELEV,MINELEV,AVGSL,MAXSL
 515   FORMAT(/1X,'TOTAL NUMBER OF LOCATIONS   = ',I8,
   1      /1X,'AVERAGE ELEVATION OF SAMPLE  = ',F8.1,
   2      /1X,'MAXIMUM ELEVATION OF SAMPLE  = ',F8.1,
   3      /1X,'MINIMUM ELEVATION OF SAMPLE  = ',F8.1,
   4      /1X,'AVERAGE SLOPE OF SAMPLE      = ',F8.1,
   5      /1X,'MAXIMUM SLOPE OF SAMPLE      = ',F8.1//)
C
     PAUSE
    endif
C
c
c=================== Finished reading all input files ================72
c              ---------------------------------
c
c---- initialize constants
c
C   DR  = degrees to radians conversion
c   RD  = radians to degrees conversion
c   GR  = gravitational accelleration (m/s)
c   PI  = pie
c   WD  = water mass to volume conversion term (water density factor)
c
    DR   = 0.0174533
    RD   = 57.29579
    PI   = 3.141592654
         GR   = 9.8
```

```
   WD   = 1000.
c
c----      define finite difference mesh parameters
C
c          Z                    = node depth in meters (positive down)
c          DZ                   = node spacing in meters (constant)
c          DT                   = time step in seconds (2 hours, constant)
c          Z(M=1)  = bottom boundary at 10 meters
c          M                    = number of nodes in model, set to 100 earlier
c          TI                   = start time = 0
c
   M    = 100
   Z(M+1) = 11.
   DZ   = .1
   DT   = 7200.
          TI   = 0.
          TSINK = 0.
          ITER = 0
c
c
C==== Loop through all locations for initializing parameters ========72
C   ----------------------------------------------------
C
   DO 90 IA = 1,NLOC
C
C---- initialize terms for calculating results
c
c   bucket mass balance terms
c
      pptloc     = 0.
      tpet       = 0.
      tet        = 0.
      dsoilmm    = 0.
      netinfil(ia) = 0.
      infilmm    = 0.
      runoffmm(ia) = 0.
      massbal    = 0.
      soilvwc(ia)  = 0.1
c
      yearppt = 0.
      yeartet = 0.
      yeardsw = 0.
      yearnet = 0.
      yearinf = 0.
      yearoff = 0.
      YEARPET = 0.
            YEARBAL = 0.
      totppt = 0.
      tottet = 0.
      totdsw = 0.
      totnet = 0.
      totinf = 0.
```

```
      totoff = 0.
      totpet = 0.
      totbal = 0.
c
c     infil mass balance terms
c
            SUMFRC(IA)  = 0.
            SUMEVP(IA)  = 0.
            SUMPND(IA)  = 0.
            SUMFLB(IA)  = 0.
            sumfin(ia)  = 0.
            sumfout(ia) = 0.
            sumfbot(ia) = 0.
            MAXFRCY(IA) = -9999.
            MAXFRCD(IA) = -9999.
            MINFRCY(IA) =  9999.
            MAXEVPD(IA) = -9999.
            MINEVPD(IA) =  9999.
            MAXPNDY(IA) = -9999.
            MAXPNDD(IA) = -9999.
            MINPNDY(IA) =  9999.
            MAXFLBY(IA) = -9999.
c
c----       Set up depth classes and root-zone depth
c     according to alluvium thickness
C     if depthflg = 0, set depths and root-zone according to depthclass
c     if depthflg = 1, set depths and root-zone to actual depths
C     maximum root-zone depth is 6 m.
c     maximum root-zone depth in bedrock is 2.0 m.
C     rootzone depths were modified on approx. 7/21/96
c
c       set root zone depths for fixed depth classes (depthflg = 0)
c
            IF(DEPTHFLG.EQ.0) THEN
              IF (DEPTHCLASS(ia) .EQ. 1.) THEN
                DEPTH(IA)   = 0.5
                RTZDPTH(IA) = 1.5
              ELSE IF (DEPTHCLASS(ia) .EQ. 2.) THEN
                DEPTH(IA)   = 1.5
                RTZDPTH(IA) = 2.0
              ELSE IF (DEPTHCLASS(ia) .EQ. 3.) THEN
                              DEPTH(IA)   = 4.5
                RTZDPTH(IA) = 4.5
              ELSE IF (DEPTHCLASS(ia) .EQ. 4.) THEN
                              DEPTH(IA)   = 6.0
                RTZDPTH(IA) = 6.0
              ENDIF
c
c       following block not yet finished (depthflg = 1 option)
c
            ELSE if (depthflg.eq.1) then
              DEPTH(IA) = DEPTHCLASS(IA)
```

```
            IF(DEPTH(IA).LE.1.5)
     1       RTZDPTH(IA) = DEPTH(IA) + 1.0
            IF((DEPTH(IA).GT.1.5).AND.(DEPTH(IA).LE.3.0))
     1     RTZDPTH(IA) = DEPTH(IA) + 0.5
                        IF((DEPTH(IA).GT.3.0).AND.(DEPTH(IA).LE.4.5))
     1     RTZDPTH(IA) = DEPTH(IA) + 0.5
            IF((DEPTH(IA).GT.4.5).AND.(DEPTH(IA).LE.6.0))
     1                   RTZDPTH(IA) = DEPTH(IA)
            IF(DEPTH(IA).GT.6.0)
     1     RTZDPTH(IA) = 6.0

c
c     following block not yet finished (depthflg = 2 option)
c     subroutine for stochastic simulation of soil depth not developed
c
c     else
c       call depthsim (ia, depthclass, depth)
c
            ENDIF

C
c---- bucket model and large grid bypass
c    imodel  = 1 for bucket model
c    ibucket  = 1 for unlimited grid sizes, location looping 1st
c
    if((imodel.eq.1).or.(iloopx.eq.2)) goto 80
    illopx = 2
c
c
c----        assign soil properties and initial conditions
c    to all elements in alluvium and bedrock
c        (DEPTH = DEPTH OF ALLUVIUM)
c
c           V                    = element storage
c    Z     = node depth below surface (meters,positive down)
c           WC                   = old water content                                    for each time step
c           WN                   = new water content after each iteration,
c                                  and at end of time step WC = WN if tolerance satisfied
c           POT                  = water potential (J/kg)
c           MINPOT               = water potential at full saturation (this was removed 8/19/96)
c           PE     = air entry potential (J/kg)
c    KS     = saturated conductivity (Kg sec / meters^3)
c           J                    = day 0 for output of initial conditions
c
c
            BR(IA) = DEPTH(IA)*10+1
            Z(1)  = 0.1
    Z(0)  = 0.
            J     = 0.
            JTIME  = 0.
c
c
```

```
          DO I=1,DEPTH(IA)*10
        PE(IA,I)     = SOILPE(soiltype(ia))
             BVAL(IA,I)   = SOILBVAL(soiltype(ia))
             BCN(IA,I)    = 2+3/BVAL(IA,I)
        vgn(ia,i)    = soilvgn(soiltype(ia))
        vgm(ia,i)    = 1-(1/vgn(ia,i))
        vgalpha(ia,i) = salpha(soiltype(ia))
        KS(IA,I)     = SOILKS(soiltype(ia))
             PORO(IA,I)   = SOILPORO(soiltype(ia))
        ALBETA(IA,I) = SOILALBETA(soiltype(ia))
        TALPHA(IA,I) = SOILTALPHA(soiltype(ia))
c                          RESID(IA,I)  = SOILRESID(soiltype(ia))
        etresid(ia,i) =          soilresid(soiltype(ia))
        SOILP(IA,I)  = SOILPOND(soiltype(ia))
        ROCKCP(IA,I) = 0.
        FRACKS(IA,I) = 0.
        FRACOUT(IA,I) = 0.
C        wc(ia,i)                  = inwats(soiltype(ia))
C        wn(ia,i)                   = wc(ia,i)
c
c---- check next two lines with Campbell
c    MOISTCR = 1 for Brooks and Corey Moisture Characteristic
c          = 0 for Van Gunucheten Moisture Characteristic
C
      IF(MOISTCR.EQ.1) THEN
                               POT(IA,I)= POTIS(soiltype(ia))
c
c        added next line on 8/18/96 for Brooks & Corey type MC
c        (potential must not be greater than air-entry)
         if (pot(ia,i).gt.pe(ia,i)) pot(ia,i) = pe(ia,i)

                               WC(IA,I) = PORO(IA,I)*(PE(IA,I)/pot(ia,i))
     1                              **(1/BVAL(IA,I))

              WN(IA,I) = WC(IA,I)
        K(IA,I)  = KS(IA,I)*(PE(IA,I)/POT(IA,I))**BCN(IA,I)
c                               MINPOT(IA,I)=PE(IA,I)*(PORO(IA,I)/RESID(IA,I))**BVAL(IA,I)
c
c---- Moistcr = 0 used for VG equation
c     began making modifications on 8/18/96
c
      ELSE
c
         pot(ia,i)= potis(soiltype(ia))
         wc(ia,i) = poro(ia,i)*
     1          (1+vgalpha(ia,i)*(-pot(ia,i)**vgn(ia,i)))
     2          **(-vgm(ia,i))
c
c        wc(ia,i) = (poro(ia,i)-resid(ia,i))*
c    1          (1+vgalpha*(-pot(ia,i)**vgn(ia,i)))**(-vgm(ia,i)
c    2          + resid(ia,i)
c
```

```
              WN(IA,I) = WC(IA,I)
        relsat  = wc(ia,i)/poro(ia,i)
c       relsat  = (wc(ia,i)-resid(ia,i))/(wc(ia,i)-poro(ia,i))
        k(ia,i) = (ks(ia,i)*(relsat)**0.5)*
     1          (1-(1-(relsat**(1/vgm(ia,i))))**vgm(ia,i))**2.
c
c                               MINPOT(IA,I)=PE(IA,I)*(PORO(IA,I)/RESID(IA,I))**BVAL(IA,I)
      ENDIF
c
                               Z(I+1) = Z(I)+DZ
                               V(I)   = WD*(Z(I+1)-Z(I-1))/2
C
C---- output initial conditions to SPY file  (modified 8/11/96)
c
      sink(ia,i) = 0.
      frac(ia,i) = 0.
      pond(ia,i) = 0.
                               IF(((LOCID(IA).EQ.ILOCOUT).and.(DBGFLAG.NE.3))
     1    .and.(ibucket.ne.1)) THEN
                                                                    WRITE(10,15)
J,-Z(I),WN(IA,I),sink(ia,i),frac(ia,i),
     1
pond(ia,i),POT(IA,i),LOCID(IA)
15
FORMAT(1X,I8,F6.1,F8.4,E10.2,E10.2,e10.2,e10.2,I10)
                               ENDIF
c
C
                               IF(((LOCID(IA).EQ.ILOCOUT).AND.(DBGFLAG.EQ.3))
     1    .and.(ibucket.ne.1)) THEN
c
c---- added sink(ia,i) to output for checking dynamic root-zone function (7/20/96)
c    modified on 8/11/96
c
              sink(ia,i) = 0.
                WRITE(10,16) JTIME,-Z(I),WN(IA,I),sink(IA,i),frac(IA,I),
     1                                pot(ia,i),LOCID(IA)
16         FORMAT(1X,E12.6,F6.1,F8.4,E10.2,E10.2,E10.2,I10)
c16        FORMAT(1X,E12.6,F7.1,F12.7,E14.6,3X,E12.6,I6)
              ENDIF
c
            ENDDO
c
c----         assign bedrock properties to all remaining elements
c         (M = 100, or 10 meters)
c
c             idepth = depth*10+1
              DO I=DEPTH(IA)*10+1,M
        PE(IA,I)     = ROCKPE(rocktype(ia))
        BVAL(IA,I)   = ROCKBVAL(rocktype(ia))
        BCN(IA,I)    = 2+3/BVAL(IA,I)
        vgn(ia,i)    = rockvgn(rocktype(ia))
```

```
      vgm(ia,i)    = 1-(1/vgn(ia,i))
      vgalpha(ia,i) = ralpha(rocktype(ia))
      KS(IA,I)     = ROCKKS(rocktype(ia))
      PORO(IA,I)   = ROCKPORO(rocktype(ia))
      ALBETA(IA,I) = ROCKALBETA(rocktype(ia))
      TALPHA(IA,I) = ROCKTALPHA(rocktype(ia))
c           RESID(IA,I)  = ROCKRESID(rocktype(ia))
      etresid(ia,i) = rockresid(rocktype(ia))
      ROCKCP(IA,I) = ROCKCAP(rocktype(ia))
      FRACKS(IA,I) = ROCKFRACKS(rocktype(ia))
      FRACOUT(IA,I) = 0.
C                          wc(ia,i)     = inwatr(rocktype(ia))
C                          wn(ia,i)                                                    = wc(ia,i)
c
c---- check next two lines with Campbell
c
    IF(MOISTCR.EQ.1) THEN
                           POT(IA,I)= POTIR(rocktype(ia))
c
c      added next line on 8/18/96
      if (pot(ia,i).gt.pe(ia,i)) pot(ia,i) = pe(ia,i)
                           WC(IA,I) = PORO(IA,I)*(PE(IA,I)/POT(ia,i))
   1            **(1/BVAL(IA,I))
           WN(IA,I) = WC(IA,I)
      K(IA,I)= KS(IA,I)*(PE(IA,I)/POT(IA,I))**BCN(IA,I)
C                          POT(IA,I)=PE(IA,I)*(PORO(IA,I)/wc(ia,i))**BVAL(IA,I)
c                          MINPOT(IA,I)=PE(IA,I)*(PORO(IA,I)/RESID(IA,I))**BVAL(IA,I)
c
C----  VG equation
c    began modifications on 8/18/96
c
    ELSE
c
      pot(ia,i) = potir(rocktype(ia))
      wc(ia,i)  = poro(ia,i)*
   1          (1+vgalpha(ia,i)*(-pot(ia,i)**vgn(ia,i)))
   2          **(-vgm(ia,i))

c      wc(ia,i) = (poro(ia,i)-resid(ia,i))*
c   1          (1+vgalpha(ia,i)*(-pot(ia,i)**vgn(ia,i)))
c   2          **(-vgm(ia,i)
c   3          + resid(ia,i)
c
           WN(IA,I) = WC(IA,I)
c
c      relsat  = (wc(ia,i)-resid(ia,i))/(wc(ia,i)-poro(ia,i))
      relsat  = wc(ia,i)/poro(ia,i)
      k(ia,i)  = (ks(ia,i)*(relsat)**0.5)*
   1          (1-(1-(relsat**(1/vgm(ia,i))))**vgm(ia,i))**2.
c
c      following still needs to be fixed for VG eq.
c                          MINPOT(IA,I)=PE(IA,I)*(PORO(IA,I)/RESID(IA,I))**BVAL(IA,I)
```

```
c
      ENDIF
C
                              Z(I+1) = Z(I)+DZ
                              V(I)   = WD*(Z(I+1)-Z(I-1))/2
c
C---- output initial conditions to SPY file  (modified 8/11/96)
c
      sink(ia,i) = 0.
      frac(ia,i) = 0.
      pond(ia,i) = 0.
                              IF(((LOCID(IA).EQ.ILOCOUT).and.(DBGFLAG.NE.3))
     1    .and.(ibucket.ne.1)) THEN
                                                                    WRITE(10,15)
J,-Z(I),WN(IA,I),sink(ia,i),frac(ia,i),
     1
pond(ia,i),POT(IA,i),LOCID(IA)
c15
FORMAT(1X,I8,F6.1,F8.4,E10.2,E10.2,e10.2,e10.2,I10)
                              ENDIF
c
c---- added sink(ia,i) to output for checking dynamic root-zone function (7/20/96)
c     modified on 8/11/96
c
                              IF(((LOCID(IA).EQ.ILOCOUT).AND.(DBGFLAG.EQ.3))
     1    .and.(ibucket.ne.1)) THEN
                 sink(ia,i) = 0.
                                WRITE(10,16) JTIME,-Z(I),WN(IA,I),sink(IA,i),frac(IA,I),
     1                               pot(ia,i),LOCID(IA)
c16         FORMAT(1X,E12.6,F6.1,F8.4,E10.2,E10.2,E10.2,I10)
                              ENDIF
c
      ENDDO
c
c
c---- assign fracture properties to bottem element of soil
c
      ROCKCP(IA,DEPTH(IA)*10) = ROCKCAP(FIELDCAP(ia))
            FRACKS(IA,DEPTH(IA)*10) = ROCKFRACKS(rocktype(ia))
C
c---- set top boundary condition
c
      Z(0)      = -1E20
      POT(IA,0)  = POT(IA,1)
      K(IA,0)    = 0.
c
c---- set bottom boundary condition
c
            POT(IA,M+1) = POT(IA,M)
            Z(m+1)     = 1E20
            IF(MOISTCR.EQ.1) THEN
c
```

```
c      following mod on 8/31/96 (for bottom flux)
       k(ia,m+1)  = 0.
c      K(IA,M+1)  = KS(IA,M)*(PE(IA,M)/POT(IA,M+1))**BCN(IA,M)
     ELSE
c
c      relsat  = (wc(ia,m)-resid(ia,m))/(wc(ia,m)-poro(ia,m))
       relsat  = wc(ia,m)/poro(ia,m)
       k(ia,i) = (ks(ia,m)*(relsat)**0.5)*
     1          (1-(1-(relsat**(1/vgm(ia,m))))**vgm(ia,m))**2.
c
     ENDIF
C
C4    PAUSE
c
C---- debugging stuff ----------
c
           IF(DBGFLAG.EQ.4) THEN
           DO I = 1,M
                          WRITE(*,95) IA,I,Z(I),PORO(IA,I),WN(IA,I),POT(IA,I),
     1          KS(IA,I)
                          WRITE(13,95) IA,I,Z(I),PORO(IA,I),WN(IA,I),POT(IA,I),
     1          KS(IA,I)

 95          FORMAT(1X,I3,I4,F8.2,F8.4,F8.4,F12.4,E12.6)
           ENDDO
           ENDIF
c-------------------------------------
c
c---- imodel and ibucket bypass returns here
 80  continue

 90  CONTINUE

C
C
C======= FINISHED INITIALIZATION PROCEDURE ==========================
C=====================================================================
c/////// If imodel = 0 or iloop = 0, loop through days 1st ////////////////
c/////// start main loop time ////////////////////////////////////////////
c
c      J    = simulation day number
c      ND   = total simulation time in days
c      IA   = location ID
c      MLOC  = total number of locations
c                                                          NDAYS = counter for spyglass output
increment
C
c---- following logic added from infil20a on 8/15/96 to allow option
c    of looping through locations 1st, time 2nd, (BUCKET method)
c    as opposed to looping through time 1st (INFIL method)
c    if ibucket = 1, then iloop is set to 1 to prevent overflow of arrays
c    iloop = 1 for looping through locations 1st (runoff routing turned off)
```

```
c    iloop = 0 for looping through time 1st (runoff routing enabled)
c
c
     if(ibucket.eq.1) iloop = 1
     if(iloop.eq.1) then
       nloc1 = nloc
           else
             nloc1 = 1
           endif
     do 8500 ia1 = 1,nloc1
c
     NDAYS = 0
c
C---- LOOP THROUGH DAYS ----------
c    ----------
c
     DO 4000 J = 1,ND
c
c
           SSPPT  = 0.
      SSET                = 0.
           SSW2           = 0.
      SSFRAC  = 0.
           SSPOND  = 0.
           ssfrin  = 0.
           ssfrout = 0.
           ssfrbot = 0.
c
      sfltop = 0.
      sflbr  = 0.
      sfl80  = 0.
      sflbot = 0.
C
           MAXITER = -999
      DTMIN2              = 9999.
C
C
C---- LOOP THROUGH ALL LOCATIONS FOR EACH DAY ----------
C    added logic to use the ILOOP option 8/15/96
C    ------------------------------------------
C
     IF(ILOOP.EQ.1) THEN
       NLOC2 = 1
           ELSE
             NLOC2 = NLOC
           ENDIF
           DO 3000 IA2 = 1,NLOC2
             if(iloop.eq.1) then
               ia = ia1
             else
               ia = ia2
             endif
```

```
c
C---- switch for bypassing ET subroutine
c
    IF(DBGFLAG.EQ.6) GOTO 8000
c
C---- call Potential ET subroutine. Solar radiation, net radiation
c    and potential ET are calculated for the day for each location.
c    1st call subroutine for calculating hourly net radiation at each site,
c    then calculate hourly potential ET at each site. Total daily ET
c    at each site is calculated within each time step of the Richards
c    equation routine using a dynamic-empirical root-zone function
c    and simulated water contents
c
          TPET = 0.
    CALL POTEVAP  (J,IA,DN,LAT,LON,SL,ASP,RIDGE,ELEV,
    1          DR,RD,PI,HSTEP,
    2          BETA,PG,CSR,WP,OZONE,VIEWFACTOR,
    3          TR,TPET)
c           dbgflag
C
8000  CONTINUE
c
c
c---- If DBGFLAG = 7, then bypass precip and ET for checking
c    redistribution of initial conditions and mass balance in profile.
c
    IF (DBGFLAG.NE.7) THEN
C
c-------- SOURCE = daily precip as flux for top node (mm/sec)
c       PPTLOC is used to calculate average daily precip for site
c       PETRS is total daily potential evapotranspiration,
c            adjusted to allow for a decrease for days having precip.
c
C-------- The next 5 lines added on 7/22/96 to use the 4JA - Yucca Mt.
c       Precip transfer equation used in the Bucket Model
c       170 = average annual precip at 1400 m at Yucca Mountain
c       133 = average annual precip at 4JA
c       avgppt = average annual precip for input file (mod 7/28/96)
c
        IF(PPTYUC.EQ.2) THEN
          PPTFACT2 = PPTFACT*(ELEV(IA)/1400.)*(170./avgppt)
        ELSE IF (PPTYUC.EQ.1) THEN
          PPTFACT2 = PPTFACT*(elev(ia)/1400.)
              ELSE
                PPTFACT2 = PPTFACT
        ENDIF
C
        PPTLOC = PPT(J)*PPTFACT2
        PETRS  = TPET/(((4*PPTLOC)/25.4)+1)
        TPET   = TPET*1.26
c
            ENDIF
```

```
c
C========== included option for bucket model here 8/18/96 ==============
c       imodel = 1 for bucket model
c       imodel = 0 for infil model
c              infil model will be organized as a seperate
c              subroutine in later version of program
c
    if(imodel.eq.1) then
      call bucket(ia,depth,soiltype,rocktype,
   1            soilporo,fieldcap,imbibe,imb,
   2            soilalbeta,soiltalpha,soilresid,
   3            pptloc,petrs,sorp,dsoilmm,tet,infilmm,
   4            soilvwc,buckmm,drainvwc,runoffmm,massbal,netinfil)
c             topoid
c
      yearppt  = yearppt + pptloc
      yearpet                  = yearpet + tpet
      yeartet  = yeartet + tet
      yeardsw  = yeardsw + dsoilmm
      yearnet  = yearnet + netinfil(ia)
      yearinf  = yearinf + infilmm
      yearoff  = yearoff + runoffmm(ia)
      yearbal                  = yearbal + massbal
c
      if((yr(j+1).gt.yr(j)).or.
   1    ((yr(j).eq.yrend).and.(dn(j).eq.dnend-1))) then
c
c---------- mod on 9/20/96 to output yearbl for softqa
c
        write(*,180)  locid(ia),yr(j),
   1              yearppt,yeartet,yeardsw,yearinf,yearoff,
   2              yearbal,yearpet
        write(15,180)  locid(ia),yr(j),
   1              yearppt,yeartet,yeardsw,yearinf,yearoff,
   2              yearbal,yearpet
 180     format(1x,i10,1x,i5,
   1         f6.1,f9.3,f9.3,f9.3,f9.3,f8.5,f8.2)
c
c       write(*,180)  locid(ia),easting(ia),northing(ia),yr(j),
c   1              yearppt,yeartet,yeardsw,yearinf,yearoff
c                 ,yearpet
c       write(15,180)  locid(ia),easting(ia),northing(ia),yr(j),
c   1              yearppt,yeartet,yeardsw,yearinf,yearoff
c                 ,yearpet
c 180     format(1x,i10,1x,f8.0,f9.0,i5,
c   1         f6.1,f9.3,f9.3,f9.3,f9.3)

        totppt = totppt + yearppt
        tottet = tottet + yeartet
        totdsw = totdsw + yeardsw
               totpet = totpet + yearpet
        totnet = totnet + yearnet
```

```
          totinf = totinf + yearinf
          totoff = totoff + yearoff
          totbal = totbal + yearbal
 c
          yearppt = 0.
          yeartet = 0.
          yearpet = 0.
          yeardsw = 0.
          yearnet = 0.
          yearinf = 0.
          yearoff = 0.
          yearbal = 0.

        endif
 c
        goto 2700
      endif
 c
 c    2700 found after 3000 loop,
 c    and before 3900 continue, 4000 loop, 4900 continue
 c
 c=============================================================================72
 C----      Begin Campbell's routine for 1-D Richards Equation flow
 c          ------------------------------------------------------
 c          initialize source/sink terms and weighting factors
 c
 c          SOURCE   = precip input (node 1 only)
 c          SINK     = root zone ET output
 c    FRACOUT   = fracture flow output for bedrock and bottom soil node
 c    FRACIN    = Imbibition from fracture back into matrix
 c          POND     = ponding output (soil nodes only)
 c    ROOTW     = root-zone weighting factor for alpha function
 c    RTZADJ    = root-zone adjusting factor for dynamic root-zone
 c
 c
          DO I=1,M
                              SOURCE(IA,I)  = 0.
                              SINK(IA,I)    = 0.
           fracout(ia,i) = 0.
       FRACIN(IA,I)  = 0.
 c     FRAC(IA,I)    = 0.
       POND(IA,I)    = 0.
                              ROOTW(I)      = 0.
                              RTZADJ(I)     = 0.
          ENDDO

 c
 C
 c---- set up root-zone element weighting factors for static
 c    root-zone function (old method)
 c    the static root-zone weighting scheme is not dependent on
 c    the simulated water content profile
```

```
c
C       IRTZ     = 0 for static root zone function
c        = 1 for dynamic root zone function
c   DEPTHFLG  = 0 for discrete depth classes
c        = 1 for variable depth classes
C   DEPTH(IA) = alluvium thickness (either discrete or variable
c        depth classes
c   ROOTW(I)  = element weighting factor for use in modified
c        Priestley-Taylor ET equation, where actual ET
c        is calculated
c
c
        IF(IRTZ.EQ.0) THEN
        IF(DEPTHFLG.EQ.0) THEN
          IF(DEPTH(IA).EQ.0.5) THEN
      DO I=1,M
            IF(I.EQ.1)          ROOTW(I) = 0.3
                              IF(I.GT.1.AND.I.LE.4)  ROOTW(I) = 0.2
                              IF(I.EQ.5)          ROOTW(I) = 0.1
          ENDDO

    ELSE IF(DEPTH(IA).EQ.1.5) THEN
      DO I=1,M
            IF(I.EQ.1)          ROOTW(I) = 0.29
                              IF(I.GT.1.AND.I.LE.5)  ROOTW(I) = 0.1
                              IF(I.GT.5.AND.I.LE.10)  ROOTW(I) = 0.05
            IF(I.GT.10.AND.I.LE.16) ROOTW(I) = 0.01
          ENDDO

    ELSE IF(DEPTH(IA).EQ.4.5) THEN
      DO I=1,M
            IF(I.LE.2)          ROOTW(I) = 0.125
                              IF(I.GT.2.AND.I.LE.6)  ROOTW(I) = 0.100
                              IF(I.GT.6.AND.I.LE.21)  ROOTW(I) = 0.025
            IF(I.GT.21.AND.I.LE.39) ROOTW(I) = 0.0025
            IF(I.GT.39.AND.I.LE.60) ROOTW(I) = 0.0015
          ENDDO

    ELSE IF(DEPTH(IA).EQ.6.) THEN
      DO I=1,M
            IF(I.LE.2)          ROOTW(I) = 0.125
                              IF(I.GT.2.AND.I.LE.6)  ROOTW(I) = 0.100
                              IF(I.GT.6.AND.I.LE.21)  ROOTW(I) = 0.025
            IF(I.GT.21.AND.I.LE.39) ROOTW(I) = 0.0025
            IF(I.GT.39.AND.I.LE.60) ROOTW(I) = 0.0015
          ENDDO
        ENDIF
      ENDIF
      ENDIF
c
c
c==== Initialize time stepping parameters and mass balance terms
```

```
c
c----       TI = simulation time (minutes)
c           DT = time step (seconds)
c           SE = mass balance error term (residual)
c    IM = mass balance tolerance
c           ITER = number of iterations
c    MAXIT = maximum number of iterations permitted
C    MITER = max number of iterations per day
c    NITER = max number of times to decrease time steps
c    NITER2 = number of increased time steps
c    sfrac2 = total water in fractures at end of day (mm)
c    sw2    = total water content change at end of day
c
            MITER  = 0
            NITER  = 0
            niter2 = 0
            DT     = MAXDT
c
c---- next line forces DT to 2 hours in the case of precip
c
            IF((pptloc.gt.0.).and.(maxdat.gt.7200)) dt = 7200.
c
            DTMIN  = DT
            dtmin2 = dt/60.
            SFRAC2 = 0.
            SW2    = 0.
            SPOND2 = 0.
            TSINK  = 0.
            sfrin  = 0.
            sfrout = 0.
            sfrbot = 0.
     NIM2   = 0
     IM     = IM2
     sumse  = 0.
c
C======= begin time stepping loop for Richards Eq. infiltration =======
c=============================================================================
c
210  TI=TI+DT/60.
            SFRAC = 0.
            sfracin = 0.
            sfracout = 0.
            ITER  = 0
            SPOND = 0.
            SSINK = 0.
C
c----       Begin Dynamic Root-zone Function ----------------------------
c    --------------------------------
C
            IF(IRTZ.EQ.1) THEN
            IF((DEPTHFLG.EQ.0).OR.(DEPTHFLG.EQ.1)) THEN
       SRTZFN  = 0.
```

```
            SRTZF2  = 0.
            SDELVWC = 0.
C
C------- for now, dynamic root-zone is not self adjusting
c       for variable alluvium thicknesses. This is a preliminary
c       function which should be correct for depth classes.
c       Modification of the static RTZD parameter to a depth-
c       dependent function will correct this problem.
c
c       errors in function corrected on 8/14/96
c
        IX    = DEPTHCLASS(IA)
              DELVWF = VWCF2(IX)
        BSOIL2 = BSOIL(IX)
c
C
C------- set up the static and dynamic conditioning functions
c       modified to use etresid, as oposed to resid
c
        DO I = 1, RTZDPTH(IA)*10 + 1
c               IF(I.GT.10) RTZADJ(I) = (Z(I)**RTZD(IX))/100.
                RTZADJ(I) = 1./((10.+1000*Z(I))**RTZD(IX))
                DELVWC(I) = WC(IA,I) - etresid(IA,I)
                IF(DELVWC(I).LT.0.) DELVWC(I) = 0.
                        SDELVWC = SDELVWC + DELVWC(I)
            ENDDO
c
c------- normalize the dynamic conditioning function and set up
c       the root density conditioning function
c
            DO I  = 1, RTZDPTH(IA)*10 + 1
              DELVWC(I) = DELVWC(I)/SDELVWC
              RTZFN(I)    = 1/(((RTZA(IX)-RTZDPTH(IA))
     1              *Z(I)**RTZB(IX))+RTZC(IX))
              SRTZFN = SRTZFN + RTZFN(I)
            ENDDO
c
c------- normalize the root density conditioning function and
c       combine with the dynamic conditioning function
C       Modified on 7/21/96 to include DELVWCF factor for reducing
c       the relative effect of the water content profile on the
c       final weighting terms (otherwise function may be too dynamic)
C       DELVWCF < 1.0 decreases effect of dynamic root zone
c       DELVWCF > 1.0 increase effect of dynamic root zone
c
c
            DO I = 1, RTZDPTH(IA)*10 + 1
              IF(I.GT.1) BSOIL2 = 0.
                        RTZFN(I) = ((RTZFN(I)*(1-BSOIL(IX)))/SRTZFN)+BSOIL2
              RTZFN(I) = RTZFN(I) * (DELVWC(I)+rtzadj(i))**VWCF2(IX)
c
c       following added 8/18/96 to reduce percentage of et from bedrock
```

```
c
                if(i.gt.(depth(ia)*10)) rtzfn(i) = rtzfn(i)/100.
                SRTZF2 = SRTZF2 + RTZFN(I)
              ENDDO
c
c----- perform final normalization to calculate root-zone
c     weighting factors
c
              DO I = 1, RTZDPTH(IA)*10 + 1
                ROOTW(I) = RTZFN(I)/SRTZF2
              ENDDO

            ENDIF
            ENDIF
c
c--------------- Calculate PPT and ET source/sink terms ----------------
c             ---------------------------------------
C
C====== set up the source/sink terms according to calculated daily fluxes
c     fluxes are defined as Kg/(m^2 sec) = cm/sec (1g = 1ml, dz = .1 m)
c
            SOURCE(IA,1) = PPTLOC/86400.
     DO I=1,M
              REALPHA(IA,I) = TALPHA(IA,I)*(1-EXP(ALBETA(IA,I)*
     1                (WC(IA,I)-etresid(ia,i))/
     2              (PORO(IA,I)-etresid(ia,i))))
C
       SINK(IA,I) = (REALPHA(IA,I)*PETRS*ROOTW(I)*ETFACT)/86400.
C
c                              root zone turned off using resid values (mod on 8/18/96)
       IF(WC(IA,I).LT.etresid(ia,i)) SINK(IA,I)=0.
c
     ENDDO
c
C
C---- calculate fracture flow and ponding terms
C     using estimated fracture conductivities and the
c     bucket model aproach
c     dbgflag = 7 keeps all sink terms set to zero
C     pondfact,fr1fact,fr2fact are multipliers used for testing
c
     IF(DBGFLAG.NE.7) THEN
     DO I=1,M
       fracout(ia,i) = 0.
c      FRAC(IA,I)   = 0.
       POND(IA,I)   = 0.
       FRACIN(IA,I) = 0.
       IF(I.LE.DEPTH(IA)*10) THEN
         IF (WC(IA,I).GT.(PORO(IA,I)-soilp(ia,i))) THEN
           POND(IA,I) = (((WC(IA,I)-PORO(IA,I)+soilp(ia,i))*V(I))
     1               /86400)*pondfact
c          POND(IA,I) = POND(IA,I)*PONDFACT
```

```
            ENDIF
          ELSE IF(I.GE.DEPTH(IA)*10)                                    THEN
            IF (WC(IA,I).GE.ROCKCP(IA,I)) THEN
              fracout(ia,i) = FRACKS(IA,I)*FR1FACT
              IF ((fracout(ia,i)*DT).GT.(V(I)*ROCKCP(IA,I)))
     1            fracout(ia,i) = ((V(I)*ROCKCP(IA,I))/DT)*FR2FACT
            ENDIF
C
          IF (SINK(IA,I)+fracout(ia,i)*DT.GT.
     1      V(I)*WC(IA,I)-etresid(IA,I)) fracout(ia,i) = 0.
c
C
C---- Cascade Fracture Model (7/25/96) ------ (original error corrected)
c    FRAC = storage term for water in fractures
c
          if(fracmod.eq.1) then
            IF((FRAC(IA,I-1)*DT).GT.(KS(IA,I)*DT)) THEN
              FRACIN(IA,I) = KS(IA,I)
            ELSE
              FRACIN(IA,I) = FRAC(IA,I-1)
            ENDIF
            FRAC(IA,I) = (FRAC(IA,I-1)-FRACIN(IA,I))+fracout(ia,i)
          endif
C
c--------- else if(fracmod.eq.0) then
c         do original bucket version of fracture flow
c
        ENDIF
            ENDDO
            ENDIF
C
C=============================================================================
C/////////////////// LOOP FOR NEWTON-RAPHSON ITERATION ////////////////////
C
220   SE=0.
      ITER=ITER+1
c
c           calculate conductivities (moistcr = 1 for Brooks & Corey)
c     fixed for VG equation
c
      DO I=1,M
        IF(MOISTCR.EQ.1) THEN
                                  K(IA,I)=KS(IA,I)*(PE(IA,I)/POT(IA,I))**BCN(IA,I)
                                ELSE
c
c         relsat  = (wc(ia,i)-resid(ia,i))/(wc(ia,i)-poro(ia,i))
          relsat  = wc(ia,i)/poro(ia,i)
          k(ia,i) = (ks(ia,i)*(relsat)**0.5)*
     1            (1-(1-(relsat**(1/vgm(ia,i))))**vgm(ia,i))**2.
c
                                ENDIF
            ENDDO
```

```
C
C
C   SETUP THE MASS BALANCE
C          ------------------------------------------------------------
    DO I=1,M
          CP(I) = -V(I)*WN(IA,I)/(BVAL(IA,I)*POT(IA,I)*DT)
          A(I)  = -K(IA,I-1)/(Z(I)-Z(I-1))+GR*BCN(IA,I-1)*
   1      K(IA,I-1)/POT(IA,I-1)
          C(I)  = -K(IA,I+1)/(Z(I+1)-Z(I))
          B(I)  =  K(IA,I)/(Z(I)-Z(I-1))+K(IA,I)/(Z(I+1)-Z(I))+CP(I)-
   1      GR*BCN(IA,I)*K(IA,I)/POT(IA,I)
          F(I)  =  ((POT(IA,I)*K(IA,I)-POT(IA,I-1)
   1      *K(IA,I-1))/(Z(I)-Z(I-1))
   2          -(POT(IA,I+1)*K(IA,I+1)-POT(IA,I)*K(IA,I))/
   3      (Z(I+1)-Z(I)))/(1-BCN(IA,I))+V(I)*(WN(IA,I)-WC(IA,I))/
   4      DT-GR*(K(IA,I-1)-K(IA,I))
   5      -SOURCE(IA,I)+SINK(IA,I)+fracout(ia,i)+POND(IA,I)
   6      -FRACIN(IA,I)
C
C     MOD ON 8/31/96
      se = se + abs(f(i))
c
c   use following for constant head upper boundary
c
C                          IF (I .GT. 1) THEN
C                                                          SE=SE+ABS(F(I))
C                          ENDIF
    ENDDO
C
C----      F(1)=0 AND C(1)=0 FOR A CONSTANT UPPER BOUNDARY
C   F(1)=0
C   C(1)=0
c
    DO I=1,M-1
      C(I)  = C(I)/B(I)
      F(I)  = F(I)/B(I)
      B(I+1) = B(I+1)-A(I+1)*C(I)
      F(I+1) = F(I+1)-A(I+1)*F(I)
    ENDDO
    DP(M)  = F(M)/B(M)
    POT(IA,M) = POT(IA,M)-DP(M)
c
c          do not allow positive head to occur
c   this corrects Brooks & Corey problem, but may introduce mass balance error
c
    IF (POT(IA,M) .GT. PE(IA,M)) pot(ia,m) = pe(ia,m)
    DO I=M-1,1,-1
      DP(I)=F(I)-C(I)*DP(I+1)
      POT(IA,I)=POT(IA,I)-DP(I)
      IF (POT(IA,I) .GT. PE(IA,I)) THEN
      POT(IA,I)=(POT(IA,I)+DP(I)+PE(IA,I))/2
      END IF
```

```
      ENDDO
c
c
      DO I=1,M
c
c             IF (POT(IA,I).LT.MINPOT(IA,I)) THEN
c       . POT(IA,I)=MINPOT(IA,I)
c       ENDIF
c
        if(moistcr.eq.1) then
                                  WN(IA,I)=PORO(IA,I)*(PE(IA,I)/POT(IA,I))**(1/BVAL(IA,I))
        else
          wc(ia,i)  = poro(ia,i)*
     1            (1+vgalpha(ia,i)*(-pot(ia,i)**vgn(ia,i)))
     2            **(-vgm(ia,i))
        endif
            ENDDO
c
c
c==== Following section is the automatic time step routine ==========
c    This algorithm could still use some improvement
c           If error greater than tolerance, do another iteration
c           Adjust time step depending on number of iterations (maxit,minit)
c           maxiter = maximum number of times DT adjusted
c           maxdt = maximum allowed time step
c
C
      if(itime.eq.1) then
C---- If error term too big, do another iteration
C
        IF ((SE.GT.IM).AND.(ITER.le.MAXIT)) GOTO 220
C
C---- If too many iterations, decrease time step and try again
C
                IF ((SE.GT.IM).AND.(ITER.Gt.MAXIT)) THEN
          TI = TI - DT/60.
          DT = DT/2.
          IF (DT.LT.DTMIN) DTMIN = DT
          NITER = NITER + 1
          IF (NITER.GE.MAXITER) THEN
            IF((NIM2.EQ.2).AND.(DT.LT.MINDT)) GOTO 3300
c
c---- next section sets the bail-out tollerance (IM3)
c
            IM = IM3
            NIM2 = NIM2 + 1
            GOTO 210
          ENDIF
          GOTO 210
        ENDIF
C
C---- If too few iterations, increase time step to run faster
```

```
C
            IF ((SE.LT.IM).AND.(ITER.LT.MINIT)) THEN
                        IF(DT.LT.MAXDT) THEN
                          DTX = DT
                                                              TI = TI-DTX/60.
                                                              DT = DT*4.
                                                              IF(DT.GT.MAXDT)
DT = MAXDT
C
C       fixed following error 8/29/96
c                                                     IF((TI+DT/60.).GT.1440.)
DT = 1440.-TI
c
IF((TI+DT/60.).GT.1440.) DT = (1440.-TI)*60.
                                                              NITER2 = NITER2 + 1

IF(NITER2.GE.MAXITER) THEN
                                                                TI = TI+DTX/60.
                                                                GOTO 1300
                                                              ENDIF
                                                              GOTO 210
                                                            ENDIF
            ENDIF
1300    CONTINUE
            IM = IM2
c
c    itime = 0 option for new automatic time stepping
c          (added 8/29/96)
c
     else if (itime.eq.0.) then
       IF ((SE.GT.IM).AND.(ITER.Le.MAXIT)) GOTO 220
       if(iter.gt.maxit) then
         ti = ti - dt/60.
         dt = dt/2.
         if(dt.lt.mindt) dt = mindt
         niter = niter + 1
         if(niter.le.maxiter) then
           goto 210
         else
           if(imflag.ne.1) then
             im    = im3
             imflag = 1
             goto 210
           else
             goto 3300
           endif
         endif
c          goto 210
       endif
c
c    do not perform time step adjustment (itime.ne. 1 or 0)
```

```
c
    else
      IF ((SE.GT.IM).AND.(ITER.Le.MAXIT)) GOTO 220
      if((se.gt.im).and.(iter.gt.maxit)) goto 3300
    endif
C
c
c
c--------- solution converged !!!! ---------------------------
C                                reset automatic time step adjustment counters
c              now calculate total water content of profile
c              set old water content = new water content before going to
c                                next time step
c
    im = im2
    niter = 0.
    imflag = 0
c
    sumse = sumse + se
    SW=0
          IF(DTMIN2.GT.DTMIN) DTMIN2 = DTMIN
          IF(MITER.LT.ITER) MITER = ITER
          NNITER  = NITER
          NITER   = 0
          NNITER2 = NITER2
          NITER2  = 0
C
C---- calculate water balance for profile at the end of time step
c
c    SW      = total water content change (mm)
c    TSINK   = total ET (mm)
c    SFRAC   = total water in fractures (?)
c    sfracout = total water drained into fractures (?)
c    sfracin  = total water imbibed back into matrix (?)
c    spond   = total water ponded (?)
c
C---- calculate water balance for profile at the end of day
c
c    SW2     = total water content change (mm)
c    TSINK   = total ET (mm)
c    SFRAC2  = total amount of water in fractures
c    sfrout  = total water drained into fractures
c    sfrin   = total water imbibed back into matrix
c    spond2  = total water ponded
c    sfrbot  = total fracture flow at 10 meters (?)
c    sfr80   = total fracture flow at 8 meters (?)
c
c
    DO I=1,M
      SW      = SW + (V(I)*(WN(IA,I)-WC(IA,I)))
      WC(IA,I) = WN(IA,I)
      SFRAC   = SFRAC + (frac(ia,i)*DT)
```

```
      sfracin  = sfracin + (fracin(ia,i)*dt)
      sfracout = sfracout + (fracout(ia,i)*dt)
      SPOND    = SPOND + (POND(IA,I)*DT)
      SSINK    = SSINK + (SINK(IA,I)*DT)
           ENDDO
           SW2    = SW2 + SW
           SFRAC2 = SFRAC2 + SFRAC
           sfrin  = sfrin + sfracin
           sfrout = sfrout + sfracout
           sfrbot = sfrbot + frac(ia,100)
           sfr80  = sfr80 + frac(ia,80)
           SPOND2 = SPOND2 + SPOND
           TSINK  = TSINK  + SSINK
C
C          CALCULATE MATRIX FLOW OUT THE BOTTOM, INTO THE BEDROCK,
c    AND INTO THE SOIL, at end of time step, in mm/day
C    modified to correct mass balance errors 8/31/96
c    added calculation for flow at 8 meter depth (fl80) 9/1/96
c
           FLBOT = ((POT(IA,M)*K(IA,M)-POT(IA,M+1)*K(IA,M+1))/
     1     ((1-BCN(IA,M+1))*(Z(M+1)-Z(M)))+GR*K(IA,M))*dt
c    2      *(86400/dt)
           FLBR  = ((POT(IA,BR(IA)-1)*K(IA,BR(IA)-1)-POT(IA,BR(IA))*
     1     K(IA,BR(IA)))/((1-BCN(IA,BR(IA)))*
     2     (Z(BR(IA))-Z(BR(IA)-1)))+GR*K(IA,BR(IA)-1))*dt
c    3      *(86400/dt)
     FLtop = ((POT(IA,1)*K(IA,1)-POT(IA,2)*K(IA,2))/
     1     ((1-BCN(IA,2))*(Z(2)-Z(1)))+GR*K(IA,1))*dt
c    2      *(86400/dt)
     fl80  = ((POT(IA,80)*K(IA,80)-POT(IA,81)*K(IA,81))/
     1     ((1-BCN(IA,81))*(Z(81)-Z(80)))+GR*K(IA,80))*dt
c    2      *(86400/dt)
c
c    added following 9/1/96 to help correct mass balance errors
c    which occurrd because end of day fluxes were used to calculate
c    total daily fluxes
c
     sflbot = sflbot + flbot
     sflbr  = sflbr  + flbr
     sfltop = sfltop + fltop
     sfl80  = sfl80 + fl80
c
c    option for writing output at end of each time step
c    (warning!!!  Use of this option can create very large files)
c
           IF (((DBGFLAG.EQ.2).or.(dbgflag.eq.3)).and.(imodel.ne.1)) THEN
       DTMIN2 = DT/60.
       write(13,9110) locid(ia),YR(J),DN(J),DTMIN2,TI2,NNITER,
     1                NNITER2,ITER,pptloc,TSINK,sw2
       write(*,9110) locid(ia),YR(J),DN(J),DTMIN2,TI2,NNITER,
     1                NNITER2,ITER,pptloc,TSINK,sw2
           ENDIF
```

```
9110      FORMAT(1x,I10,I4,I4,F8.2,F8.1,I3,I3,I4,
     1    F7.1,F7.3,F10.5)
c
c   modified following on 8/11/96
c   do not use for bucket model (imodel = 1)
c
          IF ((DBGFLAG.EQ.3).and.(imodel.ne.1)) THEN
      JTIME = J-1 + TI/1440.
      DO I=1,M
        WRITE(10,16) JTIME,-Z(I),wn(ia,i),sink(IA,I),frac(IA,I),
     1                pot(IA,I),LOCID(IA)
c
c16       FORMAT(1X,E12.6,F6.1,F10.5,F8.5,E15.6,3X,E12.6,I6)
C
      ENDDO
          ENDIF
C
c
c==== Now go to next time step
c   do time steps until day is finished
c   ti = simulation time in minutes
c          (1440 minutes = 24 hours)
c
c   modified following for itime option 8/29/96
c
    if(itime.eq.0) then
      IF (TI.LT.1440) then
        if (((1440.-ti)*60.).gt.maxdt) then
          if(pptloc.gt.0.) then
            dt = 7200.
            goto 210
          else
            dt = maxdt
            GOTO 210
          endif
        else
          dt = (1440.-ti)*60.
          goto 210
        endif
      endif
    else
      if(ti.lt.1440.) goto 210
    endif
    IF(DT.LT.DTMIN2) DTMIN2=DT
C
C---- sum water balance terms for all locations
c   these terms are used for calulating average daily water balance
c   needs further work to use with iloop =1 option
c
          SSPPT = SSPPT + PPTLOC
          SSET  = SSET + TSINK
          SSW2  = SSW2 + SW2
```

```
            SSFRAC = SSFRAC + SFRAC2
            ssfrin = ssfrin + sfrin
            ssfrout = ssfrout + sfrout
            ssfrbot = ssfrbot + sfrbot
            ssfr80 = ssfr80 + sfr80
            SSPOND = SSPOND + SPOND2

            SUMFRC(IA)  = SUMFRC(IA) + SFRAC2
            SUMEVP(IA)  = SUMEVP(IA) + TSINK
            SUMPND(IA)  = SUMPND(IA) + SPOND2
            SUMFLB(IA)  = SUMFLB(IA) + sflbot
c           SUMFLB(IA)  = SUMFLB(IA) + (FLBOT*86400.)
            sumfbot(ia) = sumfbot(ia) + sfrbot
            sumfin(ia)  = sumfin(ia) + sfrin
            sumfout(ia) = sumfout(ia) + sfrout

            IF(MAXFRCD(IA).LT.SFRAC2) MAXFRCD(IA) = SFRAC2
            IF(MAXEVPD(IA).LT.TSINK)  MAXEVPD(IA) = TSINK
            IF(MAXPNDD(IA).LT.SPOND2) MAXPNDD(IA) = SPOND2
            IF(MINEVPD(IA).GT.TSINK)  MINEVPD(IA) = TSINK
c
c
c------------ Output to file (UNIT 12: *.FLX) ----------------------
c-------------                  write total fluxes at end of day ----------------------
c
c                              sfltop   = flux at top (mm/day)
c                              sflbr    = flux at bedrock contact (mm/day)
c                              sflbot   = flux at 9.9 meters                                    (mm/day)
c     sfl80    = flux at 7.9 meters (mm/day)
c     sumse    = total mass balance error at end of day (mm)
c
            IF ((LOCID(IA).EQ.ILOCOUT).and.(imodel.ne.1)) THEN
            WRITE (12,9200)YR(J),DN(J),sFLtop,sFLBR,sFL80,
     1     sflbot,sfrin,sfrout,sumse
c           sfrbot,sfrac2
 9200       FORMAT(1X,I4,I4,F9.5,F9.5,F9.5,f9.5,f8.3,f8.3,E8.2)
            ENDIF
c
c
c-----      reset daily flux terms
c
            FL=0
            FLBOT=0
            TI2 = TI
            TI=0
c
C============== END RICHARDS EQUATION ROUTINE ========================72
c-----------------------------------------------------------------------
c
c    return from bucket model here
C
 2700 continue
```

```
c
c
C---- NEXT SECTION MAKES THE DEPTH PROFILE OUTPUT FILE
c    use only if imodel = 0 (infil model)
c    modified from previous versions on 8/11/96
c    ilocout  = location id for generating profile,
c    ndayout  = number of days to skip between profiles)
C    DBGFLAG2 = 1 for output of fracture flow terms (7/28/96)
c
c
           JULIAN = J
           IF(LOCID(IA).EQ.ILOCOUT) NDAYS = NDAYS + 1
           IF(((NDAYS.EQ.NDAYOUT).and.(DBGFLAG.NE.3)).and.(imodel.ne.1))THEN
            DO I=1,M
         WRITE(10,15) J,-Z(I),WN(IA,I),sink(ia,i),frac(ia,i),
     1
pond(ia,i),POT(IA,i),LOCID(IA)
C
            ENDDO
c
c      this output option needs to be fixed
            IF ((DBGFLAG2.EQ.1).and.(imodel.ne.1)) THEN
            DO I=1,M
                              WRITE(15,17) J,-Z(I),sink(ia,i),WN(IA,I),FRAC(IA,I),
     1          FRACIN(IA,I),FRACOUT(IA,I)
 17      FORMAT(1X,I8,F5.1,5F10.4)
C
            ENDDO
            ENDIF
            NDAYS = 0
           ENDIF
C
C
C---- set bucket model output
C    daily mass balance terms for a specific location
c
     if((locid(ia).eq.ilocout).and.(imodel.eq.1)) then
       TSINK  =  tet
       sw2    =  dsoilmm
       spond2 =  runoffmm(ia)
       sfrac2 =  infilmm
     endif
C
c------- write daily output to screen ---------------------------------
c------- and to main output file (UNIT 13 = *.DB1) --------------------
c
c
c---- modified on 9/20/96
c    balance term needed for softqa
c
           balance = pptloc-tsink-sw2-sfrac2-spond2
```

```
          IF((DBGFLAG.EQ.1.OR.DBGFLAG.EQ.6.OR.DBGFLAG.EQ.7.OR.
     1  DBGFLAG.EQ.9).AND.LOCID(IA).EQ.ILOCOUT) THEN
         DTMIN = DTMIN/60.
         write(13,9100) locid(ia),YR(J),DN(J),
     1              pptloc,TSINK,sw2,SFRAC2,spond2,balance
c
c
c          IF((DBGFLAG.EQ.1.OR.DBGFLAG.EQ.6.OR.DBGFLAG.EQ.7.OR.
c     1  DBGFLAG.EQ.9).AND.LOCID(IA).EQ.ILOCOUT) THEN
c        DTMIN = DTMIN/60.
c        write(13,9100) locid(ia),YR(J),DN(J),DTMIN2,MITER,
c     1              pptloc,TSINK,sw2,SFRAC2,spond2
c                    sumse
c
       IF((DBGFLAG.EQ.9).or.(imodel.eq.1)) GOTO 2800
       write(*,9100) locid(ia),YR(J),DN(J),DTMIN2,MITER,
     1              pptloc,TSINK,sw2,SFRAC2,spond2
c                    sumse
          ENDIF
c
c----- mod on 9/20/96 to include balance term
c
 9100      FORMAT(1x,I10,I4,I4,
     1    F7.2,1X,F7.4,1X,F8.4,F10.4,f10.4,f8.5)
c
c 9100    FORMAT(1x,I10,I4,I4,E9.3,I4,
c    1    F7.2,1X,F7.4,1X,F8.4,F10.4,f10.4)
c
c 9100    FORMAT(1x,I10,I4,I4,F9.2,I4,
c    1    F7.2,1X,F7.4,1X,F8.4,F10.4,e10.3)
 2800 CONTINUE
C
c
c////////////// end of location loop, go to next location ////////////////
c          ------------------------------------------
c
 3000 CONTINUE
c
C
C---- calculate average water balance terms for each day
c          (needs to be fixed to handle bucket model output)
c
          AVGPPT2 = SSPPT/NLOC
          AVGET   = SSET/NLOC
          AVGSW2  = SSW2/NLOC
          AVGFRAC = SSFRAC/NLOC
          AVGPOND      = SSPOND/NLOC

          avgfrin = ssfrin/nloc
          avgfrout = ssfrout/nloc
          avgfrbot = ssfrbot/nloc
c
```

```
c---- output daily averages to screen and file (UNIT 9 = ???)
c-------------------------------------------------------------
c
          IF (DBGFLAG.EQ.9) THEN
            WRITE(*,9215) YR(J),DN(J),DTMIN2,MITER,AVGPPT2,AVGET,
     1                    AVGSW2,AVGFRAC,avgfrbot,AVGPOND
            WRITE(9,9215) YR(J),DN(J),DTMIN2,MITER,AVGPPT2,AVGET,
     1                    AVGSW2,AVGFRAC,avgfrbot,AVGPOND
9215    FORMAT(1X,I4,I5,F6.0,I4,F6.1,F8.3,F8.3,F8.3,F8.3,f8.3)
    ENDIF
C
C////////////// end of day loop, go to next day ////////////////////////
C          -------------------------------
c
3900  continue
4000  CONTINUE
4900  CONTINUE
c
c    8500 loop added to use ILOOP option 8/15/96
c
8500  continue
    if(ibucket.eq.1) goto 500
c
C
          WRITE (*,5) '  SIMULATION SUCCESSFULLY COMPLETED'
          GOTO 3500
c
c
c---- Line 3300 is used as error trap if convergence is
c    not achieved in Newton-Raphson iteration according to criteria
c    specified by the user
c    need to update format statements
c
c
3300      WRITE (*,5) '  SOLUTION DID NOT CONVERGE'
c     DTMIN = DTMIN/60.
c          WRITE (12,9200)YR(J),DN(J),FL*86400,FLBR*86400,FLBOT*86400,
c     1          SW2,SFRAC2,SPOND2
c     DO I=1,M
c       WRITE(10,15) J,-Z(I),WN(IA,I),POT(IA,I),K(IA,I),LOCID(IA)
c     ENDDO
c
C
c          WRITE(13,9110) LOCID(IA),YR(J),DN(J),DTMIN,TI2,NITER,NITER2,ITER,
c     1          pptloc,TSINK,SW2
c     WRITE(*,9110) LOCID(IA),YR(J),DN(J),DTMIN,TI2,NITER,NITER2,ITER,
c     1          pptloc,TSINK,SW2
C
c
c---- calculate average terms for all locations and output
c    mass balance statistics to file (UNIT 14 = *.MAP) for mapping
c    some minor errors here need to be fixed
```

```
c
3500  DO IA = 1,NLOC

            AVGFRCY(IA) =  (SUMFRC(IA)/ND)*365.25
            AVGEVPY(IA) =  (SUMEVP(IA)/ND)*365.25
            AVGEVPD(IA) =  SUMEVP(IA)/ND
            AVGPNDY(IA) =  (SUMPND(IA)/ND)*365.25
            AVGFLBY(IA) =  (SUMFLB(IA)/ND)*365.25
            avgfbot(ia) =  (sumfbot(ia)/nd)*365.25
            avgfin(ia)  =  (sumfin(ia)/nd)*365.25
            avgfout(ia) =  (sumfout(ia)/nd)*365.25

            WRITE(14,9515) EASTING(IA),NORTHING(IA),LOCID(IA),
     1       AVGEVPY(IA),MAXEVPD(IA),MINEVPD(IA),
     2       AVGFRCY(IA),MAXFRCY(IA),MAXFRCD(IA),
     3       avgfbot(ia),avgfin(ia),avgfout(ia),
     4       AVGPNDY(IA),MAXPNDY(IA),MAXPNDD(IA),
     5       AVGFLBY(IA),MAXFLBY(IA)

9515    FORMAT(1X,F10.1,F10.1,I10,14F10.3)
          ENDDO
c
c 9900 continue
     CLOSE(9,STATUS='KEEP')
     CLOSE(10,STATUS='KEEP')
          CLOSE(11,STATUS='KEEP')
     CLOSE(12,STATUS='KEEP')
          CLOSE(13,STATUS='KEEP')
          CLOSE(14,STATUS='KEEP')
          CLOSE(15,STATUS='KEEP')
          STOP
     END
C
C
c==================== END OF MAIN PROGRAM ==============================
C///////////////////////////////////////////////////////////////
C
C///////////////////////////////////////////////////////////////
C/////////////////   ATMOS SUBROUTINE  ////////////////////////////////
C      ******** set atmospheric parameters, **********************
c            ***** updated 12/11/95 by Don Burrows and Alan Flint ******
C
C     calulate clear sky solar radiation
c
C     OZONE -- ozone layer thickness (CM)
C     WP    -- water in atmosphere(CM)
C     BETA  -- mean atmospheric turbidity
C     CSR   -- circumsolar radiation
C     ELEV  -- meters elevation
C     PG    -- reflectivity (surface)
C
     SUBROUTINE ATMOS(OZONE,WP,BETA,CSR,PG)
```

```
C
      DOUBLE PRECISION BETA(366),PG(366),WP(366),CSR(366),OZONE(366)
C
      DOUBLE PRECISION OZONE1,OZONE2,OZONE3,OZONE4,OZONE5,OZONE6,OZONE7,
     1    OZONE8,OZONE9,OZONE10,OZONE11,OZONE12,
     2    WP1,WP2,WP3,WP4,WP5,WP6,WP7,WP8,WP9,WP10,WP11,WP12,
     3    BETA1,BETA2,BETA3,BETA4,BETA5,BETA6,BETA7,
     4    BETA8,BETA9,BETA10,BETA11,BETA12,
     5    CSR1,CSR2,CSR3,CSR4,CSR5,CSR6,CSR7,CSR8,CSR9,
     6    CSR10,CSR11,CSR12,
     7    PG1,PG2,PG3,PG4,PG5,PG6,PG7,PG8,PG9,PG10,PG11,PG12
C
      COMMON DBGFLAG
C
c
      OZONE1=.29
      OZONE2=.31
      OZONE3=.32
      OZONE4=.33
      OZONE5=.33
      OZONE6=.32
      OZONE7=.30
      OZONE8=.29
      OZONE9=.28
      OZONE10=.27
      OZONE11=.27
      OZONE12=.28
      WP1=1.000
      WP2=1.000
      WP3=1.050
      WP4=1.100
      WP5=1.500
      WP6=1.800
      WP7=2.200
      WP8=2.440
      WP9=2.000
      WP10=1.400
      WP11=1.050
      WP12=0.950
      BETA1=.075
      BETA2=.075
      BETA3=.075
      BETA4=.085
      BETA5=.085
      BETA6=.090
      BETA7=.090.
      BETA8=.084
      BETA9=.077
      BETA10=.075
      BETA11=.075
      BETA12=.075
      CSR1=.85
```

```
      CSR2=.85
      CSR3=.85
      CSR4=.85
      CSR5=.74
      CSR6=.74
      CSR7=.57
      CSR8=.57
      CSR9=.66
      CSR10=.74
      CSR11=.90
      CSR12=.90
      PG1=.24
      PG2=.24
      PG3=.24
      PG4=.24
      PG5=.24
      PG6=.24
      PG7=.24
      PG8=.24
      PG9=.24
      PG10=.24
      PG11=.24
      PG12=.24
c
c         set ozone and atmospheric turbidity terms as average for middle
c         of each month (leep-year logic included as 1 extra day for December)
c
      DO N=1,366
C
c         December
          IF (N .LE. 15.) THEN
                              OZONE(N)=OZONE1 - ((OZONE1 - OZONE12) * ((15. - N) / 15.))
                              WP(N) = WP1 - ((WP1 - WP12) * ((15. - N) / 15.))
        BETA(N) = BETA1 - ((BETA1 - BETA12) * ((15. - N) / 15.))
        CSR(N) = CSR1 - ((CSR1 - CSR12) * ((15. - N) / 15.))
        PG(N) = PG1 - ((PG1 - PG12) * ((15. - N) / 15.))
C
      ELSE IF (N .GT. 349.) THEN
        OZONE(N) = OZONE1 - ((OZONE1 - OZONE12) * ((365. - N) / 15.))
        WP(N) = WP1 - ((WP1 - WP12) * ((365. - N) / 15.))
        BETA(N) = BETA1 - ((BETA1 - BETA12) * ((365. - N) / 15.))
        CSR(N)= CSR1 - ((CSR1 - CSR12) * ((365. - N) / 15.))
        PG(N) = PG1 - ((PG1 - PG12) * ((365. - N) / 15.))

C
c         January
      ELSE IF (N .GT. 15 .AND. N .LE. 46) THEN
        OZONE(N) = OZONE2 - ((OZONE2 - OZONE1) * ((46.- N) / 31))
        WP(N) = WP2 - ((WP2 - WP1) * ((46.- N) / 31))
        BETA(N) = BETA2 - ((BETA2 - BETA1) * ((46.- N) / 31))
        CSR(N)= CSR2 - ((CSR2 - CSR1) * ((46.- N) / 31))
        PG(N) = PG2 - ((PG2 - PG1) * ((46.- N) / 31))
```

```
C
c          February
      ELSE IF (N .GT. 46. .AND. N .LE. 74.) THEN
        OZONE(N) = OZONE3 - ((OZONE3 - OZONE2) * ((74. - N) / 28.))
        WP(N) = WP3 - ((WP3 - WP2) * ((74. - N) / 28.))
        BETA(N) = BETA3 - ((BETA3 - BETA2) * ((74. - N) / 28.))
        CSR(N)= CSR3 - ((CSR3 - CSR2) * ((74. - N) / 28.))
        PG(N) = PG3 - ((PG3 - PG2) * ((74. - N) / 28.))
C
c          March
      ELSE IF (N .GT. 74. .AND. N .LE. 105.) THEN
        OZONE(N) = OZONE4 - ((OZONE4 - OZONE3) * ((105. - N) / 31.))
        WP(N) = WP4 - ((WP4 - WP3) * ((105. - N) / 31.))
        BETA(N) = BETA4 - ((BETA4 - BETA3) * ((105. - N) / 31.))
        CSR(N)= CSR4 - ((CSR4 - CSR3) * ((105. - N) / 31.))
        PG(N) = PG4 - ((PG4 - PG3) * ((105. - N) / 31.))
C
c          April
      ELSE IF (N .GT. 105. .AND. N .LE. 135.) THEN
        OZONE(N) = OZONE5 - ((OZONE5 - OZONE4) * ((135. - N) / 30.))
        WP(N) = WP5 - ((WP5 - WP4) * ((135. - N) / 30.))
        BETA(N) = BETA5 - ((BETA5 - BETA4) * ((135. - N) / 30.))
        CSR(N)= CSR5 - ((CSR5 - CSR4) * ((135. - N) / 30.))
        PG(N) = PG5 - ((PG5 - PG4) * ((135. - N) / 30.))
C
c          May
      ELSE IF (N .GT. 135. .AND. N .LE. 166.) THEN
        OZONE(N) = OZONE6 - ((OZONE6 - OZONE5) * ((166. - N) / 31.))
        WP(N) = WP6 - ((WP6 - WP5) * ((166. - N) / 31.))
        BETA(N) = BETA6 - ((BETA6 - BETA5) * ((166. - N) / 31.))
        CSR(N)= CSR6 - ((CSR6 - CSR5) * ((166. - N) / 31.))
        PG(N) = PG6 - ((PG6 - PG5) * ((166. - N) / 31.))
C
c          June
      ELSE IF (N .GT. 166. .AND. N .LE. 196.) THEN
        OZONE(N) = OZONE7 - ((OZONE7 - OZONE6) * ((196. - N) / 30.))
        WP(N) = WP7 - ((WP7 - WP6) * ((196. - N) / 30.))
        BETA(N) = BETA7 - ((BETA7 - BETA6) * ((196. - N) / 30.))
        CSR(N)= CSR7 - ((CSR7 - CSR6) * ((196. - N) / 30.))
        PG(N) = PG7 - ((PG7 - PG6) * ((196. - N) / 30.))
C
c          July
      ELSE IF (N .GT. 196. .AND. N .LE. 227.) THEN
        OZONE(N) = OZONE8 - ((OZONE8 - OZONE7) * ((227. - N) / 31.))
        WP(N) = WP8 - ((WP8 - WP7) * ((227. - N) / 31.))
        BETA(N) = BETA8 - ((BETA8 - BETA7) * ((227. - N) / 31.))
        CSR(N)= CSR8 - ((CSR8 - CSR7) * ((227. - N) / 31.))
        PG(N) = PG8 - ((PG8 - PG7) * ((227. - N) / 31.))
C
c          August
      ELSE IF (N .GT. 227. .AND. N .LE. 258.) THEN
        OZONE(N) = OZONE9 - ((OZONE9 - OZONE8) * ((258. - N) / 31.))
```

```
        WP(N) = WP9 - ((WP9 - WP8) * ((258. - N) / 31.))
        BETA(N) = BETA9 - ((BETA9 - BETA8) * ((258. - N) / 31.))
        CSR(N)= CSR9 - ((CSR9 - CSR8) * ((258. - N) / 31.))
          PG(N) = PG9 - ((PG9 - PG8) * ((259. - N) / 31.))
C
c          September
      ELSE IF (N .GT.258. .AND. N .LE. 288.) THEN
        OZONE(N) = OZONE10 - ((OZONE10 - OZONE9) * ((288. - N) / 30.))
        WP(N) = WP10 - ((WP10 - WP9) * ((288. - N) / 30.))
        BETA(N) = BETA10 - ((BETA10 - BETA9) * ((288. - N) / 30.))
        CSR(N)= CSR10 - ((CSR10 - CSR9) * ((288. - N) / 30.))
        PG(N) = PG10 - ((PG10 - PG9) * ((288. - N) / 30.))
C
c          October
      ELSE IF (N .GT. 288. .AND. N .LE. 319.) THEN
        OZONE(N) = OZONE11 - ((OZONE11 - OZONE10) * ((319.- N) / 31.))
        WP(N) = WP11 - ((WP11 - WP10) * ((319.     - N) / 31.))
        BETA(N) = BETA11 - ((BETA11 - BETA10) * ((319.- N) / 31.))
        CSR(N)= CSR11 - ((CSR11 - CSR10) * ((319. - N) / 31.))
        PG(N) = PG11 - ((PG11 - PG10) * ((319. - N) / 31.))
C
c          November
      ELSE IF (N .GT.319. .AND. N .LE. 349.) THEN
        OZONE(N) = OZONE12 - ((OZONE12 - OZONE11) * ((349.- N) / 30.))
        WP(N) = WP12 - ((WP12 - WP11) * ((349. - N) / 30.))
        BETA(N) = BETA12 - ((BETA12 - BETA11) * ((349. - N) / 30.))
        CSR(N)= CSR12 - ((CSR12 - CSR11) * ((349. - N) / 30.))
        PG(N) = PG12 - ((PG12 - PG11) * ((349. - N) / 30.))
      ENDIF
      ENDDO
C
c---- debugging stuff ---------
c
C     IF(DBGFLAG.EQ.3) THEN
C     WRITE(*,7005) OZONE(N-50),WP(N-50),BETA(N-50),CSR(N-50),PG(N-50)
C     WRITE(13,7005) OZONE(N-50),WP(N-50),BETA(N-50),CSR(N-50),PG(N-50)
C 7005 FORMAT(1X,E12.6,E12.6,E12.6,E12.6,E12.6,E12.6,E12.6)
C     ENDIF

      RETURN
      END
C
C=============================================================================
c//////////////////////////////////////////////////////////////////////////
C////////////////// POTEVAP SUBROUTINE ////////////////////////////////////
C
c          start solar radiation routine
c          find position of sun for each hour for each day
c          no modifications needed here
C
      SUBROUTINE POTEVAP  (J,IA,DN,LAT,LON,SL,ASP,RIDGE,ELEV,
     1              DR,RD,PI,HSTEP,
```

```
     2            BETA,PG,CSR,WP,OZONE,VIEWFACTOR,
     3            TR,TPET)
c                 dbgflag
C
C
      INTEGER DN(40000)
      INTEGER J,IA,DBGFLAG
      DOUBLE PRECISION LAT(200),LON(200),LAT2(200)

      REAL H1,H2,HSTEP
      REAL SL(200),SL2(200),ASP(200),ELEV(200)
      REAL RIDGE(200,0:36),RIDGE2(200,0:36),SLOPE(200,0:36),
     1   HORIZ(200,0:36)

      DOUBLE PRECISION BETA(366),PG(366),WP(366),CSR(366),OZONE(366)
C
      DOUBLE PRECISION TAU,DEC,ET,ALT,AZ,STD,
     1   HASS,HASR,CF,LST,T,MA,IDR,IDA,IDM,ID,IR,ISS,IB
C
      DOUBLE PRECISION II,COSTHETA,THETA,
     1   HA,ISC,PO,P,WO,AMSP,W,U1,U3,EO,TRR,TRO,ABO,TRG,ABW,TRW,
     2   TRA,TRAA,TRAS,FC,PAP,INN,SUNAZ,RNHORIZ
C
c
      REAL zenith,idhoriz,ibhoriz,ibslope,rnslope
      REAL YRAD,DRAD,RAD,RN,GH,SSG,ALPHA
      REAL DR,RD,PI,TR,VIEWF,TA,PET,VIEWFACTOR
C
C     standard meridian
      STD=120
C
C     latitude in radians
      LAT2(ia) = LAT(ia) * DR
c
C     slope in degrees
      SL2(ia) = ATAN(.01 * SL(ia)) * RD
      YRAD=0.
C
C
C     ***** input elevation data for the surrounding ridges each 10 ******
C     ****************** startiNg at 10 degrees  ******************
C     Input ridge elevation data each 10 deg starting at 10 deg
C     This is the most questionable routine for accuracy, particularly for
C     high ridges.  A good geometrist is needed to improve this.
c
c
      VIEWFACTOR = 0.
      DO II=1,36
       RIDGE2(ia,ii) = 90. - RIDGE(ia,II)
       COSTHETA = COS(SL2(ia)*DR)*COS((RIDGE2(ia,ii))*DR)
     1        +SIN(SL2(ia)*DR)
     2        *SIN((RIDGE2(IA,II))*DR)*COS((II*10.-ASP(ia))*DR)
```

```
      THETA = -ATAN(COSTHETA / SQRT(-COSTHETA ** 2. + 1.)) + 90. * DR
      THETA = 90. - THETA * RD
      VIEWF = 90. - THETA
      IF (VIEWF .GE. 90.) THEN
       VIEWF = 90.
      ENDIF
      VIEWFACTOR = VIEWFACTOR + VIEWF
     END DO
     VIEWFACTOR = VIEWFACTOR / (36. * 90.)
     II = 0

c
C    SOLAR ROUTINE
C    This subroutine is written to calculate the location of the sun
C
C
C ALT   ALTITUDE OF THE SUN (RADIANS)
C AZ    AZIMUTH OF THE SUN (RADIANS)
C LAT   LATITUDE OF THE SITE  (DEGREES)
C LON   LONGITUDE OF THE SITE (DEGREES)
C STD   STANDARD MERIDIAN OF THE SITE (DEGREES)
C DR    DEGREES TO RADIANS (DEGREES/RADIAN)
C RD    RADIANS TO DEGREES (RADIANS/DEGREE)
C CF    CORRECTION FACTOR FOR THE EQUATION OF TIME AND LONGITUDE CORRECTION (HOURS)
C LST   LOCAL STANDARD TIME (HOURS)
C T     LOCAL APPARENT TIME (HOURS)
C H1    STARTING HOUR FOR THE SIMULATION (HOURS)
C H2    ENDING HOUR FOR THE SIMULATION (HOURS)
C HSTEP TIME STEP OF THE SIMULATION (HOURS)
C DN    DAY NUMBER (DAY OF THE YEAR, UNITLESS)
C DNN1  DAY OF THE YEAR TO BEGIN THE SIMULATION (UNITLESS)
C DN2   DAY OF THE YEAR TO END THE SIMULATION   (UNITLESS)
c
C
c    TA  = air temperature (Kelvin) as a function of Julian day number
c    TAU  = day angle (radians)
c    DEC  = solar declination (radians)
c    ET   = equation of time (minutes)
c    HASR = hour angle of the sun at sunrise (radians)
c    HASS = hour angle of the sun at sunset (radians)
c
     TA  = (17.3-11.74*SIN(DN(J)/366*2*PI+1.3))+273.15
     TAU = 2*PI*(DN(J)-1)/365
     DEC = (0.006918-0.399912*COS(TAU)+0.07257*SIN(TAU)
    1    -0.006758*COS(2*TAU)+0.000907*SIN(2*TAU)-0.002697*COS(3*TAU)
    2    +0.00148*SIN(3*TAU))
     ET  = (0.000075+0.001868*COS(TAU)-0.032077*SIN(TAU)
    1    -0.014615*COS(2*TAU)-0.04089*SIN(2*TAU))*229.18

     HASR = DACOS(-TAN(LAT2(ia))*TAN(DEC))
     HASS = -HASR
     H1   = 12.-HASR*RD/15.
```

```
      H2   = 12.-HASS*RD/15.
c
C     CORRECTION FACTOR FOR STANDARD TIME AT LOCAL LONGITUDE IN HOURS
      CF=(4*(STD-LON(ia))+ET)/60.
C
C----- LOOP THROUGH DAYLIGHT HOURS
C     HOUR OF THE DAY LOOP MODEL RUNS FROM SUNRISE TO SUNSET
C
      DO 2000 LST=H1,H2,HSTEP
c
C       CORRECTION FOR LOCAL TIME
        T  = LST+CF
        HA = 15.*(T-12.)*DR
C
C       ALTITUDE OF THE SUN AT HOUR ANGLE HA
        ALT = DASIN(SIN(DEC)*SIN(LAT2(ia))+COS(DEC)
     1       *COS(LAT2(ia))*COS(HA))
c
C       AZIMUTH OF THE SUN AT HOUR ANGLE HA
        AZ = DACOS((SIN(ALT)*SIN(LAT2(ia))-SIN(DEC))/(COS(ALT)
     1      *COS(LAT2(ia))))
        IF (HA .LT. 0.) THEN
          AZ = PI-AZ
        ELSE IF (HA .GE. 0.) THEN
          AZ = AZ+PI
        END IF

        ALT = ALT*RD
        AZ  = AZ*RD

        IF (ALT .LE. 0.) THEN
          ZENITH = 90
        ELSE IF (ALT .GT.0.) THEN
          ZENITH = 90-ALT
        ENDIF

C       END OF SOLAR POSTION ROUTINE
C
C
C---- begin routine for calculating net radiation ----------
c
c     ISC = solar constant
c     PO  = pressure at sea level
c     P   = pressure at site
c     WO  = single scatter albedo by aerosols
c
        ALPHA = 1.
        ISC   = 1367.
        PO    = 1013.25
        P     = EXP(-.0001184 * ELEV(ia)) * PO
        WO    = .9
c
```

```
C----- set coefficients
c
      AMSP = (COS(ZENITH*DR)+.15 * (93.885-ZENITH)**(-1.253))**(-1.)
      MA   = AMSP * (P / PO)
      P    = EXP(-.0001184 * 0) * PO
c
C----- pressure at beta measurement
c
      W  = WP(DN(J)) * (P / PO)**.75 * (273. / TA)**.5
      U1 = W * AMSP
      U3 = OZONE(DN(J)) * AMSP
      EO = 1. + .033 * COS((2 * 3.14159 * DN(J) / 365.))
c
C----- eccentricity correction
c
      TRR  = EXP(-.0903 * MA**.84 * (1. + MA - MA**1.01))
      ABO  = ((.1611 * U3 * ((1 + 139.48 * U3)**(-.3035)))
     1      - .002715 * U3 * ((1.+.044*U3+.0003*(U3**2))**(-1)))
      TRO  = 1. - ABO
      TRG  = EXP(-.0127 * MA**.26)
      ABW  = 2.4959 * U1 *
     1      ((1.+79.034*U1)**.6828 + 6.385 * U1)**(-1.)
      TRW  = 1. - ABW
      TRA  = (.12445 * ALPHA - .0162) + (1.003 - .125 * ALPHA)
     1      * EXP(-BETA(DN(J)) * ALPHA * MA * (1.089 + .5120001))
      TRAA = 1. - (1. - WO) * (1. - MA + MA**1.06) * (1. - TRA)
      IDR  = EO*.79*ISC*COS(ZENITH*DR)*TRO*TRG*TRW*TRAA
     1      * .5 * (1. - TRR) * (1. - MA + MA**1.02) ** (-1.)
      TRAS = TRA / TRAA
      FC   = .84
      IDA  = EO*.79*ISC*COS(ZENITH*DR)*TRO*TRG*TRW*TRAA
     1      *FC*(1.-TRAS)/(1.-MA+MA**1.02)
      PAP  = .0685 + (1. - FC) * (1. - TRAS)
c
C----- direct beam (normal to surface)
c
      INN = EO * .9751 * ISC * TRR * TRO * TRG * TRW * TRA
c
C----- direct beam (horizontal surface)
c
      IB = INN * COS(ZENITH * DR)
c
C----- diffuse (multiple reflected)
c
      IDM = (IB+IDA+IDR) * (PG(DN(J)) * PAP / (1.-PG(DN(J))*PAP))
c
C----- block all radiation
c
      IF (ZENITH .GE. 90.) THEN
        IB = 0.
        INN = 0.
        IDR = 0.
```

```
        IDA = 0.
        IDM = 0.
      ENDIF
      SUNAZ = INT(AZ / 10. + .5)
c
C----- block by east-west ridge
c
      IF (RIDGE2(ia,SUNAZ) .LE. ZENITH) THEN
        IB = 0
      ENDIF
      IF ((RIDGE2(ia,SUNAZ) - 4.) .LE. ZENITH) THEN
        IDA = (1. - CSR(DN(J))) * IDA
      ENDIF
c
C----- diffuse radiation on a horizontal surface
c
      ID = IDR + IDA + IDM
c
C----- calculate solar angle of incidence, (90-THETA)
c
      COSTHETA = COS(SL2(ia)*DR) * COS(ZENITH*DR) + SIN(SL2(ia)*DR)
     1          * SIN(ZENITH*DR) * COS((AZ-ASP(ia))*DR)
      THETA    = -ATAN(COSTHETA / SQRT(-COSTHETA**2.+1.)) + 90. * DR
      THETA    = THETA * RD
      IF (THETA .GT. 90.) THEN
        THETA = 90.
      ENDIF
c
C     add for ground reflection and subtract blocked sky
c
      IR = (ID + IB) * PG(DN(J)) * (1. - VIEWFACTOR)
      ISS = ID * VIEWFACTOR
c
C     DIFFUSE RADIATION, SLOPE OR HORIZONTAL
c
      IDHORIZ = ISS + IR
      IDSLOPE = ISS + IR
c
C     DIRECT BEAM RADIATION, SLOPE OR HORIZONTAL
c
      IBHORIZ = IB
      IBSLOPE = IBHORIZ * (COS(THETA * DR) / COS(ZENITH * DR))

      RNHORIZ = (IBHORIZ + IDHORIZ)
      RNSLOPE = (IBSLOPE + IDSLOPE)
      IF (RNHORIZ .LT. 0.) THEN
        RNHORIZ = 0.
      ENDIF
      IF (RNSLOPE .LT. 0.) THEN
        RNSLOPE = 0.
      ENDIF
```

```
      HORIZ(ia,II) = IBHORIZ + IDHORIZ
      SLOPE(ia,II) = IBSLOPE + IDSLOPE
c
C    RADIATION (RAD) IS IN J/m^2 PER TIME STEP
c
      RAD = RNSLOPE*HSTEP*3600.
      TR  = TR + RAD
c
C    CALCULATE NET RADIATIION (fixed error 8/2/96)
c
c      RN = -71+.72*RAD
      RN = (-71*hstep*3600.)+.72*RAD
c
C    CALCULATE SOIL HEAT FLUX (fixed error 8/2/96)
c
c      GH  = -20+.386*RN
      GH  = (-20*hstep*3600)+.386*RN
c
      SSG  = -13.281+.083864*TA-.00012375*TA**2
      PET  = SSG*(RN-GH)/2.45E6
            TPET =  TPET + PET
c
C
c       IF(DBGFLAG.EQ.3) THEN
c         WRITE(*,75) J,IA,DN(J),TR,RN,PET
c         WRITE(13,75) J,IA,DN(J),TR,RN,PET
c 75       FORMAT(1X,I5,I5,I5,F14.7,F14.7,F14.7)
c       ENDIF
C
C

2000  CONTINUE
C
C---- END OF HOUR LOOP
C
c---- DRAD = total daily radiation ---------------------------
C
    DRAD=TR
    TR = 0.
c
C
    RETURN
    END
c
C=======================================================================================
c//////////////////////////////////////////////////////////////////////////
c////////////////// added BUCKET subroutine 8/15//96 ////////////
c
    subroutine bucket(ia,depth,soiltype,rocktype,
    1              soilporo,fieldcap,imbibe,imb,
    2              soilalbeta,soiltalpha,soilresid,
    3              pptloc,petrs,sorp,dsoilmm,tet,infilmm,
```

```
     4              soilvwc,buckmm,drainvwc,runoffmm,massbal,
     5              netinfil)
c                   topoid
c
      integer ia
              real depth(200)
              integer soiltype(200),rocktype(200),topoid(200)
              real soilporo(20),fieldcap(20),imbibe(0:300)
              real soilalbeta(20),soiltalpha(20),soilresid(20)
      real soilvwc(200),buckmm(200),drainvwc(200),runoffmm(200)
      real netinfil(200)
      real sorp(200)
      real massbal,dsoilmm,infilmm,imb
c
              real extra,tet,buckvwc,initvwc,finalvwc
      real fieldcp,pptloc,pptvwc
c     real totwat, dailyet, dailypet
c
c---- initialize parameters
c
      if(soiltype(ia).eq.8) then
       soilks = imbibe(rocktype(ia))
       sorp(ia) = .01
      endif
c
      fieldcp  = fieldcap(soiltype(ia))
      spor     = soilporo(soiltype(ia))
      a        = soiltalpha(soiltype(ia))
      b        = soilalbeta(soiltype(ia))
      sresid   = soilresid(soiltype(ia))
      imb      = imbibe(rocktype(ia))
c
c
      infilmm     = 0.
              runoffmm(ia) = 0.
              drainvwc(ia) = 0.
c
C----         add precip to channels to help account for run-on
c     note:  this violates the overall mass balance
c
c     removed this 8/28/96
c             IF (topoid(ia).EQ.1) THEN
c               pptloc = pptloc*1.2
c             ENDIF
c
c---- convert mass balance terms to average volumetric water content
c     for entire soil profile
c     divide by depth because piston flow assumed for infiltration
c     divide by 1000 because depth is in meters
c
      buckvwc  = buckmm(ia)/depth(ia)/1000.
      initvwc  = soilvwc(ia)+buckvwc
```

```
          pptvwc   = pptloc/depth(ia)/1000.
c
    soilvwc(ia) = soilvwc(ia)+pptvwc
c
C----       CALCULATE RUNOFF IN MM
c
    IF (soilvwc(ia)+buckvwc.GT.spor) THEN
      RUNOFFmm(ia)  = (soilvwc(ia)+buckvwc-spor)*DEPTH(ia)*1000
      soilvwc(ia) = spor
            buckmm(ia)    = 0.
    ENDIF
c
c---- calculate evapotranspiration (Flint and Childs original equation)
c    PETRS = daily potential ET calculated using POTEVAP subroutine
c
    ALPRIME = a*(1-EXP(b*(soilvwc(ia)-sresid)/(spor-sresid)))
c
    TET = ALPRIME*petrs
    IF (TET .LT. 0) THEN
       TET = 0.
    ENDIF
c
c---- Alan's correction for PET on rainy days
c---- correction for PET on rainy days calculated in main program
c
c     IF (DAYPPT .GT. 0) THEN
c        TET=TET*.25
c     ENDIF
c
C    CALCULATE SOIL WATER COTENT IN VOLUMETRIC WATER CONTENT
c
    SOILvwc(ia)=SOILvwc(ia)-TET/DEPTH(ia)/1000
c
c
C----       TAKE SOME ET FROM THE DRN, IF THE DRAIN IS DEEP TAKE LESS ET
c
    IF (buckmm(ia).GT.0) THEN
      buckmm(ia) = buckmm(ia)-((1/DEPTH(ia))*.25)*TET
      if(buckmm(ia).LT.0.) THEN
        EXTRA      = 0.-buckmm(ia)
              buckmm(ia)  = 0.
            endif
c
C----       ADD BACK THE ET WATER TO THE SOIL AND THE EXTRA FROM THE DRAIN
c
      soilvwc(ia) = soilvwc(ia)+(1/DEPTH(ia)*.25)
   1            *(TET/DEPTH(ia)/1000)-(EXTRA/DEPTH(ia)/1000)
            EXTRA=0.
    ENDIF
c
C---- CALCULATE EXCESS WATER AND PUT IT IN DRAIN IN VOLUMETRIC WATER CONTENT
c
```

```
      IF (soilvwc(ia).GT.FIELDCP) THEN
        DRAINvwc(ia)  = soilvwc(ia)-FIELDCP
        soilvwc(ia) = FIELDCP
      ENDIF
c
C---- IF ET TAKES TOO MUCH WATER PUT SOILWAT BACK TO RESIDUAL
c
      IF (soilvwc(ia).lt.sresid) THEN
        TET       = TET-(sresid-soilvwc(ia))
              soilvwc(ia) = sresid
      ENDIF
c
c---- following needed only if bucket model run on hourly basis
c
c     DAILYET  = DAILYET  + TET
c     DAILYPET = DAILYPET + PETrs
c
c2000  CONTINUE
c
C ****************** END OF HOURS *************************
c
C---- CALCULATE SUMMATION OF DRAIN INTO DRN FOR STORAGE
c
      buckmm(ia) = buckmm(ia) + (drainvwc(ia)*DEPTH(ia)*1000.)
c
c
C           SET THE FINALWAT TO THE FINAL SOILWAT AND DRN TO USE IN THE MASS BALANCE CHECK
C     IF 2 MM OF WATER EXISTS THEN TAKE IMBIBE OUT AS NET INFILTRATION
c
      IF (buckmm(ia).GT.2) THEN
        IF (imb.GT.buckmm(ia)) THEN
              infilmm = buckmm(ia)
            ELSE
              infilmm = imb
            ENDIF
            NETINFIL(ia) = NETINFIL(ia) + infilmm
        buckmm(ia) = buckmm(ia) - infilmm
      ENDIF

            finalvwc = soilvwc(ia) + (buckmm(ia)/1000/DEPTH(ia))
c           FINALWAT = TOTWAT

      dsoilmm = (finalvwc - initvwc)*DEPTH(ia)*1000
            MASSBAL  = pptloc - tet - dsoilmm - infilmm - runoffmm(ia)
c
c     YRAD=YRAD+DRAD
c     TPPT=TPPT+DAYPPT
c     TRUNOFF=TRUNOFF+RUNOFF
C           WRITE(9,15)YR,DN,DAYPPT,DRAD/1000
c           WRITE(9,15)YR,DN,DAYPPT,DAILYET,INFLOW
c
c     INFLOW=0.
```

```
c     DAILYET=0.
c     DAILYPET=0.
c     DRAIN=0.
c     RUNOFF=0.
c
c2100  CONTINUE
C     END OF DAYS

      return
      end
c
c////////////////////////////// end of program ////////////////////////////////////
c////////////////////////////////////////////////////////////////////////////////
```

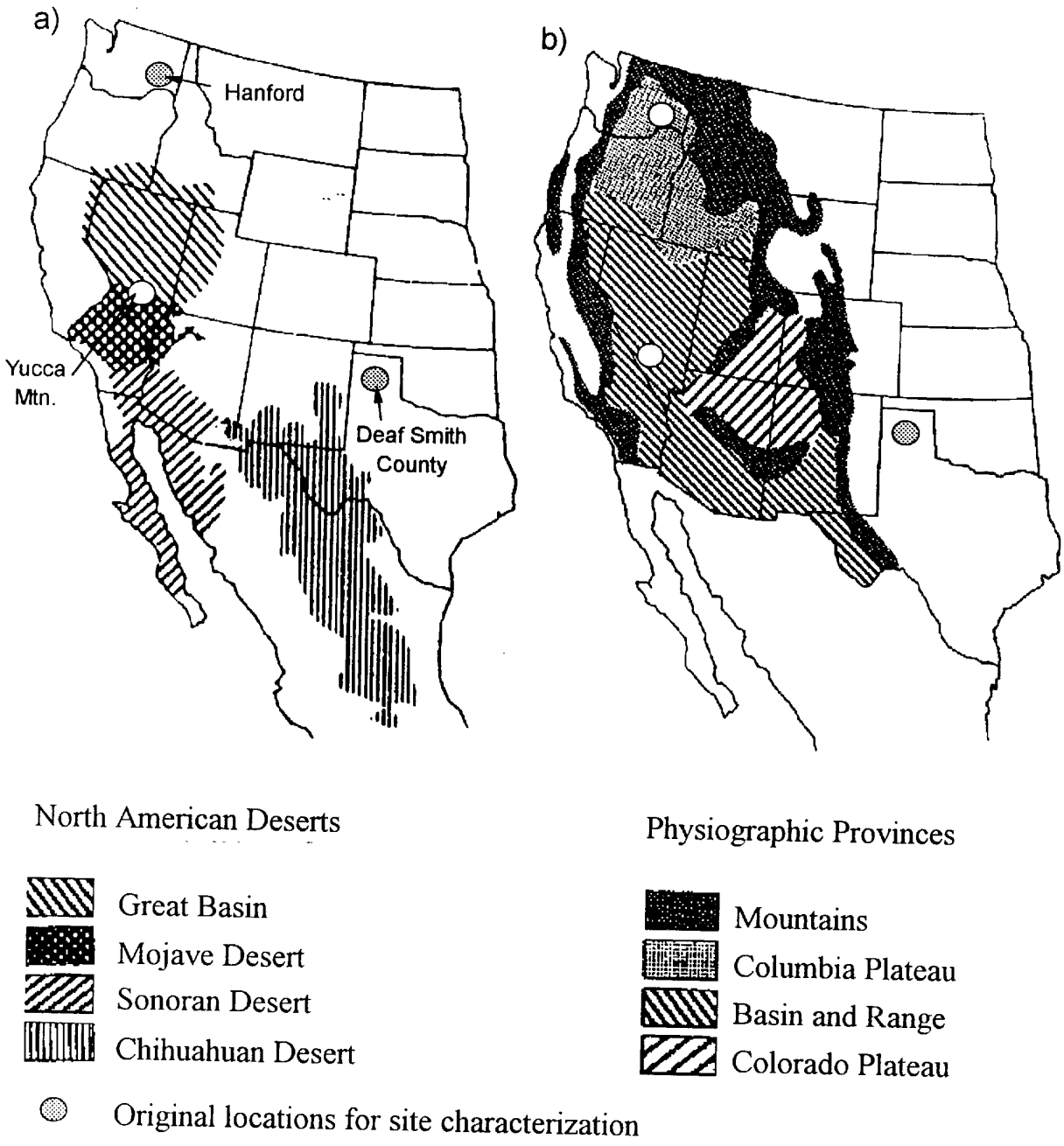

Figure 1. Locations of a) North American Deserts and the original 3 sites for characterization, and b) physiographic provinces.

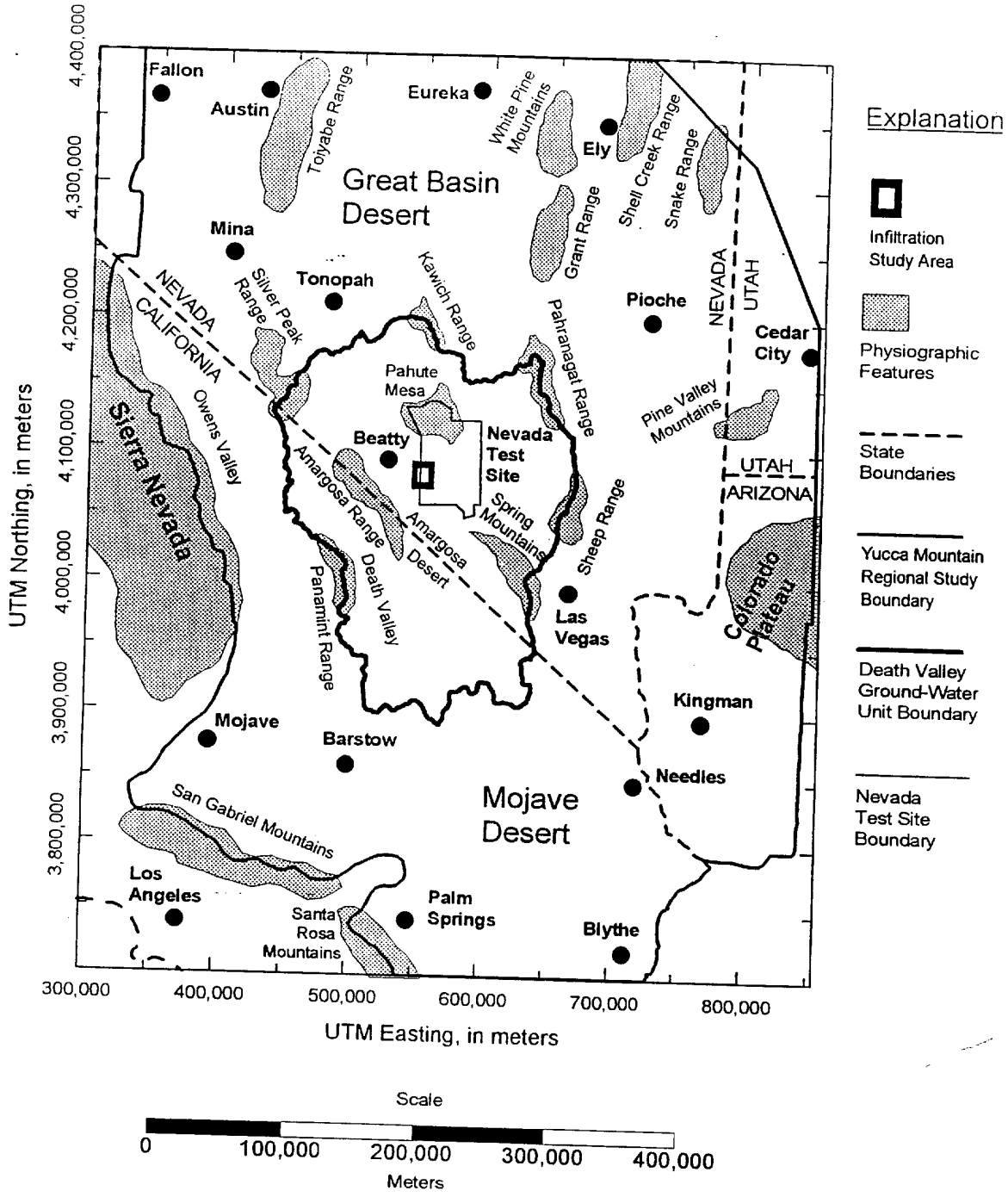

Figure 2. Yucca Mountain regional study area with Death Valley Ground-Water Unit and infiltration study boundary.

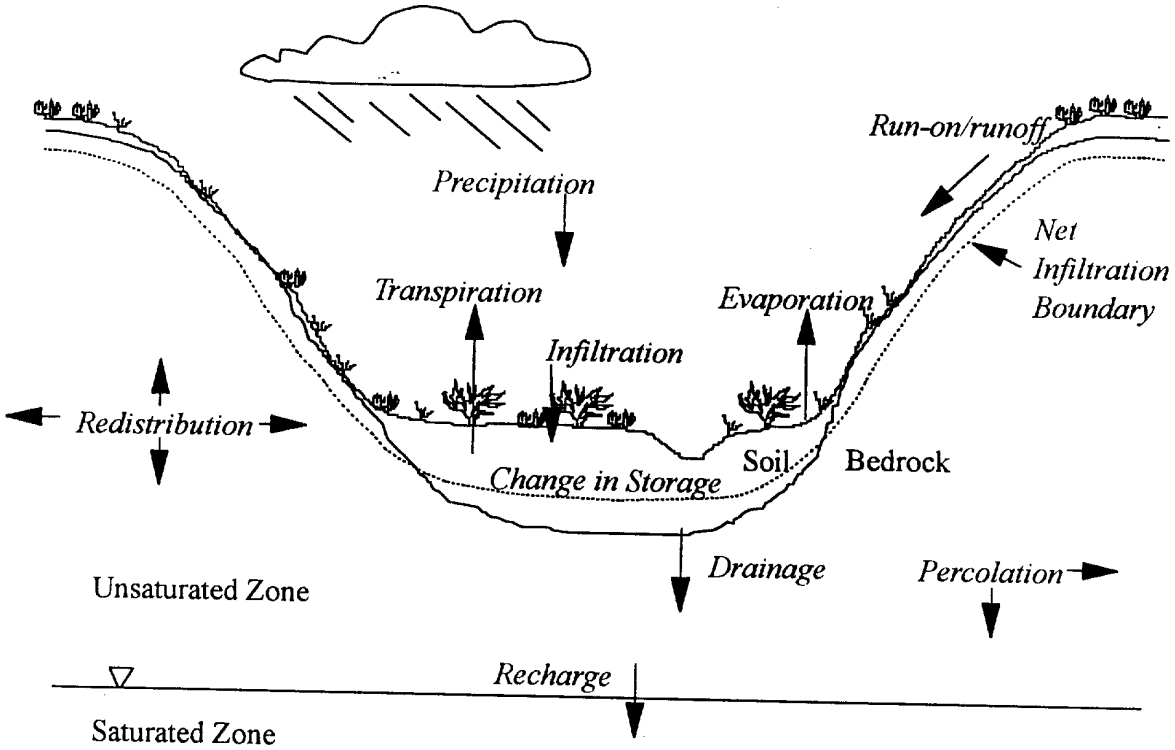

Figure 3. Field scale schematic of infiltration.

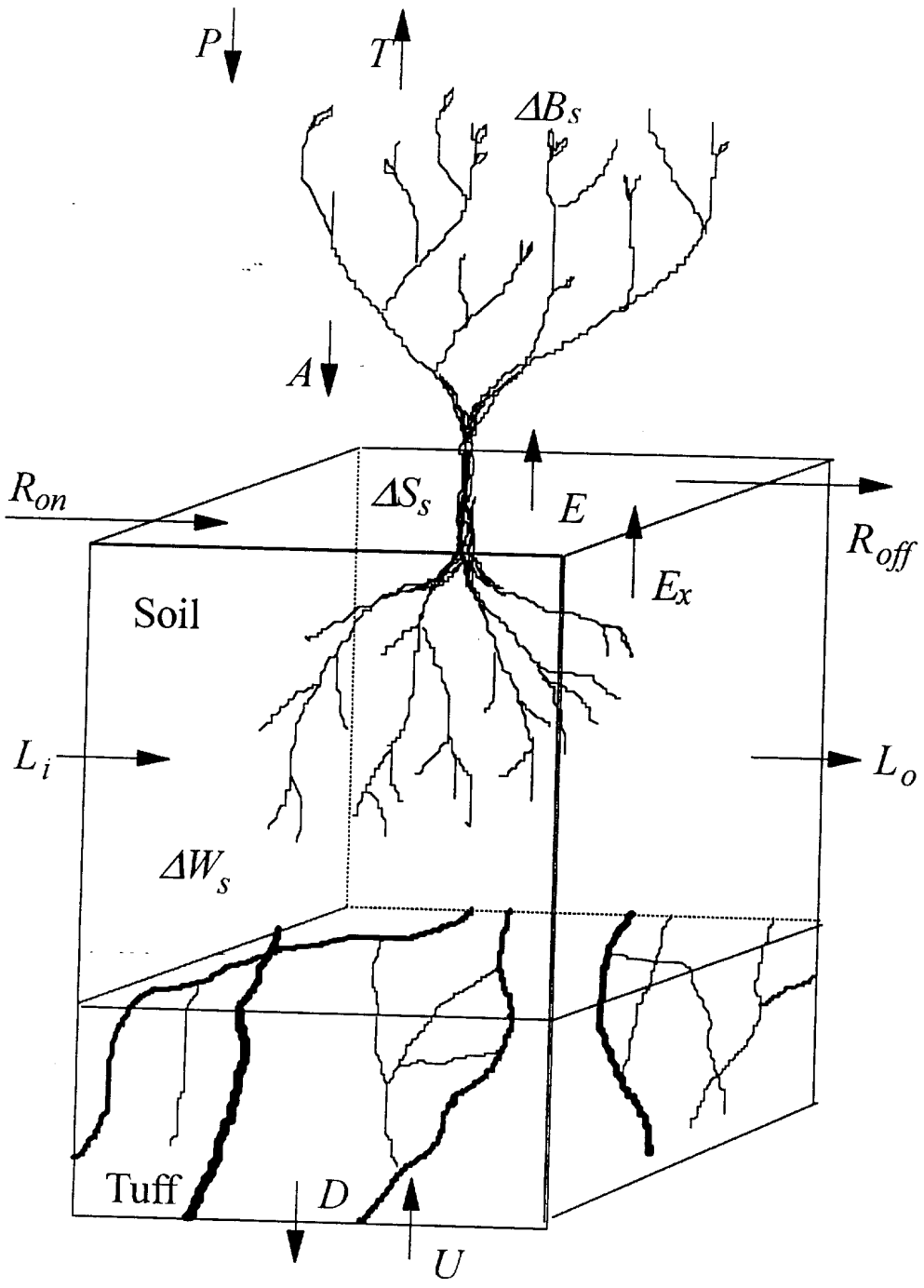

Figure 4. Diagrammatic water balance components using notation described in equation 1.

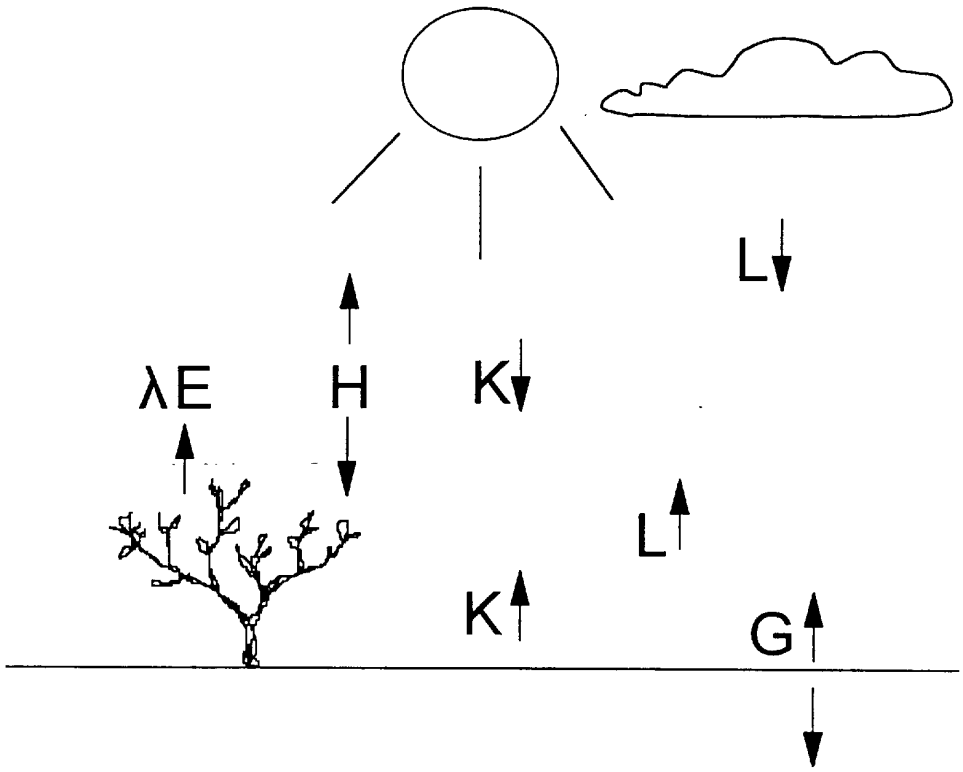

Figure 5. Conceptual model of the energy balance equation for evapotranspiration.

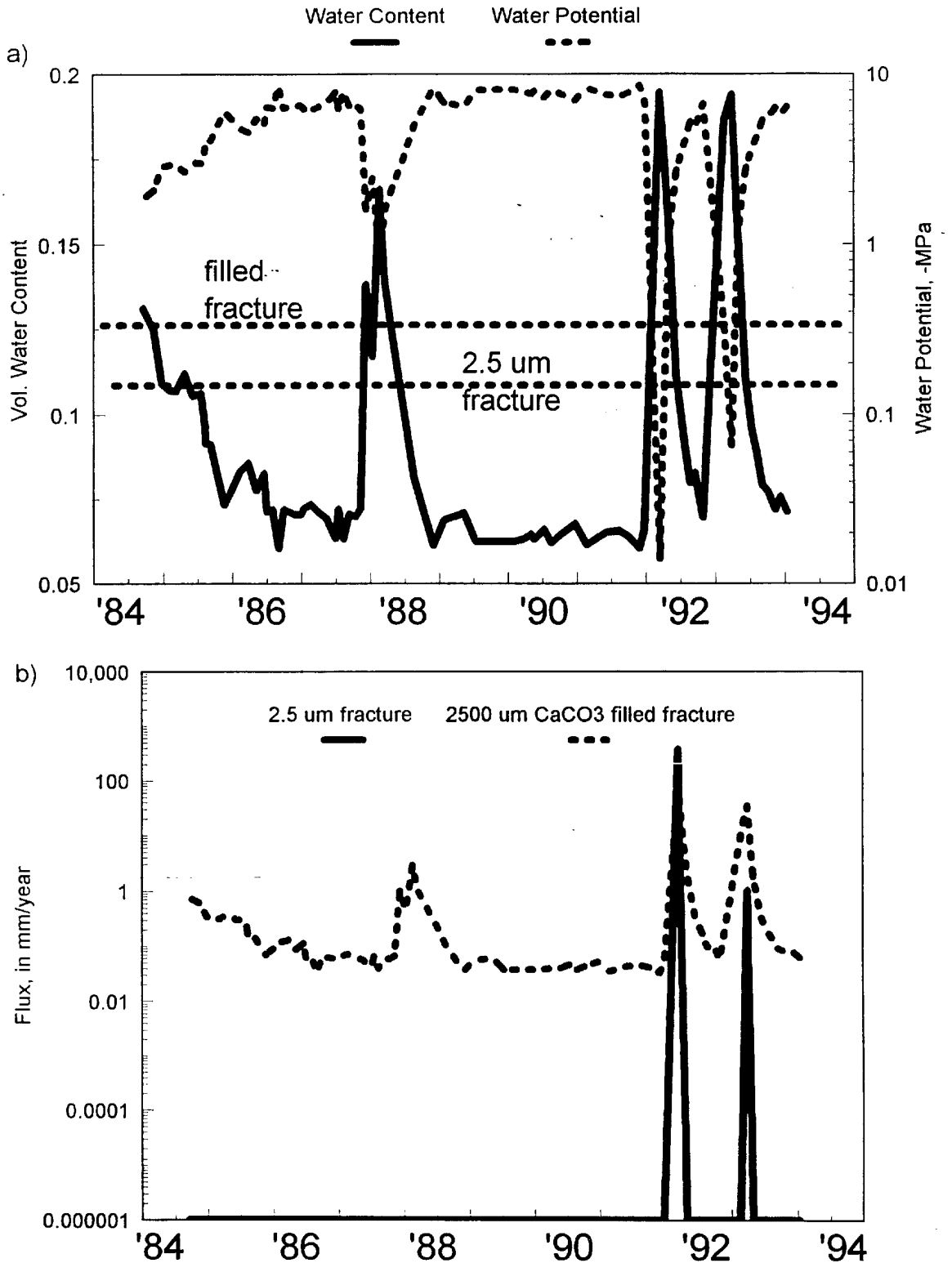

Figure 6. a) Water content and water potential at the soi-bedrock interface at a depth of 2.1 m in borehole USW UZ-N52 (the horizontal lines are the air-entry potentials for a 2.5 um open fracture and a 2500-um filled fracture), and b) associated flux calculated as the hydraulic conductivity of the fractures times a unit gradient.

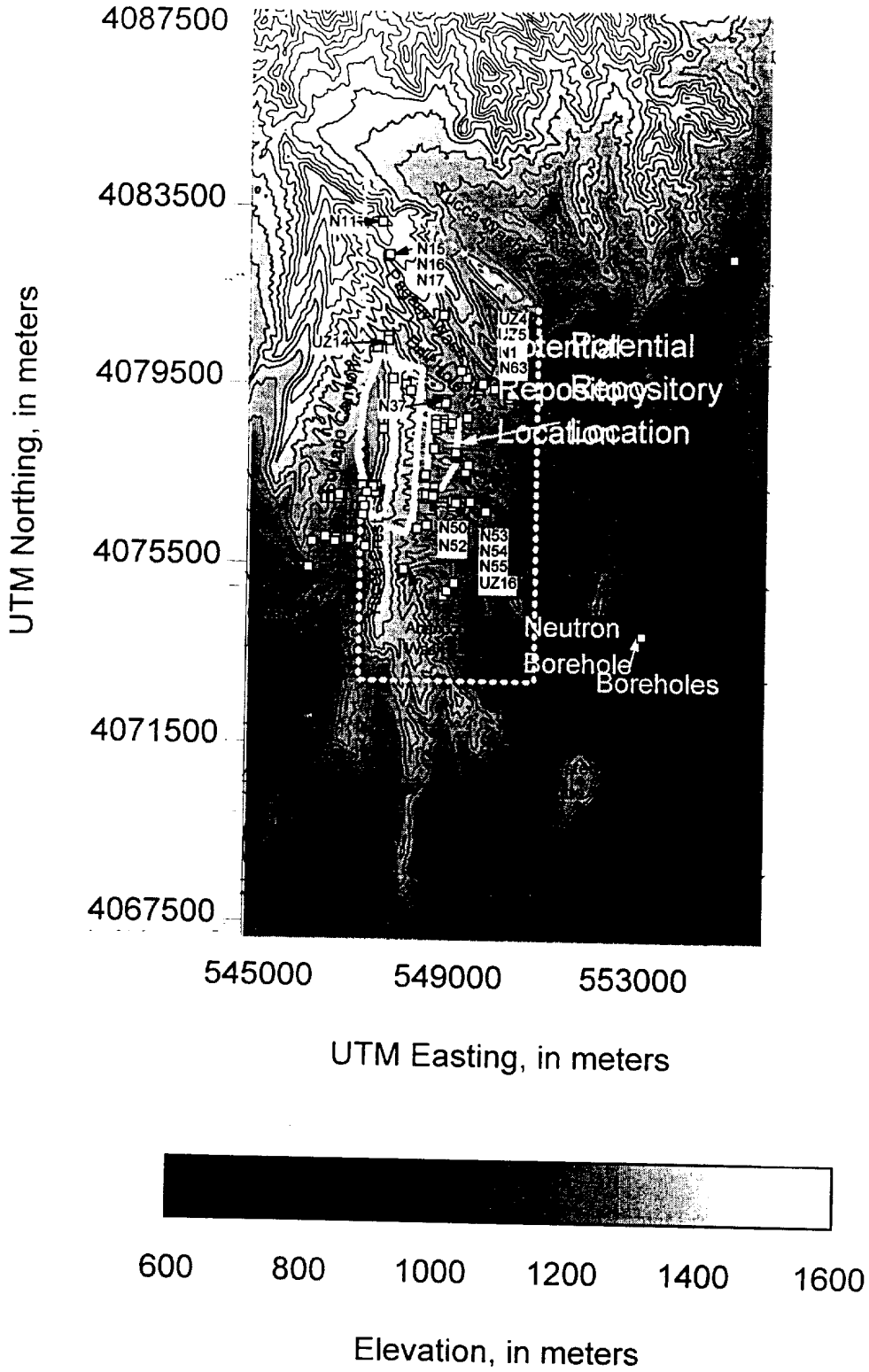

Figure 7. Infiltration study area and modeling domain with original site-scale model boundary (Wittwer and others, 1992) and potential repository location.

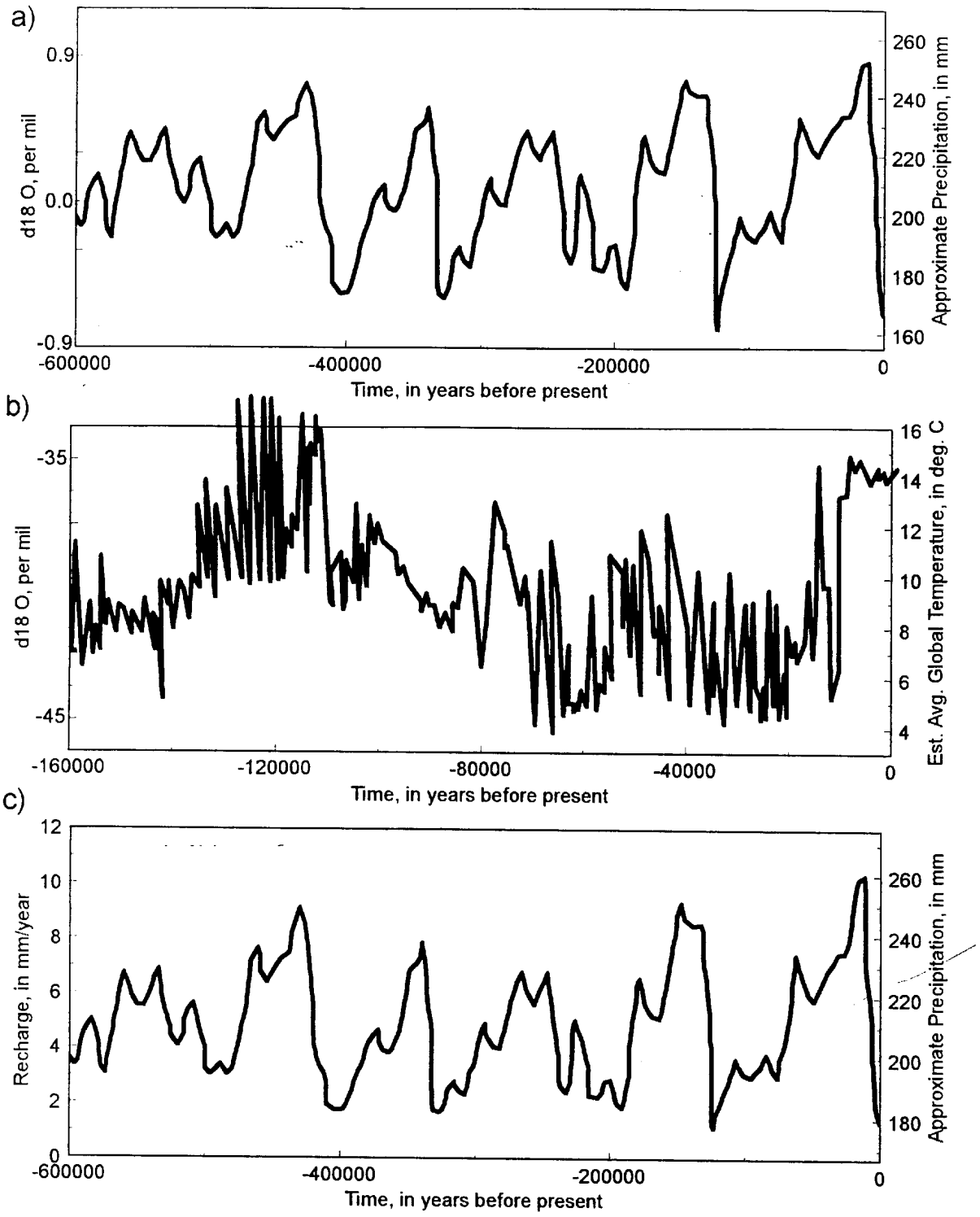

Figure 8. Historical climate change estimates from a) SPECMAP studies with a hypothetical transfer to precipitation, b) high-frequency fluctuations in climate change from the GRIP studies and c) recharge estimated from climate change cycles using the Maxey-Eakin method.

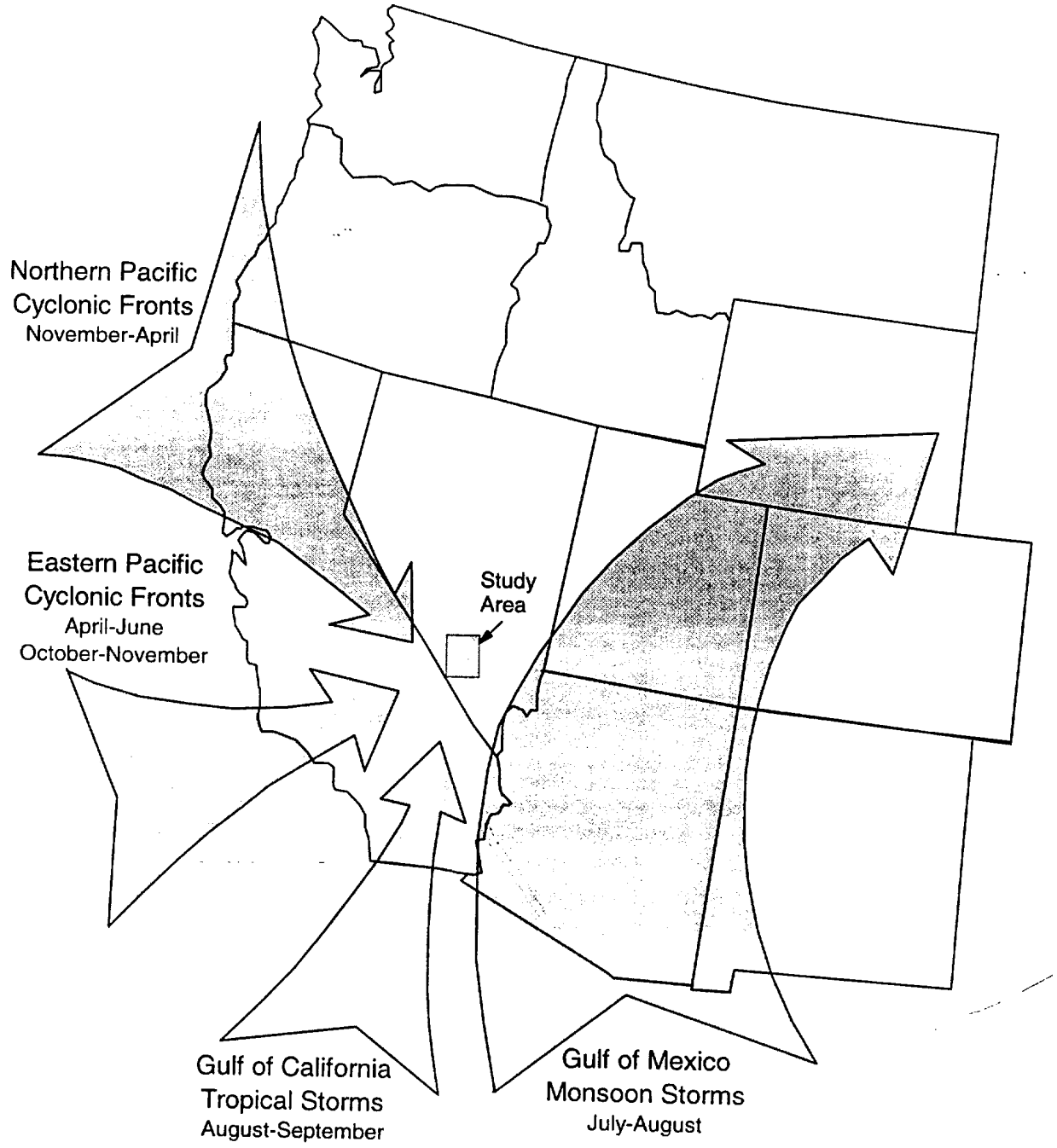

Figure 9. Predominate direction of weather patterns and seasonal sources of moisture across the southwestern U.S. (after Grasso, 1996).

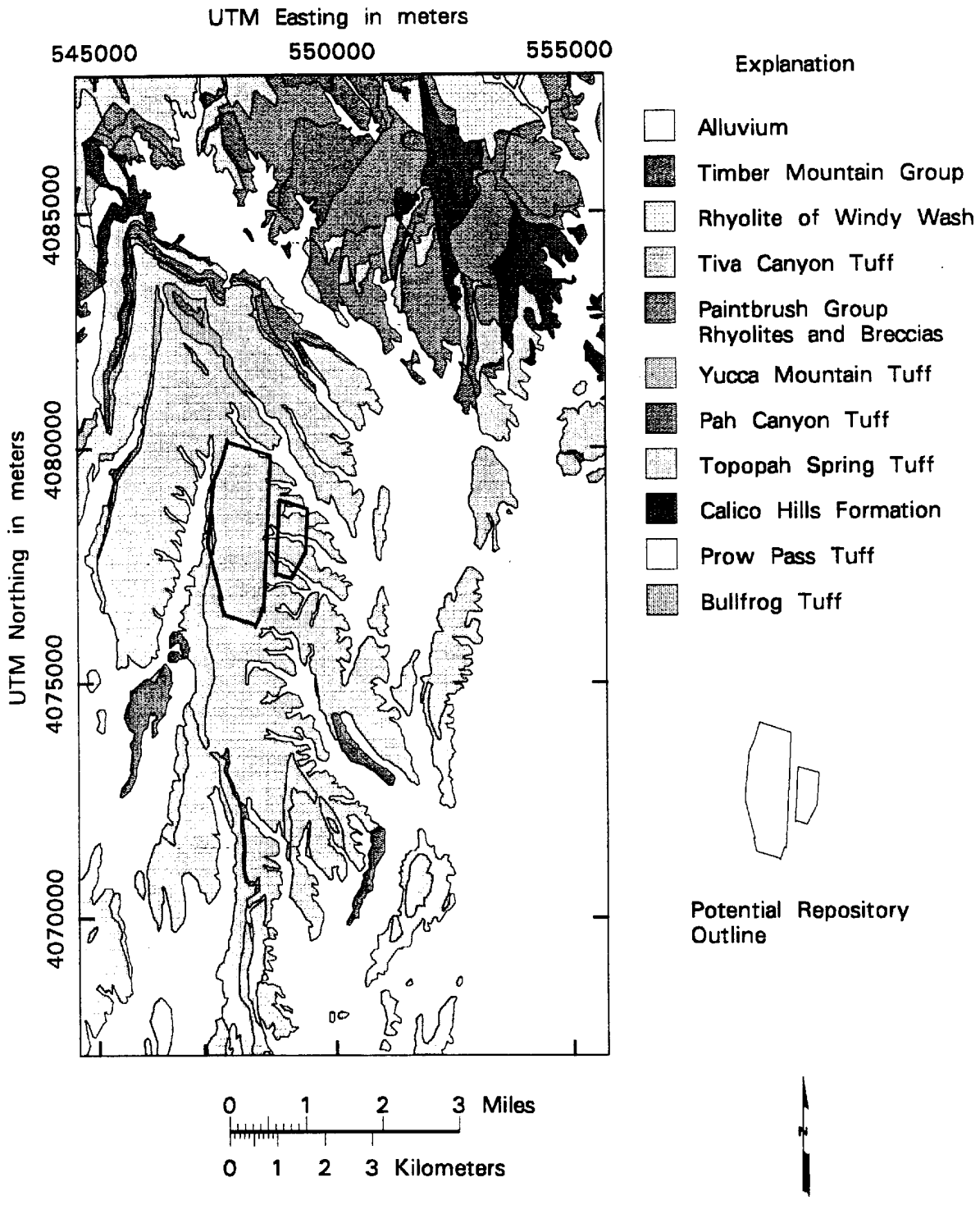

Figure 10. Map of area with general geologic designations.(after Sawyer and others, 1994).

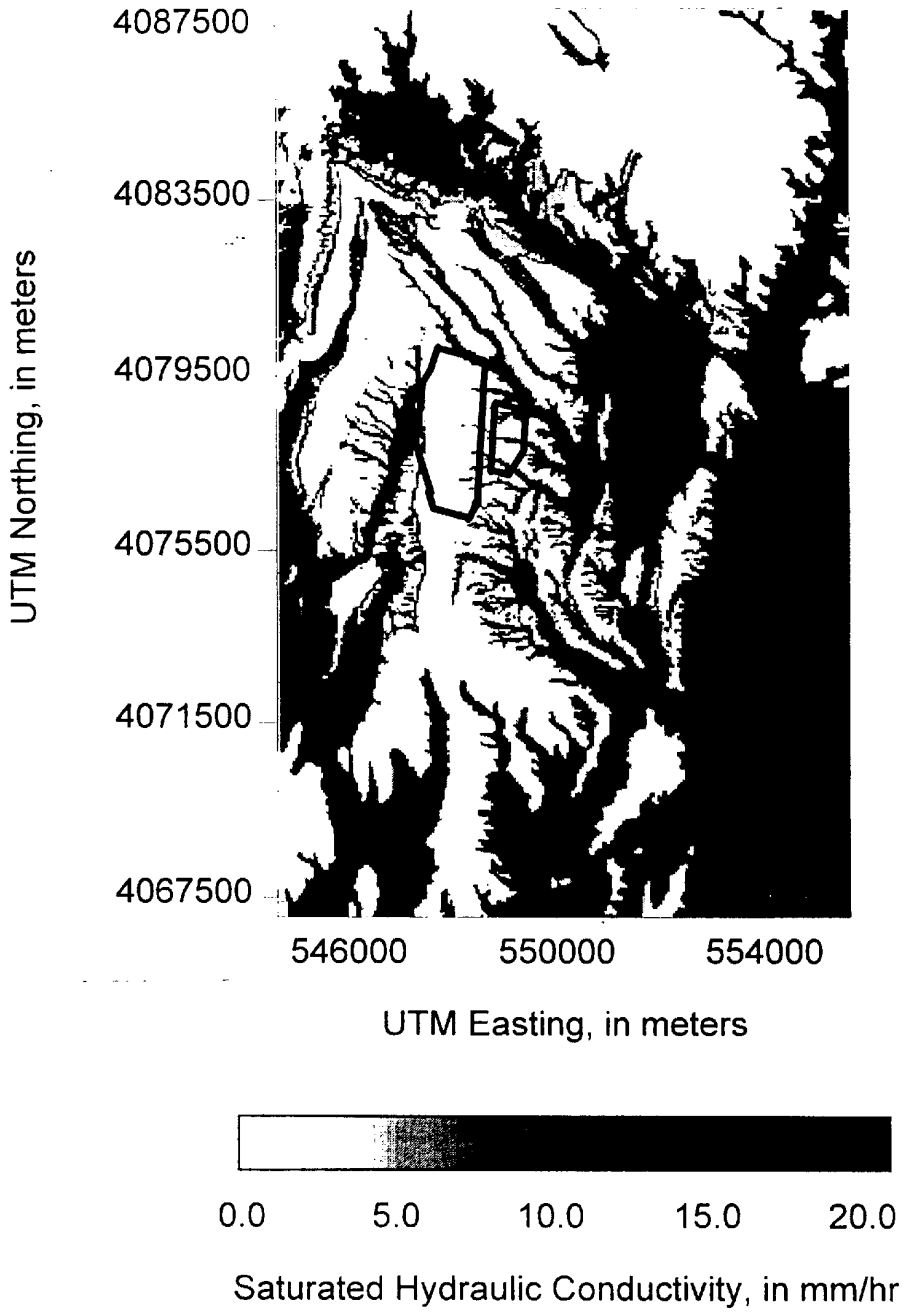

Figure 11. Saturated hydraulic conductivity of surficial bedrock units.

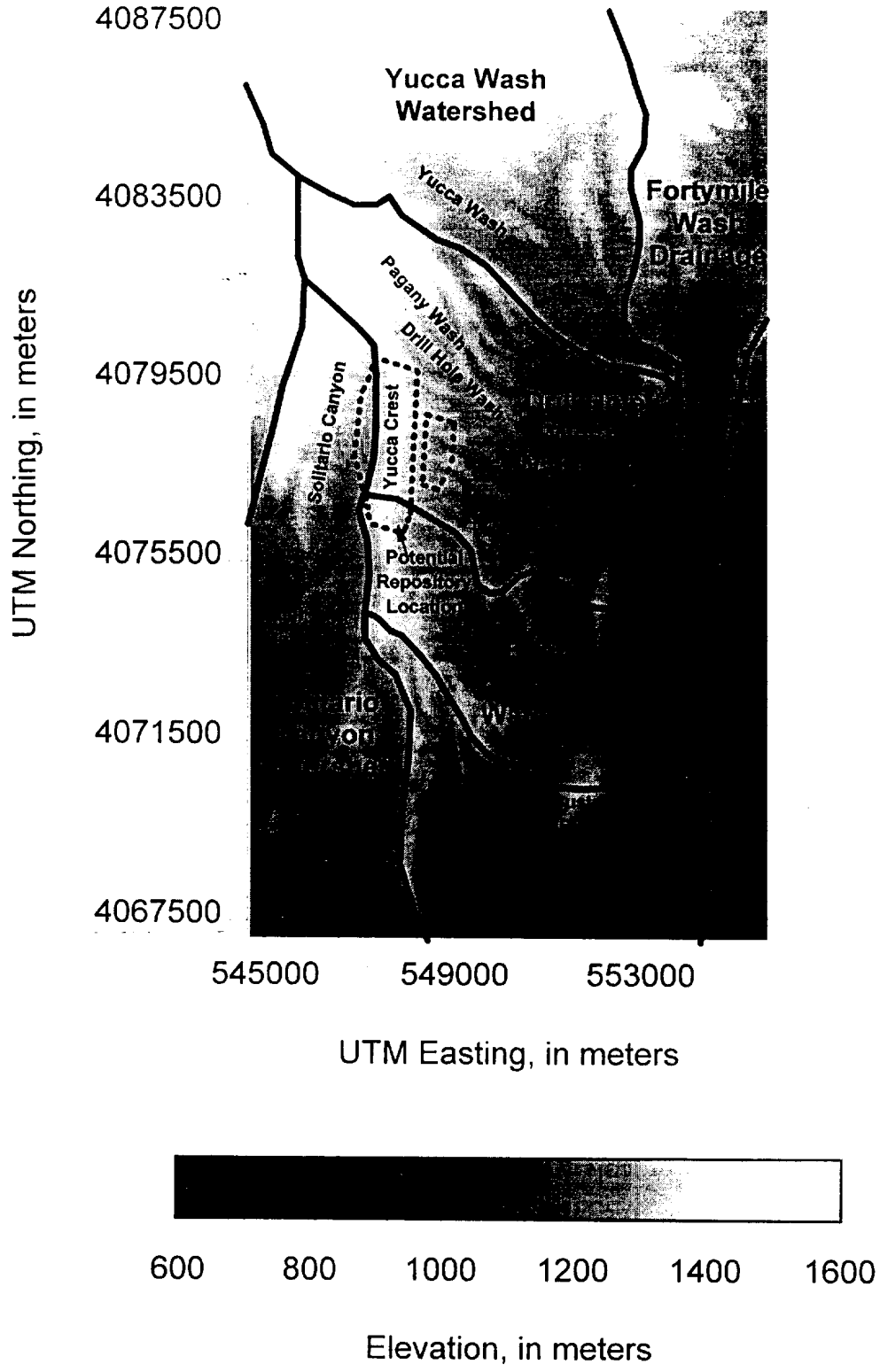

Figure 12. Map of major watersheds at Yucca Mountain.

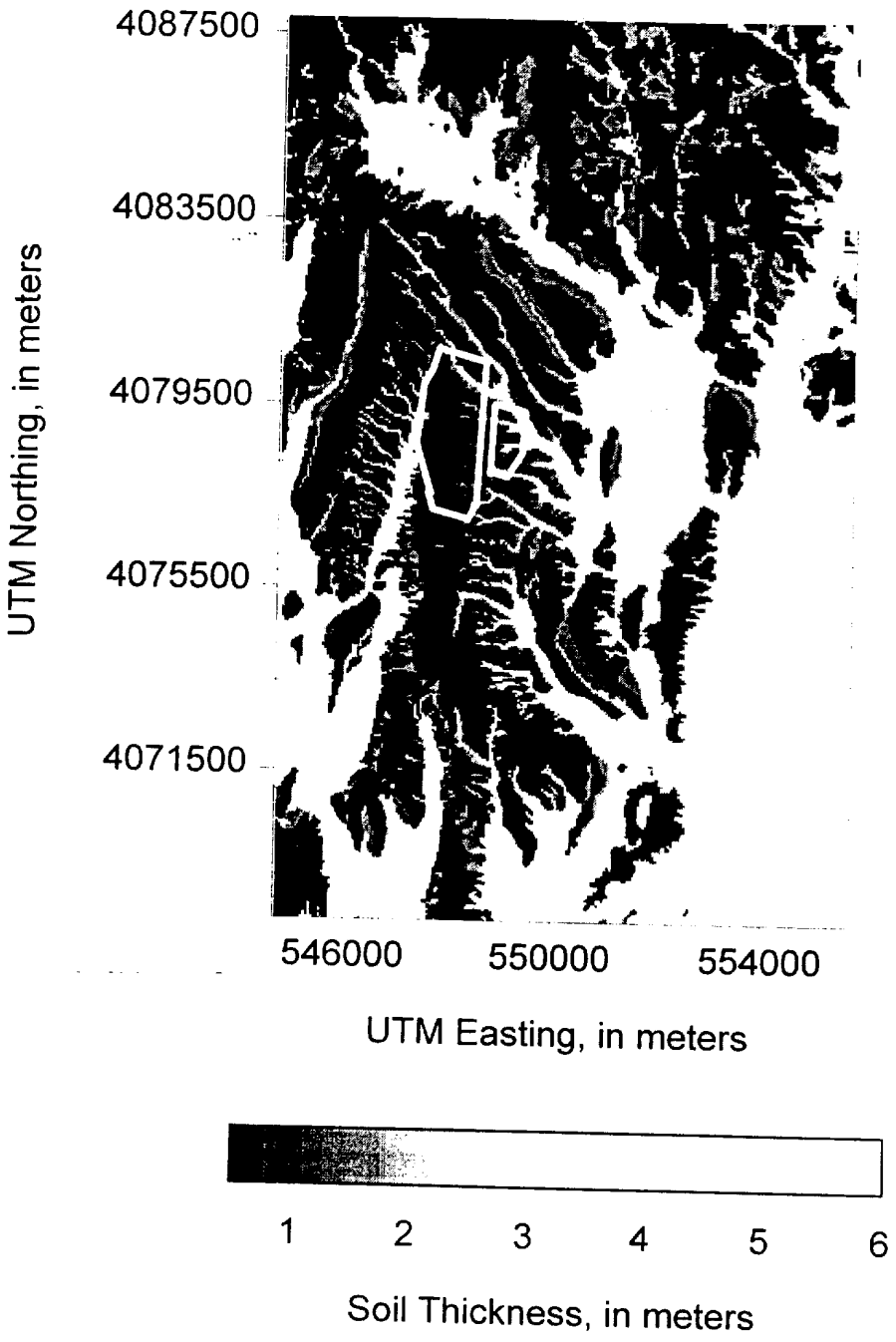

Figure 13. Map of soil thickness designated in 4 categories, 0 - <0.5 m, 0.5 - <3 m, 3 - <6 m and >/= 6 m.

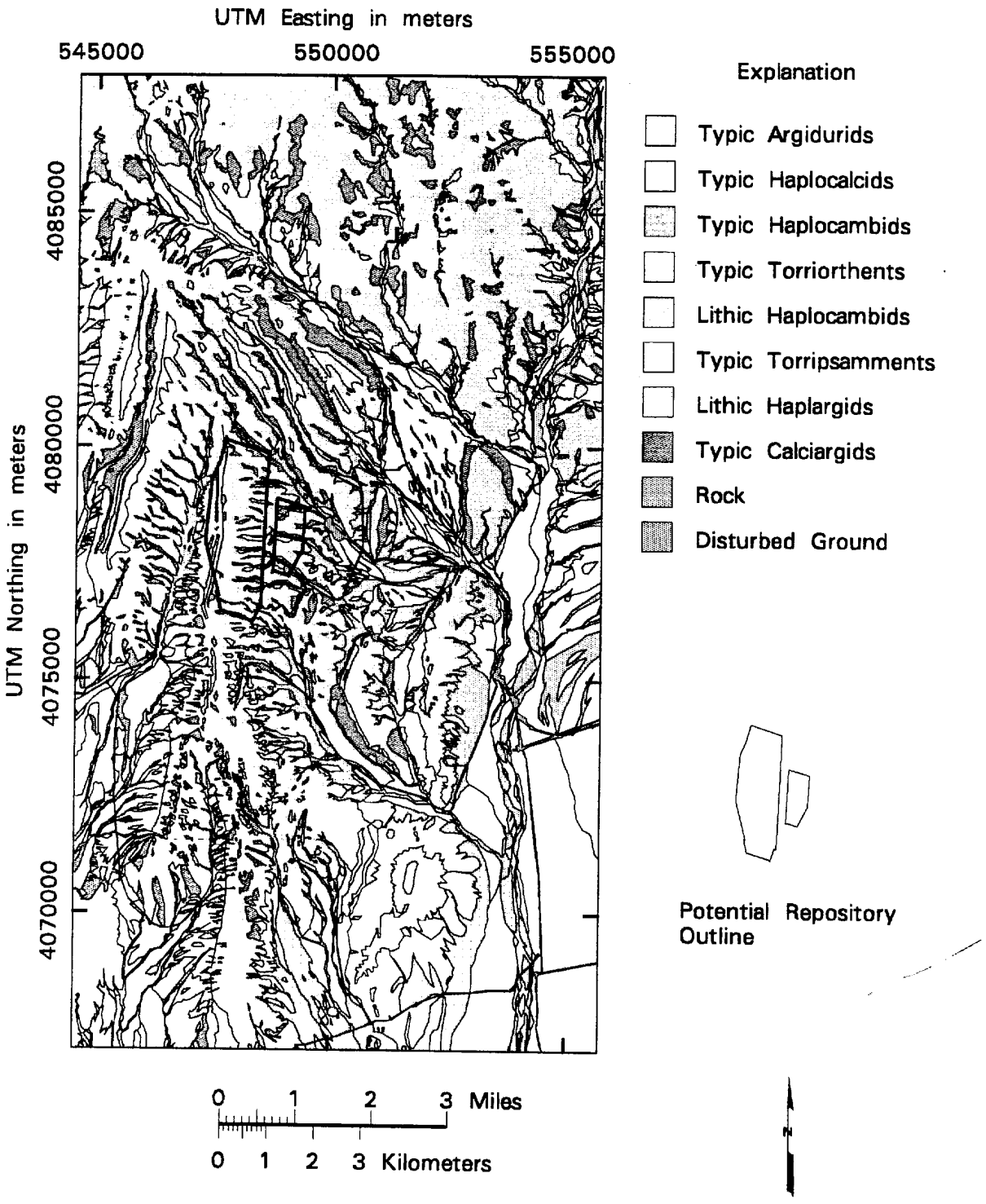

Figure 14. Map of surficial soils.

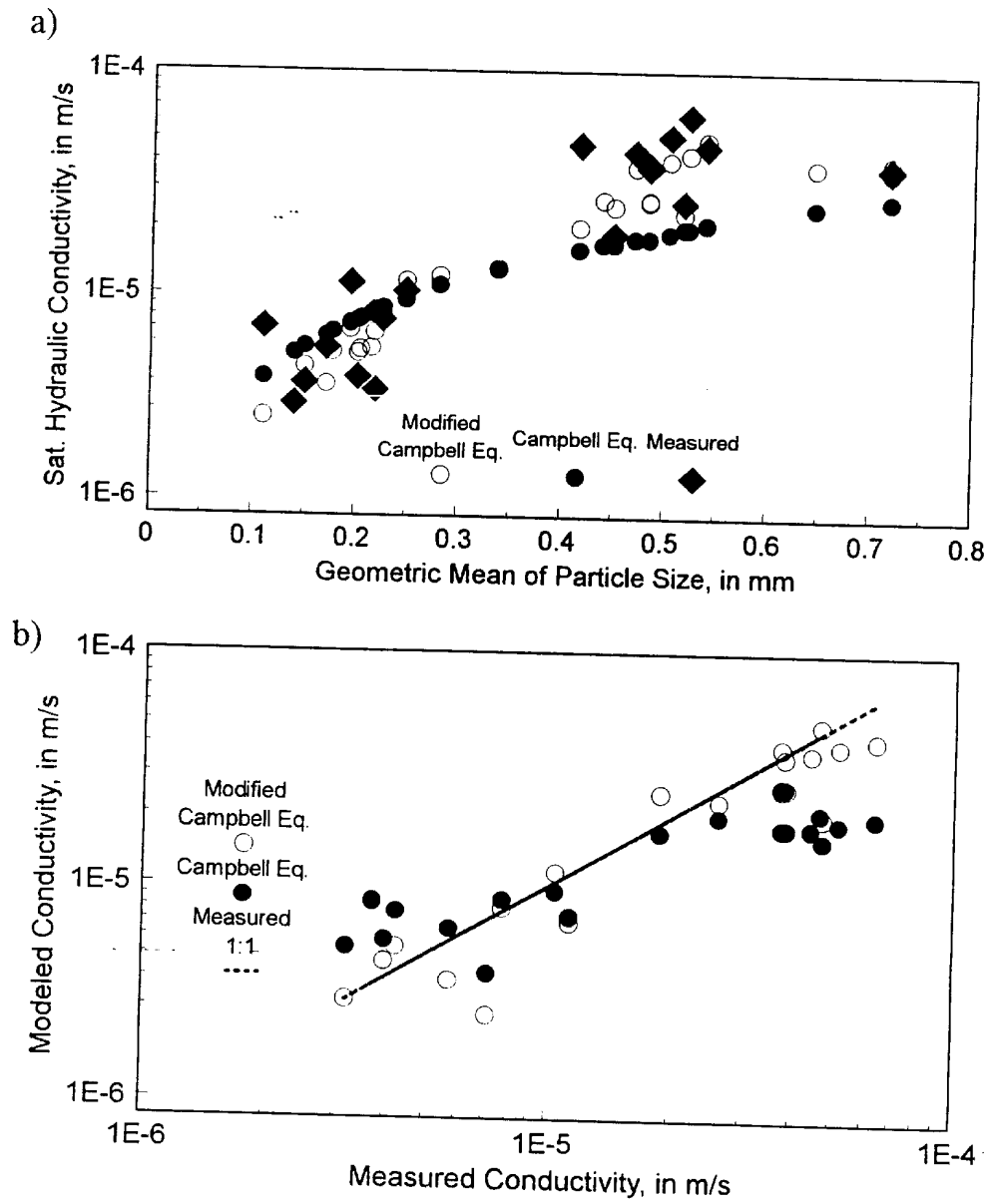

Figure 15. Relationship of a) soil texture to saturated hydraulic conductivity using Campbell (1985) for soil without rock fragments and modified to correct for percent rock fragments, and b) modeled versus measured conductivity.

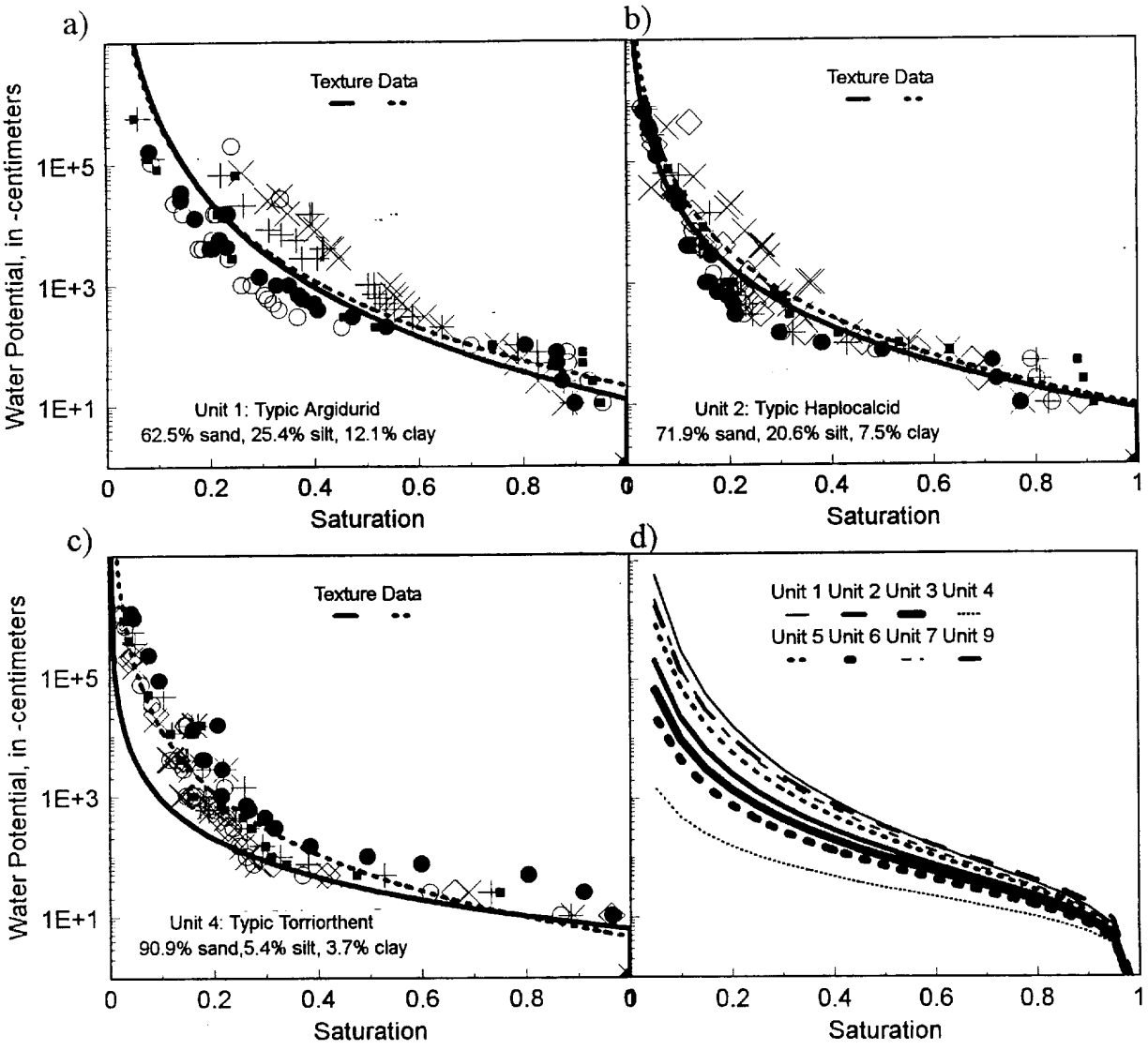

Figure 16. Moisture retention curves calculated from measured soil texture (Campbell, 1985) compared to measured data for soil model units a) 1, b) 2, and c) 4, and texture models for d) all soil model units.

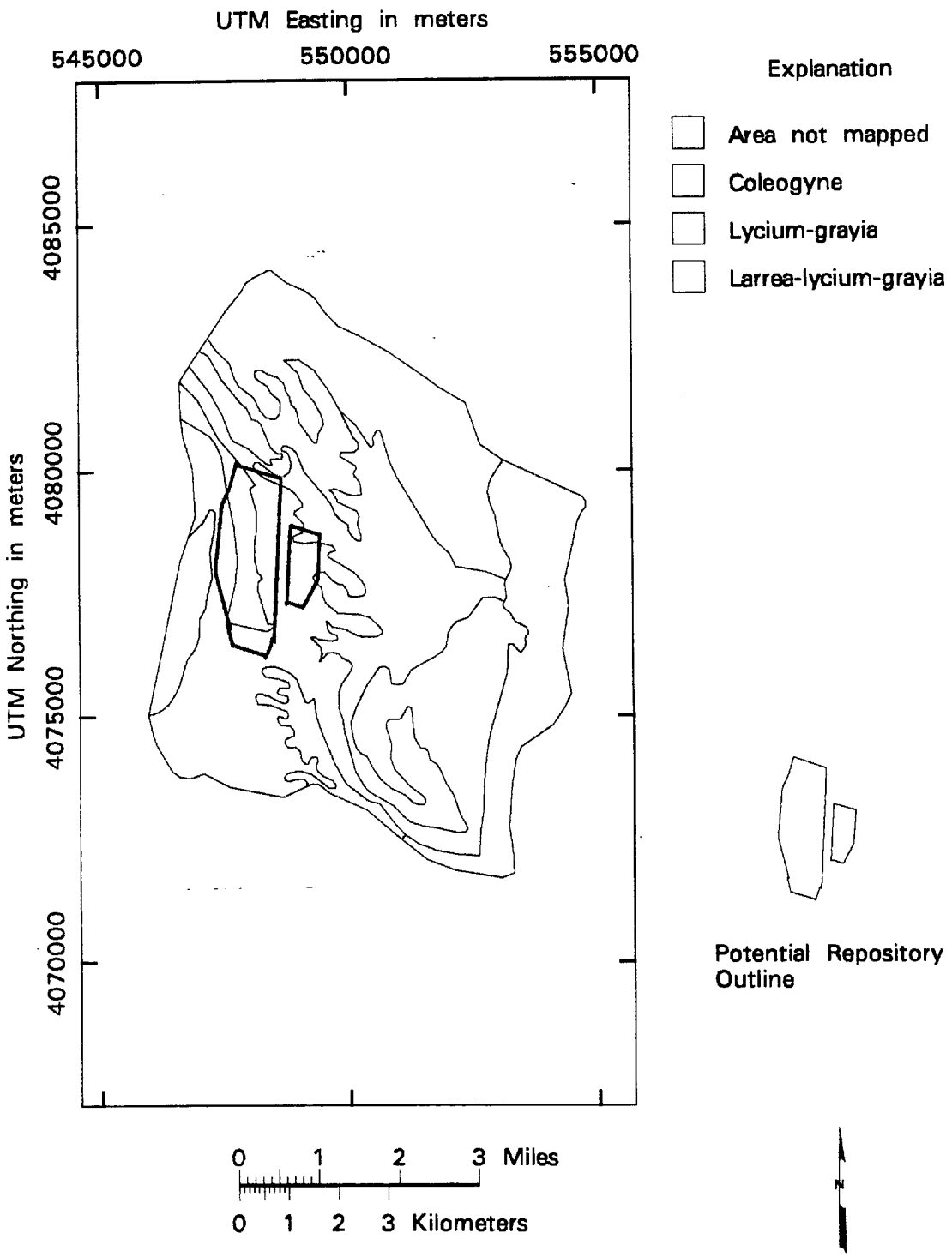

Figure 17. Map of vegetation associations.

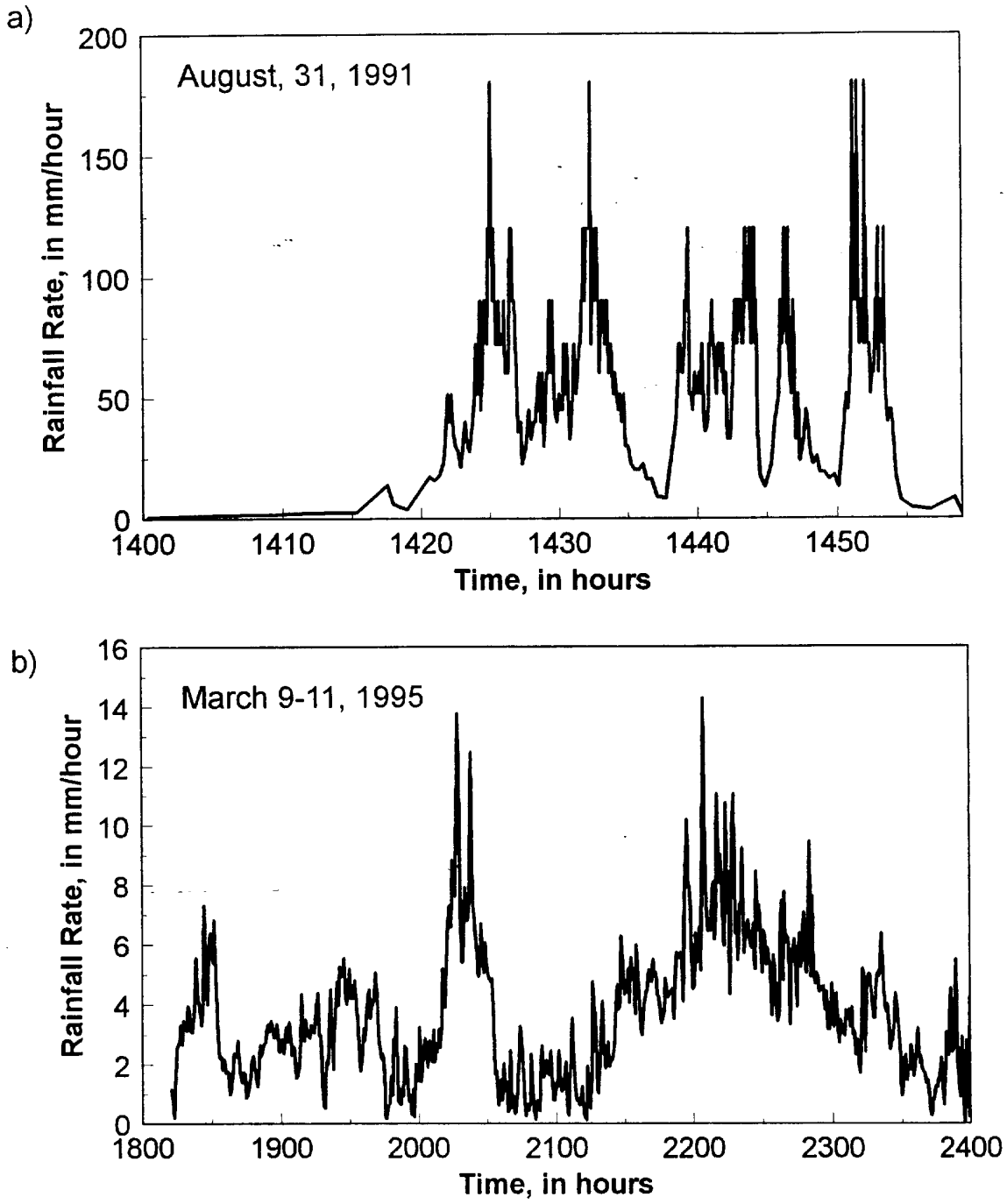

Figure 18. Rate of rainfall for a) a summer thunderstorm and b) winter precipitation.

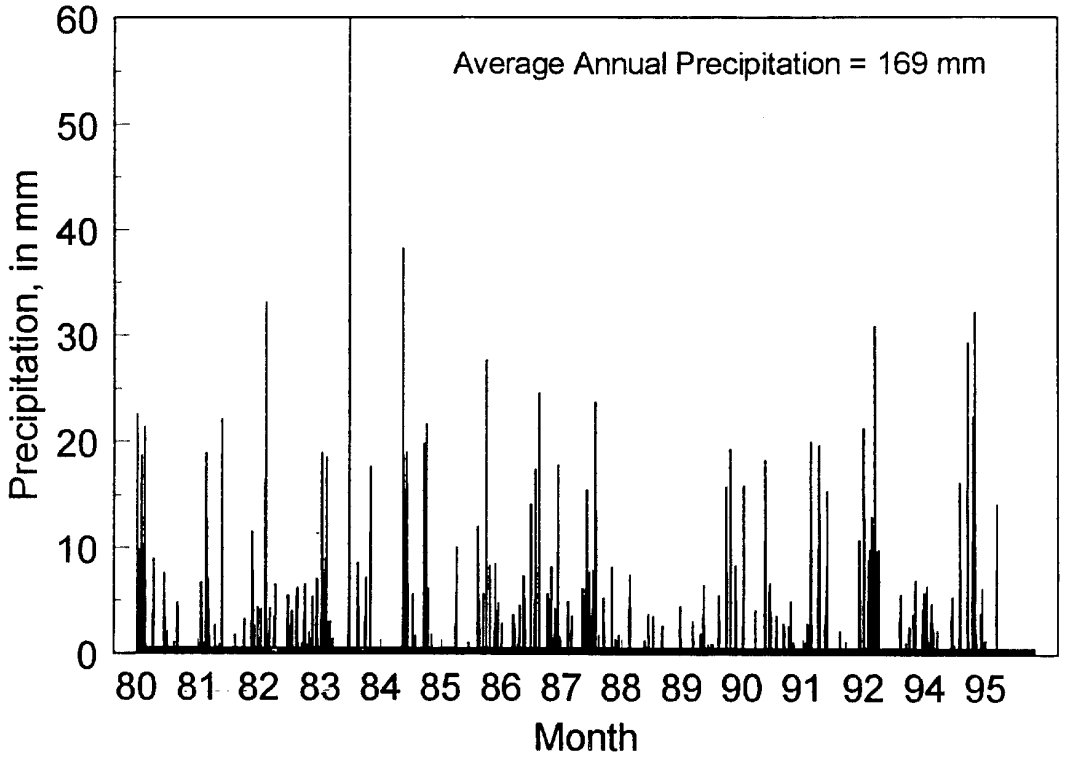

Figure 19. Estimated daily precipitation for Yucca Mountain using 15 years of measured data simulated at 90 neutron boreholes.

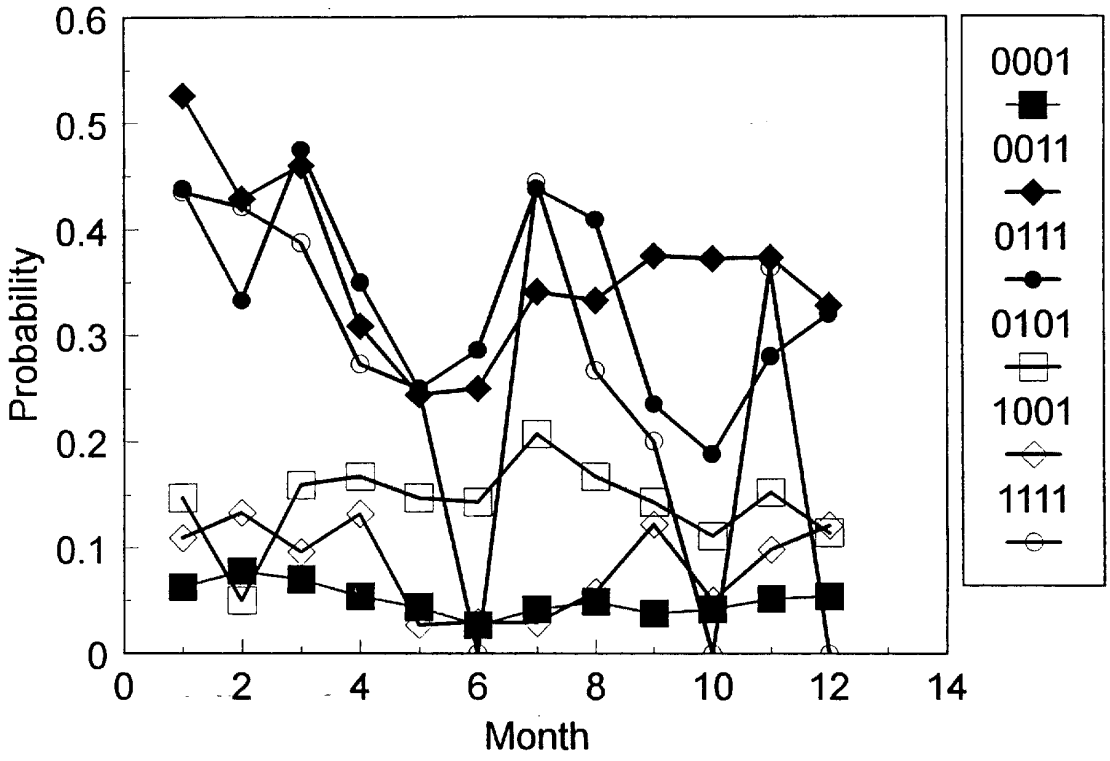

Figure 20. Probability of occurrence of daily precipitation at Yucca Mountain using 3rd order Markov chain. A 4-day window was used and 1 equals precipitation.

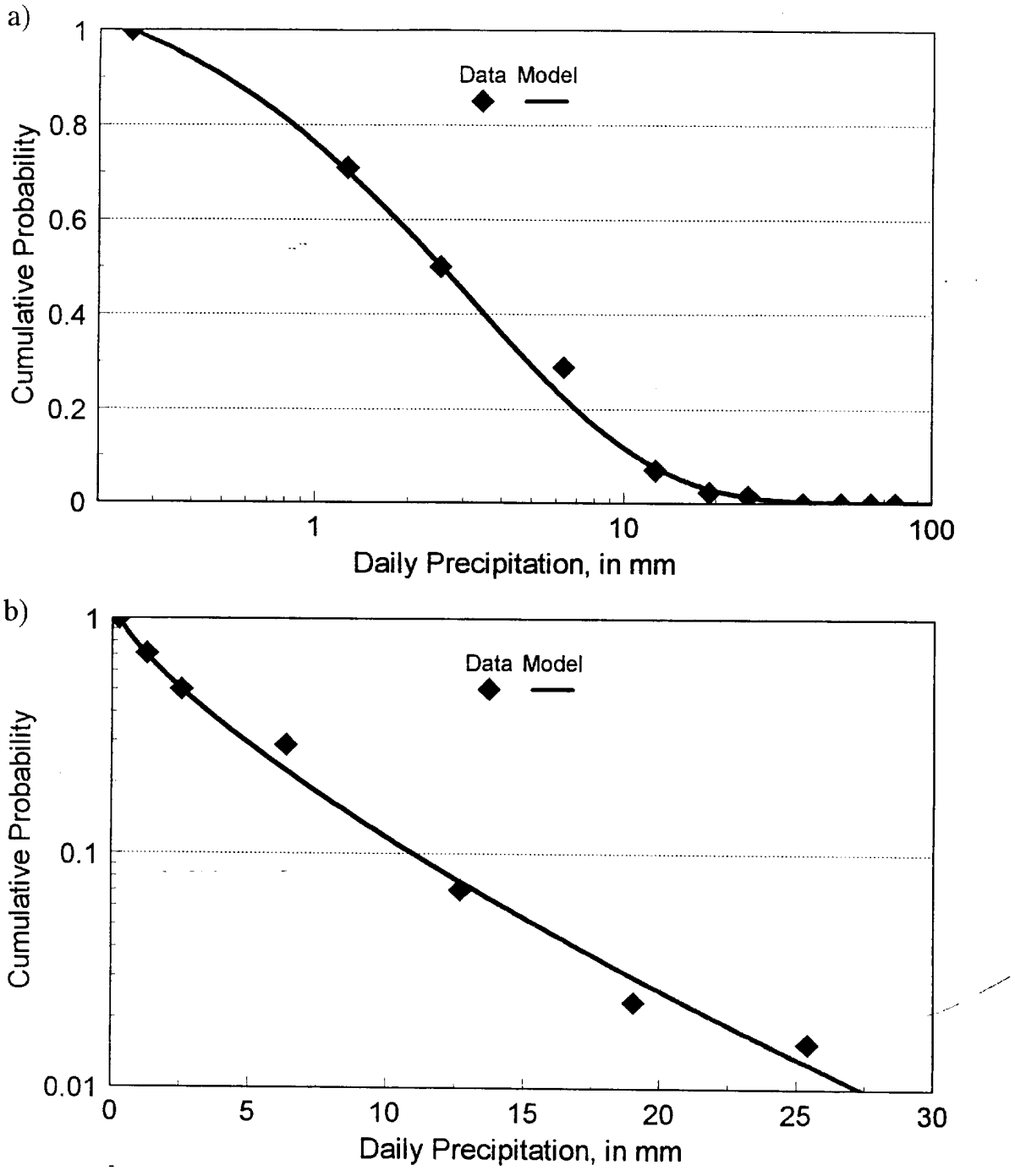

Figure 21. Data and fitted model for the cumulative probability distribution of precipitation quantity at station 4JA a) for the month of February and b) for the month of July.

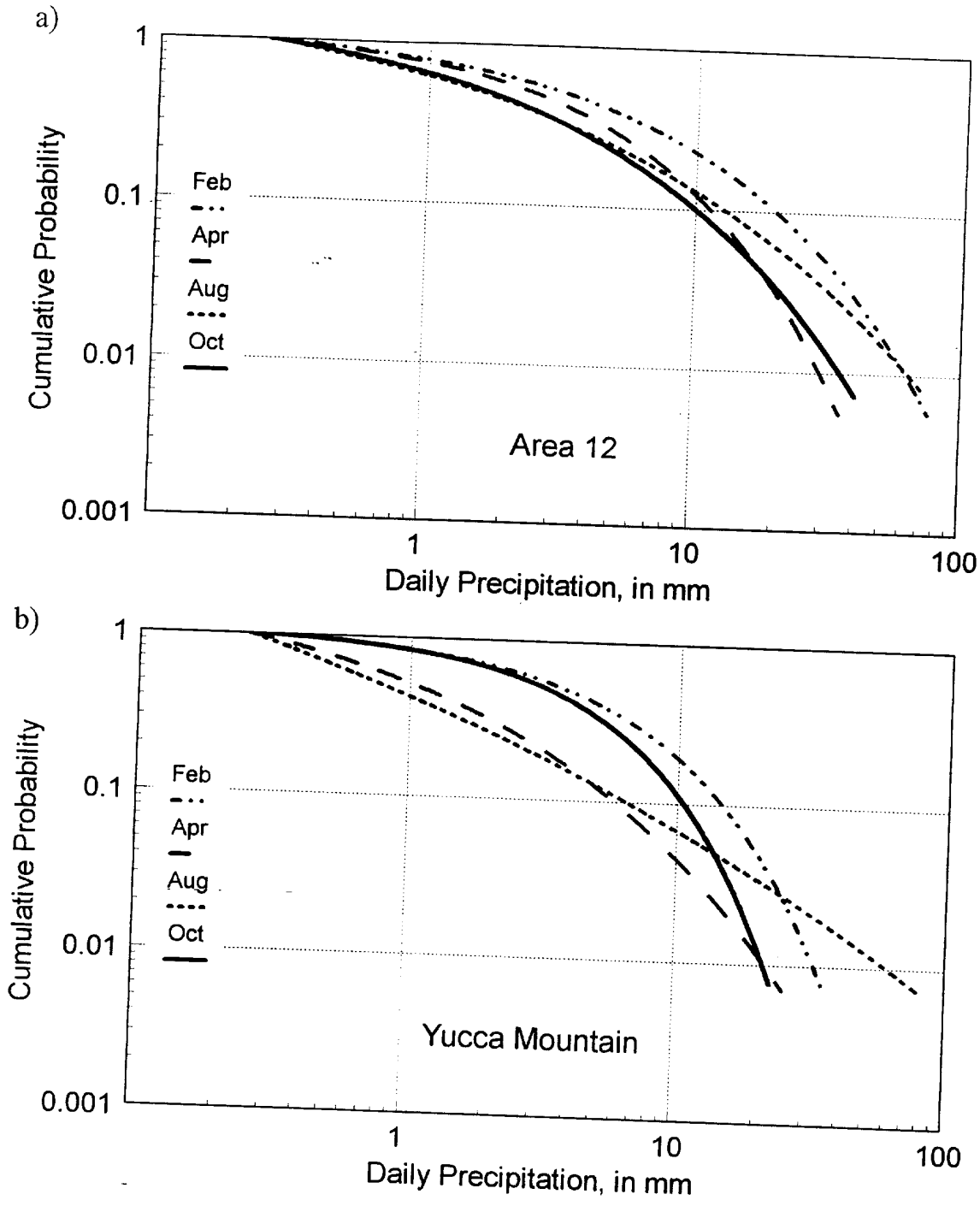

Figure 22. Modeled probability distribution of precipitation quantity for a) precipitation data from Area 12 and b) precipitation data from Yucca Mountain.

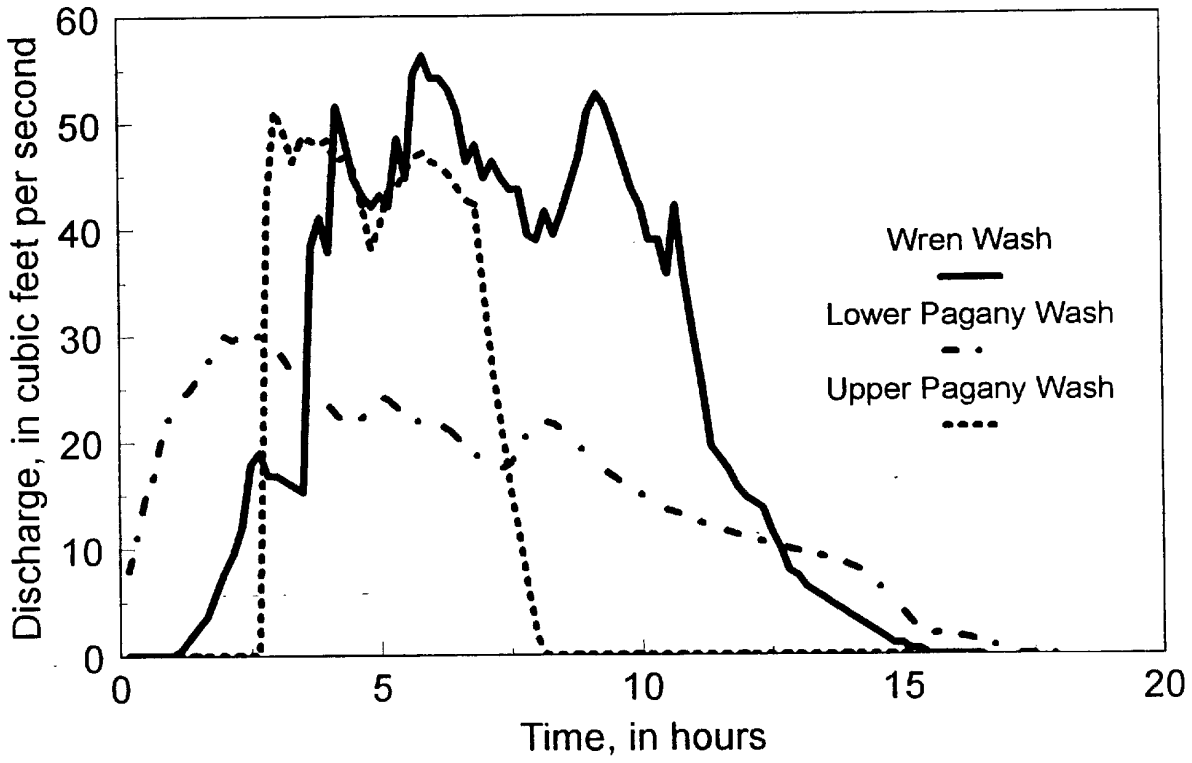

Figure 23. Hydrographs for Pagany Wash and Wren Wash, March 11, 1995.

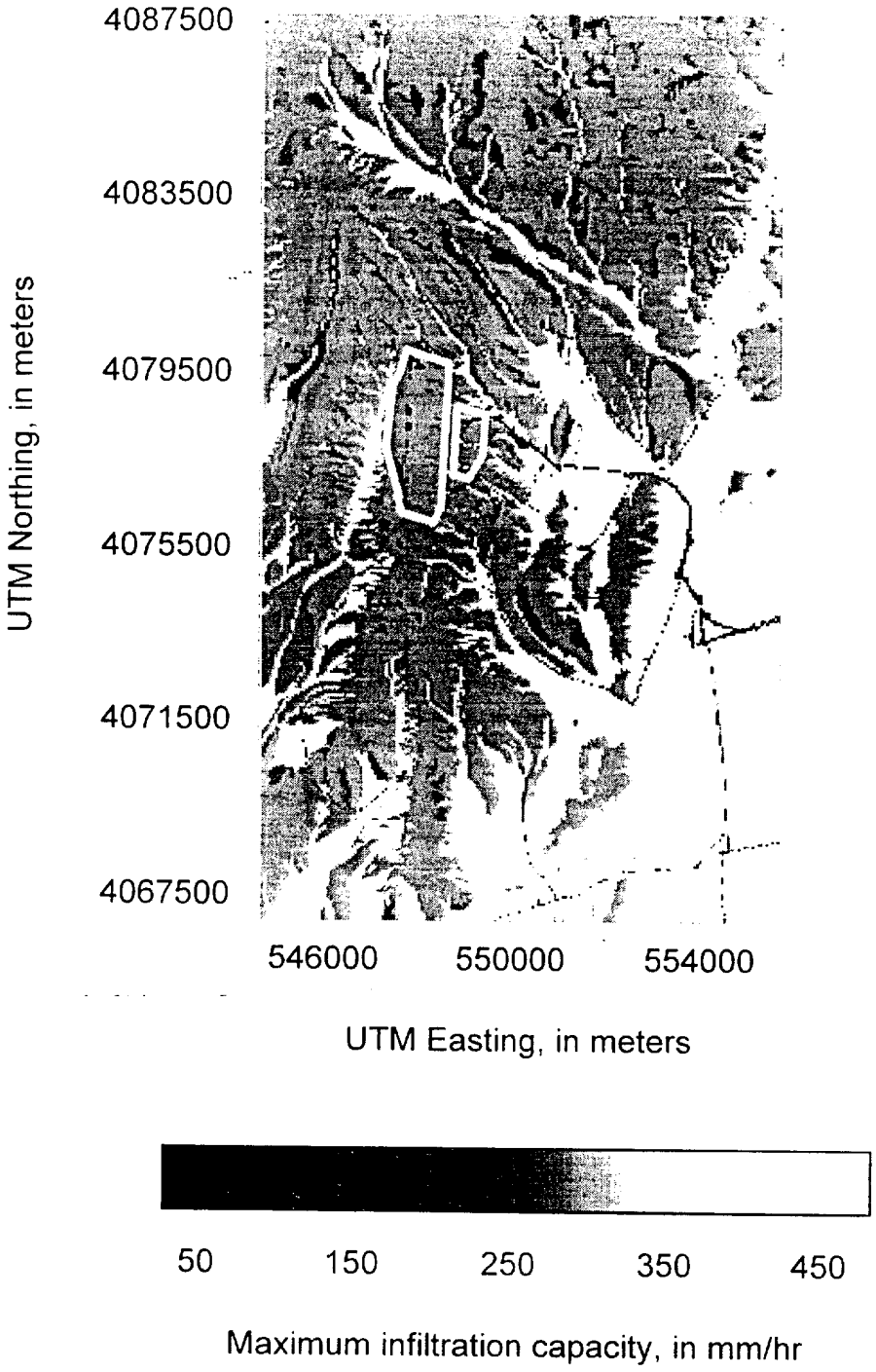

Figure 24. Map of maximum infiltration capacity into initially air dry soil.

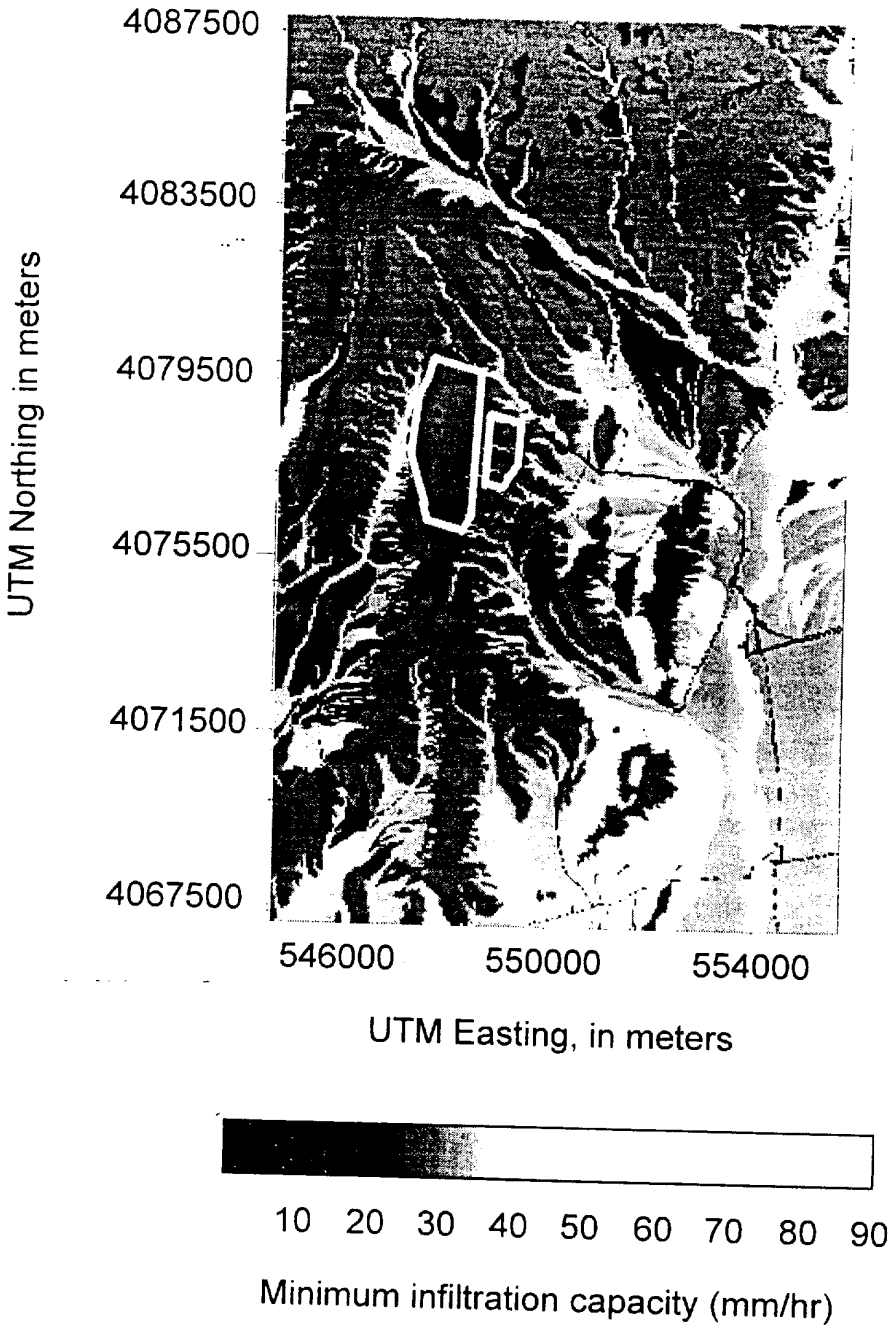

Figure 25. Map of minimum infiltration capacity.

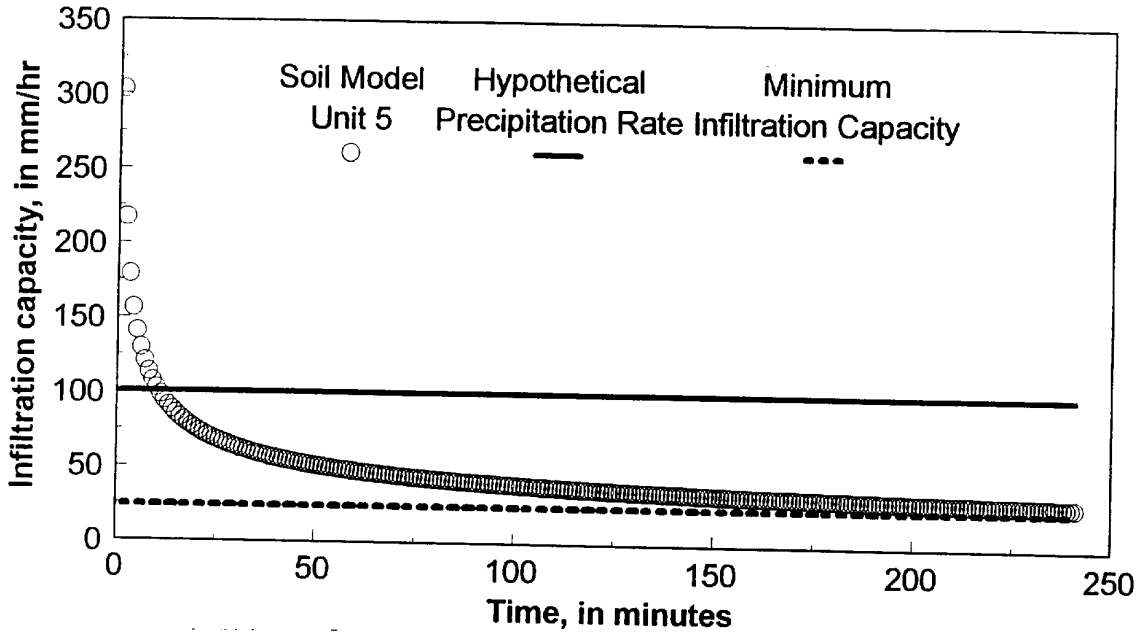

Figure 26. Illustration of the change in infiltration capacity for soil model unit 5 with time, related to precipitation rate and minimum infiltration capacity.

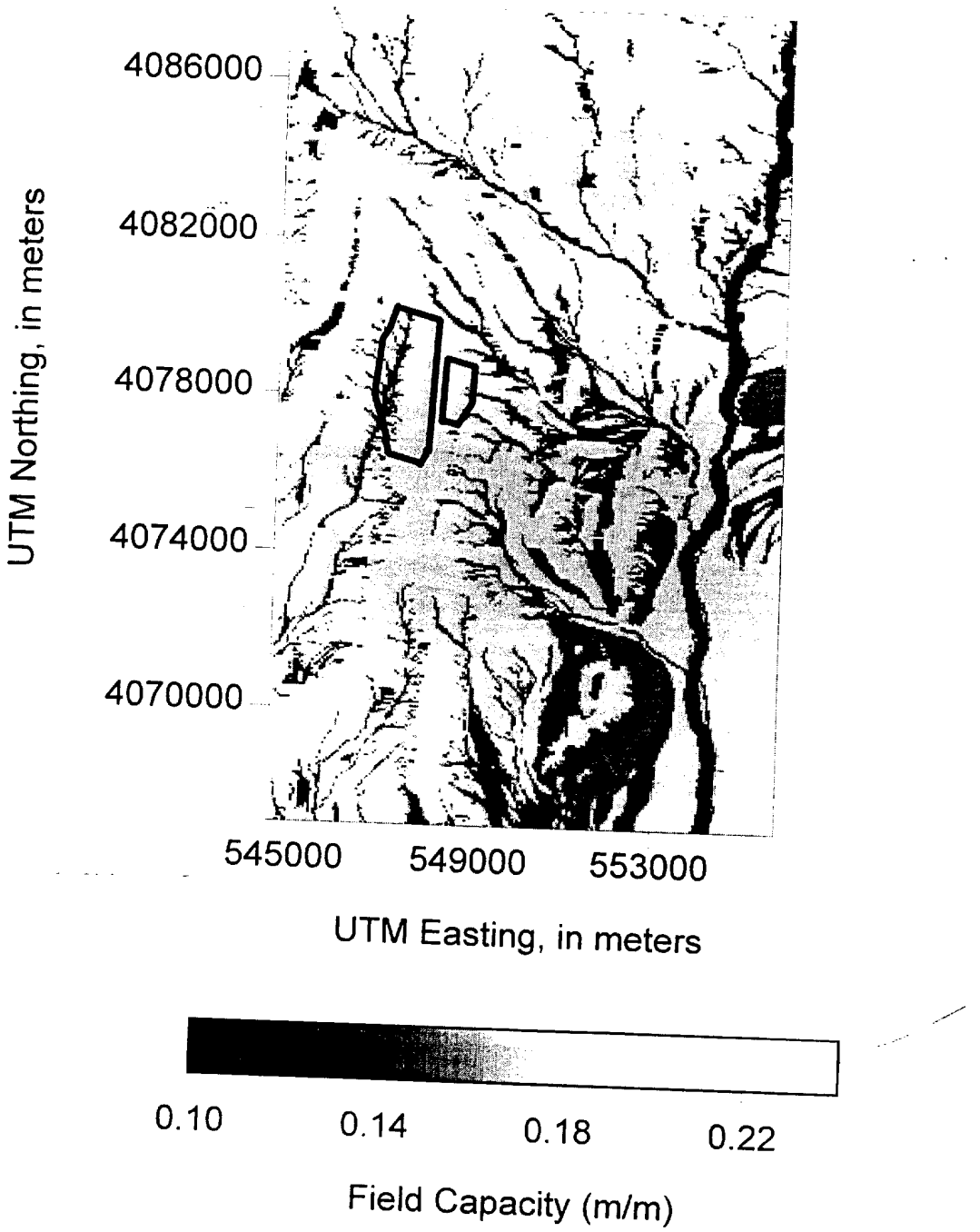

Figure 27. Map of the field capacity of the surficial soils.

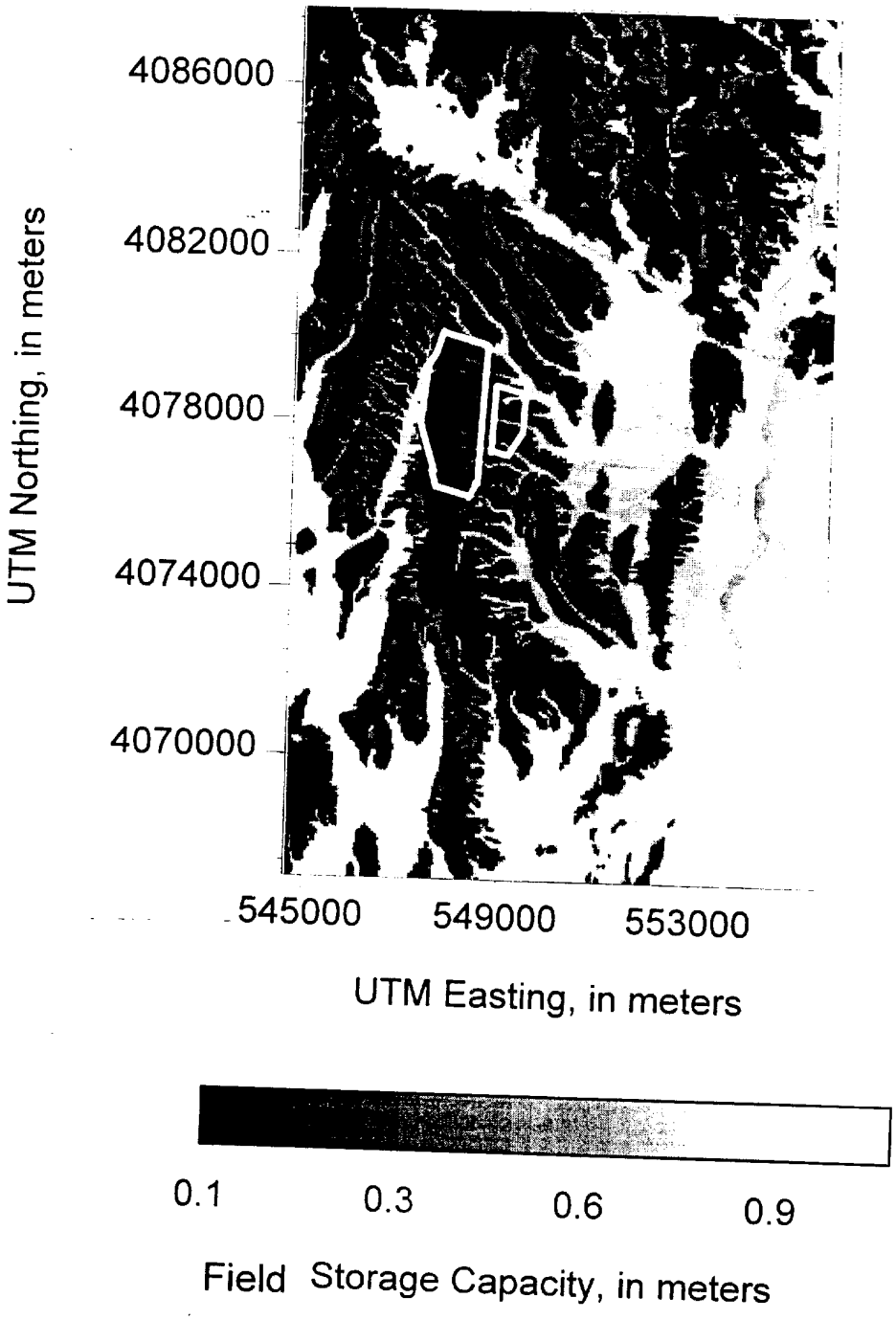

Figure 28. -Field storage capacity of soils calculated as field capacity multiplied by soil depth.

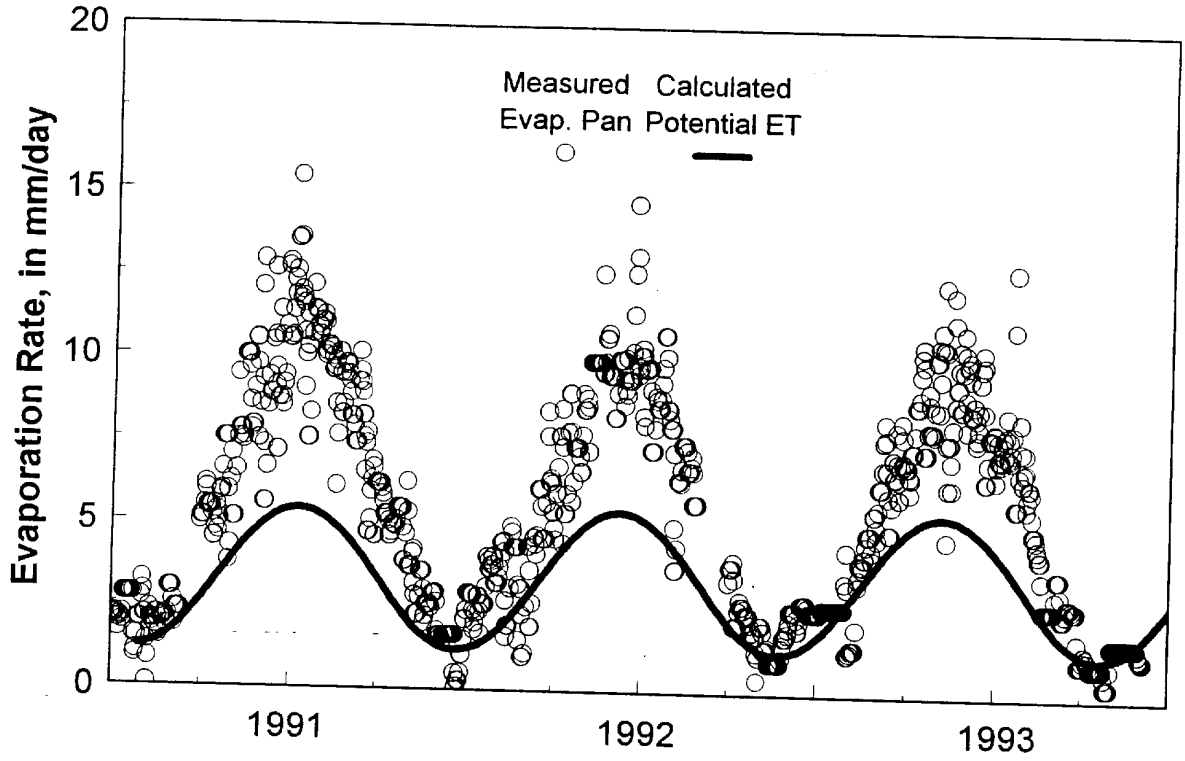

Figure 29. Measured evaporation pan data and calculated potential evapotranspiration using energy balance for 1991-1993.

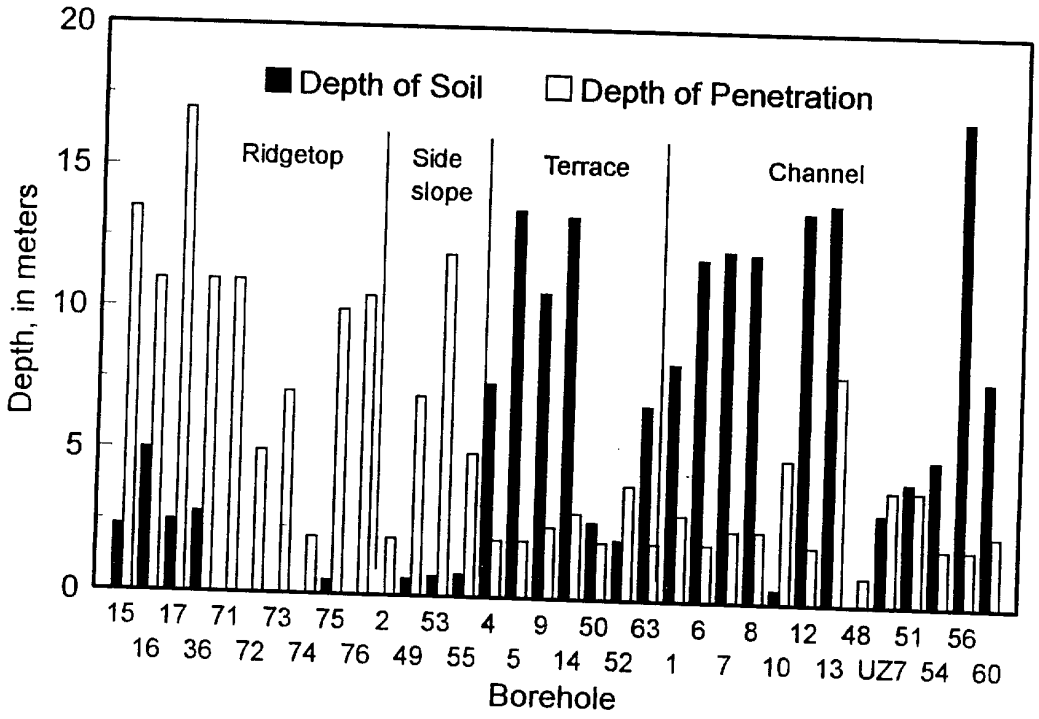

Figure 30. Average depth of penetration of the wetting front for years 1990-1993 and soil depth for 34 boreholes (Flint and Flint, 1995).

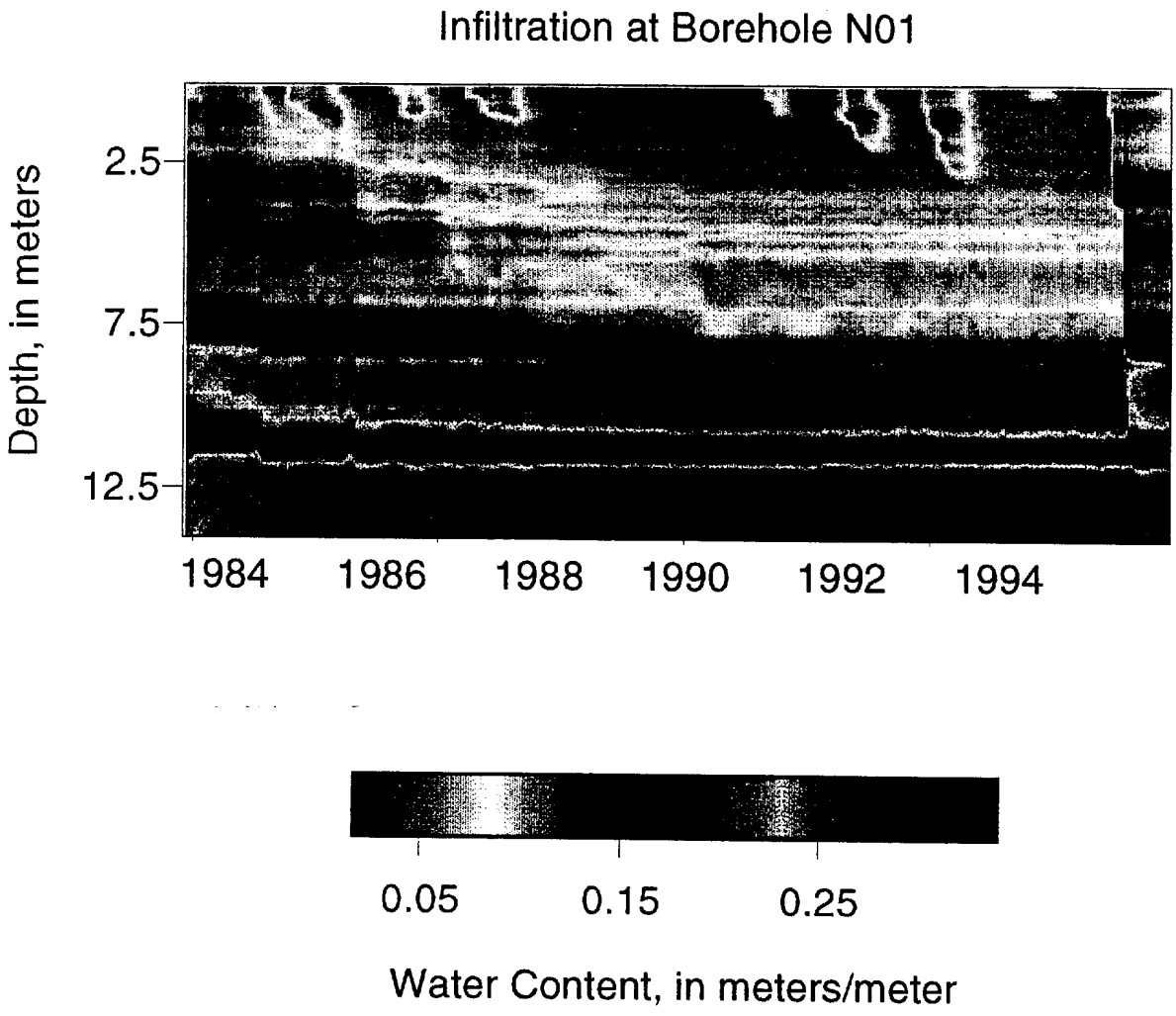

Figure 31. Changes in water content over time and depth for borehole USW UZ-N1.

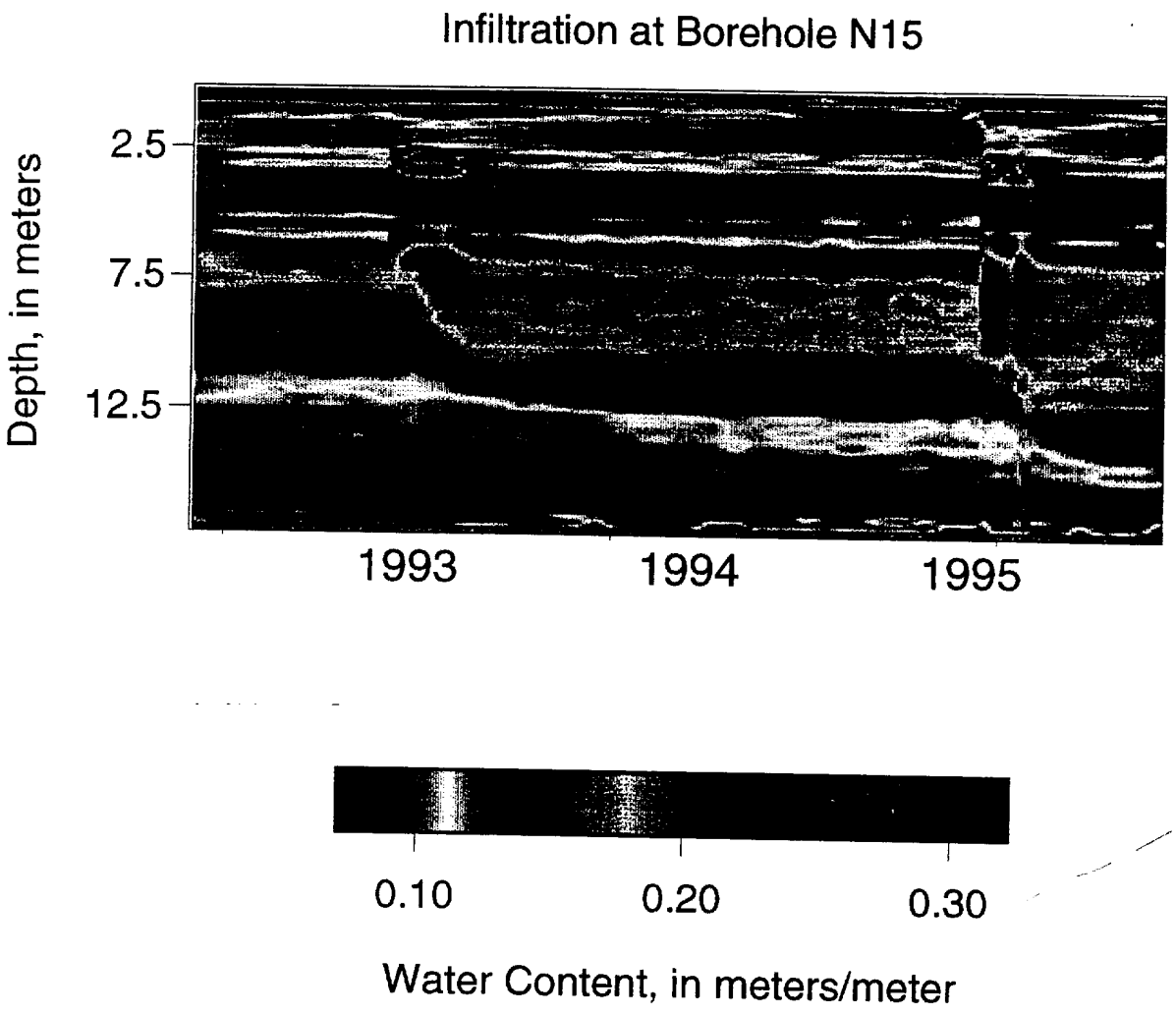

Figure 32. Changes in water content over time and depth for borehole USW UZ-N15.

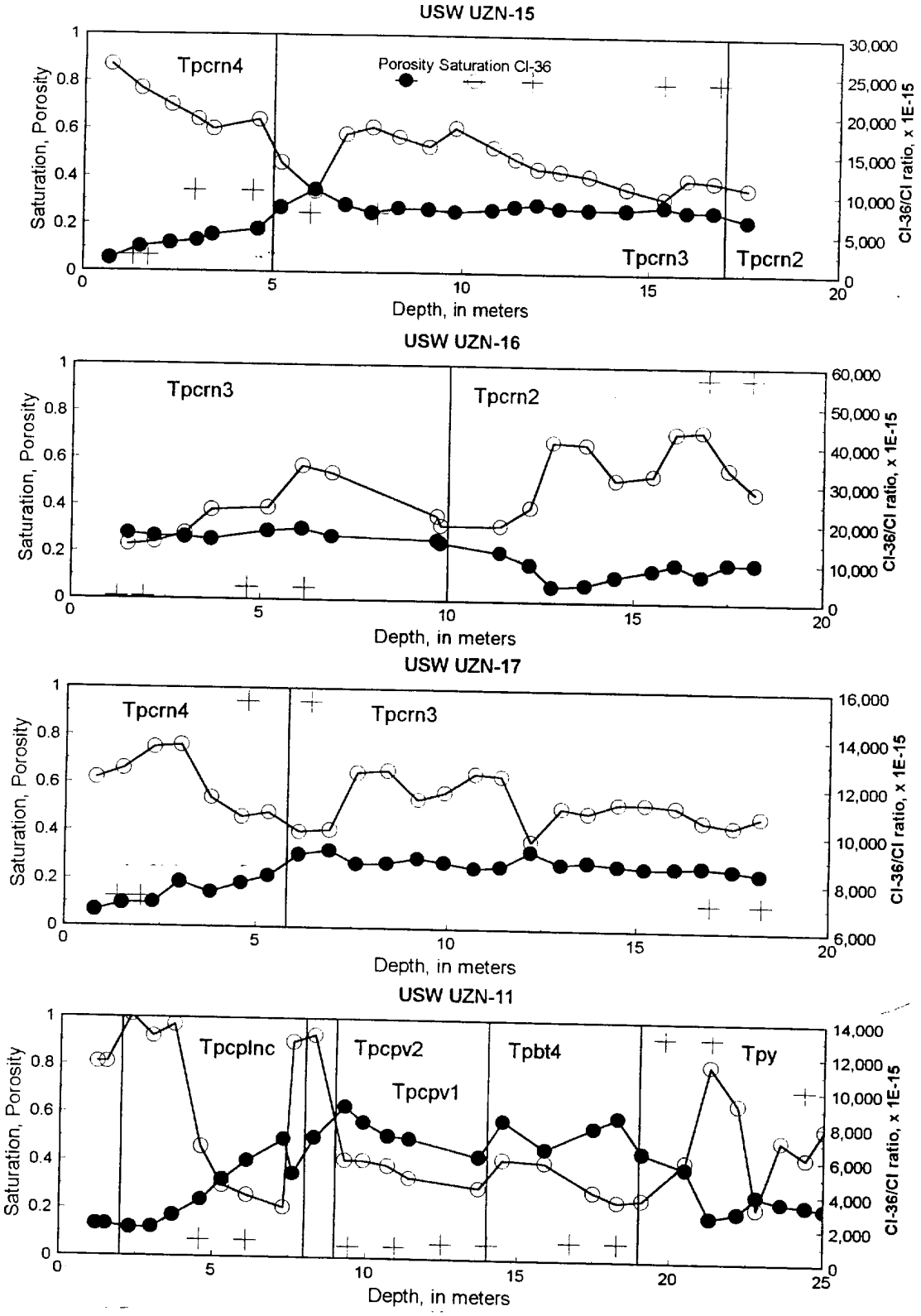

Figure 33. Saturation, porosity and Cl-36/Cl ratio for boreholes USW UZ-N15, USW UZ-N16, USW UZ-N17, and USW UZ-N11. Cl-36 data is indicated for depth ranges as between pairs of points.

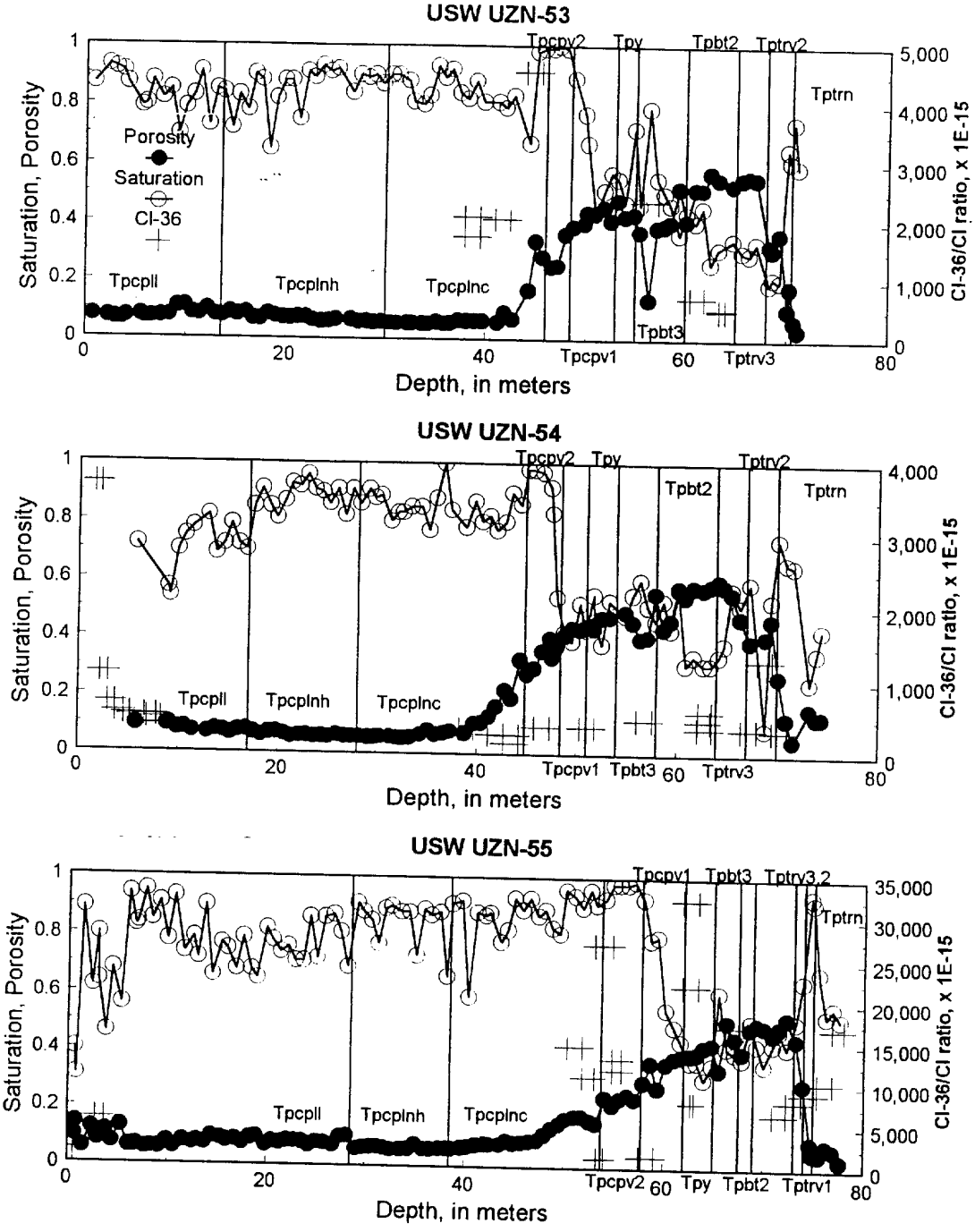

Figure 34. Saturation, porosity and Cl-36/Cl ratio for boreholes USW UZ-N53, USW UZ-N54, and USW UZ-N55. Cl-36 data is indicated over a depth range.

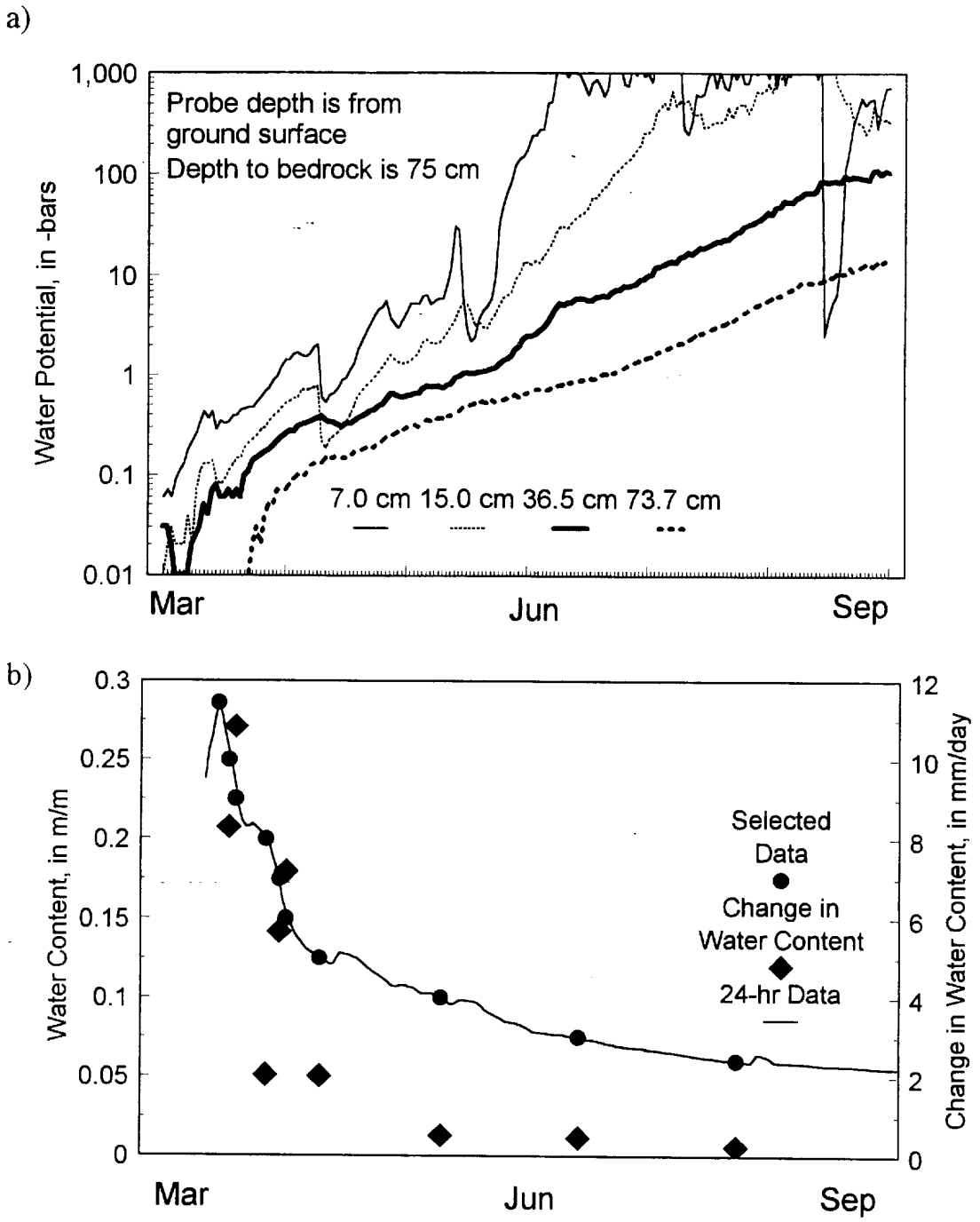

Figure 35. Water potential measurements near borehole USW UZ-N15 using heat dissipation probes, a) measured at 4 depths for 1995 and b) used to calculate flux.

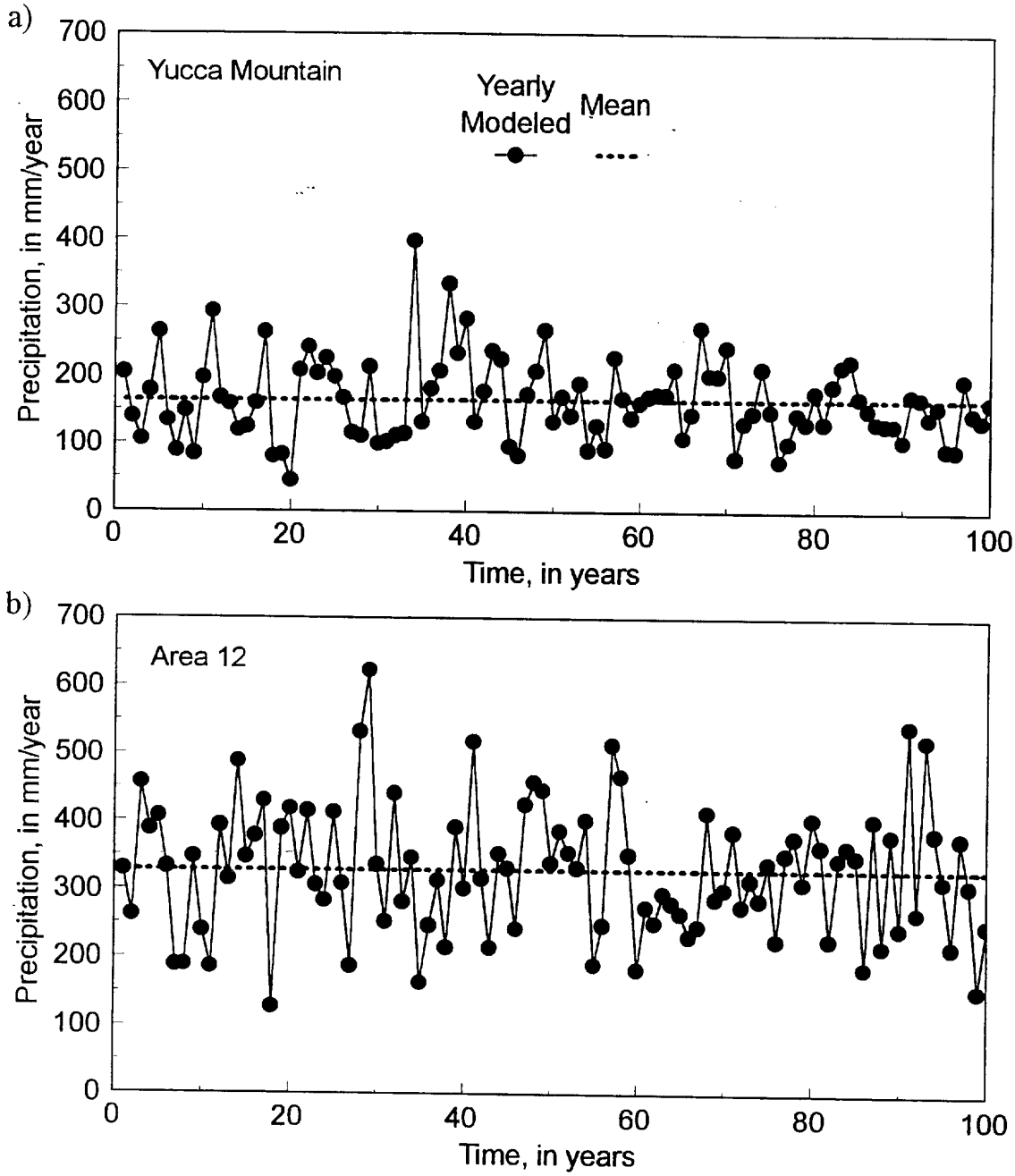

Figure 36. One hundred-year stochastic simulations of precipitation at a) Yucca Mountain and b) Area 12.

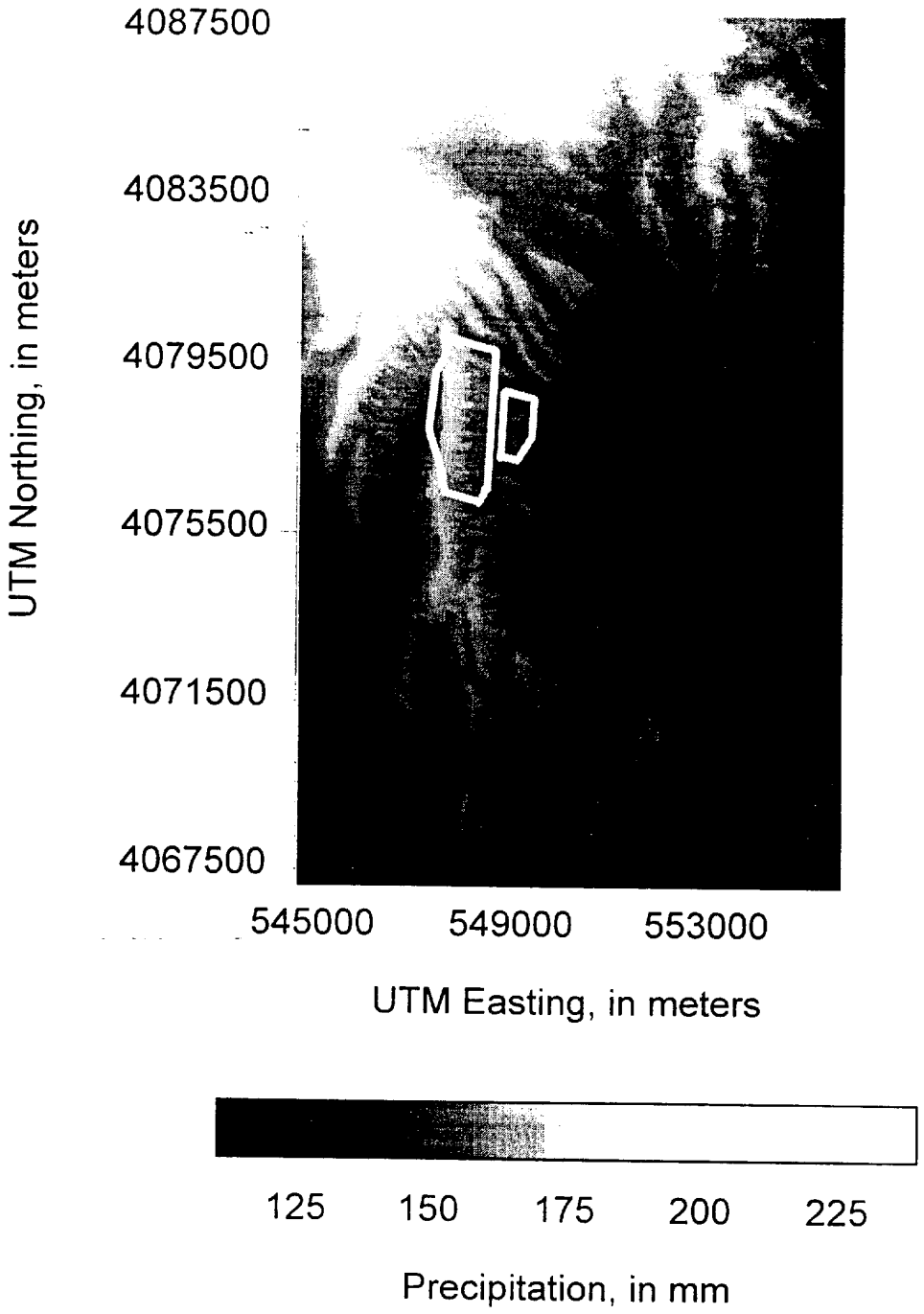

Figure 37. Average annual precipitation distributed spatially using an elevation correlation.

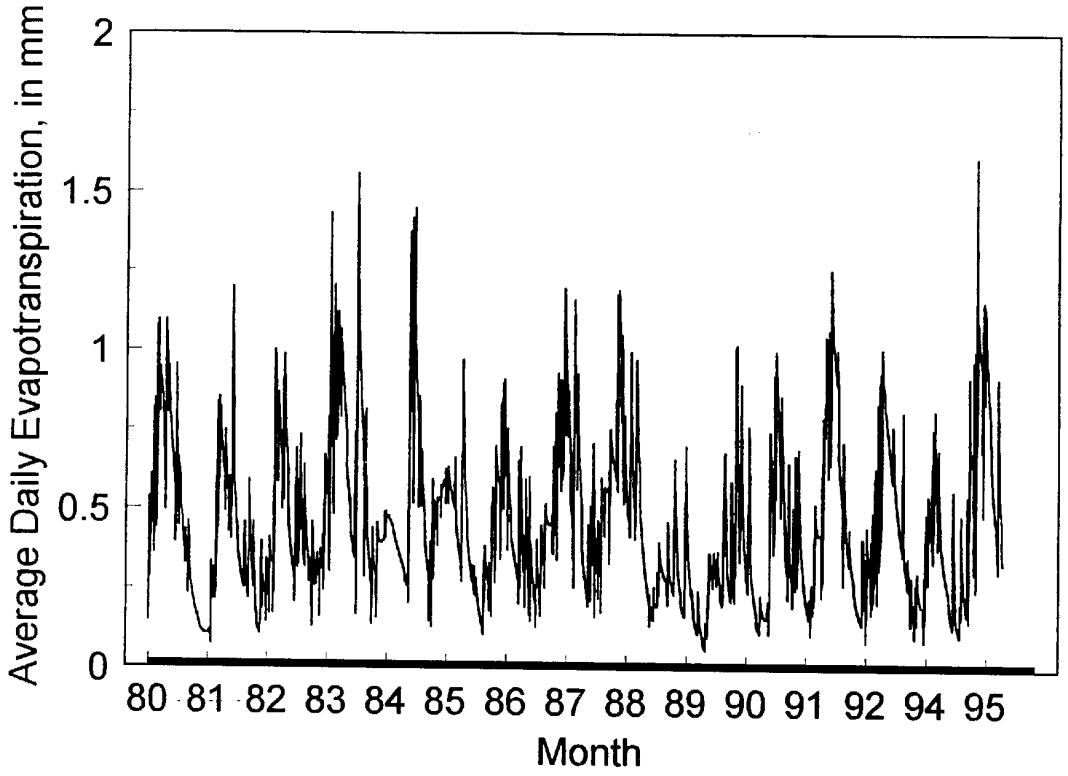

Figure 38. Simulated daily evapotranspiration for Yucca Mountain using 15 years of measured precipitation simulated at 90 neutron boreholes.

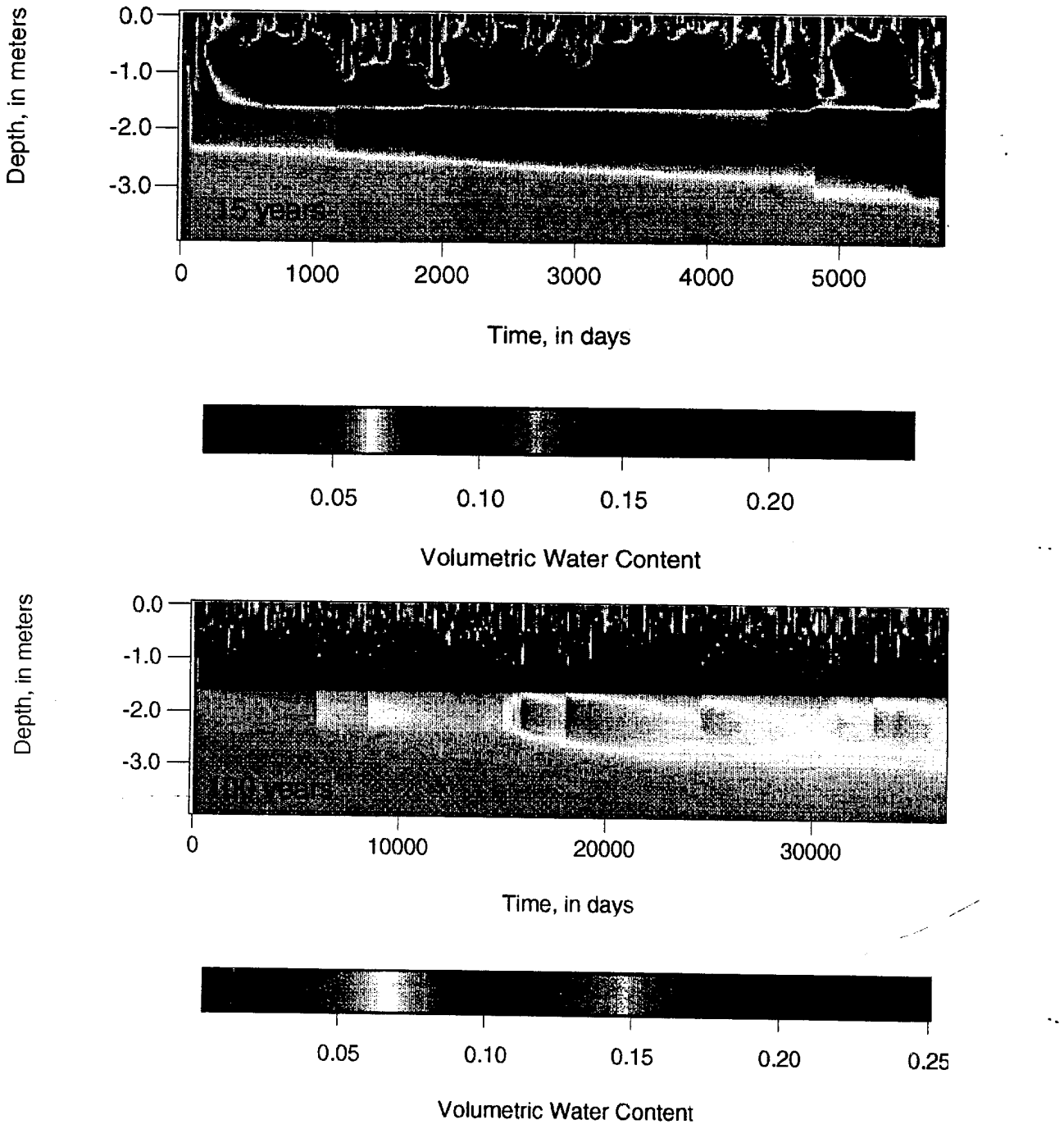

Figure 39. Volumetric water content simulated at one location in Split Wash for a) 15 years and b) 100 years using the YM stochastic rainfall model.

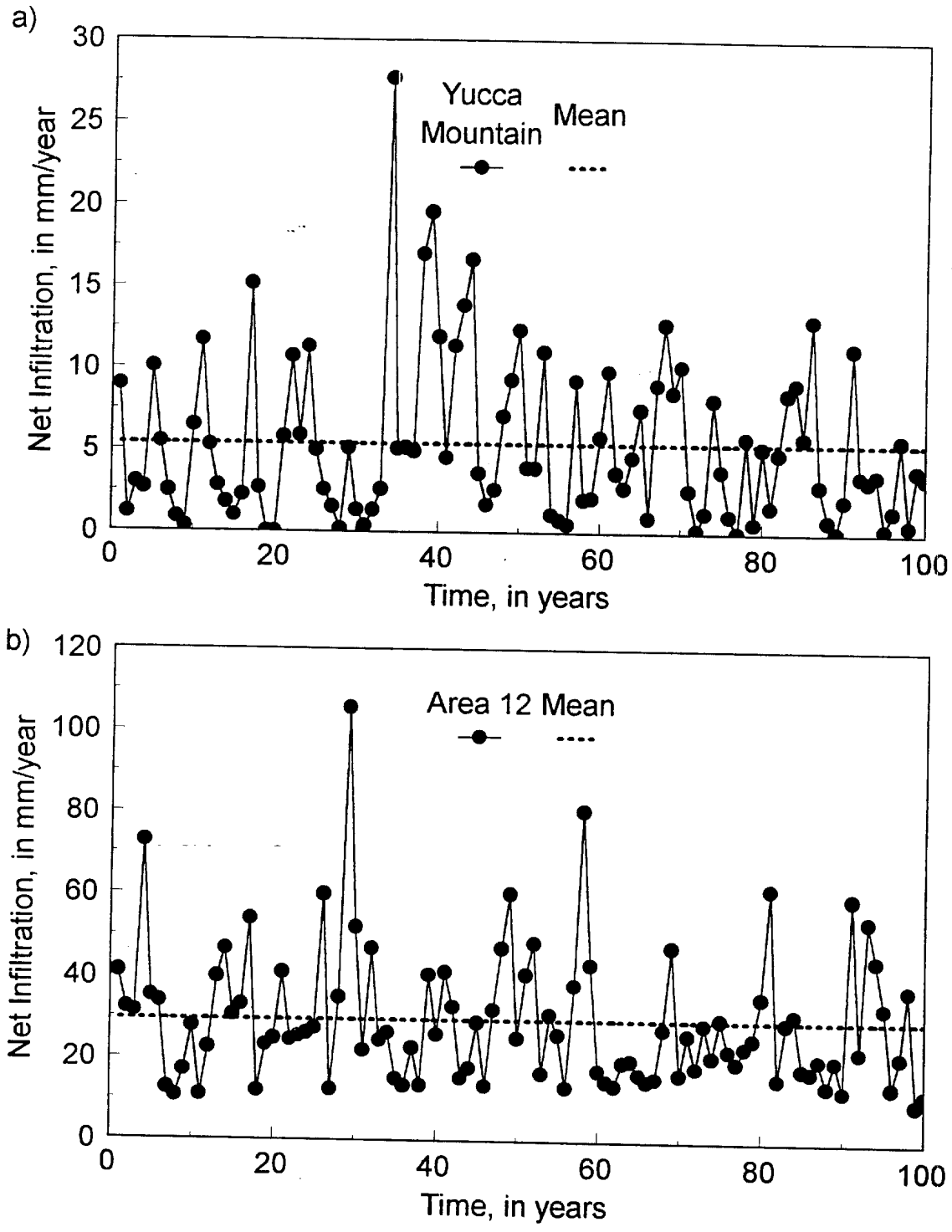

Figure 40. Simulation of mean net infiltration for neutron boreholes using 100-year stochastic simulations of precipitation from a) Yucca Mountain and b) Area 12.

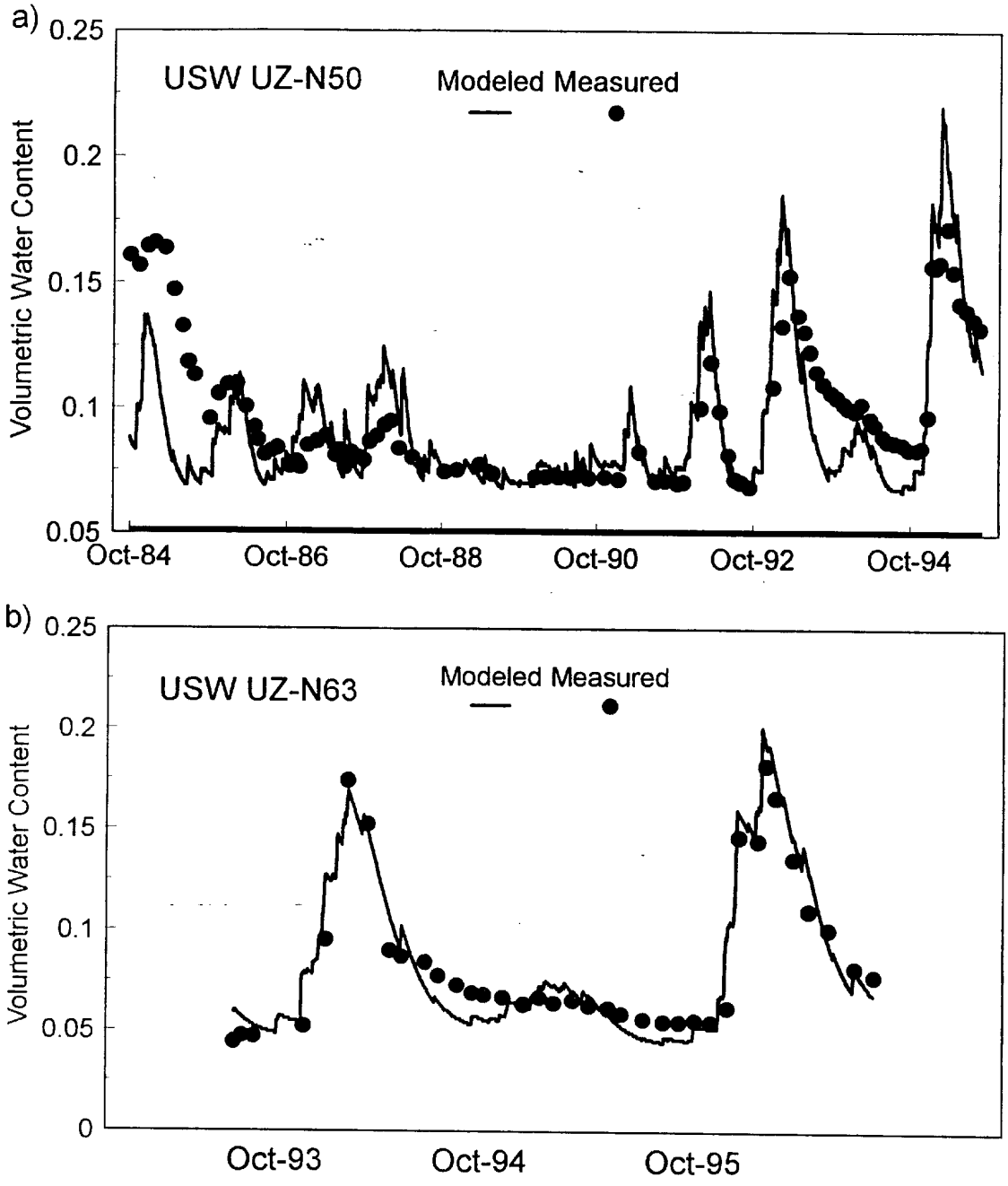

Figure 41. Calibration of modeled net infiltration using neutron boreholes a) USW UZ- N50 and b) USW UZ-N63.

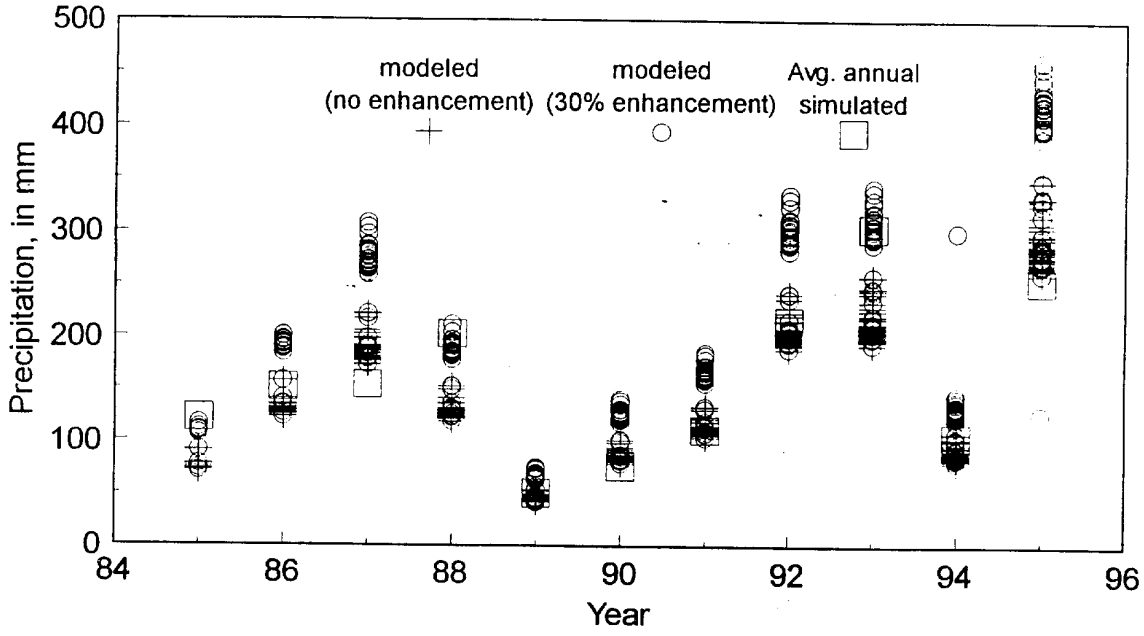

Figure 42. Precipitation modeled with no channel enhancement factor and with 30 percent channel enhancement factor compared to simulated average annual precipitation from 15 years of data.

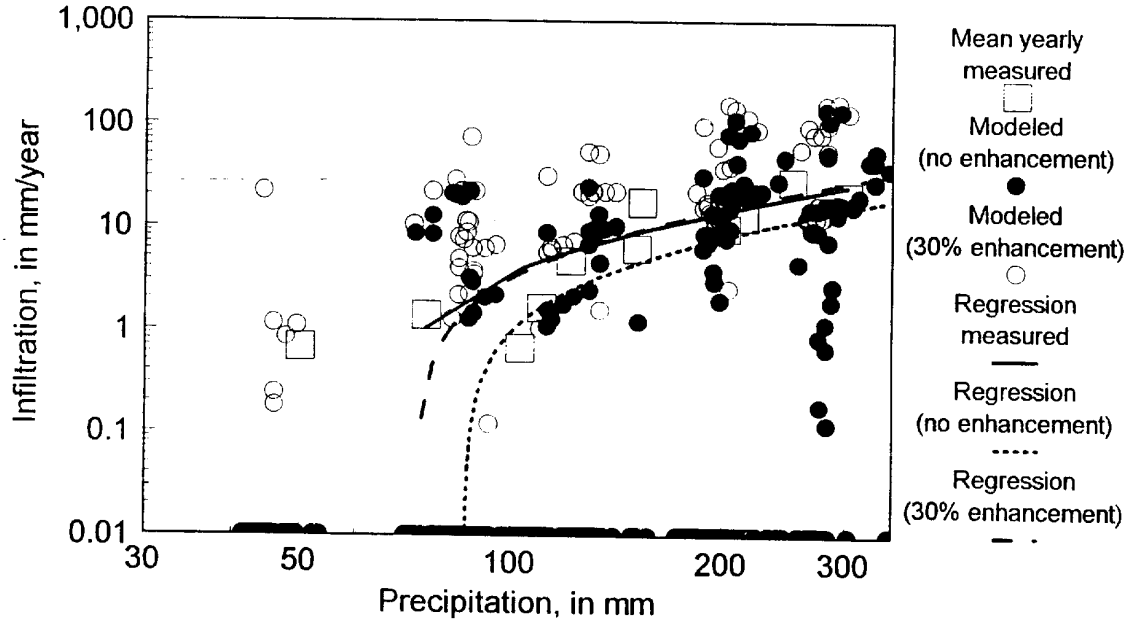

Figure 43. Precipitation versus infiltration modeled for each borehole with no channel enhancement factor and with 30 percent channel enhancement factor, and mean yearly infiltration for all boreholes. Linear regressions predicting values for each data set are shown.

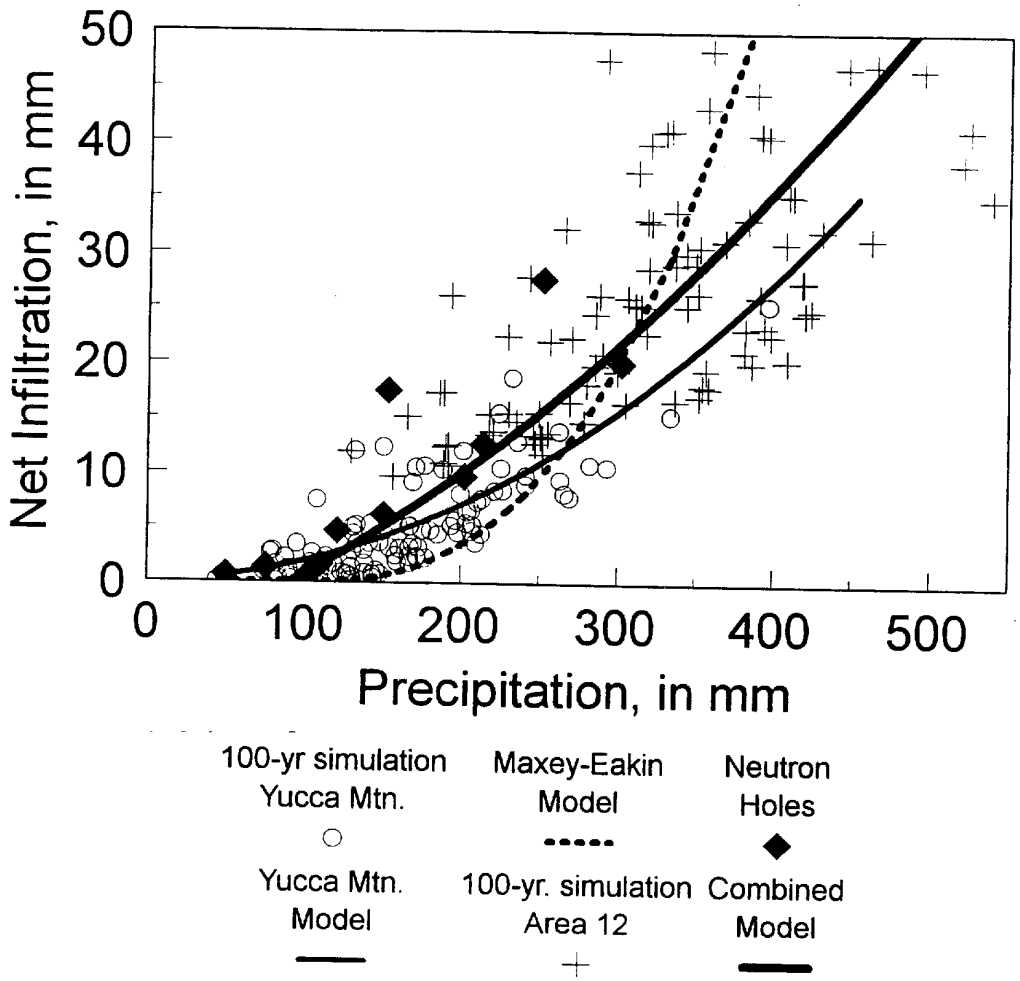

Figure 44. Precipitation versus net infiltration, modeled 100-year simulation, estimated using Maxey-Eakin method and calculated from neutron borehole data.

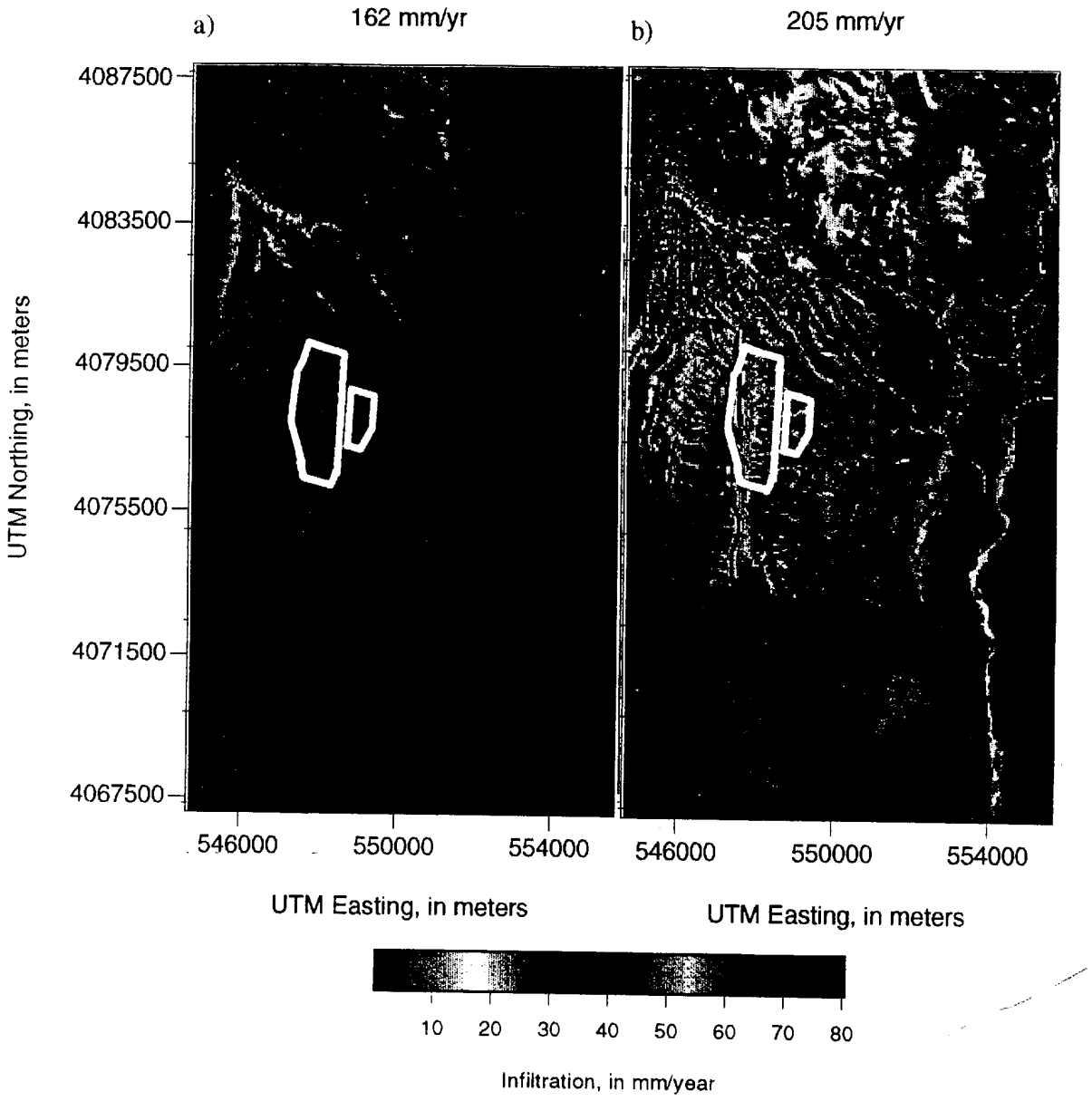

Figure 45. Infiltration simulated using stochastic precipitation simulations with average annual precipitation values of a) 165 mm/year and b) 205 mm/yr.

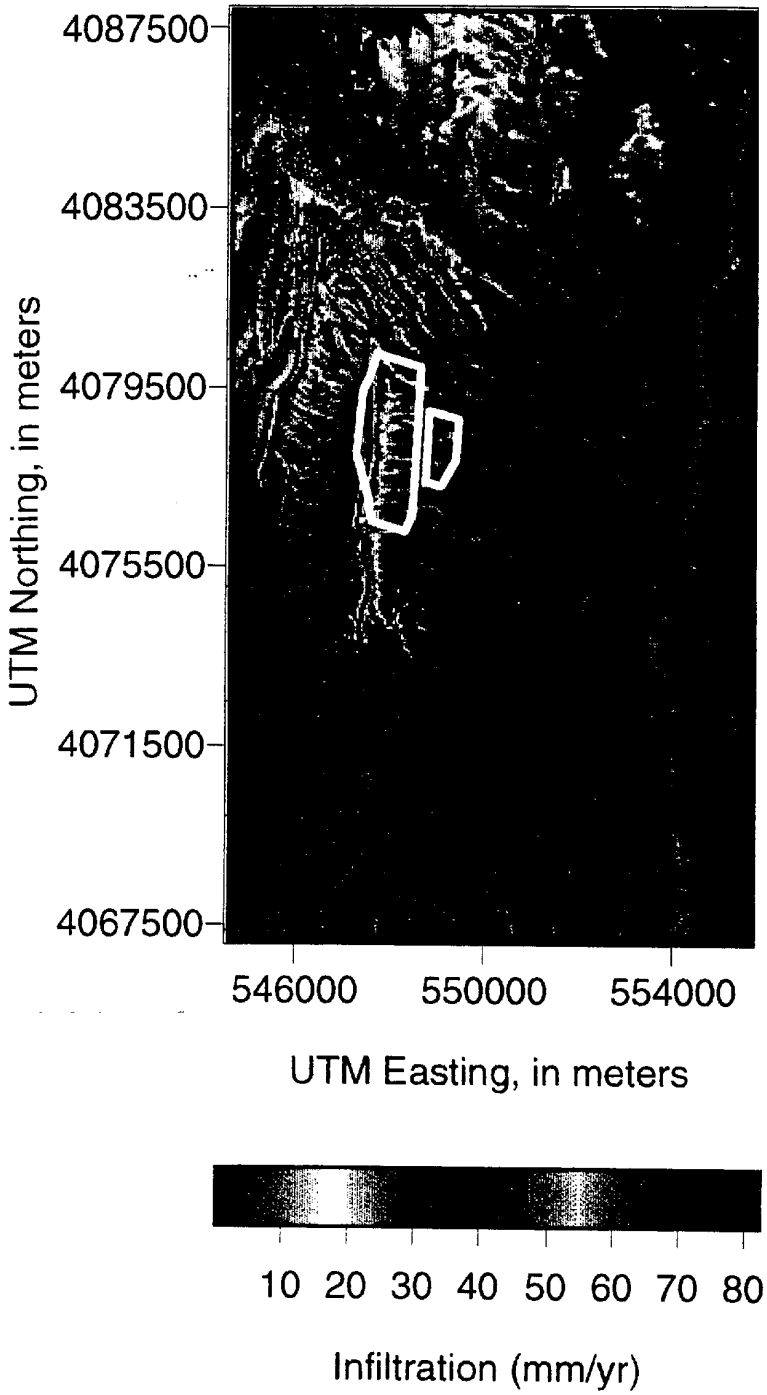

Figure 46. Conceptual model of infiltration numerically modeled using average annual precipitation and resulting in an average of 4.5 mm/year flux over the modeling domain.

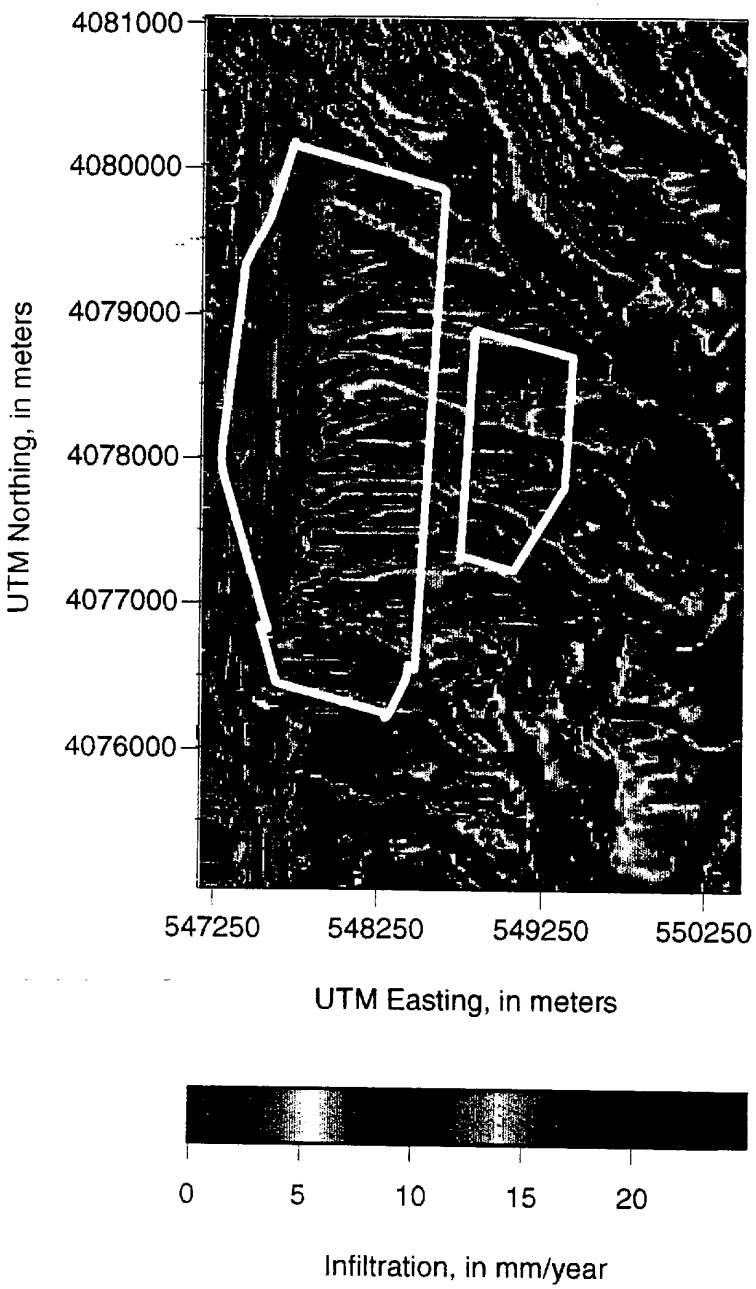

Figure 47. Close-up view of the potential repository area in figure 46.

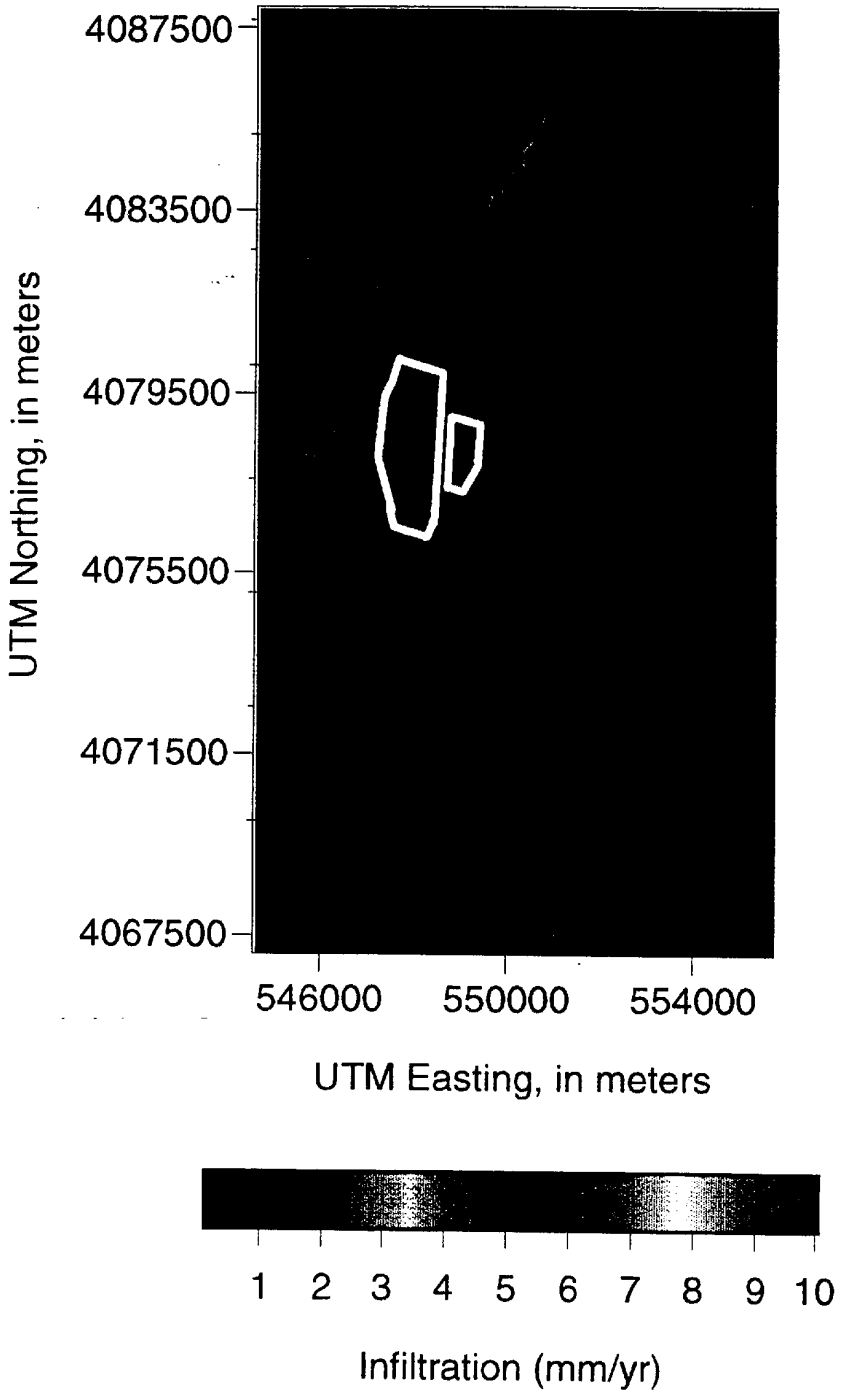

Figure 48. Alternate conceptual model of infiltration numerically modeled assuming all infiltration is through the channels. An infiltration rate of 10 mm/yr is input to the channels, resulting in an average flux over the modeling domain of 0.5 mm/yr.

Table 2 Properties of matrix and fractures for all lithostratigraphic units exposed in study area

[GIS code corresponds to those listed in Appendix V and Appendix VI; mm, millimeter, v/v, dimensionless volume, F, fractures, m, meter, m2, square meter, um, micron, * after Scott and Bonk (1984) and Sawyer and others (1995).** after Buesch and others (1994), ***after Flint (1996)]

GIS code	Formation	Lithostratigraphic Unit*	Corresponding Lithostratigraphic Unit**	Corresponding Hydrogeologic Unit***	Mean Saturated Hydraulic Conductivity (mm/day)	Mean Porosity (v/v)	Residual Water Content (v/v)	Moisture Retention Parameters alpha (1/bars)	n	m [1-(1/n)]
	Rhyolite of Fortymile Canyon									
2, 206	Rhyolite of Pinnacles Ridge	Lava flows	Tptrv1	TC	0.138	0.048	0.01	0.885	1.249	0.199
3, 207		Pyroclastic rocks	Tpbt2	BT3	45.286	0.406	0.07	41.540	1.234	0.190
4, 210	Rhyolite of Comb Peak	Lava flows	Tpcpll	TCW	0.005	0.082	0.01	0.124	1.690	0.408
5		Pyroclastic rocks	Tpbt3	BT3	45.286	0.406	0.07	41.540	1.234	0.190
6, 205	Rhyolite of Vent Pass	Lava flows	Tptrv1	TC	0.138	0.048	0.01	0.885	1.249	0.199
7		Pyroclastic rocks	Tpbt3	BT3	45.286	0.406	0.07	41.540	1.234	0.190
8	Rhyolite of Black Glass Canyon	Lava flows	Tpcpll	TCW	0.005	0.082	0.01	0.124	1.690	0.408
9		Pyroclastic rocks	Tpbt3	BT3	45.286	0.406	0.07	41.540	1.234	0.190
10	Basalt Dikes of Yucca Mountain		Tpcplnc	TCW	0.005	0.082	0.01	0.124	1.690	0.408
11, 202	Timber Mountain Tuff-Rainier Mesa	Welded ash-flow tuff	Tptpmn	TMN	0.003	0.110	0.02	0.064	1.470	0.320
12		Nonwelded ash-flow tuff	Tpcpv1	CNW	45.555	0.393	0.04	2.420	1.380	0.275
13	Bedded Tuff		Tpbt4	BT4	348.228	0.435	0.04	17.889	1.233	0.189
14, 203	Rhyolite of Windy Wash	Lava flows	Tpcpll	TCW	0.005	0.082	0.01	0.124	1.690	0.408
15		Pyroclastic rocks	Tpbt3	BT3	45.286	0.406	0.07	41.540	1.234	0.190
	Paintbrush Group									
16, 201	Tiva Canyon Tuff	Undifferentiated	Tpcpll	TCW	0.005	0.082	0.01	0.124	1.690	0.408
17		Caprock	Tpcrv	TC	0.138	0.048	0.01	0.885	1.249	0.199
18		Upper cliff	Tpcrn	CUC	3.291	0.253	0.01	0.827	1.840	0.457
19		Upper lithophysal	Tpcpul	CUL	1.079	0.164	0.01	1.404	1.529	0.346
20		Clinkstone	Tpcpmn	TCW	0.005	0.082	0.01	0.124	1.690	0.408
21		Lower cliff	Tpcpmn	TCW	0.005	0.082	0.01	0.124	1.690	0.408
22		Gray clinkstone	Tpcpmn	TCW	0.005	0.082	0.01	0.124	1.690	0.408
23		Red clinkstone	Tpcpmn	TCW	0.005	0.082	0.01	0.124	1.690	0.408
24		Upper clinkstone	Tpcpmn	TCW	0.005	0.082	0.01	0.124	1.690	0.408
25		Middle lithophysal	Tpcpmn	TCW	0.005	0.082	0.01	0.124	1.690	0.408
26		Lower clinkstone	Tpcpmn	TCW	0.005	0.082	0.01	0.124	1.690	0.408
27		Rounded step	Tpcpmn	TCW	0.005	0.082	0.01	0.124	1.690	0.408
28		Lower Lithophysal	Tpcpli	TCW	0.005	0.082	0.01	0.124	1.690	0.408
29		Lower lith. & hackly undiff.	Tpcpll	TCW	0.005	0.082	0.01	0.124	1.690	0.408
30		Hackly zone	Tpcplnh	TCW	0.005	0.082	0.01	0.124	1.690	0.408
31		Columnar	Tpcplnc	TCW	0.005	0.082	0.01	0.124	1.690	0.408
32		Bedded Tuff	Tpbt4	BT4	348.228	0.435	0.04	17.889	1.233	0.189
33	Yucca Mountain Tuff	Undifferentiated	Tpbt4	BT4	348.228	0.435	0.04	17.889	1.233	0.189
34		Upper	Tpbt4	BT4	348.228	0.435	0.04	17.889	1.233	0.189
35, 209		Middle	Tpy	TCW	0.005	0.082	0.01	0.124	1.690	0.408
36		Lower	Tpy	BT3	45.286	0.406	0.07	41.540	1.234	0.190
37		Rhyolite Flows	Tpcpll	TCW	0.005	0.082	0.01	0.124	1.690	0.408
38		Bedded Tuff	Tpbt3	BT3	45.286	0.406	0.07	41.540	1.234	0.190
39	Pah Canyon Tuff	Undifferentiated	Tpp	TPP	75.613	0.499	0.05	40.016	1.494	0.331
40		Upper	Tpp	TPP	75.613	0.499	0.05	3.412	1.427	0.299
41		Middle	Tpp	TCW	0.005	0.082	0.01	0.124	1.690	0.408
42		Lower	Tpbt2	BT2	365.471	0.490	0.05	52.638	1.278	0.218
43		Bedded Tuff	Tpbt2	BT2	365.471	0.490	0.05	52.638	1.278	0.218
44	Topopah Spring Tuff	Undifferentiated	Tptpll	TCW	0.005	0.082	0.01	0.273	1.294	0.227
45		Caprock	Tptrv1	TC	0.138	0.048	0.00	0.885	1.249	0.199
99		Caprock/rounded	Tptrn	TC	0.138	0.048	0.00	0.885	1.249	0.199
46		Rounded	Tptrn	TR	0.144	0.156	0.01	3.776	2.399	0.583
47		Thin lithophysal	Tptpul	TUL	0.017	0.154	0.01	0.657	1.331	0.249
48		Red lithophysal	Tptpul	TUL	0.017	0.154	0.01	0.657	1.331	0.249
49		Upper lithophysal	Tptpul	TUL	0.017	0.154	0.01	0.657	1.331	0.249
50		Lower lithophysal	Tptpul	TUL	0.017	0.154	0.01	0.657	1.331	0.249
51		Lithophysal	Tptpul	TUL	0.017	0.154	0.01	0.657	1.331	0.249
52, 213		Nonlithophysal	Tptpmn	TMN	0.003	0.110	0.02	0.064	1.470	0.320
53		Gray nonlithophysal	Tptpmn	TMN	0.003	0.110	0.02	0.064	1.470	0.320
54		Orange	Tptpmn	TMN	0.003	0.110	0.02	0.064	1.470	0.320
55		Brick	Tptpmn	TMN	0.003	0.110	0.02	0.064	1.470	0.320
56		Orange brick	Tptpmn	TMN	0.003	0.110	0.02	0.064	1.470	0.320
57		Orange brick lithophysal	Tptpmn	TMN	0.003	0.110	0.02	0.064	1.470	0.320
58		Orange brick	Tptpmn	TMN	0.003	0.110	0.02	0.064	1.470	0.320
59		Brownish-orange brick	Tptpmn	TMN	0.003	0.110	0.02	0.064	1.470	0.320
60, 212		Grayish-red lithophysal	Tptpll	TLL	0.020	0.130	0.01	0.273	1.294	0.227
61		Orangish-red lithophysal	Tptpll	TLL	0.020	0.130	0.01	0.273	1.294	0.227
62		Mottled lithophysal	Tptpll	TLL	0.020	0.130	0.01	0.273	1.294	0.227
63		Purplish-brown lothophysal	Tptpll	TLL	0.020	0.130	0.01	0.273	1.294	0.227
64		Reddish-brown brick	Tptpll	TLL	0.020	0.130	0.01	0.273	1.294	0.227
65		Brownish-orange lithophysal	Tptpll	TLL	0.020	0.130	0.01	0.273	1.294	0.227
66		Mottled	Tptpln	TM1	0.006	0.094	0.03	0.022	2.141	0.533
67		Vitrophyre	Tptpv3	PV3	0.004	0.036	0.02	0.010	1.582	0.368
68		Partially welded	Tptpv2,1	PV2	0.063	0.173	0.02	1.255	1.310	0.237
69	Calico Hills Formation	Pyroclastic rocks	Tac	CHZ	0.004	0.332	0.07	0.394	1.290	0.225
70, 208		Lava flows	Tptpln	TM1	0.006	0.094	0.03	0.022	2.141	0.533
71		Autobrecciated lavas	Tac	CHZ	0.004	0.332	0.07	0.394	1.290	0.225
	Crater Flat Group									
72	Prow Pass Tuff	Partially welded	Tcp, unit3	PP3	0.033	0.322	0.02	1.817	1.455	0.313
73, 214		Moderately welded	Tcp, unit2	PP2	0.328	0.237	0.02	0.072	1.603	0.376
74		Undifferentiated	Tcp, unit2	PP2	0.328	0.237	0.02	0.072	1.603	0.376
75		Bedded Tuffs	Tcp, unit1	PP1	0.015	0.286	0.05	0.179	1.454	0.312
76, 211	Bullfrog Tuff	Ash-flow tuff	Tcb, unit3	BF3	0.035	0.117	0.01	0.036	1.680	0.405

---------------- Calculated Flux for Fracture + Matrix ----------------

Estimated Fracture Density (F/m)	Fracture Aperture 2.5 um % area (m2/m2)	Fracture Aperture 25 um % area (m2/m2)	Fracture Aperture 250 um % area (m2/m2)	Open 2.5 um Fractures flux (mm/day)	Open 25 um Fractures flux (mm/day)	Open 250 um Fractures flux (mm/day)	Filled 2.5 um Fractures flux (mm/day)	Filled 25 um Fractures flux (mm/day)	Filled 250 um Fractures flux (mm/day)	Weighted average (mm/day)
17.0	4.3E-05	4.3E-04	4.3E-03	0.156	6.811	3166.388	0.140	0.157	0.322	16.357
3.7	9.3E-06	9.3E-05	9.3E-04	45.290	46.738	734.411	45.287	45.290	45.326	48.816
10.5	2.6E-05	2.6E-04	2.6E-03	0.015	4.126	1955.630	0.006	0.016	0.118	10.022
3.7	9.3E-06	9.3E-05	9.3E-04	45.290	46.738	734.411	45.287	45.290	45.326	48.816
17.0	4.3E-05	4.3E-04	4.3E-03	0.156	6.811	3166.388	0.140	0.157	0.322	16.357
3.7	9.3E-06	9.3E-05	9.3E-04	45.290	46.738	734.411	45.287	45.290	45.326	48.816
10.5	2.6E-05	2.6E-04	2.6E-03	0.015	4.126	1955.630	0.006	0.016	0.118	10.022
3.7	9.3E-06	9.3E-05	9.3E-04	45.290	46.738	734.411	45.287	45.290	45.326	48.816
10.5	2.6E-05	2.6E-04	2.6E-03	0.015	4.126	1955.630	0.006	0.016	0.118	10.022
19.1	4.8E-05	4.8E-04	4.8E-03	0.023	7.500	3557.378	0.006	0.024	0.210	18.226
8.7	2.2E-05	2.2E-04	2.2E-03	45.564	48.969	1665.930	45.556	45.564	45.649	53.855
4.4	1.1E-05	1.1E-04	1.1E-03	348.232	349.955	1167.728	348.228	348.232	348.275	352.425
10.5	2.6E-05	2.6E-04	2.6E-03	0.015	4.126	1955.630	0.006	0.016	0.118	10.022
3.7	9.3E-06	9.3E-05	9.3E-04	45.290	46.738	734.411	45.287	45.290	45.326	48.816
10.5	2.6E-05	2.6E-04	2.6E-03	0.015	4.126	1955.630	0.006	0.016	0.118	10.022
17.0	4.3E-05	4.3E-04	4.3E-03	0.156	6.811	3166.388	0.140	0.157	0.322	16.357
9.2	2.3E-05	2.3E-04	2.3E-03	3.300	6.902	1716.791	3.292	3.301	3.390	12.068
7.8	2.0E-05	2.0E-04	2.0E-03	1.087	4.141	1453.829	1.080	1.088	1.163	8.521
10.5	2.6E-05	2.6E-04	2.6E-03	0.015	4.126	1955.630	0.006	0.016	0.118	10.022
10.5	2.6E-05	2.6E-04	2.6E-03	0.015	4.126	1955.630	0.006	0.016	0.118	10.022
10.5	2.6E-05	2.6E-04	2.6E-03	0.015	4.126	1955.630	0.006	0.016	0.118	10.022
10.5	2.6E-05	2.6E-04	2.6E-03	0.015	4.126	1955.630	0.006	0.016	0.118	10.022
10.5	2.6E-05	2.6E-04	2.6E-03	0.015	4.126	1955.630	0.006	0.016	0.118	10.022
10.5	2.6E-05	2.6E-04	2.6E-03	0.015	4.126	1955.630	0.006	0.016	0.118	10.022
10.5	2.6E-05	2.6E-04	2.6E-03	0.015	4.126	1955.630	0.006	0.016	0.118	10.022
10.5	2.6E-05	2.6E-04	2.6E-03	0.015	4.126	1955.630	0.006	0.016	0.118	10.022
10.5	2.6E-05	2.6E-04	2.6E-03	0.015	4.126	1955.630	0.006	0.016	0.118	10.022
10.5	2.6E-05	2.6E-04	2.6E-03	0.015	4.126	1955.630	0.006	0.016	0.118	10.022
10.5	2.6E-05	2.6E-04	2.6E-03	0.015	4.126	1955.630	0.006	0.016	0.118	10.022
10.5	2.6E-05	2.6E-04	2.6E-03	0.015	4.126	1955.630	0.006	0.016	0.118	10.022
4.4	1.1E-05	1.1E-04	1.1E-03	348.232	349.955	1167.728	348.228	348.232	348.275	352.425
4.4	1.1E-05	1.1E-04	1.1E-03	348.232	349.955	1167.728	348.228	348.232	348.275	352.425
4.4	1.1E-05	1.1E-04	1.1E-03	348.232	349.955	1167.728	348.228	348.232	348.275	352.425
10.5	2.6E-05	2.6E-04	2.6E-03	0.015	4.126	1955.630	0.006	0.016	0.118	10.022
3.7	9.3E-06	9.3E-05	9.3E-04	45.290	46.738	734.411	45.287	45.290	45.326	48.816
10.5	2.6E-05	2.6E-04	2.6E-03	0.015	4.126	1955.630	0.006	0.016	0.118	10.022
3.7	9.3E-06	9.3E-05	9.3E-04	45.290	46.738	734.411	45.287	45.290	45.326	48.816
2.4	6.0E-06	6.0E-05	6.0E-04	75.616	76.555	522.613	75.613	75.616	75.639	77.903
2.4	6.0E-06	6.0E-05	6.0E-04	75.616	76.555	522.613	75.613	75.616	75.639	77.903
10.5	2.6E-05	2.6E-04	2.6E-03	0.015	4.126	1955.630	0.006	0.016	0.118	10.022
2.2	5.5E-06	5.5E-05	5.5E-04	365.473	366.334	775.221	365.471	365.473	365.494	367.570
2.2	5.5E-06	5.5E-05	5.5E-04	365.473	366.334	775.221	365.471	365.473	365.494	367.570
16.0	4.0E-05	4.0E-04	4.0E-03	0.021	6.285	2980.005	0.006	0.022	0.177	15.270
17.0	4.3E-05	4.3E-04	4.3E-03	0.156	6.811	3166.388	0.140	0.157	0.322	16.357
17.0	4.3E-05	4.3E-04	4.3E-03	0.156	6.811	3166.388	0.140	0.157	0.322	16.357
9.2	2.3E-05	2.3E-04	2.3E-03	0.154	3.755	1713.644	0.145	0.154	0.243	8.922
7.8	2.0E-05	2.0E-04	2.0E-03	0.025	3.079	1452.767	0.018	0.026	0.102	7.459
7.8	2.0E-05	2.0E-04	2.0E-03	0.025	3.079	1452.767	0.018	0.026	0.102	7.459
7.8	2.0E-05	2.0E-04	2.0E-03	0.025	3.079	1452.767	0.018	0.026	0.102	7.459
7.8	2.0E-05	2.0E-04	2.0E-03	0.025	3.079	1452.767	0.018	0.026	0.102	7.459
7.8	2.0E-05	2.0E-04	2.0E-03	0.025	3.079	1452.767	0.018	0.026	0.102	7.459
19.1	4.8E-05	4.8E-04	4.8E-03	0.023	7.500	3557.378	0.006	0.024	0.210	18.226
19.1	4.8E-05	4.8E-04	4.8E-03	0.023	7.500	3557.378	0.006	0.024	0.210	18.226
19.1	4.8E-05	4.8E-04	4.8E-03	0.023	7.500	3557.378	0.006	0.024	0.210	18.226
19.1	4.8E-05	4.8E-04	4.8E-03	0.023	7.500	3557.378	0.006	0.024	0.210	18.226
19.1	4.8E-05	4.8E-04	4.8E-03	0.023	7.500	3557.378	0.006	0.024	0.210	18.226
19.1	4.8E-05	4.8E-04	4.8E-03	0.023	7.500	3557.378	0.006	0.024	0.210	18.226
19.1	4.8E-05	4.8E-04	4.8E-03	0.023	7.500	3557.378	0.006	0.024	0.210	18.226
19.1	4.8E-05	4.8E-04	4.8E-03	0.023	7.500	3557.378	0.006	0.024	0.210	18.226
16.0	4.0E-05	4.0E-04	4.0E-03	0.036	6.300	2980.020	0.021	0.037	0.192	15.285
16.0	4.0E-05	4.0E-04	4.0E-03	0.036	6.300	2980.020	0.021	0.037	0.192	15.285
16.0	4.0E-05	4.0E-04	4.0E-03	0.036	6.300	2980.020	0.021	0.037	0.192	15.285
16.0	4.0E-05	4.0E-04	4.0E-03	0.036	6.300	2980.020	0.021	0.037	0.192	15.285
16.0	4.0E-05	4.0E-04	4.0E-03	0.036	6.300	2980.020	0.021	0.037	0.192	15.285
16.0	4.0E-05	4.0E-04	4.0E-03	0.036	6.300	2980.020	0.021	0.037	0.192	15.285
19.4	4.9E-05	4.9E-04	4.9E-03	0.026	7.621	3613.256	0.009	0.027	0.216	18.515
19.2	4.8E-05	4.8E-04	4.8E-03	0.024	7.540	3576.004	0.006	0.025	0.212	18.322
4.9	1.2E-05	1.2E-04	1.2E-03	0.068	1.986	912.688	0.064	0.069	0.116	4.738
4.9	1.2E-05	1.2E-04	1.2E-03	0.009	1.927	912.629	0.004	0.009	0.057	4.679
19.4	4.9E-05	4.9E-04	4.9E-03	0.026	7.621	3613.256	0.009	0.027	0.216	18.515
4.9	1.2E-05	1.2E-04	1.2E-03	0.009	1.927	912.629	0.004	0.009	0.057	4.679
4.9	1.2E-05	1.2E-04	1.2E-03	0.038	1.956	912.658	0.033	0.038	0.086	4.708
4.9	1.2E-05	1.2E-04	1.2E-03	0.333	2.252	912.953	0.329	0.334	0.381	5.003
4.9	1.2E-05	1.2E-04	1.2E-03	0.333	2.252	912.953	0.329	0.334	0.381	5.003
4.9	1.2E-05	1.2E-04	1.2E-03	0.020	1.938	912.640	0.015	0.020	0.068	4.690
4.9	1.2E-05	1.2E-04	1.2E-03	0.040	1.959	912.660	0.036	0.041	0.088	4.710